Dynamique des blooms phytoplanctoniques dans le gyre subpolaire de l'Atlantique Nord

Léo Lacour

Université Pierre et Marie Curie

Ecole doctorale des Sciences de l'Environnement d'Iles-de-France

Laboratoire d'Océanographie de Villefranche

Optique Marine et Télédétection : Applications à la Biogéochimie

Dynamique des blooms phytoplanctoniques dans le gyre subpolaire de l'Atlantique Nord

Par Léo LACOUR

Thèse de doctorat en Océanographie

Dirigée par Hervé CLAUSTRE

Présentée et soutenue publiquement le 8 décembre 2016

Devant un jury composé de :

M. Laurent MEMERY	Directeur de recherche	Rapporteur
M. Pierre-Yves LE TRAON	Directeur de recherche	Rapporteur
M. Stéphane BLAIN	Professeur	Examinateur
M. Jean-Baptiste SALLEE	Chargé de recherche	Examinateur
M. Daniele IUDICONE	Directeur de recherche	Invité
M. Hervé CLAUSTRE	Directeur de recherche	Directeur de thèse

Résumé

Le gyre subpolaire de l'Atlantique Nord est le siège de la plus importante floraison (bloom) phytoplanctonique de l'océan global. Cet événement biologique majeur joue un rôle crucial sur le fonctionnement des écosystèmes océaniques et sur le cycle global du carbone. L'objectif de cette thèse est de mieux comprendre les processus bio-physiques qui contrôlent la dynamique du bloom phytoplanctonique et l'export de carbone à différentes échelles spatio-temporelles.

Dans une première étude, basée sur des données satellites climatologiques, le gyre subpolaire a été biorégionalisé en fonction des différents cycles annuels de biomasse phytoplanctonique. En particulier, la mer du Labrador semble divisée en deux biorégions de part et d'autre de 60°N, celle située au nord étant caractérisée par un bloom beaucoup plus précoce et intense. Une analyse climatologique de données de flotteurs Argo récoltées dans la région nord a montré une forte stratification hivernale liée aux apports d'eau dessalée d'origine Arctique. Cette stratification haline augmente le temps de résidence des cellules phytoplanctoniques dans la couche éclairée permettant ainsi d'atteindre prématurément la dose de lumière nécessaire pour initier le bloom printanier.

La nouvelle génération de flotteurs BGC-Argo a permis, dans une deuxième étude, d'explorer des processus à des échelles plus fines, en particulier pendant la période hivernale jusqu'à présent très peu étudiée. En hiver, des restratifications intermittentes et locales de la couche de mélange liées à des processus de sous-mésoéchelle impactent la structure de la communauté phytoplanctonique en favorisant la croissance de diatomées. Ces blooms hivernaux, en maintenant une population active de diatomées, semblent influencer l'initiation et l'intensité du bloom printanier. Un tel pré-conditionnement biologique, lié à l'intermittence des conditions hivernales de mélange, n'avait encore jamais été évoqué dans le débat actuel sur la dynamique du bloom printanier.

Enfin, une troisième étude a montré que la variabilité de la profondeur de la couche de mélange pendant la transition hiver-printemps joue aussi un rôle crucial sur l'export de carbone. En effet, la pompe physique générée par l'alternance entre mélange convectif et restratification temporaire permet d'exporter dans la zone mésopélagique une quantité non négligeable de carbone organique particulaire avant l'initiation du bloom printanier et constitue ainsi une alternative à l'export de carbone par sédimentation.

Mots clés : Bloom phytoplanctonique, composition des communautés phytoplanctoniques, interactions bio-physiques, disponibilité en lumière, export de carbone, flotteurs Argo et BGC-Argo, couleur de l'eau, gyre subpolaire de l'Atlantique Nord.

Abstract

The North Atlantic Subpolar Gyre exhibits the largest phytoplancton bloom of the global ocean. This major biological event plays a crucial role for the functioning of marine ecosystems and the global carbon cycle. The aim of this thesis is to better understand the bio-physical processes driving the dynamics of the phytoplankton bloom and carbon export at various spatiotemporal scales.

In a first study, based on satellite data at a climatological scale, the subpolar gyre is bioregionalized according to distinct annual phytoplankton biomass cycles. In particular, the Labrador Sea appears to be well delineated into two regions on either side of the 60°N parallel, with the northern region being characterized by an earlier and more intense bloom. A climatological analysis of Argo data retrieved from the northern region revealed strong winter stratification due to fresh-water inputs from the Arctic. This haline stratification increases the residence time of phytoplankton cells in the sunlit layer, thus allowing them to reach the light level required to initiate the spring bloom in advance.

In a second study, the new generation of BGC-Argo floats allowed for processes to be explored at a finer scale, especially during the overlooked winter season. In winter, intermittent and local restratification of the mixed layer, triggered by sub-mesoscale processes, impact the phytoplankton community structure, enhancing diatom growth. These winter blooms, which maintain an active diatom population, seem to influence the timing and magnitude of the spring bloom. Such a biological preconditioning, related to winter mixing intermittency, has never yet been mentioned in the present debate on spring bloom dynamics.

Finally, a third study showed how the high variability of the mixed layer during the winter-spring transition plays a crucial role on carbon export. Indeed, the physical pump, induced by alternating convective mixing and transient restratification, enables the export of a significant fraction of particulate organic carbon to the mesopelagic zone before the onset of the spring bloom, thus representing an alternative to carbon export by sedimentation.

Key words : Phytoplankton bloom, phytoplankton community composition, bio-physical interactions, light availability, carbon export, BGC-Argo and Argo float, ocean color, North Atlantic subpolar gyre.

Table des matières

CHAPITRE 1

Introduction générale

1.1 Contexte général

Le phytoplancton est constitué d'organismes photosynthétiques unicellulaires qui dérivent au gré des courants. Ces producteurs primaires utilisent l'énergie lumineuse et les nutriments tels que le nitrate, le phosphate ou le fer pour transformer le CO_2 en matière organique nécessaire à leur métabolisme. Ils contribuent à environ 50% de la production primaire globale (Field, 1998 ; Behrenfeld *et al.*, 2006 ; Arrigo, 2007). Dans les océans, l'intensité de la lumière décroit exponentiellement avec la profondeur ce qui restreint la production à la couche éclairée de surface que l'on appelle couche euphotique. Dans cette couche, les stocks de nutriments sont rapidement consommés par le phytoplancton et deviennent alors limitants. En revanche, ces nutriments sont abondants en profondeur, où ils sont régénérés par l'activité microbienne. Le mélange vertical de la colonne d'eau permet de recharger la couche de surface en nutriments mais entraîne aussi en profondeur les organismes phytoplanctoniques. La lumière devient alors l'élément limitant. La croissance du phytoplancton est donc intimement liée au mélange vertical de la colonne d'eau qui régule les ressources nécessaires à la photosynthèse.

Au printemps, aux hautes latitudes, la stratification de la colonne d'eau permet d'initier une accumulation rapide de la biomasse phytoplanctonique en surface, il s'agit de la floraison printanière plus communément appelée bloom printanier. L'accumulation intense du phytoplancton se traduit par une coloration de l'océan qui est visible par satellite. Cet événement biologique majeur impacte l'ensemble de l'écosystème océanique et joue un rôle crucial sur le cycle global du carbone. Les caractéristiques (date d'initiation, intensité, durée) du bloom sont très variables selon les conditions environnementales (Longhurst *et al.*, 1995) et sont susceptibles d'évoluer avec les changements climatiques à venir (Ji *et al.*, 2010 ; Racault *et al.*, 2012). Il est donc primordial de bien comprendre la dynamique du bloom aux hautes latitudes et d'identifier les mécanismes bio-physiques à l'origine de sa variabilité.

Le bloom phytoplanctonique est particulièrement intense dans le gyre subpolaire de l'Atlantique Nord (Figure 1a), et caractérisé par une forte variabilité spatio-temporelle (Figure 1b). Cette région particulièrement bien documentée est une zone d'étude idéale pour comprendre la dynamique de la biomasse phytoplanctonique.
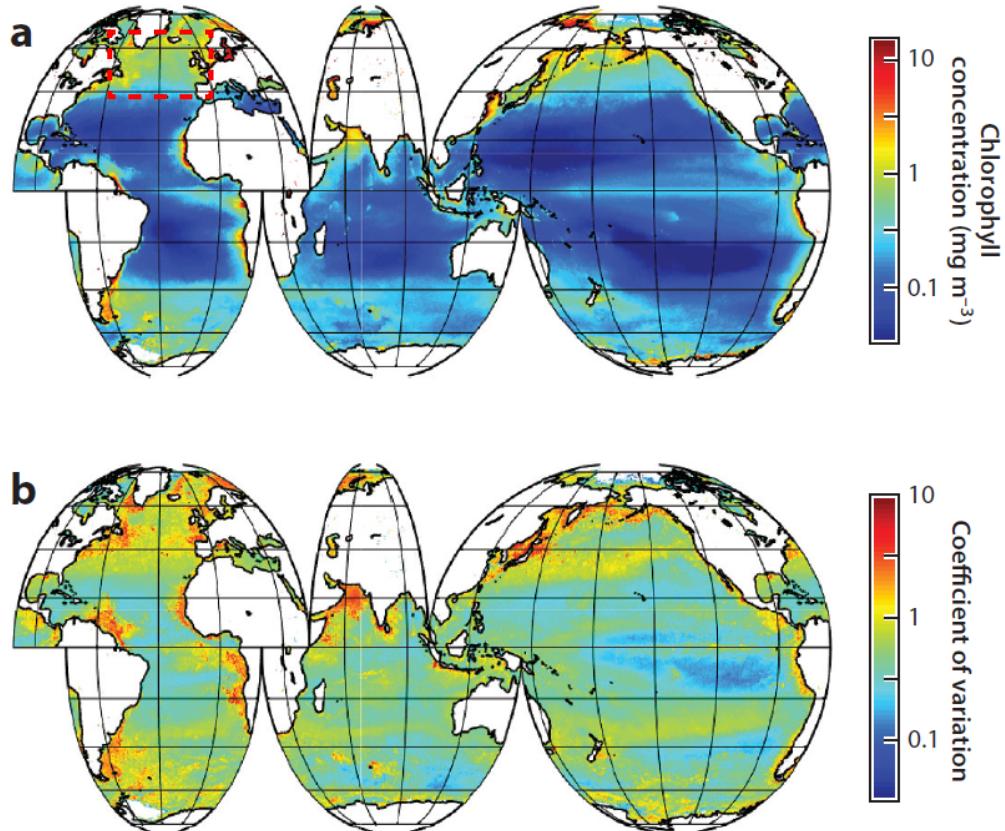
Figure. 1. (a) Moyenne annuelle de la concentration en Chla calculée à partir de données SeaWiFS de niveau 3 pour les années 1997 à 2010. La Chla est un proxy de la biomasse phytoplanctonique (b) Coefficient de variation (écart type divisé par la moyenne) de la concentration en Chla calculé sur la même période. Le rectangle rouge en tirets délimite le gyre subpolaire de l'Atlantique Nord. (source : Mahadevan (2016))

1.2   Zone d'étude : le gyre subpolaire de l'Atlantique Nord

Le gyre subpolaire de l'Atlantique Nord (45°-65°N) est divisé en 3 bassins principaux : le bassin d'Islande à l'est, la mer d'Irminger au centre et la mer du Labrador à l'ouest (Figure 2). Le bassin d'Islande et la mer d'Irminger sont séparés physiquement par la crête de Reykjanes. Le gyre cyclonique de surface est composé du courant Nord Atlantique (NAC), du courant d'Irminger (IC) qui contourne la crête de Reykjanes, du courant est et ouest du Groenland (EGC et WGC respectivement) et du courant du Labrador (LC) le long de la côte Canadienne. Le NAC et l'IC transportent des eaux chaudes et salées (8-18°C, 35,2-36,7‰) d'origine subtropicale tandis que l'EGC, le WGC et le LC transportent des eaux froides et peu salées (0-4°C, 34-35‰) d'origine arctique (Figure 3a et b ; Emery (2001). Le gyre subpolaire est donc une zone de rencontre entre deux types de masse d'eau très contrastés à
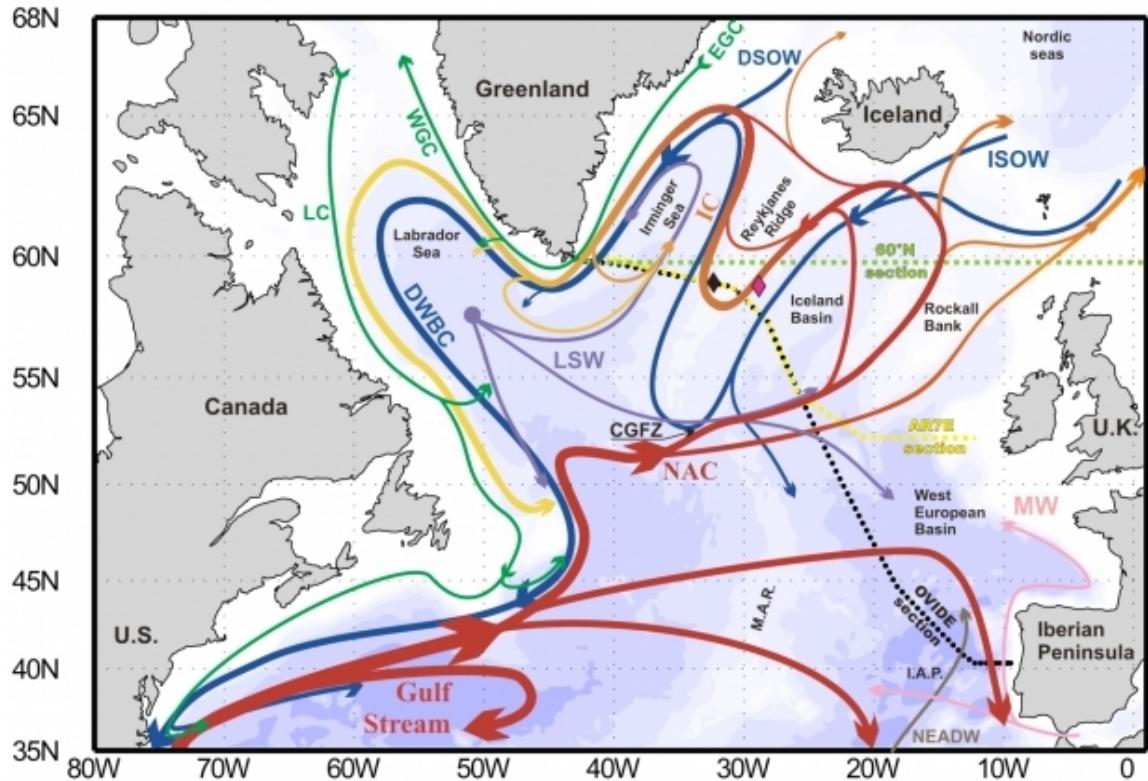
Figure. 2. Circulation océanique dans le gyre subpolaire de l'Atlantique Nord. Les principaux acronymes utilisés dans cette étude sont les suivants : courant Nord Atlantique (NAC), courant d'Irminger (IC), courant est et ouest du Groenland (EGC et WGC respectivement) et courant du Labrador (LC). (source : Pascale Lherminier, Ifremer)

l'origine de forts gradients horizontaux de densité (Figure 3c ; Caniaux *et al.* (2001). Ces gradients horizontaux de densité génèrent des instabilités baroclines qui convertissent l'énergie potentielle du fluide en énergie cinétique à l'origine de la formation de structures de mésoéchelle (10-100 km) et sous-mésoéchelle (0,1-10 km) (Fox-Kemper *et al.*, 2008). Ces structures, telles que les tourbillons, les fronts ou les filaments, sont très énergétiques et participent au transport vertical et horizontal des masses d'eau (Lévy, 2008). Elles peuvent ainsi moduler localement le stock de nutriment dans la couche euphotique (Klein et Lapeyre, 2009). A l'échelle du gyre subpolaire, le champ de tourbillon de mésoéchelle exporte des eaux de surface riches en nutriments vers le fond et constitue ainsi un puits net de nutriments (McGillicuddy, 2015). De la même manière, le transport horizontal de masses d'eau par les tourbillons cohérents constitue sur l'ensemble du gyre un flux négatif de nutriments (McGillicuddy, 2015). En effet, les tourbillons transportent des eaux pauvres en nutriments d'origine subtropicale vers l'intérieur du gyre subpolaire.

A l'échelle du gyre subpolaire, ce puits net de nutriments, lié à l'activité mésoéchelle, est largement compensé par le mélange vertical induit par les forçages atmosphériques hivernaux très intenses. Les flux de chaleur et le vent sont les principaux forçages qui influencent la stabilité de la colonne d'eau. En effet, la perte de chaleur de l'océan vers l'atmosphère (flux de chaleur négatif) entraîne un refroidissement de la couche de surface. De même, l'évaporation, favorisée par l'intensification
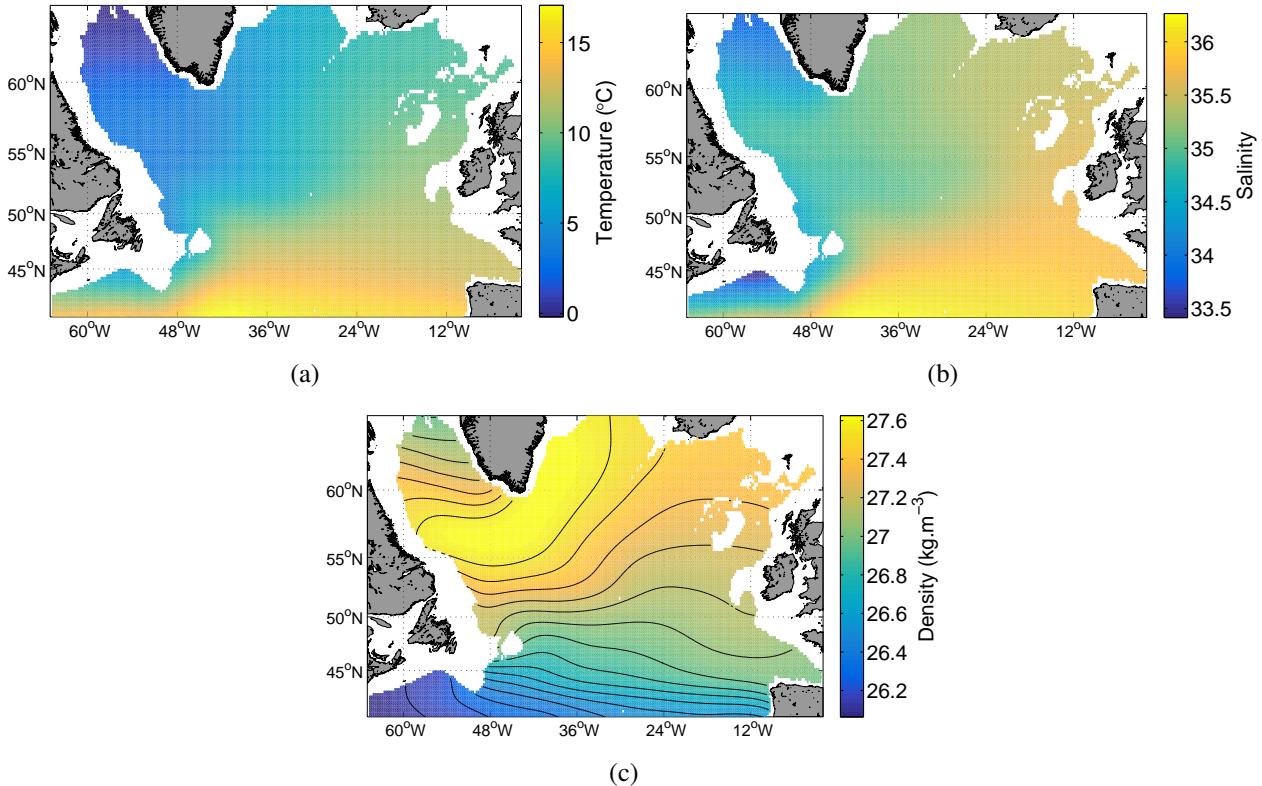
Figure. 3. Climatologie annuelle (2005-2015) de température (a), salinité (b) et densité issue des flotteurs Argo dans le gyre subpolaire de l'Atlantique Nord. Les lignes noires de la figure (c) représentent les isopycnes de surface (intervalle 0,1 kg m^{-3}).

des vents (flux de chaleur latente), peut augmenter la salinité de surface (Schulze *et al.*, 2016). Ces deux processus participent à l'augmentation de la densité de la couche de surface qui plonge alors jusqu'à sa profondeur d'équilibre. La masse d'eau de surface exportée est remplacée par une masse d'eau profonde formant ainsi une cellule convective. La couche de mélange convective peut atteindre plusieurs centaines de mètres de profondeur en hiver ce qui permet de recharger la couche de surface en nutriments (Figure 4a). Les couches de mélange convectives sont particulièrement profondes dans le sud de la mer du Labrador et de la mer d'Irminger (Figure 4a). Ces zones de formation d'eau dense sont particulièrement importantes car elles alimentent la circulation thermo-haline mondiale. Au printemps, l'augmentation du flux radiatif et la diminution de l'intensité du vent inverse les échanges océan-atmosphère de chaleur (flux de chaleur positif). L'océan commence à se réchauffer, la convection s'arrête et la colonne d'eau commence à se stratifier (Figure 4b). Les structures de méso- et sous-mésoéchelle jouent aussi un rôle crucial sur la restratification des couches de mélange hivernales. Ces structures permettent localement et en quelques jours de restratifier des couches de mélange profondes alors que les flux de chaleur sont toujours négatifs (Boccaletti *et al.*, 2007; Fox-Kemper *et al.*, 2008; Fox-Kemper et Ferrari, 2008; Mahadevan *et al.*, 2010). Cette restratification est d'autant plus intense que la couche de mélange est profonde et que le gradient latéral de densité est fort. Ce mécanisme est donc très répandu sur une grande partie du gyre subpolaire (Johnson *et al.*, 2016).

Ces différents forçages physiques régulent la disponibilité en lumière et en nutriments pour la croissance du phytoplancton et ont donc une influence majeure sur la dynamique des blooms phyto-planctoniques.
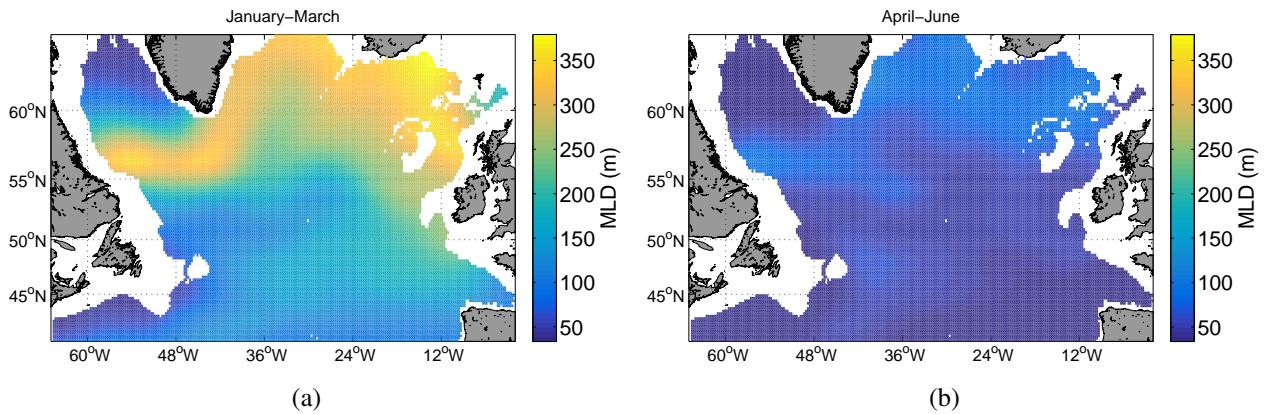
Figure. 4. Climatologie (2005-2015) de la profondeur de la couche de mélange, dérivé des données Argo, dans le gyre subpolaire de l'Atlantique Nord pour la période de janvier à mars (a) et d'avril à Juin (b).

1.3   Dynamique des blooms phytoplanctoniques aux hautes latitudes

Les travaux de Gran et Braarud (1935) et Riley (1942) ont marqué le début d'un long débat sur la dynamique des blooms phytoplanctoniques. Sverdrup (1953) s'est basé sur ces travaux pour concep-tualiser une théorie sur l'initiation des blooms en Atlantique Nord ("Critical depth hypothesis"). Cette théorie, devenue une référence en océanographie, stipule que l'accumulation de la biomasse phyto-planctonique n'est possible que lorsque la profondeur de la couche de mélange (MLD) est plus faible qu'une certaine profondeur critique. Cette profondeur critique délimite la couche océanique dans la-quelle la production par photosynthèse est égale aux pertes par respiration (Figure 5 et Figure 6a). Connaissant l'éclairement de surface, le coefficient d'atténuation diffuse et l'éclairement de compen-sation (*i.e.* l'intensité lumineuse à laquelle la photosynthèse est égale à la respiration), on peut estimer la profondeur critique. Ainsi, Sverdrup (1953) a montré que la couche de mélange hivernale était plus profonde que la profondeur critique et ne permettait pas d'accumuler de la biomasse. En revanche, au printemps, l'intensification des flux radiatifs pouvaient limiter la couche de mélange à une profondeur inférieure à la profondeur critique et ainsi permettre d'initier le bloom printanier. Les principales hy-pothèses soutenant cette théorie sont : (1) Il existe une couche de mélange dans laquelle la turbulence est suffisante pour homogénéiser le plancton. (2) Dans cette couche de mélange, la production n'est pas limitée en nutriment. (3) La production est linéairement proportionnelle à la lumière disponible, d'où la décroissance exponentielle de la production avec la profondeur (Figure 5). (4) Le taux de perte est constant dans le temps et sur la profondeur (Figure 5). (5) L'éclairement de compensation est connu.
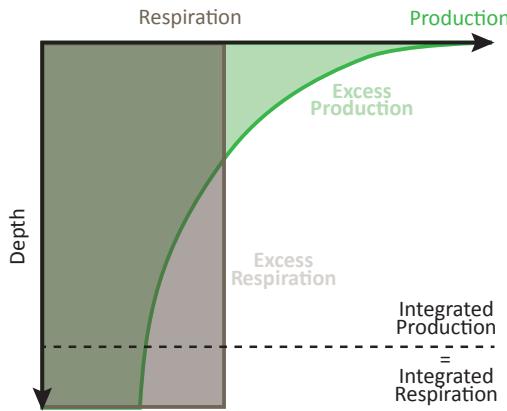
Figure. 5. Représentation schématique de la profondeur critique (Sverdrup, 1953). (source : Fischer *et al.* (2014))

Avec le nombre grandissant d'outils d'observation et de données disponibles, et l'avènement de la modélisation numérique, cette théorie et les hypothèses sur lesquelles elle repose ont été régulièrement appliquées, affinées et même contestées. Siegel *et al.* (2002), en utilisant des données satellites à l'échelle du bassin Nord Atlantique, ont inversé le modèle conceptuel de Sverdrup pour en déduire l'éclairement de compensation nécessaire à l'initiation du bloom printanier. Cet éclairement de compensation peut doubler si le taux de perte de l'ensemble de la communauté planctonique (incluant le zooplancton) est considéré et non une espèce de phytoplancton unique. Il convient alors de parler d'éclairement de compensation communautaire. Celui-ci semble relativement uniforme sur une grande partie du gyre subpolaire.

Backhaus *et al.* (2003) ont observé *in situ* un stock de phytoplancton relativement élevé dans les couches convectives hivernales ainsi qu'une production non négligeable. Ils ont émis l'hypothèse que le mélange convectif permet de limiter les pertes par sédimentation et assure une exposition régulière du phytoplancton à la lumière ("Phyto-convection" sur la Figure 8). La couche de mélange est alors assimilée à une couche euphotique virtuelle où la production est constante sur la profondeur et non exponentiellement décroissante comme supposée dans le modèle de Sverdrup (hypothèse (3)). La production intégrée peut alors être supérieure aux pertes et permettre l'accumulation de biomasse même en hiver.

La définition de la couche de mélange est un point critique du modèle de Sverdrup. L'hypothèse (1) précise bien que la turbulence (*i.e.* l'intensité du mélange) doit être suffisamment élevée pour homogénéiser le phytoplancton dans la MLD. Cependant, les mesures de turbulence océanique ne sont pas systématiques. La plupart des études ayant testé le modèle de Sverdrup ont estimé la MLD à partir de méthodes simples basées sur des mesures discrètes de température et de conductivité dont on dérive la densité. La méthode la plus couramment utilisée est la méthode par différence de densité par rapport à une valeur de référence en surface. La base de la couche de mélange est définie comme étant la profondeur à laquelle la différence de densité dépasse un certains seuil compris généralement entre 0,005 et 0,1 kg m^{-3}. Les mesures *in situ* de turbulence ont cependant montré que la dynamique de la couche turbulente est très difficile à capter avec des mesures discrètes de densité (Brainerd *et al.*, 1995). La convection hivernale induit une forte turbulence relativement homogène dans toute
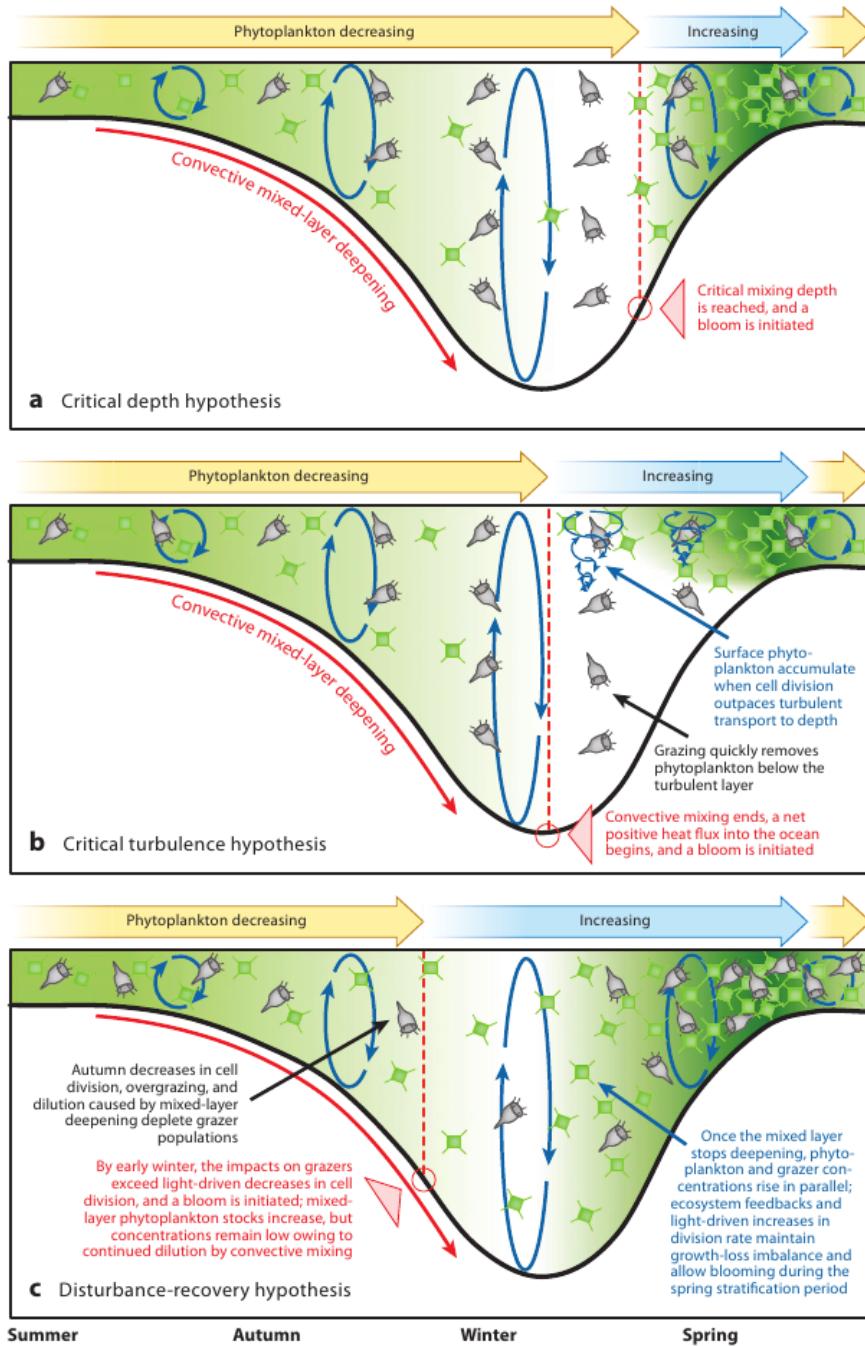
Figure. 6. Représentation schématique des principales théories d'initiation du bloom. (source : Behrenfeld et Boss (2014))

la couche de mélange (Franks, 2014). En revanche, en fin d'hiver, le réchauffement de la couche de surface par les flux radiatifs peut inhiber la convection en seulement quelques heures (Brainerd et Gregg, 1993). De même, la diminution de la salinité de surface liée à des événements de pluie intense stratifie très rapidement la colonne d'eau (Price, 1979; Hosegood *et al.*, 2006) (Figure 7a). Ces deux mécanismes induisent seulement une très faible variation de densité mais suffisent à inhiber la turbulence dans la couche de mélange. Les méthodes couramment utilisées pour estimer la MLD ne peuvent détecter de si faibles variations. Le modèle de Sverdrup n'a donc jamais pu être vraiment

testé *in situ* (Franks, 2014). Finalement, ce modèle ne pourrait être applicable qu'en hiver où les hypothèses de Sverdrup sont satisfaites (Chiswell, 2011).

Certaines études ont révélé le développement d'un bloom de surface dans une couche de mélange apparemment profonde (Townsend *et al.*, 1992; Stramska et Dickey, 1994; Dale *et al.*, 1999). Ces observations, bien que potentiellement biaisées par la méthode d'estimation de la MLD, ont conduit à la formulation d'une nouvelle théorie, basée cette fois sur l'intensité du mélange et non la profondeur de mélange ("Critical turbulence hypothesis", Huisman *et al.* (1999); Ebert *et al.* (2001); Huisman *et al.* (2002); Taylor et Ferrari (2011b)). Cette théorie, basée sur une approche de modélisation, stipule que le bloom est initié à un niveau de turbulence intermédiaire, suffisamment élevé pour maintenir en suspension les cellules qui sédimentent, mais pas trop élevé pour les maintenir suffisamment longtemps dans la couche euphotique. Ce niveau de turbulence est atteint en fin d'hiver lorsque les flux de chaleur sont réduits. Sur la base de cette théorie, Ferrari *et al.* (2014) ont montré, en compilant 7 années de données satellites, que l'accumulation de la biomasse phytoplanctonique en suface est maximale quand les flux de chaleur, moyennés sur 8 jours, passent de négatifs à positifs (Figure 6b). Le bloom pourrait alors être initié avant la stratification de la couche de mélange. Dans ces couches peu stratifiées, le frottement du vent peut induire du mélange turbulent. Le changement de signe des flux de chaleur n'implique donc pas nécessairement une réduction de la turbulence. Cependant, l'énergie du vent est rapidement dissipée sur la profondeur ce qui implique que la couche turbulente reste limitée à la surface. Brody et Lozier (2014) et Brody et Lozier (2015) ont alors proposé que l'initiation du bloom n'est pas liée à un changement de l'intensité du mélange mais plutôt à la profondeur caractéristique du mélange selon qu'il est induit par la convection ou le vent. Finalement, cette approche est basée sur les mêmes hypothèses que le modèle de Sverdrup.

Toutes ces théories reposent sur une vision 1D de l'océan. Cependant, des mécanismes 3D, liés aux structures de méso- et sous-mésoéchelle, peuvent restratifier en quelques jours les couches de mélange profondes alors même que les flux de chaleur sont toujours négatifs (Boccaletti *et al.*, 2007; Fox-Kemper *et al.*, 2008). Les tourbillons qui se développent au niveau des gradients horizontaux de densité conduisent à un transport horizontal des masses d'eau denses sous les masses d'eau moins denses qui restent en surface (Figure 7b). Les isopycnes initialement verticales dans la couche de mélange se retrouvent inclinées ("slumping", voir figure 7a). Le vent joue aussi un grand rôle au niveau de ces gradients de densité en renforçant ou en inhibant la restratification à travers le transport d'Ekman (selon la direction du vent par rapport au front (Thomas et Lee, 2005; Mahadevan *et al.*, 2010)). Indépendamment de la formation de tourbillons, des instabilités symétriques se développent au niveau des fronts et participent à la restratification de la couche de mélange hivernale (Taylor et Ferrari, 2011a). Une approche innovante de Mahadevan *et al.* (2012), basée sur une utilisation complémentaire de différents outils d'observation (satellites, flotteurs, planeurs sous-marins, campagnes) et de modélisation, a permis de montrer que les tourbillons de sous-mésoéchelle dans le bassin d'Islande pouvait conduire à une initiation précoce du bloom avant la restratification saisonnière induite par les flux radiatifs. Ces structures de méso- et sous-mésoéchelle expliquent en partie la forte variabilité spatio-temporelle de la biomasse phytoplanctonique (Lévy, 2008; Taylor et Ferrari, 2011a; Mahadevan *et al.*, 2012; Cetinić *et al.*, 2015).
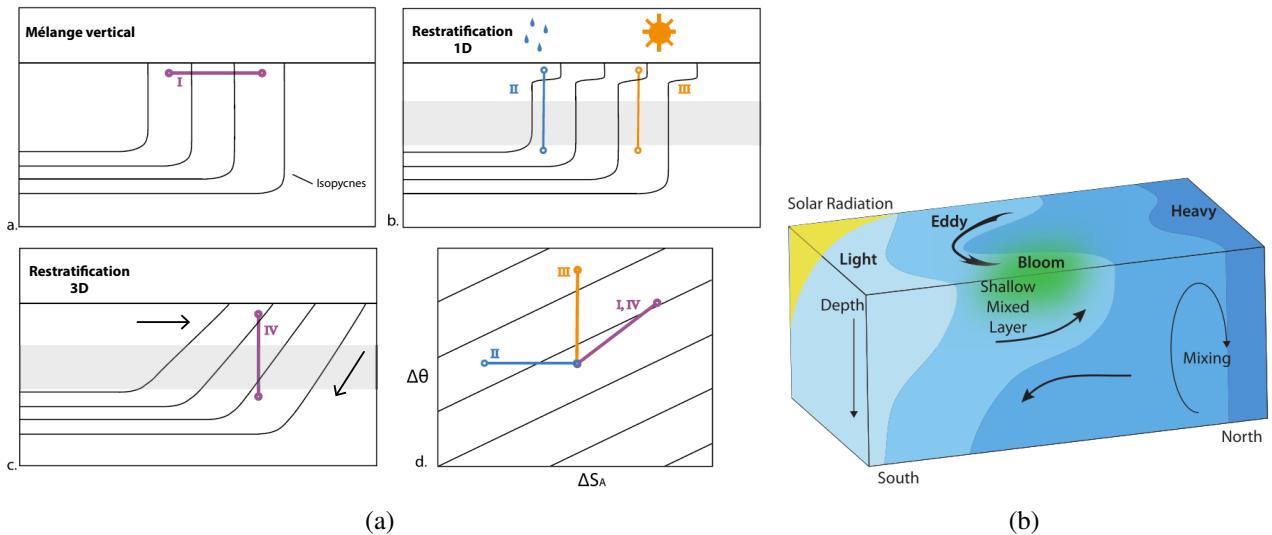
Figure. 7. (a) Restratification 1D et 3D de la couche de mélange. Le gradient horizontal de température et de salinité (I) est similaire au gradient vertical (IV) induit par le transport latéral de masses d'eau représenté par les flèches noires. (source : modifié de Johnson *et al.* (2016)). (b) Mécanisme de restratification de la couche de mélange par un tourbillon de sous-mésoéchelle. (source : Mahadevan *et al.* (2012))

Comme défini par le modèle conceptuel de Sverdrup, le bloom démarre lorsque le taux d'accumulation ou croissance nette du phytoplanton est positif, c'est à dire lorsque la croissance brute (*i.e.* taux de division cellulaire) est supérieure au taux de pertes. Les différentes théories présentées jusqu'alors se sont focalisées sur les mécanismes physiques qui contrôlent la croissance phytoplanctonique par l'intermédiaire de la disponibilité en lumière. D'autres études ont cependant montré que le taux de perte, supposé constant dans le modèle de Sverdrup (hypothèse 4), est très variable, à la fois dans le temps et sur la profondeur, et peut impacter la dynamique de la biomasse phytoplanctonique (Riley et Bumpus, 1946; Cushing, 1959; Frost, 1991; Banse, 1994; Behrenfeld, 2010; Lindemann *et al.*, 2015). Lindemann *et al.* (2015) ont souligné notamment l'importance de prendre en compte les adaptations physiologiques du phytoplancton pour comprendre la dynamique de la biomasse. En effet, le phytoplancton a la capacité de réguler son taux de respiration à l'obscurité ce qui permet de réduire les pertes dans les couches de mélange hivernales. De même, Behrenfeld (2010) et Boss et Behrenfeld (2010) ont montré, par une approche satellite et *in situ*, que les forçages physiques hivernaux peuvent moduler les relations prédateur-proie. En effet, l'approfondissement de la MLD en hiver dilue le plancton dans un plus grand volume ce qui limite le taux de prédation par le zooplancton et donc réduit les pertes du phytoplancton. Il n'existe donc pas de corrélation entre le taux d'accumulation et le taux de croissance brute, la biomasse pouvant s'accumuler dans les couches de mélange profondes malgré un taux de croissance brute très faible ("Disturbance-recovery hypothesis"). Selon la définition de Sverdrup, le bloom pourrait alors commencer en hiver quand la MLD s'approfondit. Le recouplage entre le phytoplancton et le zooplancton quand la colonne d'eau se stratifie au printemps peut limiter l'intensité et la durée du bloom.

L'apparente contradiction entre les différentes théories exposées précédemment repose en partie sur un problème de sémantique et sur des divergences méthodologiques. La définition même de bloom

phytoplanctonique est très variable selon les auteurs. Bien que le travail pionnier de Sverdrup en 1953 précise que le bloom correspond à une accumulation de biomasse intégrée sur la profondeur, la plupart des études qui ont suivi se sont focalisées sur la biomasse de surface. Cette déviation à la définition est liée à l'avènement des algorithmes satellitaires qui ont permis de déduire, des propriétés optiques de l'océan, la biomasse phytoplanctonique dans la couche de surface (*i.e.* première profondeur optique). Cependant, la variation de la biomasse de surface ne reflète pas seulement des processus biotiques mais est aussi modulée par des effets purement physiques tels que la dilution. En effet, l'approfondissement de la couche de mélange en automne-hiver réduit la biomasse de surface (*i.e.* concentration) sans pour autant impacter la biomasse intégrée (*i.e.* stock). C'est une des raisons pour lesquelles la production hivernale a longtemps été négligée. Il est donc crucial de distinguer le cycle annuel de biomasse de surface du cycle annuel de biomasse intégrée (Dale *et al.*, 1999; Körtzinger *et al.*, 2008; Behrenfeld *et al.*, 2013; Chiswell *et al.*, 2015). De même, la définition de la couche de mélange, et surtout la méthode pour en estimer sa profondeur, est un point critique à la compréhension des blooms phytoplanctoniques. Il faut bien distinguer une couche turbulente, dans laquelle le mélange est actif ("mixing layer"), d'une couche de mélange ("mixed layer") qui a été mélangée dans un passé proche (Brainerd *et al.*, 1995). Une fois ces distinctions prises en compte, il est possible d'intégrer les différentes théories exposées précédemment dans un schéma cohérent pour expliquer le cycle annuel de biomasse phytoplanctonique (Lindemann et St. John, 2014; Chiswell *et al.*, 2015) (Figure 8).
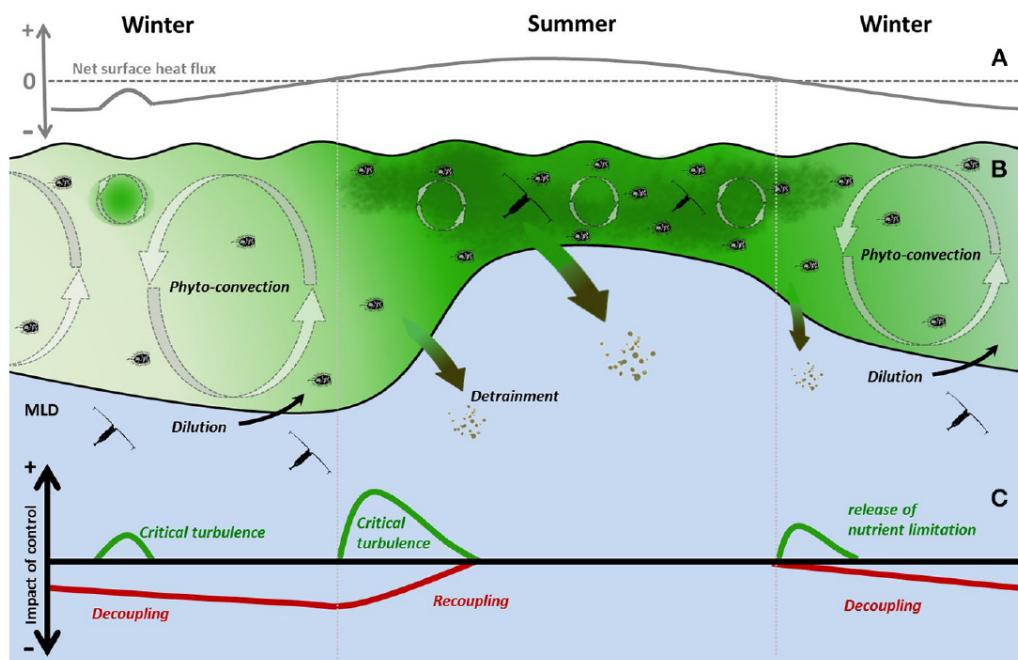

Figure. 8. Théorie unificatrice de la dynamique de la biomasse phytoplanctonique. (source : Lindemann *et al.* (2015))

Si la dynamique de la biomasse phytoplanctonique aux hautes latitudes a suscité autant d'intérêt de la part de la communauté des océanographes, c'est en partie lié au rôle crucial du phytoplancton, et de l'océan en général, sur le climat à travers les pompes de carbone.

1.4   Pompes de carbone

L'océan influence le climat de la planète en régulant le contenu en dioxyde de carbone (CO_2) de l'atmosphère. L'Atlantique Nord en particulier est un puits important de CO_2 atmosphérique (Sabine *et al.*, 2004; Takahashi *et al.*, 2009). En effet, un certain nombre de processus particulièrement efficaces dans le gyre subpolaire permettent de transporter le carbone dissous depuis les couches de surface vers les couches profondes des océans où il sera séquestré à l'échelle de quelques mois à plusieurs années. Nous détaillerons principalement deux de ces processus connus sous le nom de pompe physique et pompe biologique de carbone.

Le CO_2 dissous dans l'eau est converti en carbonate et bicarbonate ou reste sous sa forme aqueuse. Ces différents composés forment le DIC ("dissolved inorganic carbon"). La pompe biologique (Figure 9) repose sur la transformation du DIC en matière organique particulaire (POC, "particulate organic carbon") ou dissoute (DOC, "dissolved organic carbon") par le phytoplancton dans la couche euphotique de l'océan. Environ 10-30% de la matière organique produite sera ensuite exportée hors de la couche euphotique, principalement par sédimentation (Buesseler et Boyd, 2009). Le reste est recyclé sur place par l'activité hétérotrophe sous forme de DOC ou respiré sous forme de CO_2. L'efficacité de l'export dépend principalement de la composition et de la structure de la communauté phytoplanctonique présente en surface, qui influencent la nature des particules et leur vitesse de sédimentation (Guidi *et al.*, 2009; Villa-Alfageme *et al.*, 2016). En effet, certaines espèces de phytoplancton, notamment les diatomées, sécrètent un mucus collant (TEP) permettant de former des agrégats (Passow, 2002; Martin *et al.*, 2011) qui sédimentent rapidement ($\sim$10-100 m d^{-1}). De plus, l'incorporation de matière minérale (opale, calcite) ou lithogénique (pousière, argile) peut accélèrer la vitesse de sédimentation en modifiant la densité des particules (effet ballast; Alldredge *et al.* (1993)). Enfin, les producteurs secondaires tels que le zooplancton contribuent à l'export de carbone en produisant des pelotes fécales qui sédimentent rapidement ($\sim$100 m d^{-1}; Turner (2002)). Ces organismes transportent aussi activement la matière organique en profondeur à travers leur migration journalière. Les proies consommées en surface la nuit sont respirées sous forme de DIC, excrétées sous forme de DOC ou remises en suspension sous forme de pelotes fécales en profondeur pendant la journée (Steinberg *et al.*, 2000; Jónasdóttir *et al.*, 2015).

Parmi la matière organique exportée, seulement une part infime ($\sim$1%) sera séquestrée à long terme dans l'océan profond. La matière exportée est considérée comme séquestrée lorsqu'elle atteint la profondeur de la pycnocline permanente ($\sim$1000 m). Ce qui est consommé dans la zone mésopélagique ($\sim$100-1000 m) par le zooplancton ou reminéralisé par l'activité bactérienne est susceptible de retourner rapidement dans l'atmosphère sous forme de CO_2 (Sanders *et al.*, 2014).

La pompe physique encore appelée pompe de solubilité repose sur le mélange et la circulation des masses d'eau à grande échelle. Les eaux froides des hautes latitudes, qui favorisent la dissolution du CO_2, peuvent être exportées en profondeur par effet purement physique. En effet, la formation des eaux profondes au niveau des zones de convection intense (Keeling et Peng, 1995; Álvarez *et al.*, 2003; Pérez *et al.*, 2013) et la formation des eaux modales ou intermédiaires par subduction (Follows
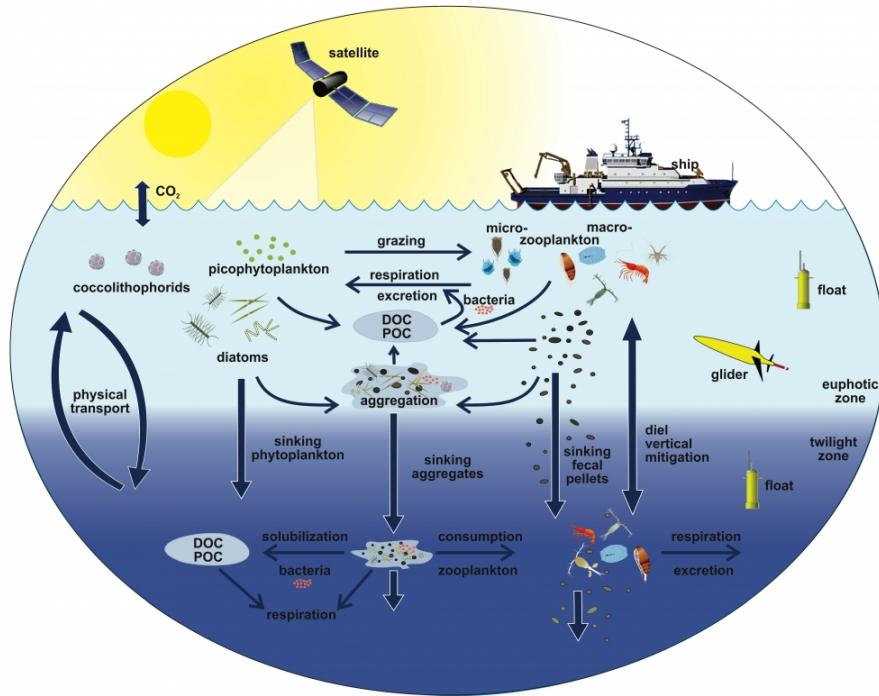
Figure. 9. Représentation schématique de la pompe biologique. (source : Siegel *et al.* (2016))

et al., 1996; Sallee *et al.*, 2012; Levy et Martin, 2013) contribuent au puits de carbone atmosphérique. Ces masses d'eau formées aux hautes latitudes alimentent la circulation thermo-haline mondiale et vont parcourir l'ensemble des bassins océaniques sur une échelle de temps de plusieurs mois à plusieurs centaines d'années. Le carbone ainsi exporté est séquestré à long terme. La pompe physique n'est pas limitée à l'export de DIC mais peut aussi exporter du carbone sous sa forme organique (Hansell *et al.*, 2009). Fontela *et al.* (2016) ont récemment démontré que la contribution du DOC à la séquestration du carbone en Atlantique Nord était considérable et représentait jusqu'à un tiers de l'assimilation du CO_2 atmosphérique dans cette région. De plus, toujours dans cette région, Tian *et al.* (2004) ont montré que l'export de DOC par la convection profonde pouvait être supérieure au flux de POC par sédimentation. Enfin, Karleskind *et al.* (2011) ont mis en évidence un export de carbone par subduction supérieur de deux ordres de grandeur à l'export lié à la pompe biologique.

Ces processus physiques impliquent la transformation et l'advection de masse d'eau à grande échelle spatiale et temporelle. Cependant, des mécanismes similaires se développent à des échelles beaucoup plus fines liées à l'activité méso- et sous-mésoéchelle. En effet, le champ tourbillonnaire renforce localement les fronts de densité (en périphérie ou entre les tourbillons) auxquels sont associés des mouvements de masses d'eau (subduction ou obduction) le long des isopycnes (Mahadevan et Tandon, 2006). Comme mentionné précédement, ces structures de sous-mésoéchelle ont aussi la particularité de restratifier localement des couches de mélange profondes et de favoriser la production primaire (Taylor et Ferrari, 2011a; Mahadevan *et al.*, 2012). Ainsi, la matière organique produite pourrait être rapidement exportée en profondeur par subduction (Lévy *et al.*, 2001; Omand *et al.*, 2015). Cette pompe de carbone, que l'on peut qualifier de pompe bio-physique, peut exporter à la

fois du DIC, du DOC et du POC indépendamment du bloom printanier. La séquestration à long terme n'est cependant pas garantie. Un autre mécanisme, lié à la variation temporelle de la profondeur de la couche de mélange, permet d'exporter du carbone en profondeur ("mixed layer pump"). Ce processus a été décrit dans un premier temps à l'échelle diurne (Woods et Onken, 1982; Ho et Marra, 1994; Gardner *et al.*, 1995). En effet, la convection de nuit, liée aux pertes de chaleur de l'océan vers l'atmosphère, mélange les cellules phytoplanctoniques et autres détritus en profondeur. De jour, le réchauffement des couches de surface, lié au flux radiatif, stratifie la colonne d'eau. L'effet mécanique du vent peut éventuellement re-mélanger la couche de surface mais sur une profondeur limitée (Woods, 1980). Le phytoplancton exporté en profondeur durant la nuit, se retrouve donc isolé sous la couche de mélange. Il peut alors sédimenter en profondeur ou être ré-entraîné dans la couche de mélange lors de la prochaine convection. L'alternance entre le mélange convectif et la restratification est le moteur qui permet de pomper du carbone en profondeur. Ce mécanisme a été quantifié pour la première fois à l'échelle saisonnière dans la mer de Norvège (Dall'Olmo et Mork, 2014). Le mélange convectif hivernal, suivi de la restratification printanière, contribue significativement à l'export annuel de carbone dans cette région en exportant environ 7 g C m^{-2} an^{-1}. Au contraire de la pompe biologique, ce mécanisme pourrait exporter toute forme de matière organique, dissoute ou particulaire (Carlson *et al.*, 1994; Dall'Olmo et Mork, 2014). Il ne serait donc pas dépendant de la production d'agrégats pendant le bloom printanier. Bishop *et al.* (1986) et Giering *et al.* (2016) ont en effet montré que des restratifications intermittentes de la couche de mélange avant la restratification saisonnière pouvaient favoriser la croissance phytoplanctonique et l'export de carbone avant le bloom printanier. Cependant, des observations de trappe à sédiments à 3000 m de profondeur ont montré seulement un faible export pendant la période pré-bloom (Lampitt *et al.*, 2010), suggérant ainsi que la majorité de la matière exportée est reminéralisée dans la zone mésopélagique.

De nombreuses études ont constaté que le budget du carbone dans la zone mésopélagique n'est pas équilibré (Steinberg *et al.*, 2008; Burd *et al.*, 2010; Giering *et al.*, 2014). En effet, la demande métabolique en carbone par les organismes hétérotrophes semble supérieure au flux vertical de carbone provenant de la surface. Ce déséquilibre indique, soit une sur-estimation de la demande métabolique en profondeur, soit qu'une source alternative de carbone n'a pas été prise en compte. Les pompes bio-physiques liées à la sous-mésoéchelle ou à la dynamique de la couche de mélange ont été effectivement négligées et pourraient contribuer à équilibrer le budget de carbone dans la zone mésopélagique. Ces processus bio-physiques sont encore peu connus car difficiles à observer *in situ*.

1.5   Outils d'observation

Les différents processus bio-physiques qui contrôlent la dynamique de la biomasse phytoplanctonique et l'export de carbone interviennent sur des échelles spatio-temporelles très variées, de l'échelle d'un bassin à la sous-mésoéchelle, de l'échelle journalière à l'échelle saisonnière (Figure 10). Il n'existe aucun outil d'observation ni même aucune approche de modélisation qui puissent résoudre une telle gamme de variabilité. Les différentes études réalisées, selon l'outil d'observation utilisé, ont

ciblé seulement une partie du problème. En revanche, l'utilisation complémentaire de l'ensemble de ces outils peut apporter une vision complète de la dynamique de la biomasse phytoplanctonique et de l'export de carbone associé. L'expérience NAB08, qui s'est déroulée dans le bassin d'Islande, est un bel exemple de ce genre d'approche. Un flotteur lagrangien a été utilisé pour suivre une même masse d'eau et ainsi observer l'évolution temporelle réelle du bloom phytoplanctonique. Un réseau de planeurs sous-marins ("gliders") a suivi le flotteur lagrangien en échantillonnant les alentours pour révéler l'hétérogénéité spatiale du bloom. Des campagnes en bateau sont venues complémenter ces observations à des périodes clés et ont offert une gamme plus large de variables échantillonnées ainsi que la possibilité de calibrer tous les instruments. Enfin, des observations satellites sur l'ensemble du bassin d'Islande ont donné un contexte général à l'étude. Une étude de modélisation a ensuite montré que les structures sous-mésoéchelles, observées par les planeurs sous-marins, peuvent influencer à la fois la dynamique du bloom et l'export de carbone à l'échelle d'une région océanique. Cette campagne s'est cependant focalisée uniquement sur la période printanière, comme la grande majorité des études sur la dynamique du bloom.
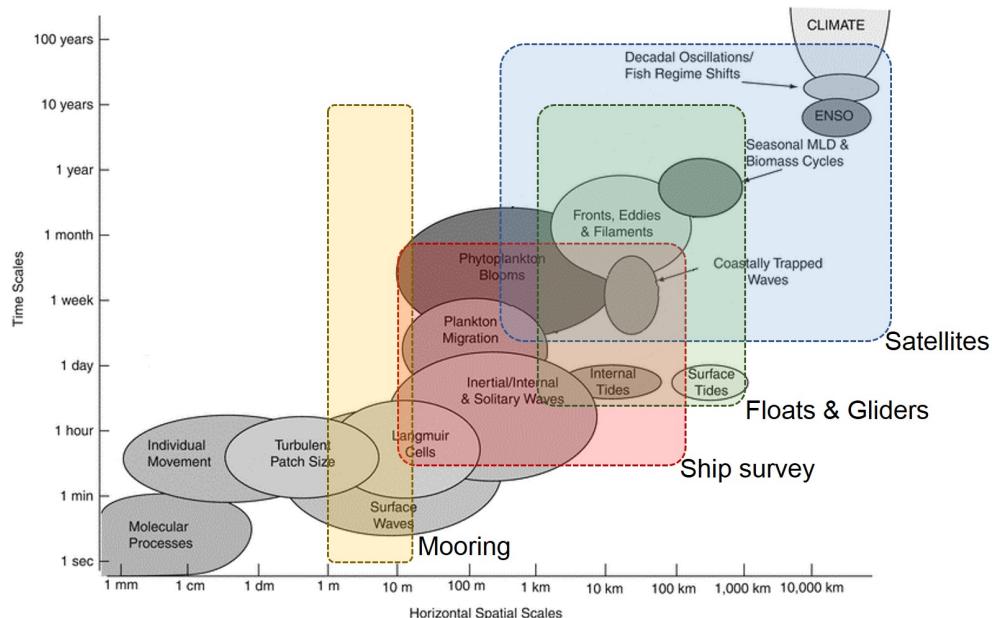
Figure. 10. Echelle spatio-temporelle de différents processus océaniques. (source : modifié de Dickey (2003))

Le laboratoire de Villefranche a déployé dans le gyre subpolaire de l'Atlantique Nord un réseau de flotteurs biogéochimiques (BGC-Argo) équipés d'un ensemble de capteurs bio-optiques. Sur le même principe que les flotteurs Argo, ces plateformes autonomes dérivent au gré des courants pendant plusieurs années et réalisent des profils de variables biogéochimiques et environnementales entre la surface et 1000 m tous les 1, 2, 5 ou 10 jours. Ils transmettent leurs données en temps réel à chaque remontée à la surface par communication iridium. La base de données BGC-Argo utilisée au cours de cette thèse est composée de plus de 3500 profils couvrant toutes les saisons depuis 2013 sur l'ensemble du gyre subpolaire de l'Atlantique Nord.

Ces flotteurs ont l'avantage de mesurer en quasi-continu certaines propriétés optiques de l'océan dont sont déduits des informations sur l'abondance et la nature des particules en suspension dans

l'eau (Claustre *et al.*, 2010). La fluorescence de la Chla et le coefficient de rétrodiffusion particulaire (b_{bp}) sont notamment deux estimateurs essentiels de la biomasse phytoplanctonique que nous allons décrire en détail dans les deux prochains paragraphes.

L'intensité de la fluorescence est corrélée à la concentration en Chla qui est elle-même un bon indicateur de la biomasse phytoplanctonique. Cependant, la relation entre ces 3 entités est complexe. La fluorescence par unité de Chla peut varier d'une espèce phytoplanctonique à une autre, mais aussi en réponse à un changement environnemental (Falkowski *et al.*, 1985; Murphy et Cowles, 1997). Un exemple bien connu de cette variabilité est le "quenching" non-photochimique (Cullen et Lewis, 1995; Sackmann *et al.*, 2008). La fluorescence par unité de Chla peut diminuer en quelque heures lorsque les cellules phytoplanctoniques sont saturées en lumière dans les couches de surface. De même, la concentration en Chla par unité de carbone répond à des variations taxonomiques ou physiologiques liées aux changements de conditions environnementales (température, nutriment, lumière). La photoacclimatation, notamment, implique une augmentation (diminution) de la concentration en Chla par unité de carbone lorsque les conditions lumineuses sont limitantes (saturantes). Ce processus peut potentiellement influencer le cycle annuel de biomasse phytoplanctonique mesurée par satellite (Morel *et al.*, 2010; Behrenfeld *et al.*, 2015) ou mesurée *in situ* Mignot *et al.* (2014).

Le second estimateur, le coefficient de rétrodiffusion particulaire, est corrélé à la concentration en carbone organique particulaire (Boss *et al.*, 2004; Cetinić *et al.*, 2012). La biomasse vivante notamment contribuerait à plus de 90% du signal de b_{bp} et 70% de sa variabilité serait liée au changement d'abondance du phytoplankton (Martinez-Vicente *et al.*, 2012). Cependant, la relation entre b_{bp} et POC est très variable selon la région du fait des différents types de particules observées mais aussi des différentes méthodes utilisées pour mesurer ces deux entités (incertitudes associées). Le changement de communauté phytoplanctonique ne semble néanmoins pas impacter cette relation (Cetinić *et al.*, 2012). Le signal de b_{bp} correspond à des particules inférieures à 10-20 μm (Martinez-Vicente *et al.*, 2013; Dall'Olmo et Mork, 2014) bien que des particules plus grandes telles que des agrégats puissent être détectées sous forme de "spike" dans le signal (Briggs *et al.*, 2011).

Les flotteurs BGC-Argo permettent ainsi d'étudier un cycle annuel complet de biomasse phytoplanctonique (surface et intégrée) tout en résolvant des échelles spatio-temporelles plus fines. Ils représentent donc un outil particulièrement adapté pour comprendre les mécanismes bio-physiques qui influencent la dynamique de la biomasse phytoplanctonique et l'export de carbone associé.

1.6   Problématique

Comme l'ont souligné Fischer *et al.* (2014), l'évolution des connaissances en Océanographie, mais aussi dans d'autres disciplines, a été rythmée par le développement d'outils d'observation innovants. En se basant sur la nouvelle génération de flotteurs BGC-Argo, nous tenterons au cours de cette thèse d'apporter des éléments nouveaux au débat actuel sur la dynamique des blooms aux hautes latitudes et sur l'export de carbone associé. Un point majeur qui a été négligé jusqu'à maintenant, faute d'outils adaptés, est le caractère épisodique des blooms phytoplanctoniques et des événements

d'export ainsi que leur variabilité spatio-temporelle. Quelles sont la fréquence et l'intensité de ces événements épisodiques et quel est leur impact à plus grande échelle spatio-temporelle ? Telle est la question qui a orienté nos réflexions et guidé nos différentes études.

Avant toute investigation du caractère épisodique et hétérogène des blooms phytoplanctoniques, il est nécessaire d'avoir une vision globale et une compréhension de l'état moyen du système. C'est l'objectif de notre première étude (Chapitre 2). Typiquement, quels sont les processus bio-physiques qui contrôlent le cycle climatologique annuel de biomasse phytoplanctonique ? Quel est le rôle de l'activité mésoéchelle sur ces cycles climatologiques de biomasse ?

La compréhension du caractère épisodique des blooms implique d'étudier des processus bio-physiques à des échelles spatio-temporelles fines, de l'ordre de grandeur de la croissance phyto-planctonique. Ceci a naturellement orienté une deuxième étude (Chapitre 3) sur l'influence des structures de sous-mésoéchelle sur l'accumulation de la biomasse phytoplanctonique. L'activité sous-mésoéchelle peut-elle modifier les conditions de mélange hivernal et initier localement des blooms transitoires ? Ces blooms peuvent-ils influencer les caractéristiques du bloom printanier ?

Si l'existence de blooms transitoires avant la restratification printanière est avérée, il convient de se demander quel est leur contribution à l'export de carbone. Nous avons orienté notre troisième étude (Chapitre 4) sur le rôle de la pompe bio-physique de carbone pendant la transition hiver-printemps. La dynamique de la couche de mélange conduit-elle à un export épisodique de matière organique en profondeur ? Quelle est la variabilité spatio-temporelle de ces événements épisodiques ? Quelle est leur influence sur les écosystèmes mésopélagiques ?

Chacun de ces trois chapitres inclut un article en anglais, publié, soumis ou en préparation dans un journal scientifique international. Chaque article sera accompagné d'une introduction, d'un résumé et d'une conclusion en français [1].

---

1. Le format de la bibliographie étant commun pour l'ensemble du document, les références apparaissent en français dans les articles.

<div style="text-align: right;">

CHAPITRE 2

</div>

Cycles de biomasse phytoplanctonique dans le gyre subpolaire de l'Atlantique Nord

---

2.1 Introduction

Bien que l'océan soit en perpétuel mouvement, il peut être partitionné en différentes régions océaniques, chacune caractérisée par des conditions environnementales uniques (*e.g.* Longhurst *et al.*, 1995; Devred *et al.*, 2007; Vichi *et al.*, 2011). Ces régions ou provinces océaniques ont souvent été utilisées comme cadre de référence dans une grande variété d'études allant des flux de carbone particulaire à la distribution des grands poissons pélagiques (Reygondeau *et al.*, 2013). Elles ont notamment permis d'extrapoler des données *in situ* rares et éparses sur un domaine cohérent plus large (Platt *et al.*, 1991; Devred *et al.*, 2007; Lavigne *et al.*, 2013; Guidi *et al.*, 2015). Sur la base de la Chla de surface mesurée par satellite, D'Ortenzio et Ribera d'Alcalà (2009) ont défini différentes régions océaniques au sein desquelles le cycle annuel de biomasse phytoplanctonique est homogène. Dans ce chapitre, nous utiliserons cette méthode pour étudier la variabilité spatio-temporelle du bloom phytoplanctonique. Les caractéristiques du bloom, aussi appelé phénologie du bloom (date d'initiation, durée, intensité) sont fortement variables à l'échelle interannuelle et décennale et sont susceptibles d'évoluer dans le futur sous l'effet du changement climatique (Henson *et al.*, 2006; Martinez *et al.*, 2009, 2016). Les cycles de biomasse ainsi que les frontières des régions associées sont donc susceptibles de varier selon les années. Cependant, nous avons fait le choix, dans cette étude, d'une approche climatologique afin d'identifier un cycle saisonnier moyen de biomasse, associé aux différentes régions océaniques. Nous pourrons alors identifier les mécanismes qui, au premier ordre, contrôlent l'accumulation de la biomasse phytoplanctonique à grand échelle.

Siegel *et al.* (2002) et Henson *et al.* (2009) ont observé dans le gyre subpolaire de l'Atlantique Nord un gradient latitudinal de la date d'initiation du bloom printanier, les régions au sud ayant un démarrage plus précoce du bloom qu'au nord. Ces observations suggèrent que l'initiation du bloom printanier est contrôlée au premier ordre par la lumière. En effet, l'angle solaire étant plus faible vers les pôles, la durée du jour et l'éclairement incident limitent la dose de lumière disponible pour la croissance du phytoplancton. Frajka-Williams et Rhines (2010) et Wu *et al.* (2008) ont cependant

montré que ce gradient latitudinal est inversé dans la mer du Labrador avec une initiation précoce du bloom dans le nord de la mer du Labrador, remettant en cause le contrôle unique de la lumière sur l'initiation du bloom à grande échelle.

Dans ce chapitre, nous examinerons le paradoxe de la mer du Labrador à l'échelle climatologique. Nous discuterons des différents mécanismes bio-physiques qui contrôlent les caractéristiques du bloom printanier et nous conclurons sur le rôle potentiel des structures de mésoéchelle sur le cycle climatologique de la biomasse phytoplanctonique dans la région nord de la mer du Labrador.

2.2   Résumé de l'étude

Cette étude est basée sur l'analyse des cycles annuels de concentration en chlorophylle *a* de surface (Chla), un proxy de la biomasse phytoplanctonique mesuré par satellite. Les données satellites utilisées sont des images composites GlobColour sur 8 jours à une résolution spatiale de 4 km. Les produits GlobColour sont issus de quatre capteurs différents (SeaWiFs, MERIS, MODIS aqua, VIIRS) et ont donc l'avantage de fournir une longue série temporelle continue en gardant une certaine cohérence sur le traitement des images (`http://www.globcolour.info`). Chaque série temporelle annuelle associée à un pixel est moyennée sur la periode 1998-2014. Nous avons donc une climatologie robuste du cycle annuel de biomasse phytoplanctonique associé à chaque pixel du gyre subpolaire de l'Atlantique Nord (40°-70°N). Une méthode statistique (K-mean, Hartigan et Wong (1979)) a été utilisée pour identifier les régions où le cycle annuel de biomasse est similaire (*i.e.* biorégions). Nous pouvons ensuite extraire un cycle annuel moyen caractéristique pour chaque biorégion (D'Ortenzio et Ribera d'Alcalà, 2009). L'écart type associé à ce cycle moyen représente la variabilité spatiale au sein de la biorégion considérée.

Cette approche a permis de biorégionaliser le gyre subpolaire en 6 biorégions distinctes. Le cycle annuel de chacune de ces biorégions permet d'identifier les caractéristiques du bloom printanier. Nous avons pu ainsi confirmer le gradient latitudinal de la date d'initiation du bloom au niveau du gyre subpolaire, et mieux caractériser l'inversion de ce gradient dans la mer du Labrador. La Mer du Labrador semble divisée en deux biorégions de part et d'autre de 60°N, celle située au nord étant caractérisée par un bloom beaucoup plus précoce, court et intense que le bloom observé au sud. Nous avons ensuite cherché à comprendre les mécanismes à l'origine de cette différence et notamment l'initiation précoce du bloom dans la région nord. Une analyse climatologique de données de flotteurs Argo échantillonnées dans la région nord a montré une forte stratification hivernale liée aux apports d'eau dessalée d'origine Arctique. Les caractéristiques des masses d'eau sur l'ensemble de la région nord du Labrador sont très similaires à celles du courant de bord est et ouest du Groenland ce qui suggère un transport latéral de masses d'eau du courant de bord vers l'intérieur du bassin. A l'inverse, la stratification plus tardive de la colonne d'eau dans la région sud serait plus d'origine thermique liée au réchauffement printanier. La stratification haline de la région nord du Labrador permet d'augmenter le temps de résidence du phytoplancton dans la couche euphotique. La dose de lumière journalière (*i.e.* PAR journalier moyenné dans la couche de mélange) augmente alors significativement. Au début

du printemps, la dose de lumière disponible pour la croissance du phytoplancton est donc plus élevée au nord qu'au sud où les couches de mélange sont encore très profondes. Le bloom peut alors être initié plus tôt au nord. La dose de lumière qui permet d'initier le bloom dans cette région est similaire à celle qui permet d'initier le bloom un mois plus tard dans la région sud (2,5 mol photons m^{-2} d^{-1}). Une dose de lumière similaire a été rapportée par d'autres auteurs pour l'initiation du bloom dans d'autres régions océaniques de l'Atlantique Nord (Riley, 1957; Siegel *et al.*, 2002; Henson *et al.*, 2006).

La date d'initiation du bloom n'est pas la seule différence entre ces deux biorégions de la mer du Labrador puisque l'intensité et la durée du bloom sont aussi très contrastées. Ces caractéristiques pourraient davantage être expliquées par la pression de broutage des producteurs secondaires ou la disponibilité en éléments nutritifs. En effet, l'intensité du bloom est fortement influencée par le temps de réponse du zooplancton par rapport au temps de réponse du phytoplancton à un changement de conditions environnementales (Franks, 2001). Le mesozooplancton impliqué lors du bloom printanier à un temps de réponse relativement long ce qui entraine un décalage entre la croissance du phytoplancton et du mesozooplancton (Edwards et Richardson, 2004). Le développement rapide et précoce du phytoplancton dans la région nord pourrait conduire à un décalage plus important entre le prédateur et sa proie, d'où l'intensité accrue du bloom au nord. Un bloom aussi intense dans une couche de surface restreinte entraîne un épuisement rapide du stock de nutriments qui pourrait être à l'origine de son déclin rapide. Cette hypothèse est renforcée par le fait que le mélange hivernal est limité dans cette région et ne permet pas forcement un réapprovisionnement complet en nutriments. Par ailleurs, les fortes biomasses phytoplanctoniques pourraient atténuer rapidement la lumière sur la profondeur et limiter la croissance des cellules les plus profondes (Platt *et al.*, 1991; Marra, 2004). L'auto-ombrage des cellules pourrait ainsi participer au déclin rapide du bloom dans la région nord.

2.3 Article : Phytoplankton biomass cyles in the North Atlantic subpolar gyre : a similar mechanism for two different blooms in the Labrador Sea (publié dans *Geophysical Research Letter*)

Le matériel supplémentaire de l'article est consultable en annexe A.

Authors : Léo Lacour[1,2], Hervé Claustre[1,2], Louis Prieur[1,2], Fabrizio D'Ortenzio[1,2]

[1]Sorbonne Universités, UPMC Univ Paris 06, UMR 7093, LOV, Observatoire océanologique, F-06230, Ville-franche/mer, France

[2]CNRS, UMR 7093, LOV, Observatoire océanologique, F-06230, Villefranche/mer, France

Corresponding author : L. Lacour (leo.lacour@obs-vlfr.fr), Sorbonne Universités, UPMC Univ Paris 06, UMR 7093, LOV, Observatoire océanologique, F-06230, Villefranche/mer, France

Key Points :

- Bioregionalization reveals two distinct regions in the Labrador Sea.
- Both bioregions present very different bloom phenology.
- The light-mixing regime can explain these two bloom phenologies.

Abstract   An analysis of seasonal variations in climatological surface chlorophyll *a* points to distinct biogeographical zones in the North Atlantic subpolar gyre. In particular, the Labrador Sea appears well delineated into two regions on either side of the 60°N parallel, with very different climatological phytoplankton biomass cycles. Indeed, north of 60°N, an early and short spring bloom occurs in late April while south of 60°N, the bloom gradually develops one month later and significant biomass persists all summer long. Nevertheless, at climatological scale, the first-order mechanism that controls the bloom is identical for both bioregions. The light-mixing regime can explain the bloom onset in both bioregions. In the Labrador Sea, the blooms seem to rely on a mean community compensation irradiance threshold value of 2.5 mol photon m^{-2} d^{-1} over the mixed layer.

Introduction

The North Atlantic subpolar gyre experiences large amplitude phytoplankton biomass cycles with major seasonal blooms (Longhurst, 2007). Future climate change will affect environmental conditions that control bloom dynamics (Edwards et Richardson, 2004). This is one important reason for the recently growing interest towards understanding bloom dynamics and particularly the timing of the bloom that can potentially influence the whole biomass cycle during the remaining productive season (Henson *et al.*, 2006). The model of Sverdrup (1953) describes bloom initiation in spring when the shoaling mixed layer depth (MLD) reaches the so-called critical depth, allowing sufficient light to induce net growth of phytoplankton. This paradigm is consequently still being refined or nuanced (Lévy, 2008; Taylor et Ferrari, 2011b; Mahadevan *et al.*, 2012), confirmed (Henson *et al.*, 2006; Chiswell, 2011) and even challenged (Townsend *et al.*, 1992; Durbin *et al.*, 2003; Behrenfeld, 2010).

Beside the lack of agreement in the definition of a bloom, part of the ongoing debate might also result from the type of data set used (in situ vs satellite) or from the specific window of observation (local vs regional, annual vs inter-annual), which might nuance, if not impact, the conclusions. For example, Henson *et al.* (2006) observed clear inter-annual variability in bloom timing and magnitude in the Irminger Sea, suggesting that several processes probably interact to modulate the bloom. This also pleads for the acquisition of a long time series to extract the "roots" of the observed variability. Similar types of conclusions were reached by Lavigne *et al.* (2013) for a blooming region of the Mediterranean Sea where bio-physical mechanisms potentially evident through analysis at the climatological scale were not obvious any more if the analysis was re-focused on specific years. It is more than likely that there is a first-order mechanism driving the bloom in a given region, on which

is superimposed the inter-annual variability of physical forcing modulating the biological response (Frajka-Williams et Rhines, 2010). The corollary is that a robust climatological approach is needed to address the first-order mechanism controlling bloom dynamics in a given region. This is the choice taken in the present analysis which addresses bloom initiation and evolution in the Labrador Sea (LS) as evidenced by climatological time series.

Our specific interest in the LS indeed results from known peculiarities in the bloom phenology (onset, duration, intensity and decline) in this area. In the northern part (>60°N) of the basin, the bloom starts earlier and is shorter and more intense with respect to the southern part of the basin and more generally to the rest of the North Atlantic subpolar gyre (Head *et al.*, 2000; Wu *et al.*, 2008; Frajka-Williams et Rhines, 2010). This pattern on bloom onset in the LS is paradoxical with observations made by Siegel *et al.* (2002) that show a northward propagation of the spring bloom in the North Atlantic. In the north LS, noticeable hydrological peculiarities have also been identified. Over the west Greenland shelf, a boundary current, called the West Greenland Current (WGC), carries West Greenland Current Water (WGCW) characterized by cold, fresh water originating from the Arctic at the surface and warm, salty Irminger water of subtropical origin from 300 to 800 m depth. Offshore advection of WGCW occurs off Cap Desolation ($\sim$ 60°N), in a region marked by high eddy-kinetic energy (Figure 11). The lateral advection of WGCW, particularly surface fresh water, significantly affects the water column stability in the northern LS (Hatun *et al.*, 2007; Schmidt et Send, 2007).
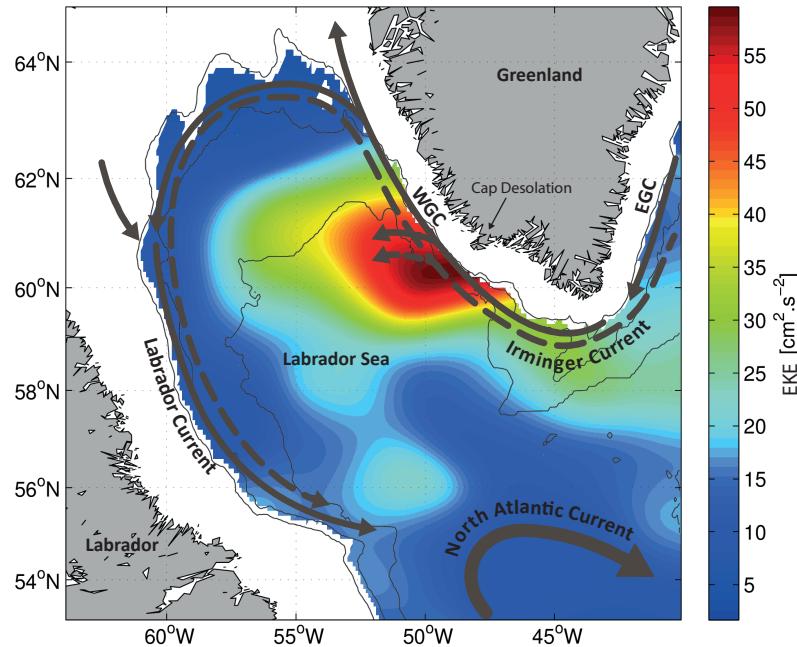
Figure. 11. General circulation in the LS superimposed on mean deep Eddy Kinetic Energy (EKE) map (1998-2010) calculated from 1,000 m depth Argo float displacement (see text S1). The dashed arrow corresponds to the Irminger Current extending from 200 to 800 m deep, below the East Greenland Current (EGC), West Greenland Current (WGC) and the Labrador Current that encircles the Labrador Sea. Note the retroflexion of the North Atlantic current south of the basin.

Few studies (Wu *et al.*, 2008; Frajka-Williams et Rhines, 2010) have investigated the potential role of haline stratification on phytoplankton phenology. These authors have identified two regions in the LS with a reversed pattern in the bloom onset. Frajka-Williams et Rhines (2010) showed that stratification was responsible for the early north LS bloom timing while light was assumed to control the south LS bloom. Wu *et al.* (2008) also reported an early bloom in the north related to the very shallow mixed layer. Yet they have concluded that light availability plays an important role but is not a determining factor for the early bloom.

Here, the paradoxical phenology of the north LS bloom is reinvestigated at climatological scale, with respect to bloom phenology of the subpolar gyre and more particularly of the south LS. Firstly North Atlantic subpolar gyre regions are identified for their similar bloom phenology (i.e. bioregionalization). Secondly, this bioregionalization is used to determine, with in situ Argo data, the regional and seasonal variations of water column stability and convolve them with seasonal variations in surface irradiance. This synergetic conjunction of hydrology and surface irradiance, as proposed by the conceptual model of Sverdrup (1953), is carried out in order to evaluate the extent to which the bloom phenology in distinct regions is driven by the light-mixing regime.

Material and methods

The bioregionalization of the North Atlantic subpolar gyre (from 40°N to 70°N) was performed according to the method described in D'Ortenzio et Ribera d'Alcalà (2009). The objective of this statistical method is to identify regions with similar patterns in the seasonal cycle of surface chlorophyll *a* concentration (hereafter called Chla), a proxy of surface phytoplankton biomass. 8-day composite satellite Chla data from the GlobColour project (`http://www.globcolour.info`) was used to create 8-day climatology (over the 1998-2014 period) for each pixel (spatial resolution of 4 km) of the basin. The GlobColour data set provides a long time series of merged L3 Ocean Colour products from different sensors (SeaWiFS, MERIS, MODIS aqua, VIIRS) which ensures data continuity and improves spatial and temporal coverage. A detailed description of the GlobColour product is given in the GlobColour Product User Guide (`http://www.globcolour.info/CDR_Docs/GlobCOLOUR_PUG.pdf`). To facilitate comparison between pixels, each 8-day value for each pixel was normalized by the maximal and minimal Chla value of each series so that the time series is scaled between 0 and 1. Due to low incident sun angle in winter, the Chla time series for each pixel last only 27 8-day periods from early March to late September. A cluster K-mean analysis (Hartigan et Wong, 1979) is then applied, allowing pixels exhibiting similar seasonal cycles of Chla to be assembled. Each pixel with more than two 8-day periods of missing data is removed from the analysis. The spatial distribution of the different clusters can subsequently be mapped with the associated centroid of each clusters corresponding to the mean seasonal cycle. The number of clusters is set before the analysis and is based on the Calinski and Harabazs index (Calinski et Harabasz, 1974; Milligan et Cooper, 1985) (see Text S2 and Figure S1). Here 6 clusters were used to regionalize the North Atlantic. In the following, the spatial distribution of the cluster are referred to as "bioregion", as proposed by D'Ortenzio et Ribera d'Alcalà (2009). The climatological seasonal phytoplankton biomass cycle

associated to each bioregion provides information on timing, duration and relative intensity of the bloom. The same analysis was also performed on the Labrador Sea alone with only 3 clusters to better characterize the bioregions in this area (see Figure S2). This region is influenced by the presence of sea ice which could limit the coverage of satellite data during winter period. However, Figure S3 shows that most of the region is free of ice as early as March due, in large part to, the West Greenland Current which carries warm waters of subtropical origin.

In order to analyze more specifically and quantitatively the biomass cycles in the bioregions identified in the LS, new un-normalized 8-day climatological cycles were created by area-averaging all Chla data for all pixels of a bioregion (see Figure S2). This pixel selection for area-averaging data within the bioregions is more accurate than a data box selection without any physical or biological meaning.

In this study, the bloom is defined as the rapid accumulation of phytoplankton biomass in the surface layer, seen by satellite. Therefore the onset is defined here as the maximum accumulation rate r, which is expressed as :

$$r = \frac{1}{Chla} \times \frac{dChla}{dt} \tag{1}$$

Argo data were used to produce monthly climatological time series of area-averaged temperature and salinity within each bioregion of the LS from the surface down to 1,000 m depth (see geographic location of Argo data profiles in Figure S4). In the LS, more than 7300 Argo profiles were available for the 1998-2014 period. The accuracy of float data is $\pm 0.002°C$ in temperature and ± 0.005 in salinity. Temperature and salinity profiles were used to estimate the mixed layer depth (MLD) according to the algorithm of Holte et Talley (2009) (see supporting information). This algorithm accounts for the vertical density compensation (de Boyer Montégut *et al.*, 2004, figure 10) that potentially occurs in the LS. A monthly climatological annual cycle of the MLD based on Argo data was estimated for both LS bioregions. 8-day climatological Photosynthetically Available Radiation (PAR) and PAR diffuse attenuation coefficient (K_{PAR}) were downloaded from the GlobColour website. The PAR was averaged over the mixed layer (PAR_{ML}) to account for the daily amount of photons received by phytoplankton (Riley, 1957; Prieur et Legendre, 1988; Morel *et al.*, 2010; Blain *et al.*, 2013; Mignot *et al.*, 2014). This proxy indeed convolves all the processes that control the amount of available light for phytoplankton cells in the water column (i.e. the surface irradiance, the thickness of the layer where phytoplankton is mixed and the irradiance attenuation within this layer). At short time scale (hours to day), the depth of the turbulent layer which mix phytoplankton cells can be shallower than the mixed layer depth (Brainerd *et al.*, 1995). Nevertheless, in the climatological context of this analysis, we assumed here that phytoplankton cells are, in average, uniformly distributed throughout the entire mixed layer over the 8-day period. The bloom is supposed to begin when the PAR_{ML} rises above a threshold value called PAR_c. PAR_c, similar to the community compensation irradiance (Siegel *et al.*, 2002), is the mean light energy over the MLD required by photosynthesis to compensate for all loss processes (including mortality and grazing), and to allow for net growth. This approach is based on the concept of Sverdrup (1953) but slightly differs from the critical depth hypothesis (CDH) in the

sense that the critical depth Z_{cr} is not used. The underlying concept is that the growth rate is not exponentially decreasing with depth, but rather constant throughout the mixed layer. The PAR below the sea surface [PAR$(0-)$], was calculated using a reduction of 7.6% of the PAR above the sea surface [PAR$(0+)$], to take into account the loss by reflection at the air/sea interface (Morel, 1991). The attenuation of PAR with depth was given by :

$$PAR(z) = PAR(0-) \times \exp(-K_{PAR} \times z) \tag{2}$$

The mean PAR over the mixed layer was estimated as :

$$PAR_{ML} = \frac{1}{MLD} \times \int_0^{MLD} PAR(z)dz \tag{3}$$

The monthly climatological MLD was linearly interpolated to match 8-day climatological PAR.

Results and discussion

Bioregionalization of the North Atlantic with a focus on the LS

The bioregionalization of the North Atlantic (Figure 12) reveals the high variability of phytoplankton biomass seasonal cycles at a climatological level. Timing, relative intensity as well as bloom duration exhibit very significant differences according to bioregions. The cycles associated with bioregions 1 and 3, are typical of temperate regions with the one-month delay between Chla maxima in both bioregions typically corresponding to the well-known northward propagation of the spring bloom (Siegel *et al.*, 2002). Bioregion 4, limited to coastal areas, is characterized by an early bloom (maximum biomass in mid-April). Bioregion 5 appears to be well representative of the overall subpolar gyre. It is characterized by a high phytoplankton biomass during 3 months, from June to September. Bioregions 6 and 2 are less spatially coherent than the others, except in the Labrador Sea.

The present bioregionalization of the North Atlantic, only based on satellite Chla, shows similar patterns to the geographical provinces described by Longhurst *et al.* (1995), who also used satellite Chla, as well as Devred *et al.* (2007), who used sea surface temperature (SST) and phytoplankton biomass data. Cluster analysis clearly distinguishes the North Atlantic Drift Province (bioregion 1) in particular the Drift retroflection south east of the LS (Figure 11), the North West Atlantic Shelf Province (bioregion 4) and the Boreal Polar Province (bioregion 2) on the Greenland shelves. However, the pattern is different in the LS with two distinct regions on either side of the 60°N parallel. In particular, the Boreal Polar Province only identified along the Greenland and Labrador shelves by Longhurst *et al.* (1995) and Devred *et al.* (2007) seems to extend into the North Labrador Sea interior as part of the present climatological analysis. The LS is well separated into two bioregions on either side of the 60°N parallel (Figure 12 and Figure S2). Both bioregions will respectively be referred to as "North LS" (bioregion 2 on Figure S2) and "South LS" bioregion 3 on Figure S2). In the South
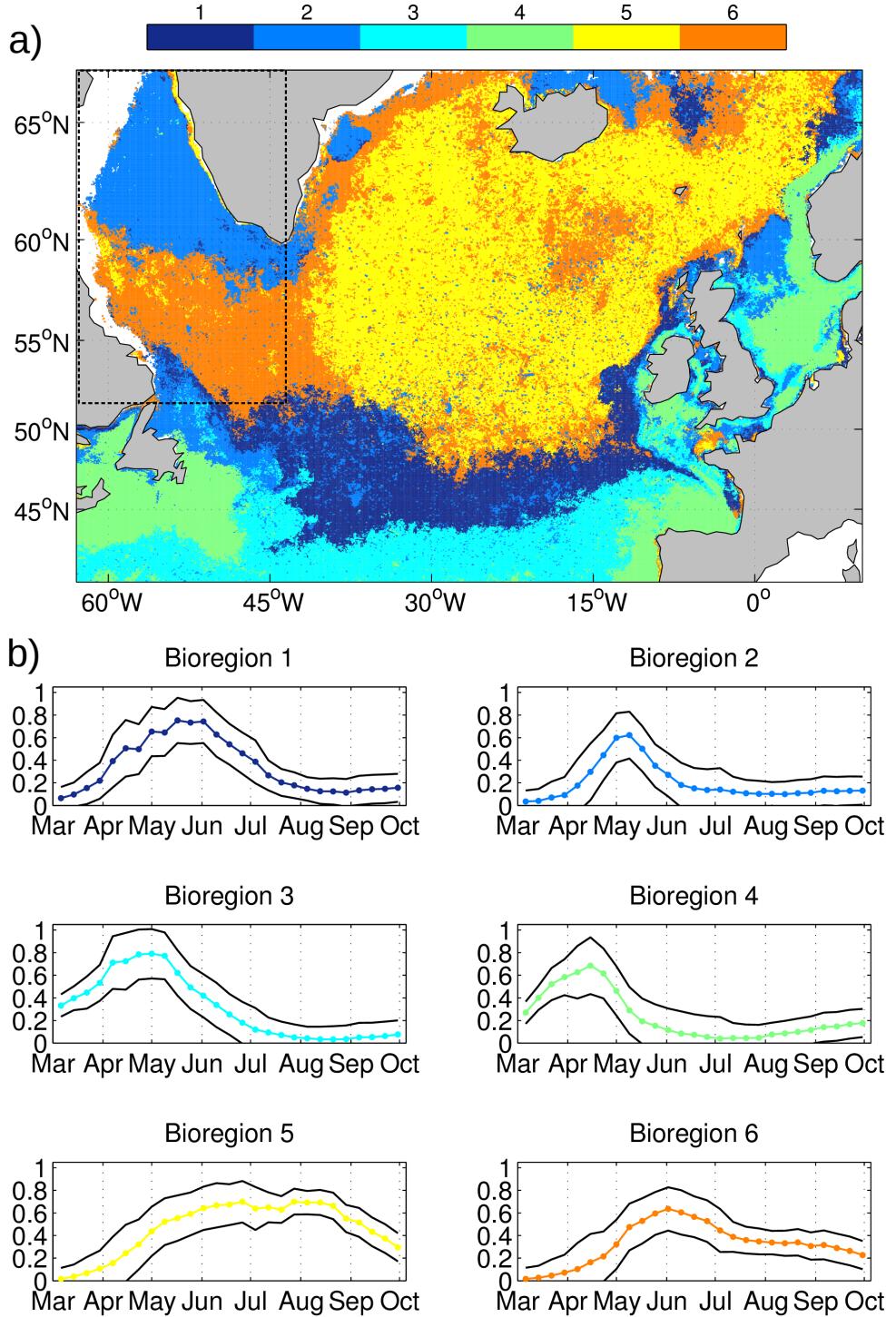
Figure. 12. Spatial distribution of the clusters obtained from the K-means analysis (a) and mean normalized Chla annual cycles in each cluster ± one standard deviation (b). Each cluster is considered as a bioregion with a spatiotemporal coherence with respect to phytoplankton biomass cycles. The dashed black box delineates the area of interest.

LS, the bloom starts in April-May and develops slowly with a relative biomass maximum occurring 2 months later in June. Unexpectedly, in the North LS, a short duration bloom starts in early April, peaks in May, and declines in June (Figure 12b). In the LS, it thus appears that the bloom does not follow an expected latitudinal progression associated with the seasonal increase in surface irradiance (Siegel *et al.*, 2002). Because of this paradoxical phytoplankton cycle dynamics, the following analysis and discussion will solely focus on the Labrador Sea.

Climatological differences in the hydrological conditions of the North and South LS

Climatological time series of temperature, salinity and density, from the surface to 1,000 m depth (Figure 13 and Figure S5 for density), clearly evidence different hydrological conditions between both bioregions of the LS (see bioregion 2 and 3 on Figure S2). The North LS is characterized by cold ($\sim$2°C) and fresh ($\sim$34.1-34.2) water at the surface from January to June. At intermediate depths (200-800 m), the relatively warm (4-5°C) and salty ($\sim$34.9) modified Irminger waters have only been identified in the North LS. These water masses are very similar to the WGCW, especially from December to March. The consequence of the presence of WGCW in the North LS is an increase in the water column stability during winter and early spring (Head *et al.*, 2000). The MLD in the North LS is indeed at least 100 m shallower than in the South LS over this period. The fresh and cold upper water layer in the North LS is present during the whole year due to different sources, such as Artic Ocean water carried by East and West Greenland currents, a high precipitation rate (DeTracey et Tang, 1997) or Greenland runoff (Hanna *et al.*, 2008). All these inputs strongly influence the stability of the water column in the North LS. Climatological buoyancy anomaly has revealed that this region is mostly stratified (MLD<100 m) due to stabilizing fresh water in spite of destabilizing cold water (Frajka-Williams et Rhines, 2010). In the South LS, the upper water layer is thermally rather than haline-stratified from May to November. Before May, solar radiation is too weak to compensate for heat loss, so the MLD is deeper (>400 m).

Impact of light and water stability on bloom onset in the North and South LS

In both bioregions of the LS, very different climatological biomass cycles are observed, when addressed quantitatively in terms of Chla. In the North LS, the peak in surface Chla reaches 3.7 mg m^{-3} in late April (Figure 14a), 7 times higher than the value in the South LS at the same period. At the date of the North LS bloom onset (early April; dashed blue line, Figure 14b), the area-averaged surface PAR in the South LS (19 mol photon m^{-2} d^{-1}) is slightly higher than the one in the North LS (16 mol photon m^{-2} d^{-1}; Figure 14c) while the bloom onset in the South LS takes place one month later. The thickness of the mixed layer plays a key role on light availability for the development of the bloom in the North LS. Indeed, the mean PAR over the mixed layer (Figure 14d) is twice higher in the North LS than in the South at the same time. In the South LS, the bloom begins one month later in early May when PAR$_{ML}$ reaches 2.5 mol photon m^{-2} d^{-1}, the same value that supported the bloom onset in the North LS.
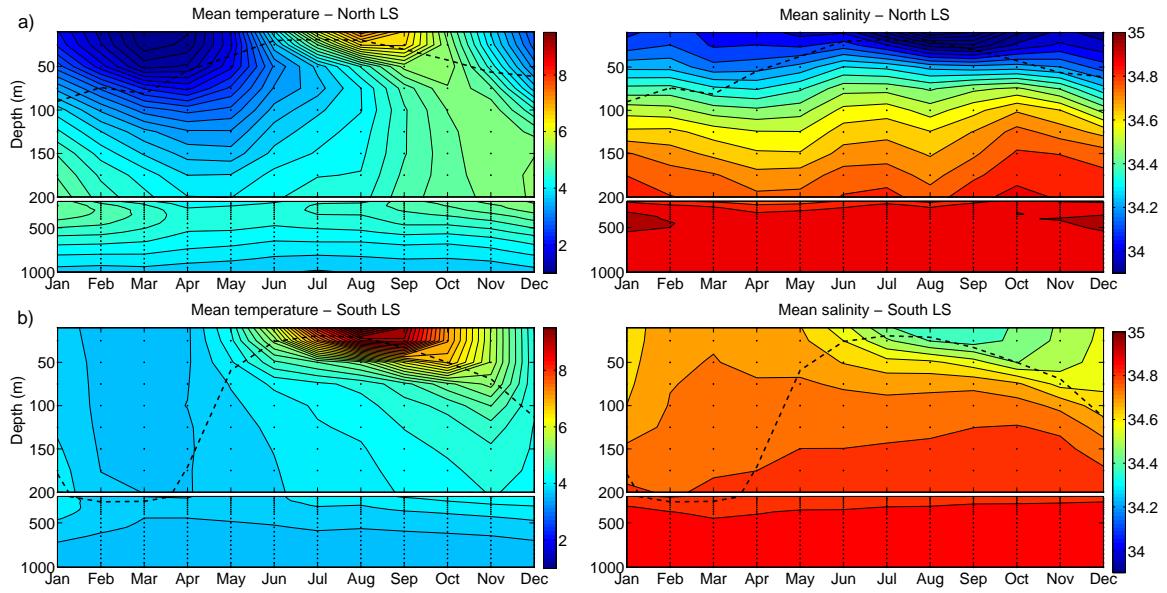
Figure. 13. Climatological area-averaged time series of temperature and salinity in the North LS (a) and in the South LS (b) over the 1998-2014 period (see geographic location of the data in Figure S4). Dashed lines denote the climatological MLD. The data (black points) were interpolated using the matlab function "contourf". Thin black lines represent contours, with a resolution of 0.2°C for temperature and 0.06 for salinity.

Wu *et al.* (2008) and Frajka-Williams et Rhines (2010) have separately studied the impact of the shoaling of the mixed layer and irradiance (PAR), using the critical depth hypothesis, on the timing of the bloom in the LS. They concluded that the early shoaling was responsible for the early bloom in the North LS, while light controlled the South LS bloom. Both factors are directly linked because the depth of the mixed layer regulates phytoplankton's time exposure to light. The mean PAR over the mixed layer takes the depth of mixing into account in the assessment of the light availability (i.e. light-mixing regime). From the present observation, the climatological analysis reveals that the light-mixing regime drives the onset of the bloom in both bioregions of the LS. The mean community compensation irradiance (PAR_c) of 2.5 mol photon m^{-2} d^{-1} could be the threshold value that triggers the bloom onset in this region. Interestingly, this value is consistent with the community compensation irradiance of 2.5 mol photon m^{-2} d^{-1} from Henson *et al.* (2006) in the Irminger Sea, 3.5 mol photon m^{-2} d^{-1} from Riley (1957) in the Sargasso Sea and of 3 mol photon m^{-2} d^{-1} from Siegel *et al.* (2002) south of 40°N, in stratified environments.

Bloom termination and summer biomass evolution

In the North LS, the bloom begins to decline one month earlier (early May) and faster than the bloom in the South LS and more generally in the subpolar gyre (early June). It is interesting to analyze the potential causes at the origin of the time-shift in bloom decline. Bottom-up (nutrient, light) as well as top-down (zooplankton, mortality) control are investigated here. In most of the North Atlantic, nutrients are replete in early spring to support the bloom onset, thanks to winter-time convection that replenishes upper layers. However, the surface haline barrier in the North LS could limit, at least partially, this wintertime recovery of nutrients. A rapid growth of large phyto-
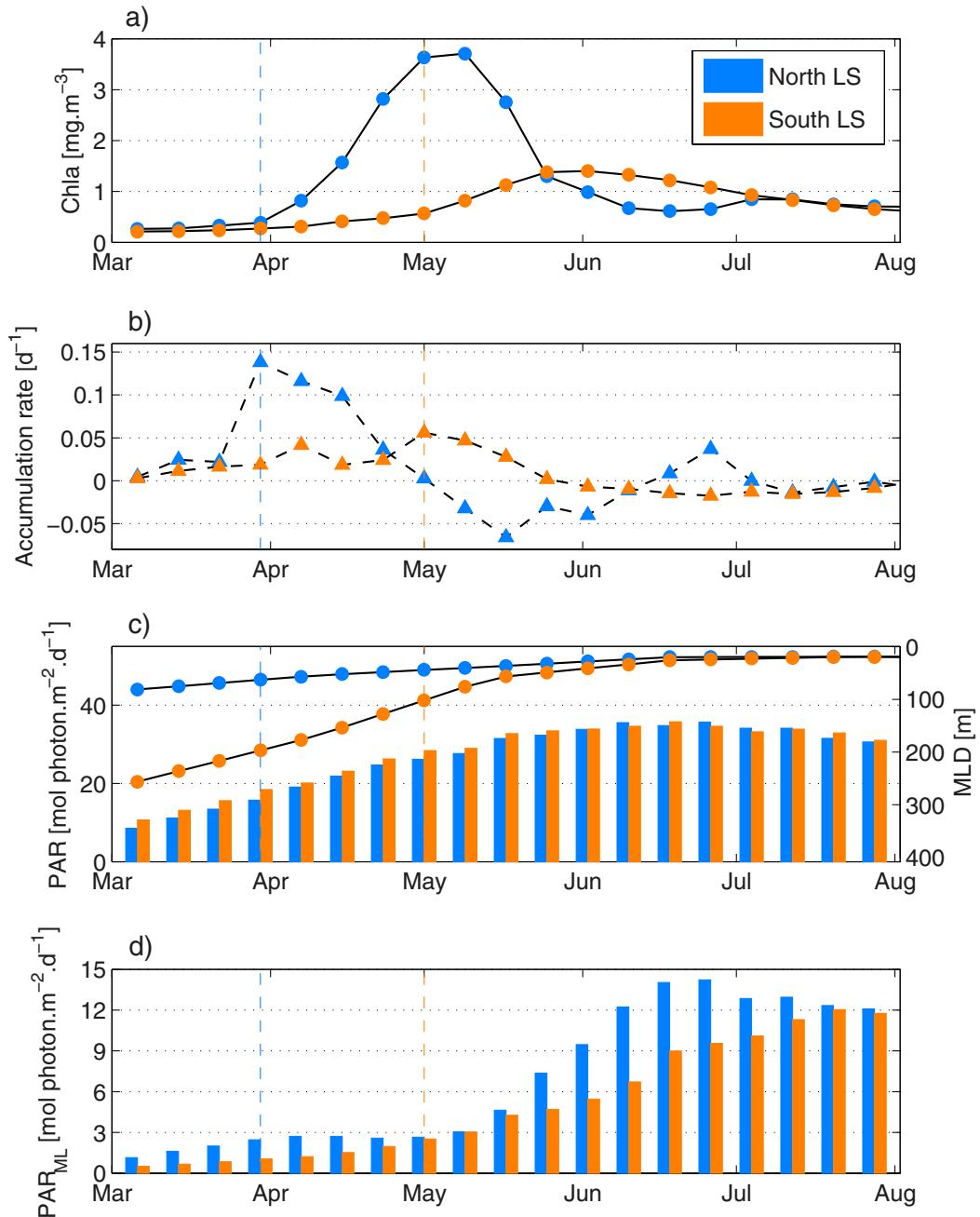
Figure. 14. Climatological cycle of area-averaged surface Chla (a), Accumulation rate (see equation 1) of the surface Chla (b), surface PAR (bars) and MLD (lines) (c) and mean PAR over the MLD (d). Vertical dashed lines denote the bloom initiation deduced from panel b. Blue correspond to the North LS and red to the South LS. Note the scale inversion for MLD on panel c. The time axis, from 1st March to 31 July is centered on the bloom period.

plankton cells, such as diatoms, could then lead to a rapid exhaustion of nutrients in the MLD, in particular silicate. This could be amplified by numerous eddies in the North LS which could constitute a net sink of nutrients by vertical advection (for Nitrate : 0.01-0.03 mol N m^{-2} y^{-1}; McGillicuddy *et al.* (2003)). However, horizontal advection of nutrient-rich Arctic water from the Greenland shelf to the North LS interior seems to compensate for these losses (0.3-1 mol N m^{-2} y^{-1}). Climatological annual cycles of nitrate and silicate concentrations (World Ocean Atlas 2009), averaged over the MLD in both bioregions of the LS, seems to indicate that nutrient concentrations are weaker in the North LS than in the South LS over a whole year. Nevertheless, these concentrations remain high (Figure S6) especially in the North LS when the bloom starts to collapse. The minimum nutrient concentration indeed occurs in both bioregions in August/September when bloom in the North LS has already collapsed 2 or 3 months before. At climatological scale, nutrients appear to not control the bloom collapse in both bioregions. However, a nitrate profile from a BGC-Argo float in the North LS (data not shown but available at `http://www.oao.obs-vlfr.fr/bioargo/PHP/lovbio044b/lovbio044b.html`; profile As_120_00) at the end of April 2015 shows a clear nitrate depletion at the surface, associated with very high Chla (above 10 mg m^{-3}). Thus, on specific years, it appears that nutrient depletion could be at the origin of the North LS bloom collapse.

The possible influence of light limitation on the North LS rapid bloom decline in nutrient-replete conditions has also to be addressed. The high Chla in a rather thin layer (<50 m) might be at the origin of self-shading and associated inhibition of growth, causing the rapid decline of the bloom (Marra, 2004). PAR$_{ML}$ is a useful criteria not only to explain bloom initiation but also to evidence a possible light limitation. At climatological scale, PAR$_{ML}$ slightly decreases in the North LS at the time of the maximum Chla. However, PAR$_{ML}$ never fall below the critical light level (PAR$_c$) so that light limitation does not appear as first-order explanation of the bloom collapse. Nevertheless, the same analysis performed on specific years shows that PAR$_{ML}$ can fall below the critical light level and leads to the end of the bloom (result not shown). In the South LS, light and nutrients are not a limiting factor but the biomass remains low possibly as a consequence of control by secondary producers.

The top-down control by grazers could indeed influence the phytoplankton biomass cycles in both bioregions of the LS. Nevertheless, the way in which the zooplankton population can regulate the spring bloom still needs to be quantitatively addressed. Observations of annual cycles of zooplankton abundance are rare especially at high latitudes, where in situ data are sparse. According to Head *et al.* (2000), the triggering of reproduction seems to be linked to the start of the spring bloom; however an early and rapid bloom as in the North LS could lead to a mismatch between primary and secondary producers which, in turn, could explain the high bloom intensity in the North LS compared to the South (Marra et Barber, 2005; Ji *et al.*, 2010). The establishment of the zooplankton population after the bloom peaks maintains low phytoplankton concentrations in summer despite high light levels. The mismatch between primary and secondary producers leading to an intense bloom in the North LS could also be at the origin of its abrupt decline. Viral infection is now recognized as a potentially significant cause of phytoplankton mortality (Lehahn *et al.*, 2014), resulting in particular in the production of transparent exopolymers. The latter are known to contribute to cell aggregation,

enhancing the sinking rate (Vardi *et al.*, 2012), and hence the draining of the upper layer from its particulate material.

Conclusion

This climatological analysis suggests that the first-order mechanism controlling the initiation of the bloom in both nutrient-replete bioregions of the Labrador Sea is the light-mixing regime, i.e. the concurrent influence of surface light and mixing. The same mechanism can explain two different bloom phenologies. The summer regime still seems to be controlled by grazing or other top-down processes. More generally, this study highlights the importance of in situ measurements to investigate and understand the underlying mechanisms of a complete annual cycle of phytoplankton biomass in remote areas. While satellite remote sensing is essential, it remains nevertheless restricted to the surface layer and thus has to be completed by in situ observations. In particular, it should be noticed that environmental conditions in the North LS are similar to those of the Arctic where a subsurface chlorophyll maximum (SCM) occurs in summer while it remains unseen by satellites. These data could be nicely complemented by observations of the BGC-Argo type that would resolve interannual variability, as well as reveal the vertical structure of the biological response to physical forcing.

2.4   Discussion supplémentaire

La biorégionalisation du gyre subpolaire de l'Atlantique Nord a révélé que la dynamique de la biomasse phytoplanctonique est particulière dans la mer du Labrador, notamment dans la région nord où la stabilité de la colonne d'eau permet d'initier le bloom un mois plus tôt que dans la région sud et plus généralement dans l'ensemble du gyre. Cette stabilité dans le nord de la mer du Labrador est liée à une stratification haline à grande échelle et quasi-permanente. Bien que les sources d'eau peu salée aient été identifiées dans cette étude, la présence de cette barrière de salinité en surface sur l'ensemble de la biorégion nord n'a pas été abordée. Les sources d'eau peu salée semblent toutes connectées par le courant de bord est et ouest Groenland qui rejoint le courant du Labrador au nord de la mer du Labrador le long des isobathes 1000 et 2000 m (Figure 11). Ces courants contournent

l'ensemble du bassin mais n'expliquent pas la présence d'eau peu salée à l'intérieur du bassin. En utilisant des flotteurs dérivants en surface, Reverdin *et al.* (2003) ont observé une seconde voie de circulation qui traverse le bassin au niveau de 60°N (isobathe 3000 m). Cette voie est empruntée par des tourbillons de mésoéchelle qui se forment sur la côte du Groenland dans une zone très énergétique (Figure 11). Chanut *et al.* (2008) ont montré par modélisation que ces tourbillons sont caractérisés par un cœur de vorticité négative entouré d'une langue de vorticité positive. Ces structures permettent donc d'isoler des masses d'eau et de les transporter sur de grandes distances (Provenzale, 1999). Cependant, les simulations numériques montrent que ces tourbillons ne se déplacent pas sous la limite de 58°N. Les masses d'eau du courant est et ouest Groenland peuvent donc être advectées par l'activité mésoéchelle vers le centre du bassin et influencer les conditions de mélange de tout le nord de la mer du Labrador (Katsman *et al.*, 2004; de Jong *et al.*, 2014). Les structures de mésoéchelle formées sur la côte du Groenland pourraient ainsi influencer le cycle annuel de biomasse phytoplanctonique observé à grande échelle par satellite.

Bien que le gradient latitudinal de la date d'initiation du bloom soit inversé par rapport au reste du gyre, c'est bien la dose de lumière (PAR$_c$ ou I$_c$) qui joue un rôle déterminant pour l'initiation du bloom dans la mer du Labrador. En effet, l'éclairement de compensation communautaire I$_c$ nécessaire à l'initiation du bloom est identique dans les deux biorégions. Siegel *et al.* (2002) ont aussi observé une relative homogénéité de I$_c$ sur l'ensemble du gyre sans pour autant en expliquer la raison. Il est possible qu'au moment de l'initiation du bloom printanier, dominé par les diatomés, le microzooplancton présent ne soit pas adapté à ce type de proie et que le mésozooplancton ne soit pas encore arrivé à maturité. Le contrôle par le zooplancton de l'initiation du bloom serait alors négligeable et ne ferait pas varier I$_c$. Néanmoins, la diversité des communautés phytoplanctoniques, chacune avec des paramètres physiologiques différents, implique certainement des besoins en lumière différents qui pourraient donc faire varier I$_c$. De même, la température devrait impacter ces paramètres physiologiques et apporter de la variabilité. Il est possible qu'à l'échelle climatologique et à l'échelle d'une région océanique, ces facteurs soient négligeables ou expliquent seulement la variabilité observée autour du cycle moyen (écart type sur la Figure 12).

L'éclairement de compensation I$_c$ est estimé au moment de l'initiation du bloom. Le choix de la date d'initiation est cependant très subjectif et varie selon la définition du bloom. Dans cette étude, nous avons considéré l'initiation du bloom comme étant le taux d'accumulation maximal de la biomasse de surface. En visualisant simplement le cycle de biomasse en échelle log des deux biorégions du Labrador (Figure 15), il apparaît que la biomasse de surface, bien que très faible, a commencé à s'accumuler bien avant la date d'initiation estimée. Par ailleurs, la biomasse faible en surface pourrait être liée à la dilution du phytoplancton dans des grands volumes d'eau. Connaissant la profondeur de la couche de mélange dans les deux biorégions, il est possible d'estimer le cycle de biomasse intégrée ($Chla \times MLD$). Le cycle intégré dans la région nord n'est pas très différent du cycle de surface, la profondeur de la couche de mélange étant faible et peu variable. En revanche, le cycle intégré dans la région sud révèle un stock de phytoplancton élevé en fin d'hiver, du même ordre de grandeur que le stock au pic du bloom printanier. Au sud, les couches de mélange profondes pourraient découpler le

zooplancton du phytoplancton ce qui favoriserait l'accumulation hivernale de ce dernier (Behrenfeld, 2010). Behrenfeld *et al.* (2013) ont montré sur l'ensemble du gyre que la profondeur de la couche de mélange hivernale régule le stock de phytoplancton (les maximums de MLD sont corrélées aux stocks maximaux). Cependant, la même relation n'existe pas avec le maximum de concentration au printemps. Malgré les conclusions quelque peu provocatrices de Behrenfeld (2010) qui stipulent notamment que le bloom commence non pas au printemps mais en hiver, l'accumulation de biomasse dans les couches de mélange profondes en hiver et l'accumulation de biomasse de surface au printemps sont deux événements distincts contrôlés par des mécanismes différents. En particulier, les relations prédateur-proie ne sont pas les mêmes car la composition des communautés phytoplanctoniques et zooplanctoniques varie selon les conditions environnementales. Cela suggère que le cycle annuel du phytoplancton ne doit pas être examiné uniquement en terme de biomasse mais aussi en terme de composition et de structure de taille de la communauté.
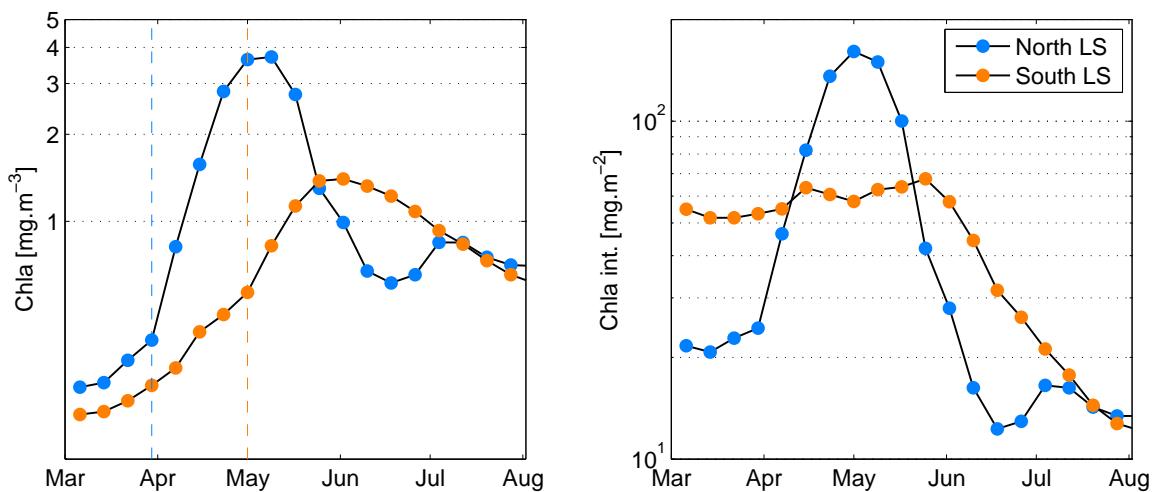
Figure. 15. Cycle de biomasse de surface (gauche) et intégrée (droite) dans les deux biorégions de la mer du Labrador. La biomasse de surface est directement mesurée par satellite alors que la biomasse intégrée est estimée en multipliant la biomasse de surface par la profondeur de la couche de mélange.

2.5   Conclusion

Cette étude a montré que les conditions de mélange couplées à l'éclairement incident contrôlent l'initiation du bloom printanier à grande échelle, mais aussi plus indirectement l'ensemble du cycle annuel de la biomasse de surface. Plus particulièrement, les conditions de mélange hivernal dans le nord de la mer du Labrador, influencées par l'activité mésoéchelle, semblent modifier complètement la dynamique du bloom printanier à l'échelle climatologique. Quel peut être le rôle de la période hivernale sur le bloom printanier ? La dynamique de la biomasse en hiver peut-elle influencer les caractéristiques du bloom printanier ?

Cette étude a également révélé les limites des observations satellites pour la compréhension des blooms phytoplanctoniques. Le cycle annuel de biomasse de surface observé par satellite ne reflète pas

exactement la dynamique réelle de la biomasse, notamment à cause de facteurs purement physiques tels que la dilution. Des données *in situ* sont nécessaires en particulier pendant la période hivernale qui pourrait jouer un rôle important sur la dynamique du bloom printanier.

CHAPITRE 3

Dynamique de la biomasse phytoplanctonique pendant la période hivernale et impact sur le bloom printanier

3.1 Introduction

Bien que le gyre subpolaire de l'Atlantique Nord soit une des régions océaniques les plus échantillonnées, en particulier pendant le bloom printanier, cette région reste quasiment méconnue pendant la période hivernale. En effet, les grandes distances à parcourir et les conditions de mer difficiles en hiver ne facilitent pas la mise en œuvre de campagnes océanographiques. En outre, à ces latitudes, même les observations satellites sont limitées, du fait de la couverture nuageuse très dense et du faible angle solaire en hiver.

En se basant sur la théorie de Sverdrup (Sverdrup, 1953), la communauté océanographique a longtemps supposé que les forçages atmosphériques hivernaux très intenses, qui mélangent la colonne d'eau sur des centaines de mètres de profondeur, couplés à un faible éclairement de surface limitaient drastiquement la croissance phytoplanctonique. Comment alors maintenir pendant l'hiver une population de phytoplancton capable d'ensemencer le bloom printanier ? Des observations *in situ* en fin d'hiver dans le bassin d'Islande ont montré que le stock de phytoplancton dans les couches de mélange profondes n'était pas négligeable (Backhaus *et al.*, 2003). En effet, le mélange convectif pourrait permettre des incursions régulières du phytoplancton dans la couche euphotique et pourrait ainsi maintenir une population active jusqu'au bloom printanier. Par ailleurs, Behrenfeld (2010) ont montré que l'approffondissement de la couche de mélange en hiver permettait de réduire la pression de broutage par le microzooplancton et diminuait ainsi les taux de perte du phytoplancton. Ainsi, malgré un taux de croissance très faible, la biomasse phytoplanctonique pourrait s'accumuler dans les couches de mélange hivernales profondes. Cependant, comme souligné dans le précédent chapitre, il est primordial d'identifier quel groupe phytoplanctonique peut endurer de telles conditions environnementales. Dale *et al.* (1999) ont observé, dans les couches de mélange hivernales profondes de la mer de Norvège, une population dominée par du pico- et du nanophytoplancton, tels que des flagellés. Typiquement, ce groupe de phytoplancton ne semble pas impliqué dans l'ensemencement du bloom printanier dominé par des diatomées (Backhaus *et al.*, 2003). L'hypothèse de la dormance

apporte un argument convainquant pour expliquer la présence de diatomées au début du printemps. Certaines espèces pourraient passer l'hiver en profondeur sous forme de spore ou de cellule végétative et s'activer au début du printemps lorsque les conditions environnementales redeviennent favorables (Smetacek, 1985; McQuoid et Hobson, 1996). Par ailleurs, des études de modélisation ont montré que des structures de sous-mésoéchelle se formant au niveau de forts gradients horizontaux de densité peuvent restratifier localement (1-10 km) et en quelques jours des couches de mélange très profondes (Boccaletti *et al.*, 2007; Fox-Kemper *et al.*, 2008; Fox-Kemper et Ferrari, 2008). La restratification modifie localement l'environnement lumineux favorisant ainsi le développement de blooms phyto-planctoniques avant même la restratification saisonnière liée aux flux radiatifs (Mahadevan *et al.*, 2012). L'occurrence de ce genre d'événements pendant la période hivernale pourrait ouvrir des fe-nêtres d'opportunité à certains groupes de phytoplancton tels que les diatomées et ainsi favoriser le maintient de certaines espèces impliquées dans le bloom printanier.

Dans ce chapitre, nous explorerons cette hypothèse à l'aide de données de flotteurs Argo et BGC-Argo. Nous montrerons comment l'activité sous-mésoéchelle induit des restratifications temporaires de la couche de mélange en hiver et comment celles-ci peuvent influencer la production et la struc-ture de la communauté phytoplanctonique. Enfin, nous montrerons, à l'aide d'un modèle simple, l'influence de cette intermittence du mélange hivernal sur les caractéristiques du bloom printanier.

Le format très court de l'article présenté dans ce chapitre implique qu'une grande partie des mé-thodes et des résultats figurent dans le matériel supplémentaire associé à l'article (voir annexe B). Dans le cadre de ce chapitre, des extraits du matériel supplémentaire seront présentés dans la section *Matériel et Méthodes*, qui précède l'article, et dans la section *Résultats et discussion supplémentaires*. Les résultats de la modélisation (développée en collaboration avec le laboratoire d'océanographie de Naples) sont consultables à la fin de l'annexe B.

3.2 Résumé de l'étude

Nous avons utilisé dans cette étude un jeu de données issu de flotteurs Argo et BGC-Argo déployés dans le gyre subpolaire de l'Atlantique Nord (43°N - 66°N). Environ 300 profils BGC-Argo et plus de 2000 profils Argo ont été exploités durant la période hivernale (janvier à mars) des années 2014 et 2015.

Le réseau de flotteurs Argo a été utilisé pour mettre en évidence l'intermittence du mélange hiver-nal. Environ 25% des profils de densité, répartis de manière relativement homogène sur l'ensemble du gyre, indiquent une MLD inférieure à 100 m (profil dit "stratifié"). La stratification verticale est par-ticulièrement intense au niveau des zones où le gradient horizontal de densité est fort, ce qui suggère le rôle potentiel de l'activité sous-mésoéchelle pour restratifier localement les couches de mélange hivernales. La structure en température et salinité des gradients horizontaux de densité (*i.e.* angle de Turner) s'avère être similaire à la structure des gradients verticaux de densité sur l'ensemble du gyre. Pour ces couches de mélange peu profondes, la stratification verticale observée est donc principale-ment liée à un transport latéral de masse d'eau initié probablement par l'activité sous-mésoéchelle.

A cette période de l'année, ces mécanismes de restratification sont en compétition avec le mélange vertical induit par le vent et la perte de chaleur de l'océan. Les événements de restratification sont donc aussi dépendants des conditions météorologiques. L'analyse de l'intensité du vent et des flux de chaleur sur la période hivernale a montré une forte intermittence de ces forçages atmosphériques avec une probabilité de 10-20% d'avoir une période de calme supérieure à 24 heures sur l'ensemble du gyre. Ces observations suggèrent que les événements de restratification sont transitoires et intermittents pendant la période hivernale.

Les événements de restratification peuvent accroître d'un ordre de grandeur la disponibilité en lumière pour le phytoplancton dans la couche de mélange ce qui induit localement une accumulation de biomasse (observée à la fois sur la Chla et le b_{bp}). Les périodes de calme semblent donc suffisamment longues pour restratifier des couches de mélange profondes et initier des blooms transitoires en hiver. Par ailleurs, cette modification de l'environnement lumineux, liée à la restratification de la couche de mélange, influence non seulement la production phytoplanctonique mais aussi la structure de la communauté. Les variations du rapport Chla/b_{bp}, considéré comme un proxy de la structure des communautés autotrophes, ont permis de révéler cette influence. Dans les couches de mélange profondes, la communauté phytoplanctonique est dominée par du pico- et nanophytoplancton. En revanche, les blooms observés lors des événements de restratification sont caractérisés par une augmentation de la proportion du microphytoplankton, représenté principalement par des diatomées. Ces blooms transitoires sont particulièrement fréquents en février-mars (10-25% des profils) lorsque les restratifications sont plus fréquentes et que la lumière disponible augmente due à l'augmentation de la durée du jour. La couverture nuageuse semble aussi jouer un rôle prépondérant sur ces blooms de diatomées en modulant l'intensité lumineuse à l'échelle de l'événement. Ces résultats ont été confirmés par des données indépendantes de la structure des communautés phytoplanctoniques (dérivées de mesures HPLC de pigments), collectées lors d'une des seules campagnes hivernales réalisées dans le gyre subpolaire (campagne CATCH en janvier-février 1997).

La grande majorité des études sur la dynamique du bloom printanier se sont focalisées sur l'influence des forçages physiques sur la biomasse phytoplanctonique. Nos observations révèlent que les restratifications intermittentes de la couche de mélange hivernale impactent surtout la structure de la communauté. Bien que les blooms transitoires ne soient pas intense en terme de biomasse, ils maintiennent néanmoins une population physiologiquement active de diatomées pendant tout l'hiver. En outre, des résultats complémentaires issus d'un modèle simple (voir annexe B) ont montré que la fréquence de ces blooms transitoires pendant la période hivernale pouvait influencer les caractéristiques du bloom printanier, notamment avancer la date d'initiation de plusieurs semaines et doubler l'intensité du bloom.

3.3 Matériel et méthodes

(extrait du matériel supplémentaire de l'article présenté à la section suivante)

BGC-Argo float data

PROVOR CTS-4 profiling floats used in this study are equipped with : a SBE 41 CTD ; an ECO3 (Combined Three Channel Sensors) composed of a chlorophyll *a* (Chla) fluorometer, a Colored Dissolved Organic Matter (CDOM) fluorometer, and an optical backscattering sensor at 700 nm and angle of 124° (b_{bp}) ; an OCR-504 radiometer measuring Photosynthetically Available Radiation integrated over 400-700 nm (PAR). Measurements were collected during upward profiles every 5 or 10 days, from the parking depth at 1,000 m to the surface. Vertical resolution of acquisition was 10 m between 1,000 m and 250 m, 1 m between 250 m and 10 m, and 0.2 m between 10 m and the surface. Radiometric measurements were acquired only in the upper 250 m. Data were transmitted via Iridium communication each time the floats surface, usually around local noon. A "real time" quality control procedure was performed on CTD data (Wong *et al.*, 2015), Chla (Schmechtig *et al.*, 2014) and PAR measurements (Organelli *et al.*, 2016) after the factory calibration was applied. The instrumental dark signal was removed from the Chla profile and the non-photochemical quenching was corrected following the method in (Xing *et al.*, 2012). Spikes were removed from Chla and b_{bp} profiles using a 5-point running median filter and a 7-point running mean filter (Briggs *et al.*, 2011).

Atmospheric data and Sea ice fraction

Net heat flux and wind data were extracted from the ECMWF ERA Interim dataset (reanalysis) freely available at `http://apps.ecmwf.int/datasets/data/interim-full-daily/levtype=sfc`. Atmospheric data, with spatial resolution of 0.25°, were averaged over 12 hours periods. Daily mean sea ice product with spatial resolution of 0.05° was provided by the OSTIA global foundation (`http://marine.copernicus.eu`). Pixels with sea ice fraction > 50% are plotted in Fig. 21D.

Stratification and Turner angle analysis

More than 2000 Argo float temperature and salinity profiles were acquired during January-March 2014 and 2015 in the North Atlantic Subpolar Gyre. Derived density profiles were used to estimate the depth of the mixed layer (see section *MLD estimation*). Buoyancy frequency $N^2 = -(g/\rho_0)\partial\rho/\partial z$ (where g is the acceleration due to gravity, ρ is the potential density and ρ_0 is a reference density) averaged over 5-100 m depth was calculated to provide a quantitative measure of stratification. Surface temperature, salinity and density data (averaged over 5-15 m depth) from Argo float were interpolated on a regular grid by a Gaussian correlation function, weighted by the local number of data, with a decorrelation radius of 200 km. Both vertical Argo profiles and surface horizontal map of temperature and salinity were used to calculate Turner angles (Matlab function gsw_Turner_Rsubrho from Gibbs Sea Water toolbox) as follow (Johnson *et al.*, 2012, 2016) :

$$Tu_v = tan^{-1}(\alpha\frac{\partial\theta}{\partial z} - \beta\frac{\partial S_A}{\partial z}, \alpha\frac{\partial\theta}{\partial z} + \beta\frac{\partial S_A}{\partial z})$$

$$Tu_H = tan^{-1}(\alpha\partial\theta - \beta\partial S_A, \alpha\partial\theta + \beta\partial S_A)$$

where ∂ is the difference between data points calculated across isopycnals, α and β are the thermal expansion and saline contraction coefficients, respectively, θ is the conservative temperature and S_A is the absolute salinity (TEOS-10, (IOC *et al.*, 2010)). Vertical Turner angle Tu_v was determined for each Argo profile using data points of θ and S_A at 5 m and the depth of the mixed layer (Fig. 16). Horizontal Turner angle Tu_H was calculated for each 0.25° grid points of the surface map using θ and S_A at the maximum and minimum density points in a 3x3 square centered around the grid point. Thus, the difference between data points is calculated across gradients. A turner angle provides a metric to quantify the relative contribution of temperature and salinity to density gradients. The slumping of horizontal density gradient induced by mixed layer eddies (MLEs) produces vertical density gradient with a similar Turner angle ($Tu_H = Tu_v$) (Johnson *et al.*, 2016). Frequency distribution of Tu_v (from all Argo profiles) and Tu_H (from all grid points), each normalized by the maximum frequency of the distribution, allows to compare temperature and salinity structure of horizontal and vertical gradients in the whole subpolar gyre in the winters 2014 and 2015. Similar distribution of horizontal and vertical Turner angle indicate that horizontal density gradients slump to produce vertical stratification. It is important to note that although MLEs seems to be a leading-order mechanism that slump horizontal density gradient, other lateral processes such as mesoscale dynamics or wind through Ekman buoyancy fluxes also modify upper-ocean stratification (Johnson *et al.*, 2016).
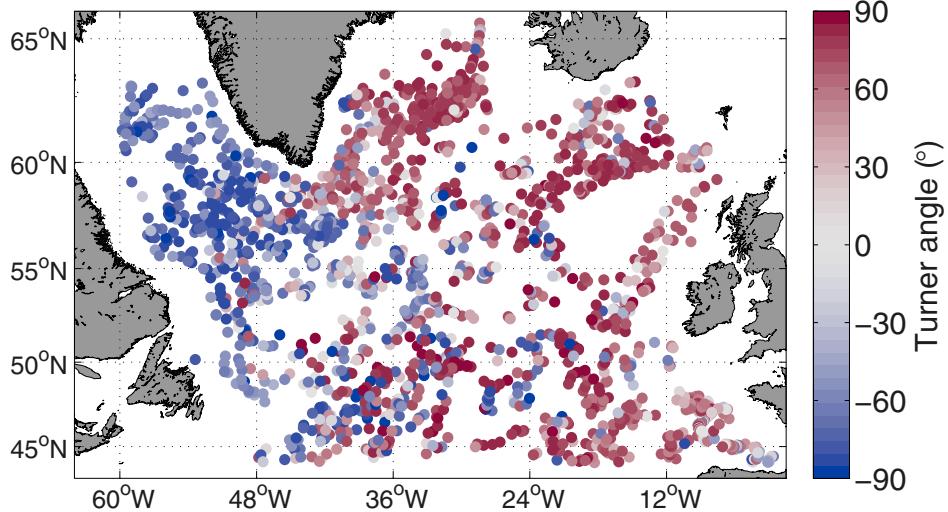
Figure. 16. Vertical Turner angle Tu_v for more than 2000 Argo float profiles in the North Atlantic Subpolar Gyre in the winters 2014 and 2015. Turner angles > 0° indicate that temperature is the main contributor to the density gradient whereas angles < 0° indicate that salinity is the main contributor. Around 0°, both temperature and salinity contribute equally to the density gradient. Angles > 45° or < -45° indicate that salinity is working against temperature and vice versa.

MLD estimation

The mixed layer depth (MLD) was estimated using a density difference of 0.01 kg m⁻³ from a reference value at 5 m depth. MLD was used to distinguish deep mixed conditions (MLD > 100 m) from stratified conditions, in the sense of shallow mixed layer (MLD < 100 m). The threshold of 100 m corresponds approximately to the deeper limit of the euphotic zone. Although we don't have any information about mixing intensity, we assumed that the mixed layer depth estimation, using a criteria of 0.01 kg m⁻³, matches well the active mixing layer depth in winter (Brainerd *et al.*, 1995). As a quality control of the mixed layer depth estimation, we checked the shape of the Chla profiles in the MLD. If the MLD is actively mixed, the Chla is expected to be homogeneous in this layer. The relative standard deviation (RSD = standard deviation / mean) was calculated to quantify the homogeneity of the Chla profile in the MLD (Fig. 17). This quality control was done before the quenching correction given that this correction needs an accurate estimation of the MLD. Therefore, in order to avoid the bias by quenching at the surface, the RSD was calculated between the isolume 20 μmol photons m⁻² s⁻¹, which marks the beginning of the quenching effect (dashed grey line), and the MLD (dashed black line, Fig. 17). All the winter profiles with RSD > 20% (57 profiles) were removed from the present analysis.

Calm periods

Calm periods were defined as a decrease of wind lower than 10 m s⁻¹ and net heat flux higher than -100 W m⁻² (i.e. positive or weakly negative) during at least 24 hours, the time scales needed to develop stratifying buoyancy flux from MLEs (Boccaletti *et al.*, 2007). The stratifying buoyancy flux, which competes with surface cooling and winds, is proportional to $(b_y H)^2 / f$ where b_y is the horizontal buoyancy gradient, H is the mixed layer depth and f is the Coriolis frequency. The wind and heat flux threshold used in this study are typical values allowing restratification by lateral buoyancy flux in the Iceland basin ($H = 300m$, $b_y = -0.3x10^{-7}s^{-2}$ and $f = 1.28x10^{-4}s^{-1}$). However, similar conditions were observed across most of the subpolar gyre, with the westward shallowing of the mixed layer depth compensated by increasing horizontal gradients (Mahadevan *et al.*, 2012). Therefore, we used the same thresholds across the whole subpolar gyre to define calm periods. Figure 18 shows an example of the wind and heat flux intermittency at a given location (55°N -40°W). Numerous data points fall below the atmospheric thresholds defined above (orange dots) during both winters 2014 and 2015. This example shows that calm periods (at least two consecutive data points) are frequent and intermittent in winter in the subpolar gyre. The probability to have calm periods during both winters 2014 and 2015 is the total duration of calm periods divided by total duration of the period of observation (180 days).

Sea state derived from BGC-Argo floats

A profiling float uses a pump to regulate his buoyancy so that it controls its ascent to the surface. From 10 m depth to the surface, the pump is off and the float is supposed to reach the surface under its own momentum. After 600 seconds, if the float does not reach the surface, the pump is reactivated.
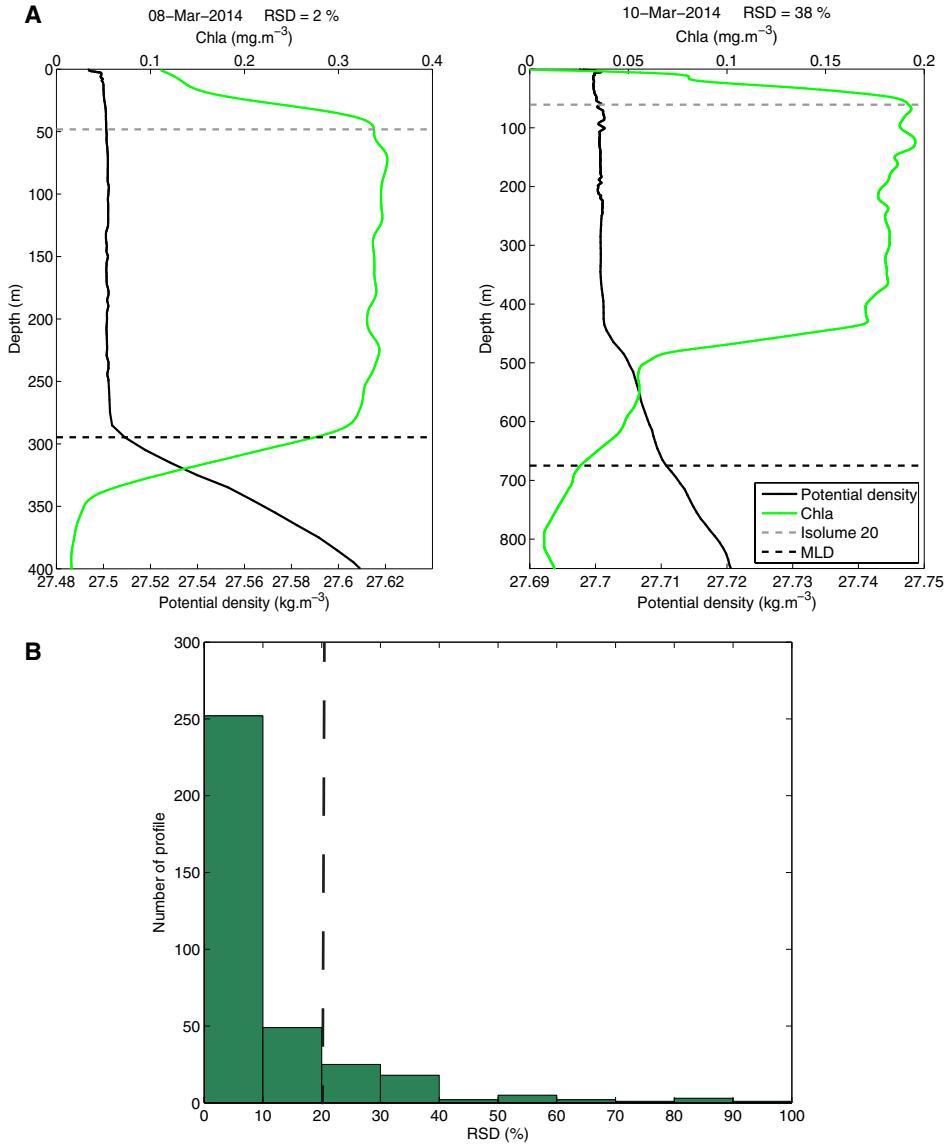
Figure. 17. Quality control of the mixed layer depth (MLD) estimation using Chla profiles. (A) Examples of a good MLD estimation (RSD = 2%, left panel) and a bad MLD estimation (RSD = 38%, right panel). Dashed grey line marks the isolume 20 μmol photons m^{-2} s^{-1} and black dashed line marks the MLD. (B) All winter profiles with RSD > 20% (57 profiles) were removed from the analysis.

The time spend during the ascent, between 10 m and the surface, where the pump is off, is well correlated with maximum wave height (Fig. 19). This proxy of the sea state is used in the North Atlantic Subpolar Gyre as an independent estimation of the frequency of calm periods with a flat sea (ascent time < 100 s) (method developed by Antoine Poteau). Note that this calm period estimation is only based on sea state and is not related to the restratification mechanism as above.

Light model

A radiative transfer model (Morel, 1991), was used to assess daily-integrated PAR along the float trajectory. This model takes into account the water vapor content (which can reduces PAR up to 0.7% when the sun is at zenith), the total ozone content (up to 1%) and the tropospheric aerosol load (up to 6%). However, the more crucial effect of the cloud cover is not taken into account in this so-
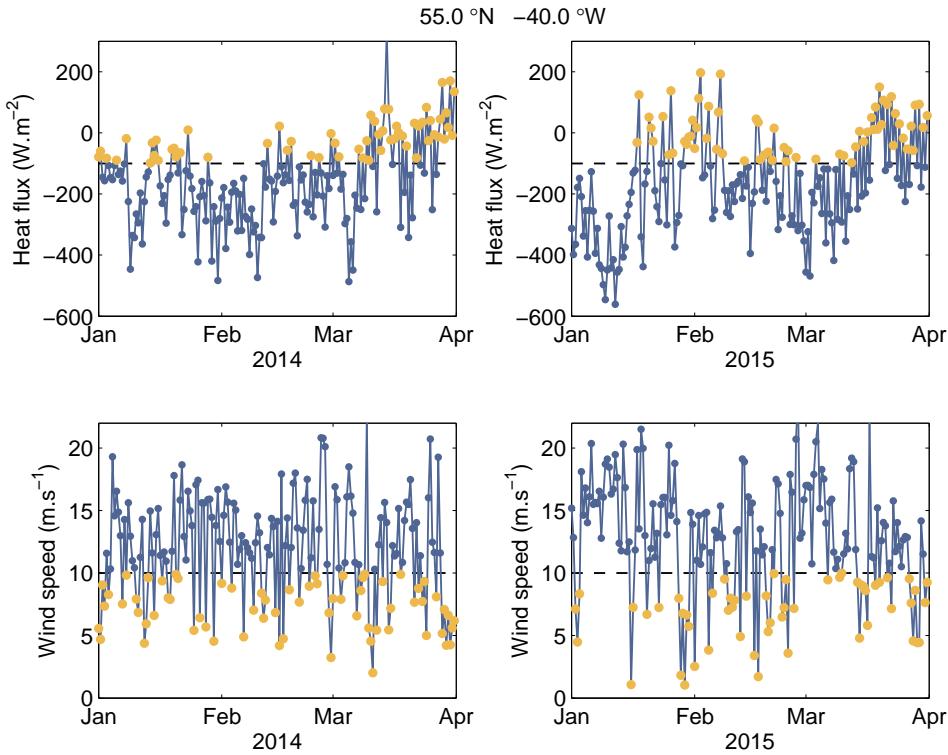
Figure. 18. Wind and heat flux intermittency at 55°N -40°W during the winters 2014 and 2015. 12h-averaged wind speed and heat flux < 10 m s^{-1} and > -100 W m^{-2} respectively are marked in orange.

called "clear sky" model. The transmission across the air-water interface is separately computed for the diffuse light component using a constant reflectance (6.6%) and for the direct component using a sun-altitude dependent reflectance. The modeled instantaneous PAR (iPAR) just below the surface is propagated through the water column using a diffuse attenuation coefficient derived from the Chla profile measured by the float (Gordon et Morel, 1983; KIRK, 1984). By comparing the clear sky iPAR profile with the float iPAR profile, the light attenuation due to the cloud cover can be estimated (Fig. 20). The median, over the vertical profile, of the ratio of float iPAR to clear sky iPAR gives a correction factor which quantifies the average light attenuation due to cloud cover during the float ascent (cloud cover is not necessarily stable, see Fig. 20). To avoid any potential bias due to dark signal at depth, the median is computed only in the upper layer where iPAR > 5 μmol photons m^{-2} s^{-1}. Assuming that the average cloud cover estimated during float ascent is representative of the entire day, this correction factor is subsequently applied to all the modeled profiles of the day (time increment 1/60th of the day length). The integration of all these cloud-corrected modeled iPAR profiles over the day length gives an estimate of daily-integrated PAR (in mol photons m^{-2}). The surface daily-integrated PAR used in this study is the first value recorded below the sea surface. In the main text, the term cloudiness refers to the correction factor (i.e. the attenuation of light). The modeled daily-integrated PAR profile is used to estimate Ze, the depth to which the euphotic zone extends. Ze is here defined as the depth of the 0.1 mol photons m^{-2} isolume, a light threshold adapted to subarctic species (Geider *et al.*, 1986; Smetacek et Passow, 1990). The modeled daily-integrated PAR profile is also used to calculate the average PAR in the mixed layer (PAR$_{ML}$).
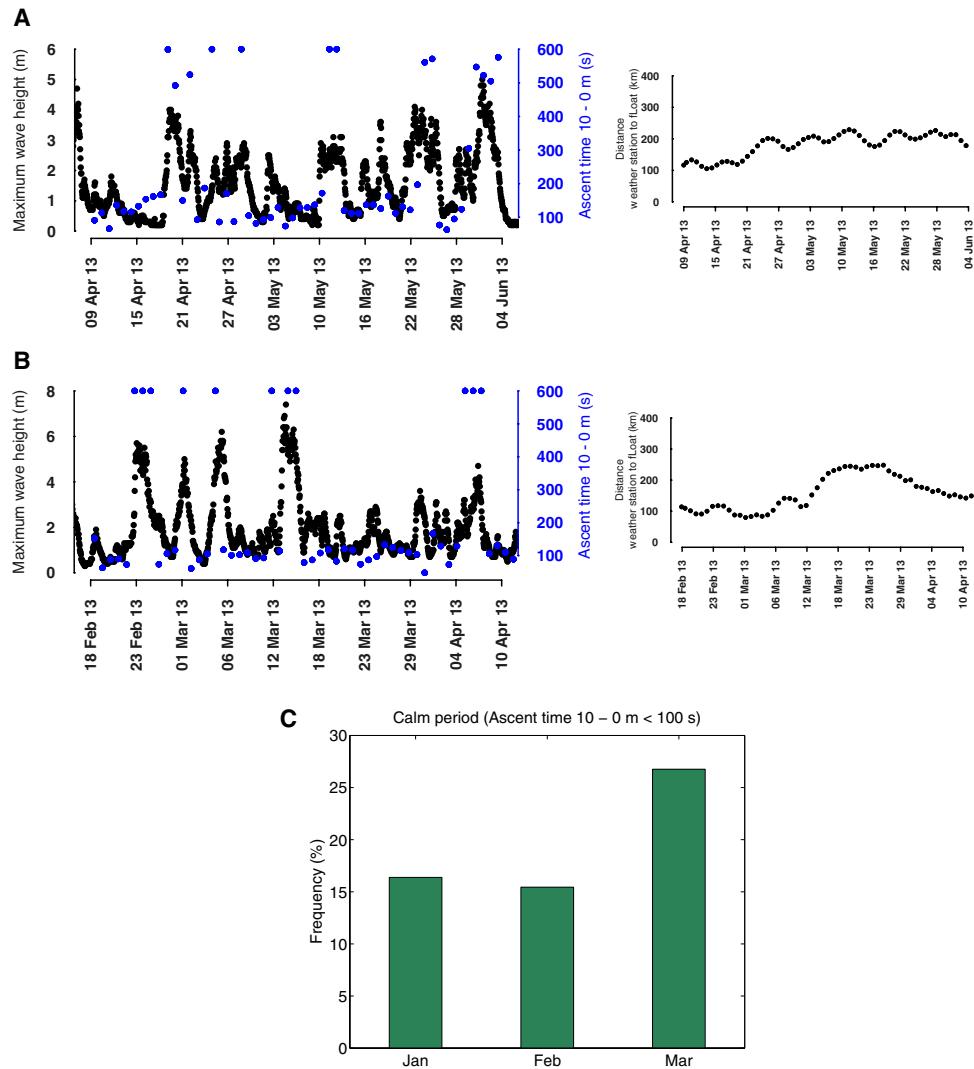
Figure. 19. Sea state estimation from BGC-Argo float profiles. Comparison of ascent time and maximum wave height for 2 BGC-Argo floats near weather station LION (A) and weather station COTE d'AZUR (B) in the North-western Mediterranean Sea. Distances between weather stations and floats are shown on the right. (C) Frequency of calm periods (ascent time 10 – 0 m < 100 s) for the 301 BGC-Argo float profiles in the subpolar gyre.

Optical community index

A simple optical community index (CI) was used to assess changes in phytoplankton community composition. Cetinić *et al.* (2015) have shown that high and low Chla fluorescence to b_{bp} ratio was correlated with diatom- and pico-nanophytoplankton-dominated communities, respectively. They chose to use Chla fluorescence (volt) and not calibrated Chla (mg m^{-3}) to homogenize their dataset which came from different platforms (with different sensors). In the present study, the optical community index was calculated with Chla and b_{bp} calibrated in the same way for all the BGC-Argo fleet used. Thus, the use of Chla instead of Chla fluorescence does not affect the interpretation of the optical index. CI was calculated as the ratio of MLD integrated values. It ranged from 50 to 1600 mg m^{-2}. For clarity, the ratio has been normalized by the minimum and the maximum value of the dataset so that the optical community index ranges from 0 to 1. The maximum of the ratio reached 60% of the
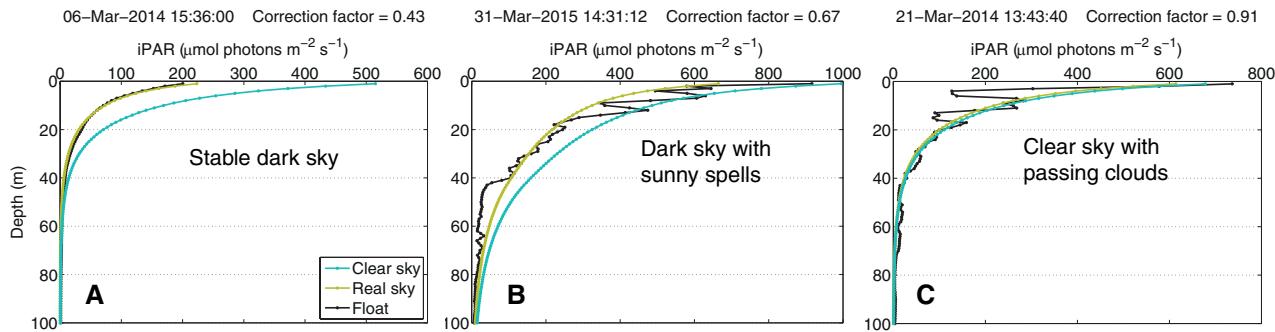
Figure. 20. Three examples of the impact of the cloud cover on the instantaneous photosynthetically available radiation (iPAR). Blue line is the modeled clear sky iPAR profile. Black line is the iPAR profile measured by BGC-Argo floats. Yellow line is the corrected modeled iPAR profile. The correction factor (see in tittle) describes the average light attenuation due to the cloud cover during the float ascent. A stable dark sky reduces the light level by 67% (A). A partly cloudy sky with sunny spells reduces by 33% on average (B). A clear sky with few passing clouds reduces by only 9% on average (C).

average value, recorded by floats in different location of the subpolar gyre, at the peak of the spring bloom when diatoms are dominant. However, at the peak of the spring bloom, the Chla to b_{bp} ratio is boosted due to physiological adaptation to silicate limitation, as shown by Cetinić *et al.* (2015) (their figure 6). In their study, 60% of the value of Chla fluorescence to b_{bp} ratio at the peak of the spring bloom ($\sim$150 V m) gives a ratio of $\sim$90 V m which corresponds to a fraction of diatom cell carbon to total autotrophic cell carbon of 40-60%. We conclude that a community index close to 1 indicates a large contribution of diatoms to the community whereas index close to 0 indicates a dominance of the pico- and nanophytoplankton.

Pigment analysis

High Performance Liquid Chromatography (HPLC) pigment data were acquired during the CATCH (Couplage avec l'Atmosphère en Conditions Hivernales) experiment (Eymard *et al.*, 1999) which took place in the Newfoundland Basin in January-February 1997 (37 stations coupled with CTD measurements). Diagnostic pigment (DP) analysis was used to explore patterns of dominance among phytoplankton assemblages (Vidussi *et al.*, 2001). DP is the sum of seven depth-integrated pigments (Table 1) :

$$BP_{pico} = \frac{Zea + Tchlb}{DP}$$

$$BP_{nano} = \frac{Allo + 19'HF + 19'BF}{DP}$$

$$BP_{micro} = \frac{Fuco + Peri}{DP}$$

where the subscripts pico, nano and micro refer to picophytoplankton (<2 μm), nanophytoplankton (2-20 μm) and microphytoplankton (20-200 μm). The use of this method allowed us to investigate the role of mixing intermittency on the community structure as a whole and not only on diatoms abundance.

Table. 1. Taxonomic pigments (modified from Vidussi *et al.* (2001))

Pigments	Abbreviations	Taxonomic significance	Size (µm)
Zeaxanthin	Zea	Cyanobacteria and prochlorophytes	< 2
Chlorophyll b+Divinylchlorophyll b	Tchl b	Green flagellates and prochlorophytes	< 2
Hexanoyloxyfucoxanthin	19'HF	Chromophytes nanoflagellates	2-20
Butanoyloxyfucoxanthin	19'BF	Chromophytes nanoflagellates	2-20
Alloxanthin	Allo	Cryptophytes	2-20
Fucoxanthin	Fuco	Diatoms	>20
Peridinin	Peri	Dinoflagellates	>20

3.4 Article : *Unexpected winter phytoplankton blooms in the North Atlantic Subpolar Gyre* (soumis à *Nature Geoscience*)

Authors : L. Lacour[1*], M. Ardyna[1], K. Stec[2], H. Claustre[1], L. Prieur[1], M. Ribera D'Alcala[2], D. Iudicone[2]

Affiliations : [1]Sorbonne Universités, UPMC Univ Paris 06, CNRS, Laboratoire d'Océanographie de Villefranche (LOV), Observatoire Océanologique, 06230 Villefranche-sur-mer, France
[2]Laboratory of Ecology and Evolution of Plankton, Stazione Zoologica Anton Dohrn, Naples, Italy

[*]Correspondence to : leo.lacour@obs-vlfr.fr

In mid- and high-latitude oceans, it has been traditionally recognized that winter conditions are unfavorable for phytoplankton growth. Strong winter surface cooling and winds drive turbulent mixing, moving phytoplankton over several hundred meters, mostly well below the sunlit layer (D'Asaro, 2008). Combined with low solar radiation, such unfavorable conditions drastically limit phytoplankton growth, especially species involved in seeding the spring bloom, the main marine annual biological event (Riley, 1942; Sverdrup, 1953). Here, using a new generation of autonomous profiling floats equipped with biogeochemical sensors, we reveal unexpected and widespread winter phytoplankton blooms in a large part of the North Atlantic Subpolar Gyre. Such biological features are triggered by intermittent restratification of the mixed layer, favoring locally a phytoplankton community shift from pico- and nanophytoplankton to microphytoplankton, mainly phototrophic diatoms. These transient blooms may have major implications for the successful overwintering of diatoms relevant to the subsequent spring bloom. The evidence of active diatoms in winter challenges current views on life strategies and contribute to better understand the mechanisms driving the spring bloom variability.

For decades, the community adopted the Sverdrup paradigm (Sverdrup, 1953) which postulates that deep winter mixing prevents phytoplankton biomass accumulation since losses exceed light-limited production. However, few wintertime in situ observations revealed significant phytoplankton stock in deep mixed layer (Backhaus *et al.*, 2003; Dale *et al.*, 1999). Based on modeling simulations, orbital motions triggered by deep convection have been suggested to allow recurrent incursions of phytoplankton to the lighted layer, and thus supporting a winter production (Große *et al.*, 2015). Furthermore, winter deepening of the mixed layer would dilute plankton concentration, thus reducing grazing pressure, and consequently, phytoplankton loss (disturbance-recovery hypothesis; Behrenfeld (2010); Behrenfeld *et al.* (2013)). Despite low phytoplankton growth, biomass may accumulate throughout winter in deep mixed layers.

Modelling studies have shown that mixed layer eddies (MLEs) growing from horizontal density gradients can generate vertical restratification of the mixed layer at spatial scales of 1-10 km and time scales of days (Boccaletti *et al.*, 2007; Fox-Kemper *et al.*, 2008), thus allowing patchy blooms to be initiated before the vernal stratification (Mahadevan *et al.*, 2012). MLEs being potentially much frequent in winter (Callies *et al.*, 2015), such restratification mechanism may provide an additional mechanism to winter phytoplankton growth.

The common view that the North Atlantic subpolar ocean is continuously deeply mixed in winter is challenged. Indeed, around 25% of the Argo density profiles were stratified (mixed layer depth (MLD) < 100 m) during the winters of 2014 and 2015 (Fig. 21A and Fig. 24). The vertical stratification was particularly strong in areas of significant horizontal density gradients (Fig. 21B), suggesting the potential role of MLEs. MLEs drive net horizontal transfer of lighter water above heavier water that can locally stratify the mixed layer. Similar temperature and salinity structure (i.e. Turner angle; Johnson *et al.* (2016)) between horizontal and vertical density gradients in the subpolar gyre (Fig. 21C) confirm the crucial role of lateral processes in restratifying the deep winter mixed layer in the North Atlantic Subpolar Gyre.

Restratification mechanisms compete with vertical mixing induced mainly by surface wind and cooling (Mahadevan *et al.*, 2012). Thus, restratification events require sufficiently long calm periods with a relaxation of this atmospheric forcing. While analysing wind speed and heat fluxes, we observed that some regions of the subpolar gyre presented up to 30% of calm periods with strong intermittency (Fig. 21D and Fig. 18). A proxy of the sea state (i.e. wave height), derived from BGC-Argo floats, also confirmed evidence of calm periods (i.e. 20% of the winter profiles, Fig. 19). Therefore, transient calm periods appear to be frequent across the North Atlantic Subpolar Gyre, allowing restratification to be a recurrent feature in winter.

As observed locally in the Icelandic basin in early spring (Mahadevan *et al.*, 2012), such restratification events triggered winter phytoplankton accumulations in the surface layer (i.e. blooms) in the whole subpolar gyre (based on both chlorophyll *a* (Chla) and particulate optical backscattering (b_{bp}); Fig. 22). These restratification events maintain phytoplankton cells in the euphotic zone (surface to Ze; see Fig. 22B), enhancing the light availability for their growth. Indeed, the light level (i.e. the average Photosynthetically Available Radiation (PAR) over the MLD) increased ten-fold in average
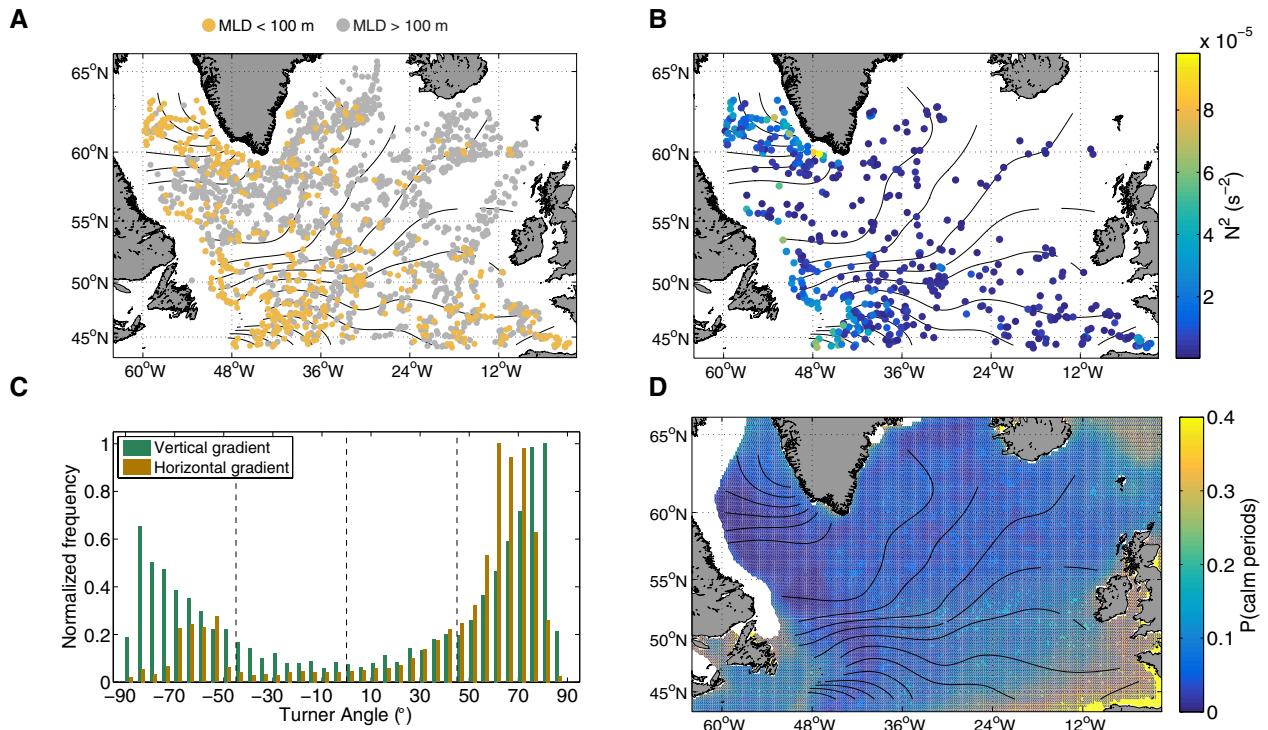
Figure. 21. Winter physical intermittency in the North Atlantic Subpolar Gyre. (A) 2022 Argo float profiles (January-March 2014-2015). Orange dots mark the location of stratified profiles (MLD < 100 m) and grey dots mark the deep mixed profiles (MLD > 100 m). (B) Stratification intensity (average value of N^2 between 5 and 100 m) of profiles with MLD < 100 m. (C) Frequency distribution of Turner angle for horizontal (orange) and vertical (green) density gradients. Each distribution is normalized by its maximum frequency. Vertical dashed lines mark angle 0°, where both temperature and salinity contribute equally to the density gradient, and angle -45° and 45° where salinity and temperature respectively are the only contributor. Angles > 45° or < -45° indicate that salinity is working against temperature and vice versa. D) Probability to have calm periods lasting at least 24 hours during January-March 2014-2015. A calm period is defined as a > 24 hour period with wind speed < 10 m s^{-1} and net heat flux > -100 W m^{-2}. White pixels indicate the presence of sea ice. Black lines in (A), (B) and (D) denote contours of surface density (contour interval of 0.1 kg m^{-3}).

in stratified conditions (MLD < 100 m; 1.3 mol photons m^{-2}) compared to deeply mixed conditions (MLD > 100 m; 0.13 mol photons m^{-2}, see an example in Fig. 27). These observations suggest that calm periods lasted long enough to initiate locally transient winter phytoplankton blooms.

Importantly, distinct light environments between stratified and deeply mixed conditions impacted not only phytoplankton production but also the structure of the community (Litchman, 2000; Walter *et al.*, 2015). An optical community index (Chla to b$_{bp}$ ratio, Cetinić *et al.* (2015)) derived from BGC-Argo float measurements, revealed a clear shift in the phytoplankton community structure during restratification events. In typical winter conditions (i.e. deep mixed layers with low surface daily-integrated PAR), pico- and nanophytoplankton clearly dominated the overall phytoplankton community in the subpolar gyre (Fig. 23A). By contrast, the proportion of diatoms temporarily increases during transient restratification events when their growth was evidently boosted by more favourable light conditions (Fig. 23A, B and Fig. 27). These Sverdrup-like blooms became particularly frequent in late February and March (10-25% of the all profiles, n = 30, Fig. 23B), when frequency of restratifi-

A
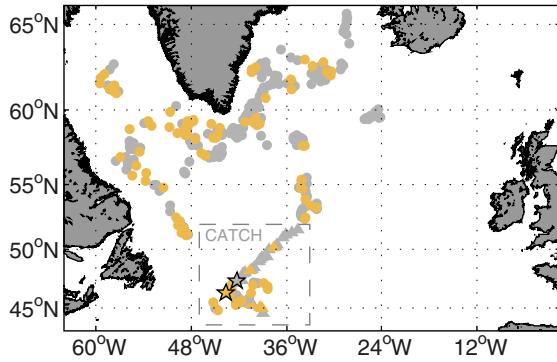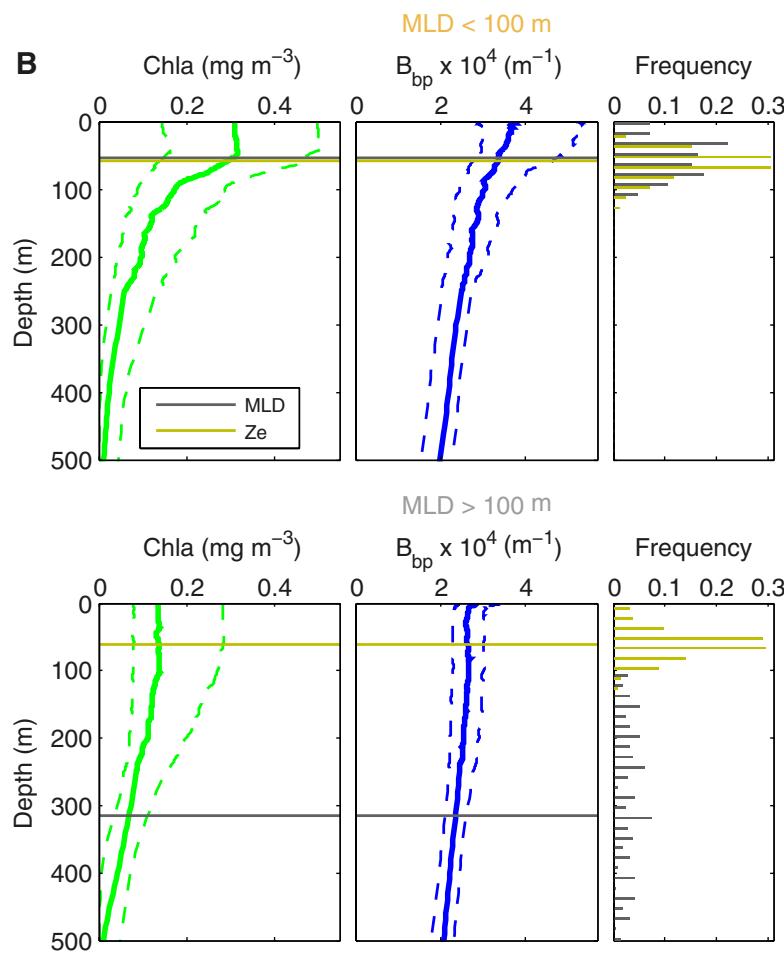
Figure. 22. Winter phytoplankton blooms in the North Atlantic Subpolar Gyre. (A) Location of the 301 BGC-Argo float profiles (dots, January-March 2014-2015) and the 37 pigment profiles from the CATCH cruise (triangles, January-February 1997). Orange symbols indicate stratified profiles (MLD < 100 m, 35% of the profiles, including CATCH profiles) and grey symbols indicate deep mixed profiles (MLD > 100 m). The dashed rectangle delineates the study area for the CATCH expedition. Stars indicate the location of the pigment profiles shown in Fig. 28A. (B) Median profile and quartiles of chlorophyll a (Chla) and backscattering (b_{bp}) from BGC-Argo floats shown in (A), for MLD < 100 m (top) and MLD > 100 m (bottom). Every single Chla and b_{bp} profile is shown in SM fig. S7. Horizontal grey and yellow lines indicate the median MLD and euphotic depth (Ze) respectively. Ze is defined as the depth of the 0.1 mol photons m^{-2} isolume. Panels on the right show the frequency distribution of MLD (grey) and euphotic depth (yellow).

cation events increased (20-40% of the all profiles, n = 86) and surface PAR was higher due to longer daylength (Fig. 23C). Variation of the cloudiness (dot size in Fig. 23C) also reinforced the critical role of light level, and its impact on changing the community composition in winter. During calm periods with clear sky conditions, higher light levels significantly boosted the growth of diatoms (Fig. 23C). These findings have been confirmed independently by rare phytoplankton pigment samples collected during a winter cruise in the North Atlantic Subpolar Gyre (CATCH, January-February 1997). While deep mixing layers were dominated by pico- and nanophytoplankton (mainly small flagellates), mi-

crophytoplankton (mainly diatoms) became a relevant group reaching almost 40% of the community when MLD shoaled above 100 m (Fig. 28B).
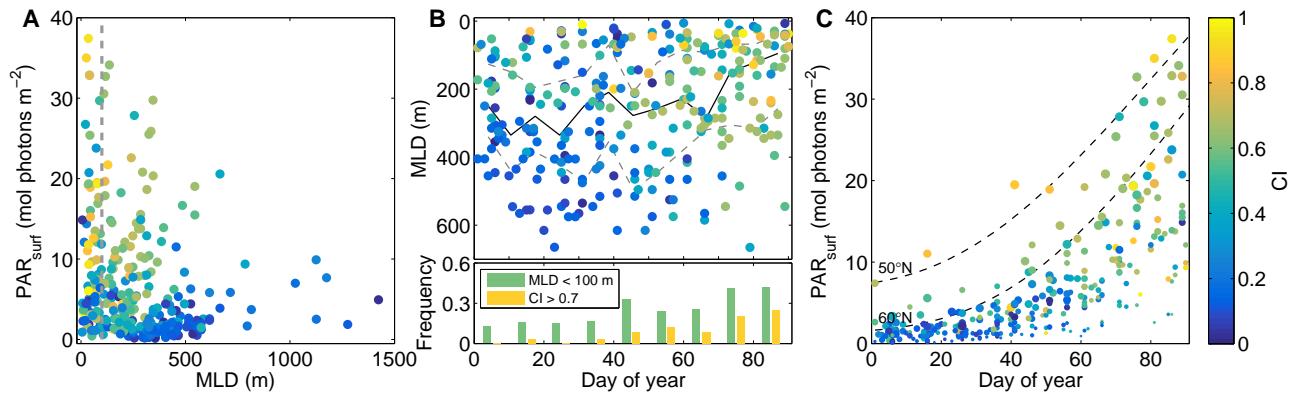

Figure. 23. The light environment impacts the phytoplankton community structure. Color scale denotes the optical community index CI (normalized chlorophyll *a* to backscattering ratio). CI close to 1 indicates a large contribution of diatoms to the community whereas CI close to 0 indicates a pico- and nanophytoplankton-dominated community. (A) Surface daily-integrated photosynthetically available radiation (PAR) and MLD derived from all BGC-Argo float profiles shown in Fig. 22A. Vertical dashed grey line marks 100 m depth. (B) MLD as function of day of year (from 1st January to 31 March, top). Black line represents the median MLD and dashed grey lines the quartiles. Frequency of stratified profiles (MLD < 100 m) and frequency of profiles with CI > 0.7 over a ten days period (bottom). (C) Surface daily-integrated PAR as function of day of year. Dot size denotes the cloudiness (large for clear sky and small for dark sky). Dashed black lines indicate temporal evolution of modeled clear sky surface PAR for two latitudes (50°N and 60°N).

Moderate to high light-adapted diatoms thriving in spring are not likely able to survive in deep winter mixed layers. A set of suitable overwintering strategies, e.g. formation of resting cells or spores (Smetacek, 1985; McQuoid et Hobson, 1996), have been pointed out to survive under harsh winter conditions. Here, we show that diatoms can remain physiologically active throughout winter by benefiting from transient restratification events and thus better light environments. By contrast, the persistence of small flagellates, and their dominance in deep mixing layers may be explained by mixotrophy, the combined used of phototrophy and heterotrophy within a single organism (Caron, 2016). The shift to heterotrophy during long period of darkness at depth could confer to these organisms a serious ecological advantage and bring an alternative hypothesis to the disturbance-recovery hypothesis (Behrenfeld, 2010; Behrenfeld *et al.*, 2013).

An extraordinary number of studies emerged during the last decade to understand the dynamics of the high-latitude spring bloom (i.e. timing and magnitude). However, the vigorous debate on spring bloom dynamics has remained mainly focused on physical controls of phytoplankton biomass accumulation. Our observations reveal that the physical environment plays a key role also in shaping the community structure during the preconditioning period of the spring bloom. Although transient winter blooms, supported by mixing intermittency, are not intense in term of biomass, they maintain an active diatom population throughout winter. Unlike resting cells or spores that require a germination period (Smayda et Mitchell-Innes, 1974), active winter diatoms can directly seed the spring bloom, hence impacting the bloom timing and potentially its magnitude.

Indeed, results of a parallel subpolar phytoplankton community model (SM S2.6) support the claim that intermittent winter stratification can affect spring bloom characteristics. Restratification events in winter boost diatom net growth rate (SM fig. S13), increasing the standing stock of diatoms towards spring. Mixing intermittency may increase by up to 2 fold the bloom magnitude and bring the bloom peak timing forward by up to 19 days (SM fig. S15 and table S4). These results not only corroborate in situ observations (i.e. BGC-Argo and CATCH data) but further suggest a possible impact of winter mixing intermittency on the observed yet unexplained (Barton *et al.*, 2014) interannual variability of spring blooms.

Unexpected wintertime occurrence of diatom blooms in the subpolar gyre could also challenge our perception of the spring bloom-dependent carbon export. Alternation of stratification and deep mixing allows transient diatom blooms along with non-sinking particles and dissolved organic and inorganic carbon to be transferred rapidly to depth (the so-called mixed layer pump (Gardner *et al.*, 1995; Dall'Olmo et Mork, 2014)). Even though a single event transfers only a low carbon stock compared to the spring bloom, cumulative events over the winter months may contribute significantly to the annual carbon export.

3.5 Résultats et discussion supplémentaires

(extrait du matériel supplémentaire de l'article présenté à la section précédente)

Historical Argo analysis

Historical MLD estimation (criteria 0.01 kg.m^{-3}) was obtained from the Argo database for a period 1995-2010 (de Boyer Montégut *et al.*, 2004). Within pixels of 9x6 degrees, we calculated for each year and each month the probability that MLD was lower than 100 m. Figure 24 shows the median probability (period 1995-2010) for January, February and March. This figure gives an historical context to demonstrate that observations made in winters 2014 and 2015 by Argo and BGC-Argo floats (Fig. 21A and 22A) are not peculiarities of these specific years.

Main drivers of optical community index variability

For assessing potential sources of variability in the community index, a Principal Component Analysis (PCA) was performed on 344 BGC-Argo float profiles (Fig. 25A). Input parameters were daily-integrated surface PAR (PAR), mixed layer depth (MLD), mean surface 0 – 20 m salinity (SAL), mean surface colored dissolved organic matter (CDOM) and optical community index (CI). Prior to analysis, these parameters were standardized by subtracting the mean and dividing by the standard deviation. Together, principal component 1 and 2 explain 73% of the variance. CI is well positively correlated with surface PAR and in a lesser extent negatively correlated with MLD. Stations with high CI show high loading on PAR and stations with low CI show high loading on MLD and SAL/CDOM (negatively correlated). A hierarchical clustering analysis allowed us to define 3 main groups (Fig. 25B and C). Cluster 3 is characterized by high surface PAR and shallow MLD, cluster 2 by deep MLD and low surface PAR and cluster 1 by low salinity and high CDOM. These last two variables allowed
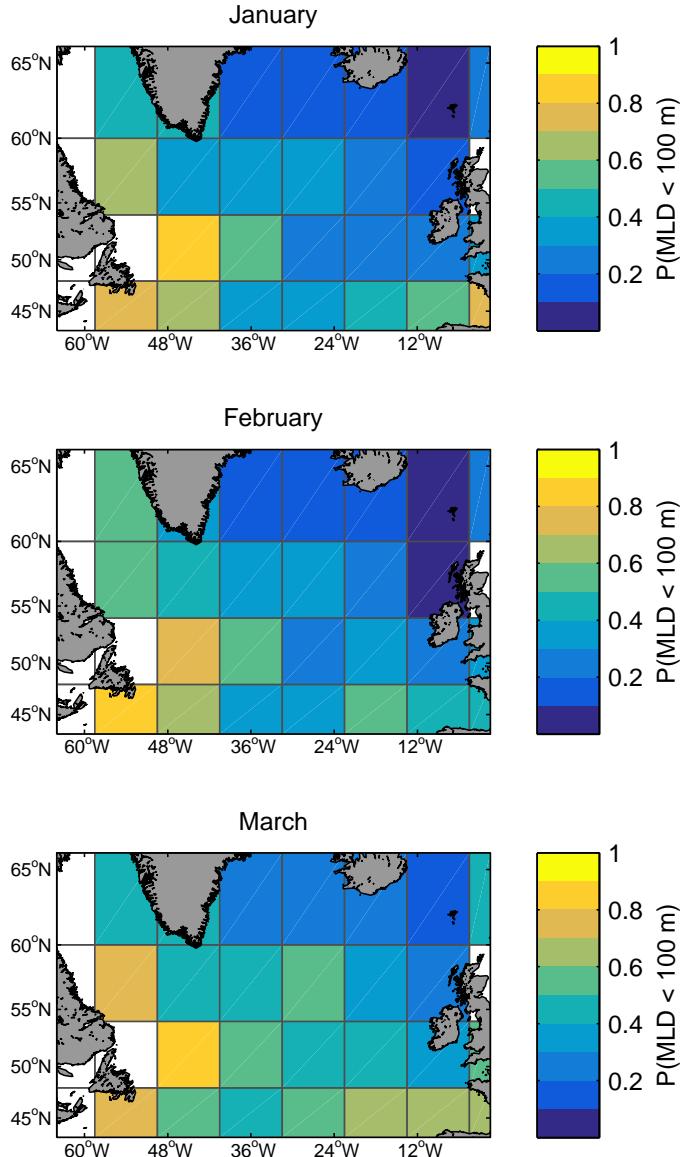
Figure. 24. Median probability that MLD was lower than 100 m for January, February and March in the North Atlantic Subpolar Gyre.

us to identify stations influenced by terrigeneous inputs from the Arctic, as already shown in previous studies (Matsuoka *et al.*, 2014; Granskog *et al.*, 2015). Terrigeneous matter strongly increased the b_{bp} signal thus decreasing the CI (< 200 mg m^{-2}). This variability being not linked to changes in community composition, stations from this cluster 1 (shown in Fig. 25D) were removed from the analysis (43 stations).

Photoacclimation

Chla is not simply a measure of phytoplankton biomass, but varies as a response of physiological adaptation to changing light (i.e. photoacclimation) (Geider, 1987). Indeed, at global scale, the seasonal variability of Chla to b_{bp} ratio seems to be mainly driven by photoacclimation (Behrenfeld *et al.*, 2015). However, at local scale, over a limited temporal window (3 months), our results show that photoacclimation is not a dominant factor. Chla to b_{bp} ratio increases when light level increases which is opposite to a photoacclimation effect (Fig. 25A and Fig. 27A and B).
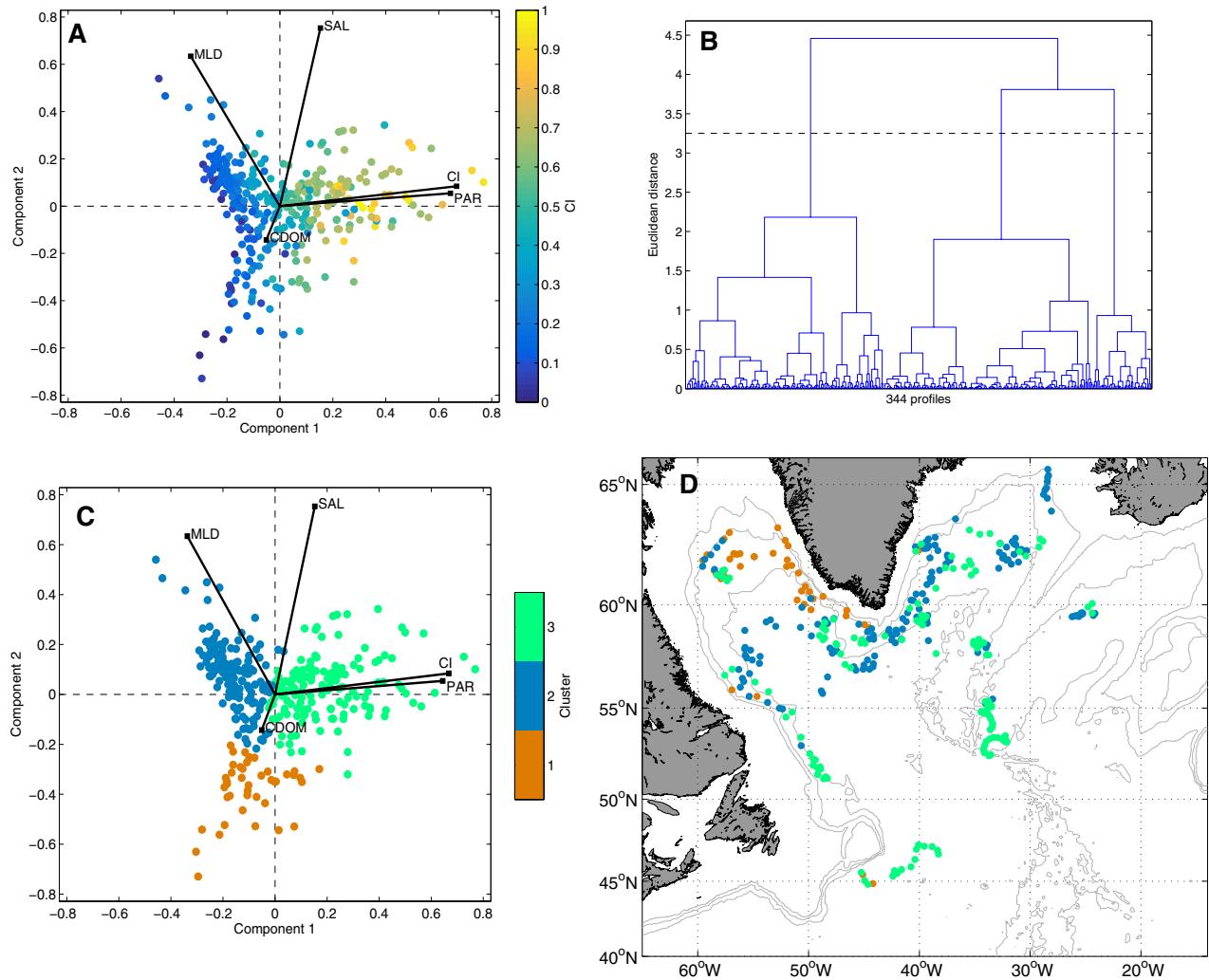
Figure. 25. Principal component analysis (PCA) applied on BGC-Argo float data (n=344). Input parameters are daily-integrated surface PAR (PAR), mixed layer depth (MLD), surface 0 - 20 m salinity (SAL), surface colored dissolved organic matter (CDOM) and optical community index (CI). Together, component 1 and 2 explain 73% of the variance. (A) Dots are color-coded by the community index. (B) A hierarchical cluster tree allows defining 3 clusters of stations. (C) Same as (A) but color-coded by the 3 clusters. (D) Location of the stations belonging to each cluster.

Light level / Light regime

The light level experienced by phytoplankton cells within an active mixed layer is not obvious to quantify. The average light in the MLD, used to estimate the light level, has clearly an influence on phytoplankton growth in such a way that it is frequently used to explain the bloom onset (Sverdrup, 1953; Siegel *et al.*, 2002; Lacour *et al.*, 2015). However, this descriptor shows only a weak correlation with the optical community index (Fig. 26), suggesting that average light in the MLD is not sufficient to characterize the light environment. The light regime (light/dark period), mainly controlled by the depth of the mixed layer relative to the depth of the euphotic zone (Ze), could also play a crucial role on the community composition (Fig. 27). Diatom growth is enhanced when cells are mixed in the euphotic layer (i.e. longer light period) as also evidenced by laboratory experiment (Walter *et al.*, 2015).
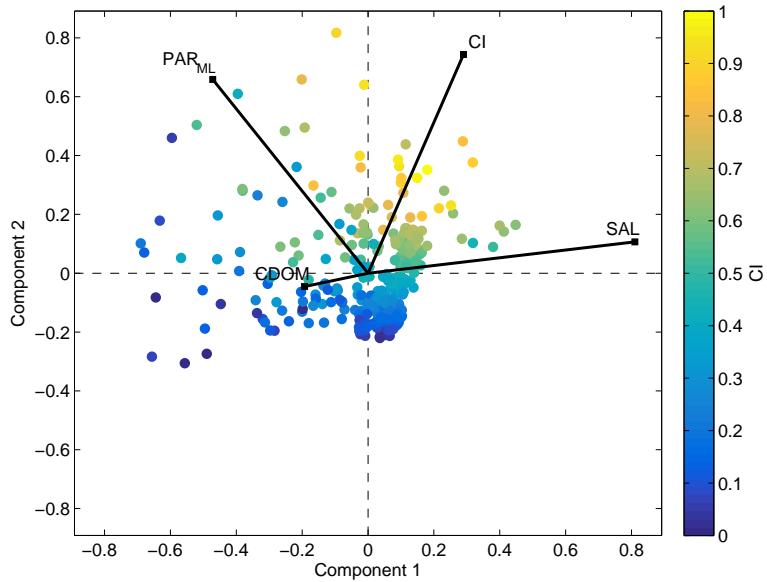
Figure. 26. Same as Fig. 25 with PAR_{ML} instead of MLD and PAR. Together, component 1 and 2 explain 77% of the variance.
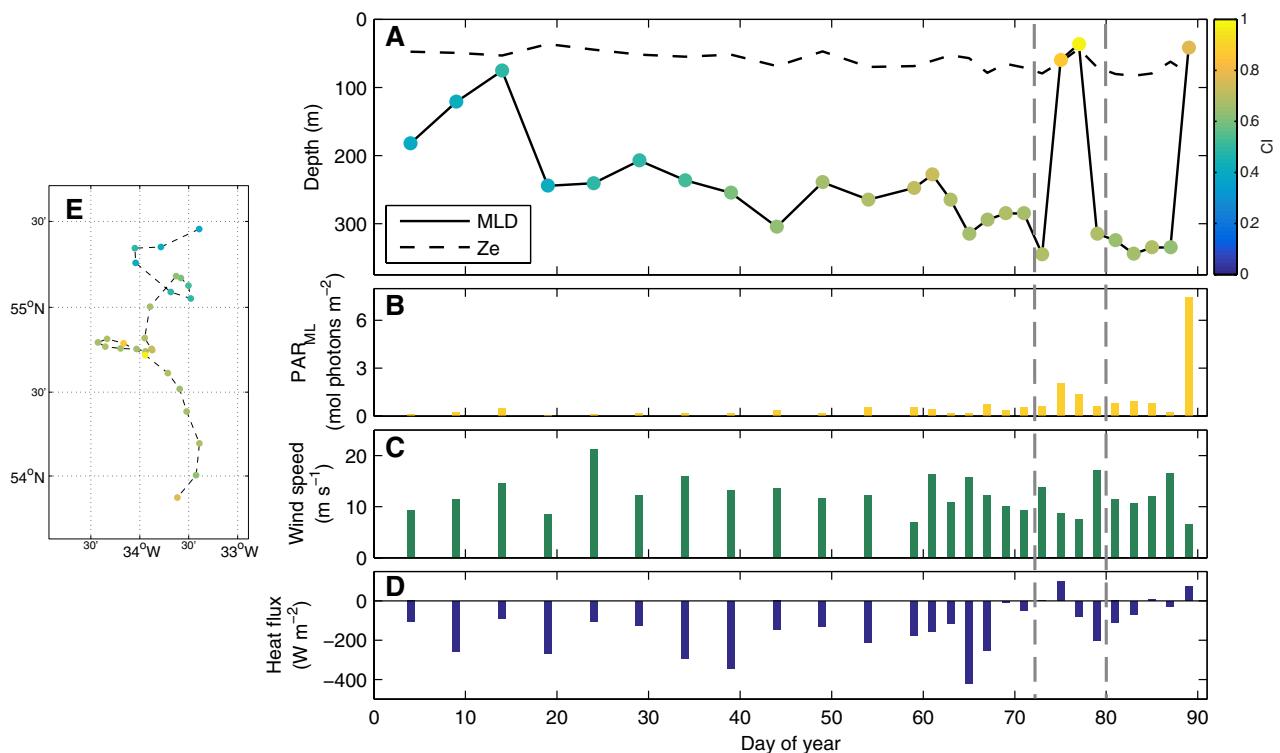
Figure. 27. A restratification event supported by a relaxation of the wind and heat flux in mid-March (∼day 75) induces a transient diatom bloom as evidenced by high community index (CI). (A) MLD and Ze along a BGC-Argo float trajectory, color-coded by CI. Match up of PARML (B), wind speed (C) and heat flux (D) at each surfacing of the float. (E) Trajectory of the float color-coded by CI.

CATCH expedition : HPLC validation

The CATCH expedition is one of the few midwinter survey carried out in the subpolar gyre with HPLC data available. The reason for the poor winter sampling in this region is evidenced by rough weather conditions suffered during the CATCH experiment. Strong storms with winds as high as 20 m s^{-1} were frequently recorded along the ship track. Even so, 25% of the wind measurements were lower than 10 m s^{-1} (Eymard *et al.*, 1999), which highlights the intermittency of the atmospheric forcing. The study area was characterised by strong horizontal density gradients due to the convergence of two contrasting waters, cold and fresh Labrador Sea water and warm and saline subtropical water. Numerous fronts and eddies were observed in this highly energetic region (Caniaux *et al.*, 2001). As a consequence, mixing length scale was highly intermittent and patchy with MLDs ranging from 20 to 800 m depth. Figure 28A shows two examples of all diagnostic pigment concentration profiles acquired within two-day interval, one in stratified conditions (MLD = 60 m) and one in deeply mixed conditions (MLD = 460 m). The concentration of diatoms (Fuco) clearly increases in the stratified case. However, in both cases, nanoflagellates (HF) concentration remains the highest. The depth of the mixed layer clearly impacts the biomass proportion of the nano- and microphytoplankton (Fig. 28B). The microphytoplankton abundance increases with MLD shallowing and reaches almost 40% of the community when MLD shoals above 100 m. The nanophytoplankton, identified as nanoflagellates, remain dominant in early winter whatever the depth of the mixed layer (50-70%). The picophytoplankton abundance ($\sim$20%, not shown) is almost unaffected by mixing, as also noted in the Iceland Basin (Paulsen *et al.*, 2015). Interestingly, before January 15th, the community structure appears to be not influenced by the MLD shallowing (grey dots in Fig. 28B). Especially, a critical light threshold could limit the diatom growth, even in shallow MLD. Based on this chemotaxonomic analysis, we confirm that short-term restratification of the water column affects not only the phytoplankton production but also the community structure, initiating transient diatom blooms, provided that daily-integrated surface PAR reaches a critical threshold.
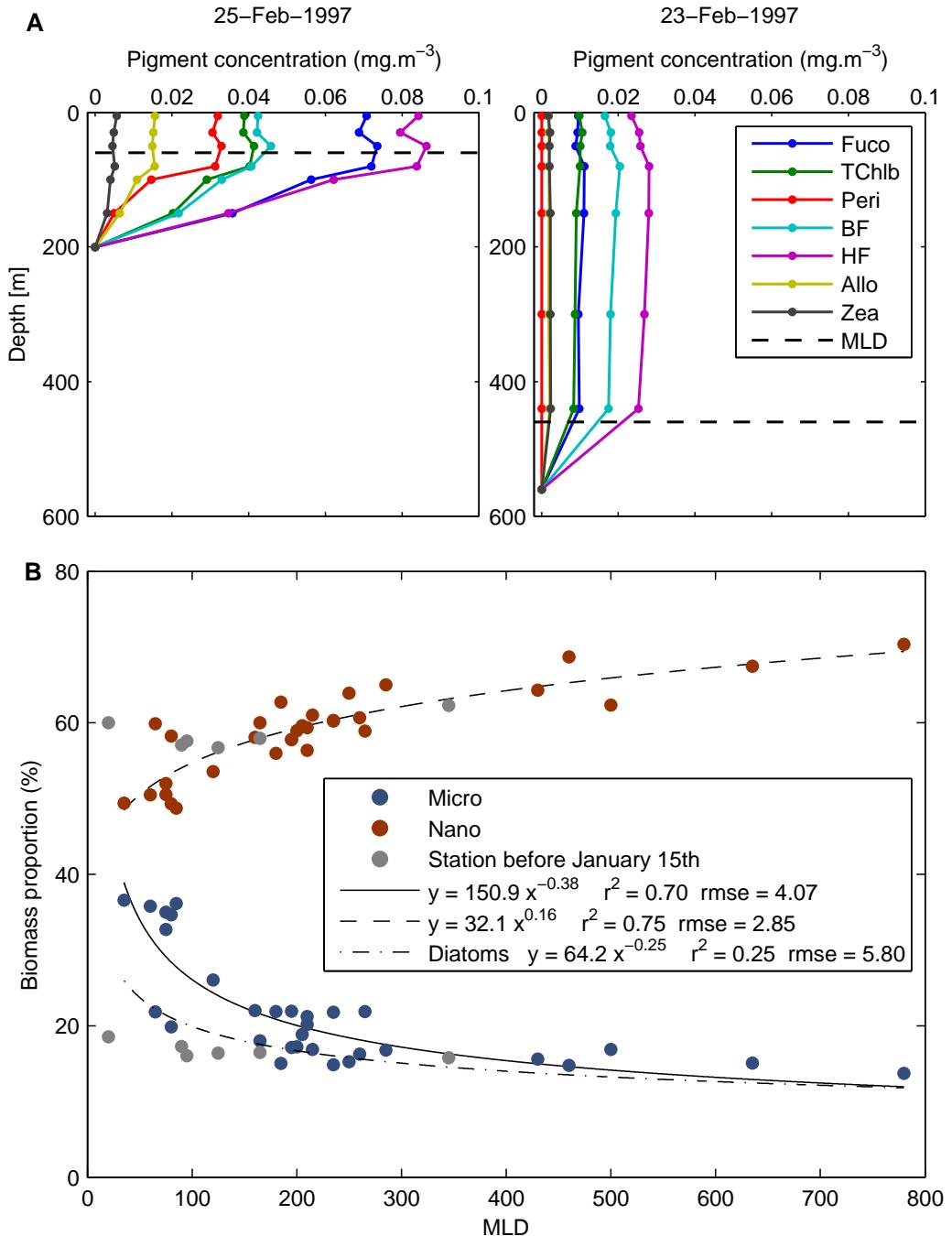
Figure. 28. Chemotaxonomic analysis from the CATCH expedition (January-February 1997), see location of the stations on Fig. 22A. (A) Examples of one stratified profile (left) and one deeply mixed profile (right) of pigment concentrations. The horizontal dashed black line marks the MLD. (B) Biomass proportion of nano- and microphytoplankton as function of MLD. Solid and dashed lines represent the best-fit power law function of the data excluding grey dots, which correspond to stations before January 15th (assumed to be extremely light limited). Dash-dot line represent the best-fit power law function of the proportion of diatoms (Fuco / DP).

3.6   Conclusion

Cette étude a démontré que des restratifications intermittentes et locales de la couche de mélange en hiver influencent la structure de la communauté phytoplanctonique en favorisant la croissance de diatomées. Le développement de blooms de diatomées en hiver n'a été confirmé, dans cette étude, que par un nombre limité de données de pigments récoltées dans une zone géographique restreinte. Les récentes campagnes NAAMES et Tara Arctique, qui se sont déroulées en début d'hiver dans le gyre subpolaire, ont déployé un "Imaging FlowCytobot" qui permet d'identifier et de quantifier les différentes espèces planctoniques présentes. Les premiers résultats confirment également la présence en quantité non négligeable de différentes espèces de diatomées de différentes tailles. Il serait intéressant de vérifier si les espèces qui se développent lors des blooms transitoires hivernaux sont les mêmes que celles impliquées dans le bloom printanier, ou si il s'agit d'espèces spécialement adaptées aux faibles conditions de lumière en hiver. Le modèle numérique utilisé dans cette étude a permis de simuler le comportement de 40 espèces de phytoplancton, dont 10 espèces de diatomées pendant la période hivernale et printanière. Bien que idéalisé, le modèle a démontré que les restratifications intermittentes de la couche de mélange en hiver favorisent le développement de certaines espèces de diatomées qui sont aussi présentes pendant le bloom printanier.

Quelque soit l'espèce de diatomée impliquée, ce groupe phytoplanctonique est connu pour sa participation active à l'export de carbone. Ces blooms transitoires de diatomées, très fréquents en fin d'hiver, ne pourraient-ils pas induire un export épisodique de carbone en profondeur ? L'intermittence du mélange ne pourrait-elle pas contribuer au transfert rapide de matière organique vers la zone mésopélagique ? Ces questions seront abordées dans le chapitre suivant.

CHAPITRE 4

Dynamique de la couche de mélange et export de carbone pendant la transition hiver-printemps

4.1 Introduction

L'écosystème mésopélagique, bien qu'étant l'un des plus vastes de la planète, est l'un des moins connus. Les premiers bilans ont montré que le budget du carbone dans cet écosystème n'est pas à l'équilibre (Steinberg *et al.*, 2008; Burd *et al.*, 2010; Giering *et al.*, 2014). Le flux entrant de carbone serait deux ordres de grandeur inférieur à la demande métabolique des organismes hétérotrophes (Giering *et al.*, 2014). Cependant, ces estimations souffrent d'un sous-échantillonnage évident. La plupart des observations sont restreintes en un lieu et un temps donné, généralement pendant le bloom printanier. Les sources de carbone alimentant l'écosystème mésopélagique en hiver, notamment, sont totalement méconnues. De même, la durée des observations est fortement limitée. Les événements épisodiques sont donc potentiellement non résolus.

La présence récurrente de blooms transitoires hivernaux (tels que décrits dans le chapitre précédent) pourrait constituer une source épisodique de carbone pour l'écosystème mésopélagique pendant une période considérée comme peu productive. Considérons alors les mécanismes pouvant potentiellement exporter en profondeur la matière produite pendant ces blooms. Les résultats du chapitre précédent ont montré que la proportion de microphytoplancton, notamment des diatomées, augmente significativement lors de ces blooms transitoires. Ces particules sont donc susceptibles de sédimenter, et ainsi de participer au flux descendant de carbone. La vitesse de sédimentation peut atteindre 10 m d^{-1} pour des diatomées sénescentes (Smayda, 1970) et de l'ordre de 100 m d^{-1} pour des agrégats (Villa-Alfageme *et al.*, 2016). Alternativement, le mélange convectif, encore actif à cette période, peut entrainer les particules à une vitesse de l'ordre de 1000 m d^{-1} (D'Asaro, 2008). C'est la raison pour laquelle nous nous sommes focalisé dans ce chapitre sur le rôle de la couche de mélange pour exporter de la matière organique en profondeur. L'intermittence du mélange en hiver et au début du printemps, caractérisée par l'alternance d'événements de convection et de restratification est un moteur potentiel à l'export de matière organique vers la zone mésopélagique.

Dans ce chapitre, nous explorerons la dynamique intra-saisonnière de la couche de mélange. Nous montrerons comment celle-ci induit un export épisodique de matière organique en profondeur. Enfin, nous discuterons du rôle potentiel de ces événements épisodiques sur le fonctionnement de l'écosystème mésopélagique.

4.2   Résumé de l'étude

La densité du réseau BGC-Argo a été exploitée pour étudier la dynamique intra-saisonnière de la couche de mélange. Nous avons utilisé un réseau de 14 flotteurs BGC-Argo déployés dans le gyre subpolaire de l'Atlantique Nord. Ces flotteurs ont réalisé 2126 profils de température, salinité, Chla et b_{bp} entre 2014 et 2016.

Cette étude repose sur la distinction entre une couche de mélange active (nommée couche turbulente par la suite) et une couche de mélange ayant été mélangée dans un passé proche. Nous avons estimé la profondeur de ces deux couches en se basant sur le gradient vertical maximal du profil de Chla et de densité. Le gradient maximal de densité (MLD_{dens}) correspond à la profondeur de la pycnocline saisonnière qui suit la profondeur maximale atteinte par la couche turbulente. En revanche, le gradient maximal de Chla (MLD_{bio}) correspond d'avantage à la profondeur de la couche turbulente, à l'échelle de temps caractéristique de la croissance du phytoplancton (1-2 jours, la variation diurne de la couche turbulente n'est donc pas résolue).

La dynamique de MLD_{bio} et MLD_{dens} est illustrée par la série temporelle d'un flotteur évoluant dans le bassin d'Islande en 2014. Comme attendu, MLD_{dens} varie à l'échelle saisonnière alors que MLD_{bio} varie à l'échelle intra-saisonnière. Pendant la transition hiver-printemps, MLD_{bio} oscille entre MLD_{dens}, pendant les événements de convection (flux de chaleur négatif), et la profondeur de la couche euphotique pendant les événements de stratification (flux de chaleur positif). La matière ainsi produite en surface lors des événements de stratification est ensuite exportée en profondeur par le mélange convectif. L'alternance entre mélange convectif et restratification est donc le mécanisme par lequel le carbone organique est pompé en profondeur. La différence entre MLD_{bio}, qui marque la profondeur d'un mélange récent, et MLD_{dens}, qui marque la profondeur d'un mélange passé, permet de délimiter une couche de mélange fossile ("remnant layer") qui contient la matière exportée par ce mécanisme. Cette signature est ensuite utilisée sur l'ensemble des profils du réseau BGC-Argo pour quantifier la fréquence et l'intensité des événements d'export. Les stocks de carbone exportés sont les plus élevés au début du printemps, quand le flux de chaleur passe de négatif à positif. Ces événements sont cependant très fréquents (~35%), jusqu'à 120 jours avant cette période et 30 jours après, et sont répartis sur l'ensemble du gyre subpolaire.

Le contenu en Chla de la matière organique présente dans la couche fossile est très élevé pendant la transition hiver-printemps, suggérant ainsi que la matière exportée est fraîche et donc potentiellement de bonne qualité nutritionnelle. La dynamique de la couche turbulente pourrait donc soutenir l'activité hétérotrophe dans la zone mésopélagique. La population de zooplancton notamment pourrait économiser de l'énergie en restant dans la couche fossile, peu turbulente, tout en bénéficiant d'un

apport intermittent de matière fraîche. Au contraire, durant le bloom printanier, la matière fraîche est limitée à la surface, ce qui contraint le zooplancton à migrer sur plusieurs centaines de mètres, même si certaines espèces, non migratrices, semblent se satisfaire de la matière qui sédimente. Les différents mécanismes d'export, entre la période de transition hiver-printemps et la période du bloom printanier, impliquent différentes stratégies d'alimentation. L'export de matière fraîche en fin d'hiver pourrait aussi initier le développement saisonnier du zooplancton, en dormance en profondeur, de sorte que leur période de reproduction coïncide avec le bloom printanier. Ainsi, la dynamique intra-saisonnière de la couche turbulente, à l'origine de l'export épisodique de matière organique, pourrait conditionner le fonctionnement de l'écosystème mésopélagique avec de possibles répercussions sur le bloom printanier.

4.3   Article : *Intra-seasonal dynamics of the mixed layer pump in the North Atlantic Subpolar Gyre : a BGC-Argo approach* (en préparation pour *Journal of Geophysical Research*)

Authors : L. Lacour[1*], H. Claustre[1], N. Briggs[1], M. Ardyna[1], G. Dall'Olmo[2]

Affiliations : [1]Sorbonne Universités, UPMC Univ Paris 06, CNRS, Laboratoire d'Océanographie de Villefranche (LOV), Observatoire Océanologique, 06230 Villefranche-sur-mer, France
[2]Plymouth Marine Laboratory, Plymouth, UK

[*]Correspondence to : leo.lacour@obs-vlfr.fr

Introduction

The export of organic matter from the surface to the ocean interior has traditionally been attributed to the biological pump (Sanders *et al.*, 2014). Mediated principally by the sinking of particulate organic carbon (POC), the biological pump at high latitudes is closely related to the spring phytoplankton bloom (Martin *et al.*, 2011). Large phytoplankton cells such as diatoms (> 20 μm) that thrive during the spring bloom contribute significantly to the downward carbon flux due to their high sinking rate (1 to 50 m d^{-1}, Villa-Alfageme *et al.* (2016)), and their ability to form large aggregates (Smetacek, 1985, 1999). Zooplankton play also a critical role, by repackaging organic matter into fecal pellets and enhancing the speed at which it sinks out of the euphotic zone (Turner, 2002, 2015). Furthermore, active transport of POC through the diurnal and seasonal migrations of zooplankton from the euphotic zone to the mesopelagic zone ($\sim$100-1,000 m) also contributes to the vertical transport of carbon into the deep ocean (Steinberg *et al.*, 2000; Jónasdóttir *et al.*, 2015). Up to 90% of the exported material may be consumed and remineralized back into dissolved organic carbon (DIC) by heterotrophic activity in the mesopelagic (Buesseler et Boyd, 2009). Finally, only $\sim$1% of the organic matter produced in the surface is sequestered for long term in the deep ocean (Ducklow *et al.*, 2001; Poulton *et al.*, 2006).

In complement to sinking flux, Lévy *et al.* (2001) and Omand *et al.* (2015) provided evidence that export of organic matter also occurs through localized (1-10 km) eddy-driven subduction of non-sinking particles, and possibly dissolved organic carbon (DOC). Such a submesoscale eddy-driven flux of POC may contribute to half of the total springtime export of POC from the subpolar oceans (Omand *et al.*, 2015). Through eddy-driven stratification, these submesoscale processes can also enhance the production of organic matter at the surface (Mahadevan *et al.*, 2012, Lacour et al., submitted) which will potentially be exported by subsequent eddy-driven subduction (Omand *et al.*, 2015). Submesoscale subduction leads to episodic injections of POC- and DOC-rich waters below the mixed layer, possibly outside the spring bloom period. Given that the current estimates of metabolic activity in the mesopelagic region exceed the influx of organic substrates generally attributed to the biological pump (Steinberg *et al.*, 2008; Burd *et al.*, 2010; Giering *et al.*, 2014), submesoscale subduction has been invoked as an alternate pathway to explain the missing factors in the balance of the carbon budget (Lévy *et al.*, 2001; Barth *et al.*, 2002; Omand *et al.*, 2015). The spatial heterogeneity of this process could stimulate hotspots of organic substrate that would likely be missed by conventional sampling methods.

Recently, Dall'Olmo et Mork (2014) and Giering *et al.* (2016) highlighted the potential impact of downward entrainment of organic matter by mixing, a process known as the mixed layer pump (ML pump) (Gardner *et al.*, 1995). A few localized studies first described this mechanism at the diurnal timescale, showing that alternation of night convection and daily restratification can lead to an entrainment-detrainment cycle of particles in the mixed layer (Woods et Onken, 1982; Ho et Marra, 1994; Gardner *et al.*, 1995). Indeed, the mixed layer deepens due to the effect of wind and heat loss to the atmosphere (Price *et al.*, 1986) but do not shoals, as commonly assumed for the sake of simplicity. Instead, the upper-ocean stratifies due to solar heating and eventually a new mixed layer re-forms from the surface (Ho et Marra, 1994), therefore isolating phytoplankton cells and other particles at depth (Fig. 29). At the diurnal timescale, the amplitude of the mixed layer depth (MLD) variation is small (Woods et Onken, 1982), so that exported stocks of particles by the ML pump are accordingly weak. However, others studies have investigated the impact of seasonal variations of MLD on the export of organic matter (Carlson *et al.*, 1994; Dall'Olmo et Mork, 2014; Dall'Olmo *et al.*, 2016). These authors have shown that winter deep convective mixing followed by spring stratification of the water column exports large amount of carbon as dissolved organic matter or small non-sinking particles. They concluded that the seasonal ML pump amounts on average to 23% of the carbon supplied by fast-sinking particles in high-latitude regions.

It is worth noting that the winter to spring evolution of MLD is not a smooth shoaling but is interspersed with restratification or shallow mixing events. Such intermittent mixing appears to enhance both phytoplankton production and POC export before the onset of the spring bloom (Bishop *et al.*, 1986; Garside et Garside, 1993; Koeve et Pollehne, 2002; Giering *et al.*, 2016, Lacour et al., submitted). In particular, Giering *et al.* (2016) have shown that the pre-bloom export rate of small particles by the ML pump was similar to the total particles export rate by sedimentation observed during, and after, the spring bloom period in the north-east Iceland basin. However, the analysis of long-term se-

diment trap data from 3000 m at the Porcupine Abyssal Plain (49°N, 16°W) revealed that pre-bloom deep flux rates are small (Lampitt *et al.*, 2010). This discrepancy suggests that most of the particulate material exported by the ML pump is consumed in the mesopelagic region (Giering *et al.*, 2016). Thus, this process may be less relevant to the long-term sequestration of carbon than for supplying energy to the mesopelagic food-web.
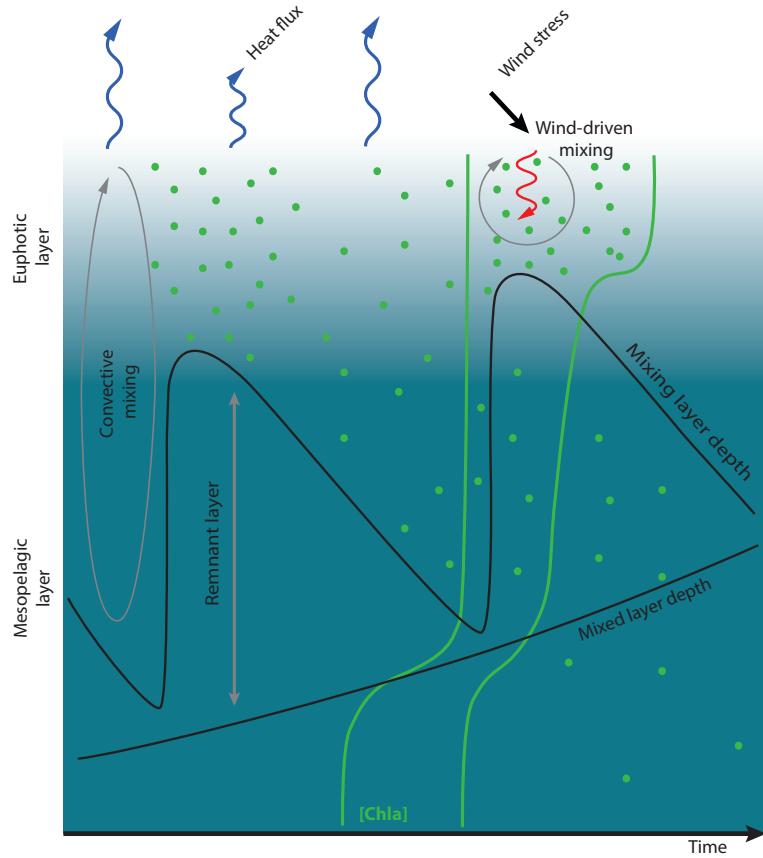
Figure. 29. Schematic of the mixed layer pump.

Despite the recent discoveries mentioned above, the intra-seasonal dynamics of the ML pump and its potential role in sustaining mesopelagic ecosystems remains poorly known. The reason is twofold. First, current methods to estimate the depth of the mixed layer are not appropriate. Brainerd *et al.* (1995) highlighted the importance in distinguishing the mixed layer, the zone of relatively homogenous water formed by the history of mixing, from the mixing layer, the zone in which mixing is currently active. They showed that current density-derived method failed to capture the high-frequency variability of the mixing layer. Second, most existing observational tools are not well suited to study such unpredictable episodic and widespread events. In the present study, using high-frequency sampling from a new generation of autonomous profiling floats equipped with bio-optical sensors, we investigate the intra-seasonal dynamics of the ML pump in the North Atlantic Subpolar Gyre. More specifically, we try to capture the frequency and intensity of episodic exports by the ML pump on a basin scale. We then discuss the importance of these events in supplying pulses of fresh organic substrate to the mesopelagic ecosystem.

Material and Methods

The BGC-Argo dataset : description and data processing

The data used in this study were acquired by a fleet of 14 BGC-Argo floats that were deployed in the North Atlantic subpolar gyre. These floats provided 2126 profiles spanning all seasons between 2014 and 2016 (Fig. 30). These floats (NKE PROVOR CTS-4) are equipped with : a SBE 41 CTD ; an ECO3 (Combined Three Channel Sensors) composed of a chlorophyll *a* (Chla) fluorometer, a Colored Dissolved Organic Matter (CDOM) fluorometer, and an optical backscattering sensor at 700 nm (b_{bp}) ; and an OCR-504 radiometer measuring Photosynthetically Available Radiation integrated over 400-700 nm (PAR). Measurements were collected during ascent every 2, 5 or 10 days, from 1,000 m (parking depth) to the surface. Vertical resolution of acquisition was 10 m between 1,000 m and 250 m, 1 m between 250 m and 10 m, and 0.2 m between 10 m and the surface. Radiometric measurements were acquired only in the upper 250 m. Data were transmitted through Iridium communication each time the floats surface, usually around local noon.
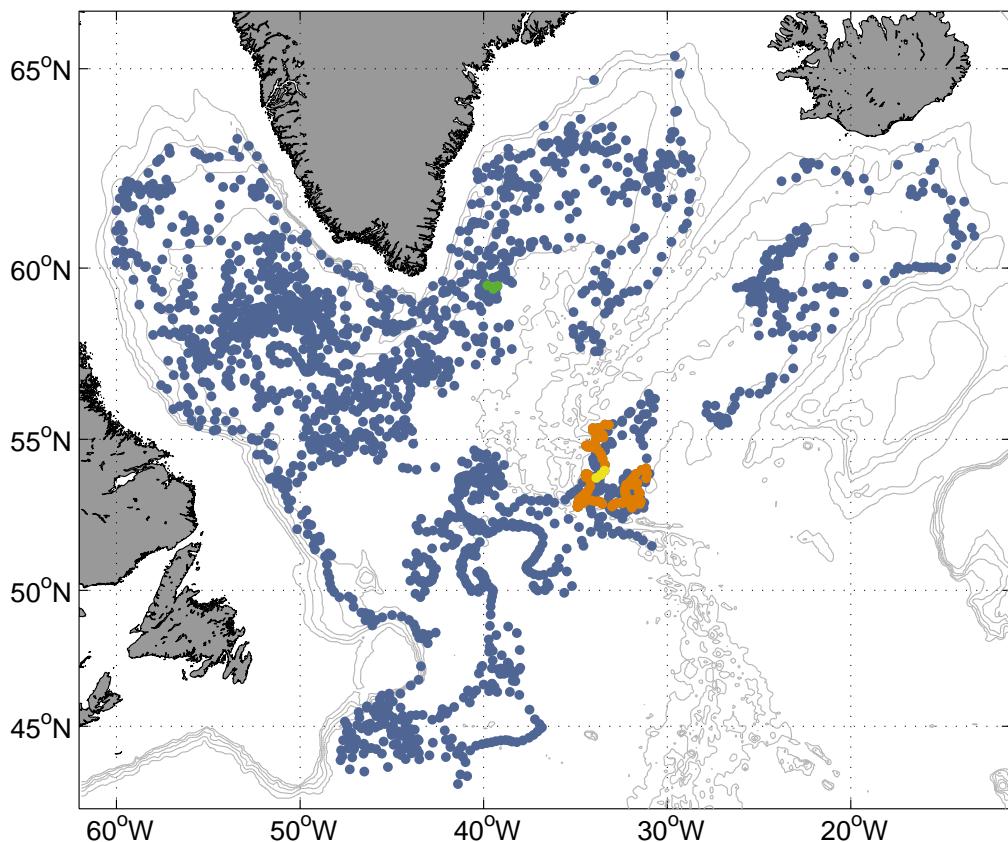

Figure. 30. Location of BGC-Argo float profiles in the North Atlantic subpolar gyre during 2014-2016. Orange dots indicate the location of float 22b trajectory (January-December 2014) shown in Fig. 33. Yellow and green dots indicate the location of profiles shown in Fig. 34a and 34b respectively.

A "real time" quality control procedure was performed on the CTD data (Wong *et al.*, 2015), Chla (Schmechtig *et al.*, 2014) and PAR measurements (Organelli *et al.*, 2016) after the factory calibration was applied. The instrumental dark signal was removed from the Chla profile following the method in Xing *et al.* (2011) and the non-photochemical quenching was corrected as follows : the maximum

Chla value above MLD, defined as a density difference of 0.01 kg m^{-3} with a reference value at 5 m, is extrapolated toward the surface. As an additional condition, the depth of the extrapolated Chla value have to be shallower than the depth of the isolume 20 μmol photons m^{-2} s^{-1} (derived from PAR profile), which marks the lower limit of the quenching effect. Optical spikes were removed from Chla and b_{bp} profiles using a 5-point running median filter and a 7-point running mean filter (Briggs *et al.*, 2011). The spike signals from b_{bp} profiles were used to detect large particles or aggregates following Briggs *et al.* (2011). Note that, because of the low vertical resolution sampling below 250 m, deep optical spikes are not well resolved which leads to a potential underestimation of large particles and aggregates. For the same reason, the depth correction for carbon loss relative to b_{bp} in aggregates used by (Briggs *et al.*, 2011) was not applied. Both baseline and spike signal from b_{bp} profiles were converted to POC using an empirical factor published for the North Atlantic (Cetinić *et al.*, 2012). Given that POC stocks are only quantified below the mixing layer in the present study, a conversion factor of 31,519 mg POC m^{-2} was applied. It is specially adapted to POC/b_{bp} relationship below the mixing layer (Cetinić *et al.*, 2012). This relationship might be biased by a background b_{bp} signal that is not necessarily related to POC. Consequently, before converting to POC, the median of deep (950-1,000 m) b_{bp} values measured by each float was subtracted from each profile of the corresponding time series. However, b_{bp} values (when not used as a POC proxies) presented in this paper are raw values (deep value not subtracted). POC derived from the baseline b_{bp} signal likely corresponds to small particles (< 10 μm, Dall'Olmo et Mork (2014)) whereas POC derived from spike signal corresponds to large particles or aggregates (Briggs *et al.*, 2011).

Atmospheric data

Net heat flux data were extracted from the ECMWF ERA Interim data set (reanalysis), freely available at `http://apps.ecmwf.int/datasets/data/interim-full-daily/levtype=sfc`. These data were averaged over 24-hour periods, with spatial resolution of 0.25°. A negative net heat flux indicates a cooling of the ocean.

Estimation of mixing and mixed layer depths

We used a single criterion, the maximum vertical gradient, to estimate the mixing and mixed layer depths from Chla and density profiles respectively. The maximum density gradient (MLD$_{dens}$) is supposed to match the depth of the seasonal pycnocline (i.e. mixed layer depth) which is the envelope of the maximum depth reached by the mixing layer (Brainerd *et al.*, 1995). In contrast, the maximum Chla gradient (MLD$_{bio}$) is more related to the mixing layer dynamics with time scales typical of phytoplankton growth (Zawada *et al.*, 2005; Boss et Behrenfeld, 2010) (Fig. 29). The underlying concept is that the Chla signal is homogeneous over the whole mixing layer, irrespective of its depth (Backhaus *et al.*, 2003). Indeed, while phytoplankton cells grow within the euphotic layer, mixing redistributes them throughout the mixing layer. However, as soon as cells are detrained from the mixing layer, the Chla signal start to decrease (Murphy et Cowles, 1997), thus intensifying the Chla gradient between mixing and remnant layers (Fig. 29). Figure 31 illustrates that MLD$_{bio}$ can change

within 2 days ($t_0 + 2$) in response to change in atmospheric forcing. In the same time, MLD_{dens} remains deep as a signature of the past mixing event (t_0). As doubling time of phytoplankton cells is on the order of a day (Eppley *et al.*, 1973; Goldman *et al.*, 1979) MLD_{bio} is not likely able to capture the diurnal variability of the mixing layer. Thus, typical timescale of the dynamics of MLD_{bio} is 1-2 days. This dynamics can be approximated with a density difference method but the criterion need to be adequately chosen. In the present study area, a density difference of 0.01 kg.m^{-3} shows the best correlation with MLD_{bio} (not shown). Higher density difference criteria do not capture the high frequency variability of the mixing layer.

Technically, Chla and density profiles were additionally smoothed before calculating the maximum gradient to suppress the influence of spikes or noise. Quenching correction on Chla profile may erase a potential gradient. Therefore, this correction was performed after calculating the maximum gradient.
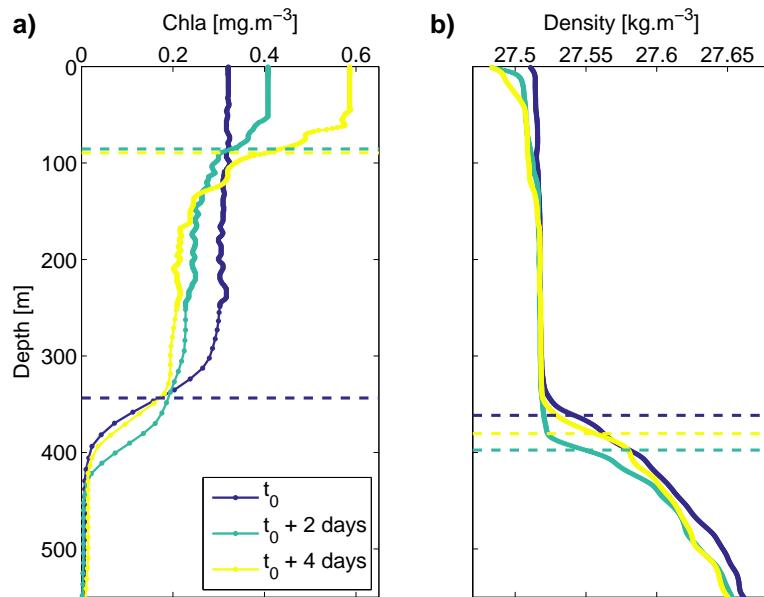

Figure. 31. Three BGC-Argo float profiles along the float 22b trajectory (yellow dots in Fig. 30) sampled in the same water mass (see Fig. 34a) in late March. Chla profiles a) and density profiles b) with 2 days interval. Horizontal dashed lines mark the depth of the maximum Chla gradient (MLD_{bio}) in a) and maximum density gradient (MLD_{dens}) in b). Constant Chla in the upper layer in a) is due to quenching correction. A visual check on the shape of b_{bp} profiles supported this correction.

Detection of submesoscale subduction events

Subduction is a 3D process involving lateral advection of water masses. Such a lateral advection can be identified on a 1D profile using a state variable called spice (Flament, 2002; Omand *et al.*, 2015). Based on anomalous temperature-salinity properties, this variable is a useful indicator of interleaving of water masses. The relative standard deviation of a spice profile (RSDspice, standard deviation / mean) from surface (5 m) to MLDdens is used to detect a potential intrusion of water in this layer. Application of this method over the entire dataset enables to identify submesoscale subduction events at a basin scale.

Results

Mixing versus Mixed layer dynamics

MLD_{bio} and MLD_{dens}, as proxies of the mixing and mixed layer depths, do not present the same dynamics depending on the season (Fig. 32). MLD_{bio} and MLD_{dens} are similar in fall and early winter when strong atmospheric forcing induces turbulent mixing down to a depth that will define the upper limit of the seasonal pycnocline. Hydrographic properties and phytoplankton cells concentration are homogeneous within the MLD_{dens}. In late winter, MLD_{bio} and MLD_{dens} start to diverge. Shallower mixing layers form above remnant mixed layers, delimited by MLD_{bio} at the top and by MLD_{dens} at the bottom (see Fig. 29). Phytoplankton cells in these remnant layers are thus isolated from the surface layer. In summer, MLD_{bio} is generally deeper than MLD_{dens} and likely corresponds to the limit of the euphotic zone. Light penetrates deeper than MLD_{dens} and allows phytoplankton growth below this layer. Hence, regardless of the seasons, MLD_{bio} is a good indicator of the depth of the productive layer, where particles are produced through photosynthesis. Note that MLD_{bio} estimation > 100 m deeper than MLD_{dens} is considered as an outlier. These outliers represent 141 profiles, so 7% of the total dataset.
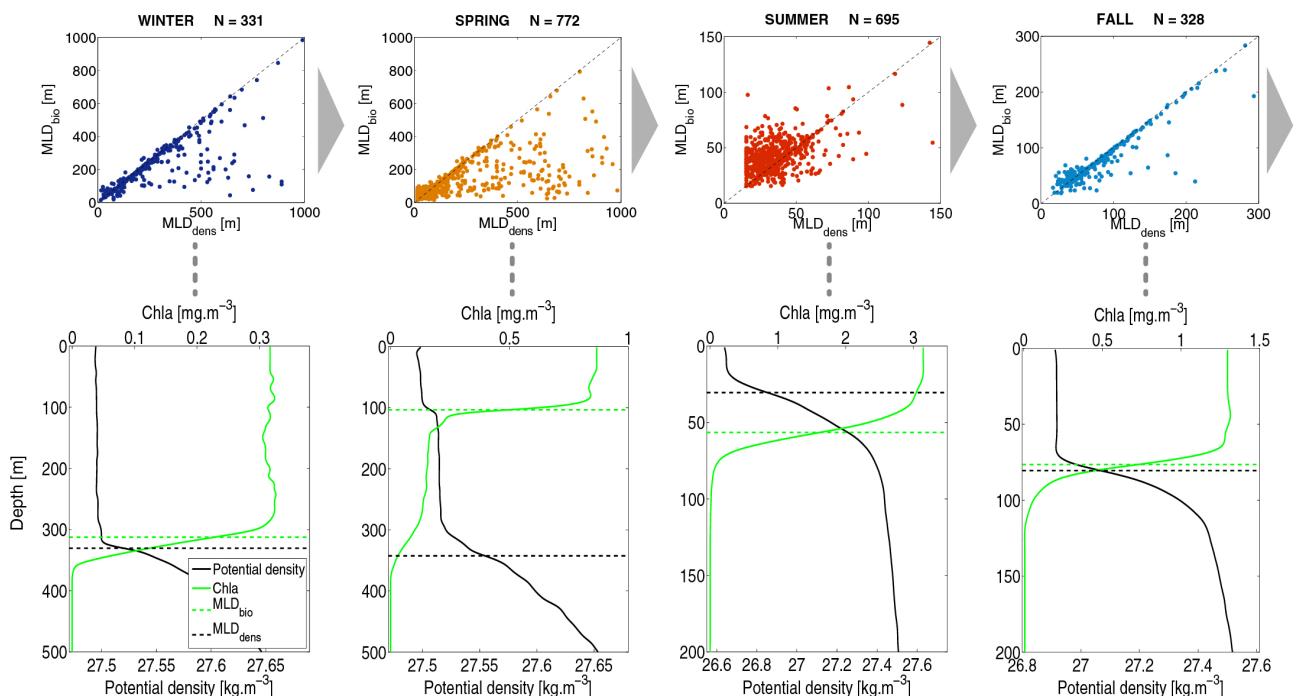

Figure. 32. Seasonal difference between MLD_{bio} and MLD_{dens} for all the profiles shown in Fig. 30 (top) and examples of Chla and density profiles by season (bottom). Horizontal dashed black and green lines mark MLD_{dens} and MLD_{bio} respectively.

Observations of vertical density and Chla profiles in late winter and spring suggest that the density-derived criteria used to estimate the MLD need to be adequately chosen and interpreted with caution. Most of these criteria do not detect subtle changes in density which affect phytoplankton vertical distribution. Studies estimating depth-integrated Chla by multiplying the concentration of surface Chla (measured by satellite) by the depth of the mixed layer could overestimate the Chla stock. Indeed, the

widely used density difference criteria of 0.1 kg.m^{-3} leads, in the present study, to a mean overestimation of 46% of the spring phytoplankton stock (comparison of the real stock measured by the float in the mixed layer with the estimated stock based on surface Chla). However, a density criterion of 0.01 kg m^{-3} leads to a mean overestimation of only 3%. Most of density difference thresholds are not adapted to capture the intra-seasonal dynamics of the mixing layer which affects the vertical distribution of phytoplankton biomass.

Impact of the mixing layer dynamics on POC export

The time series of a specific float (float 22b, see the float trajectory in Fig. 30) is used to illustrate the impact of the mixing layer dynamics on POC export (Fig. 33). While MLD$_{dens}$ roughly varies at the seasonal time scale, MLD$_{bio}$ varies at higher frequency (Fig. 33b). MLD$_{bio}$ oscillates between MLD$_{dens}$ during convective mixing events (negative net heat flux, see Fig. 33c) and a shallower depth during stratification (positive heat flux) or shallow mixing events. The particles produced during stratification/shallow mixing events are thus entrained to depth by the next convective mixing event. Finally, new stratification/shallow mixing events isolate particles in the remnant layer.

High variability of the mixing layer occurs when net heat flux (Q) is near zero during winter-spring transition (Fig. 33c). The switch from negative to positive net heat flux is not a smooth transition. Rather, it occurs over more than a one-month period and is associated with an intermittent reversal of the sign of this flux. This intermittency drives the high variability of MLD$_{bio}$ which acts as a physical pump. Interestingly, zero-crossing net heat flux in fall does not affect the dynamics of MLD$_{bio}$ which remains closely related to MLD$_{dens}$.

The water mass history of mixing can be retraced using a single 1D profile. Indeed, MLD$_{bio}$ marks the depth limit of recently active mixing while MLD$_{dens}$ marks the depth limit of past mixing. It is thus assumed that each POC stock isolated in the remnant layer along the float trajectory has been exported by the ML pump. The amount of POC exported through the ML pump is maximal during the winter-spring transition when net heat fluxes are nearly null. This maximum occurs before the main spring bloom (Fig. 33d and 33a). Occasionally, the contribution of large particles or aggregates to the exported POC stock can be significant.

A quasi-lagrangian approach of the ML pump

We identified two sections of float trajectories with quasi-langrangian behavior (i.e. tracking coherent water masses). The first section contains 3 profiles from float 22b (yellow dots in Fig. 30) with 2-day intervals, and the second one contains 4 profiles from float 24c (green dots in Fig. 30) with also 2-day intervals. The first profile of each section is well mixed up to 250 m depth and 600 m depth for float 22b and 24c respectively. Then, mixing stops and a new mixing layer forms to a depth of around 100 m in both sections. The quasi-lagrangian framework allows us to investigate the fate of Chla and b$_{bp}$ in 3 pre-defined layers (surface, remnant and deep layer, Fig. 34). Each data points of each profile within these 3 layers are identified on a temperature-salinity diagram to test the assumption of quasi-lagrangian behavior (Fig. 34). Only small changes in temperature and salinity are recorded between
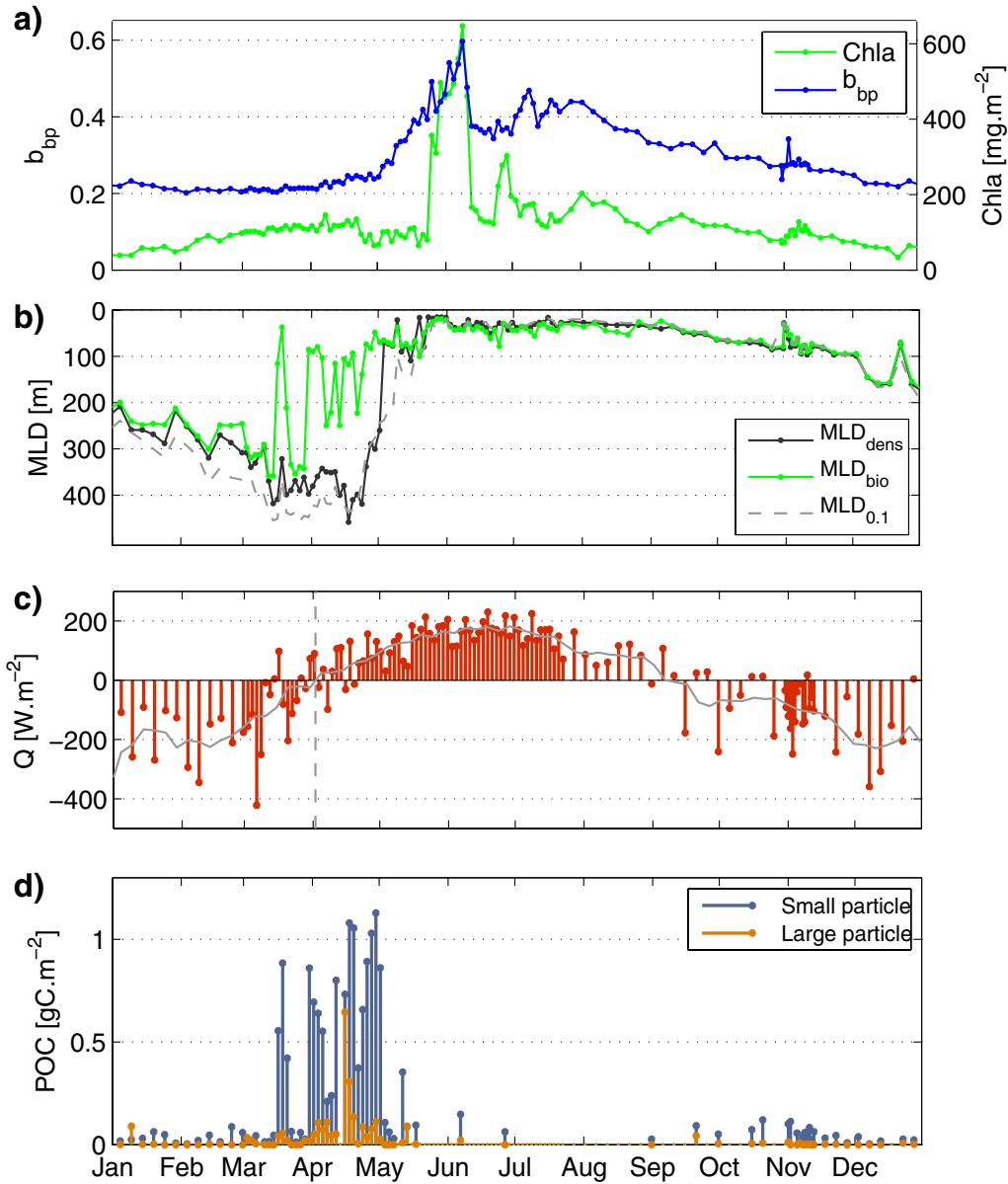
Figure. 33. a) Chla and b_{bp} integrated over 0-1,000 m depth, b) MLD_{dens} and MLD_{bio}, c) daily-averaged net heat flux (Q) and d) exported particulate organic carbon (POC) via mixed layer pump along the float 22b trajectory (January-December 2014). Continuous grey line and vertical dashed grey line in c) show 30-day smoothed net heat flux and the date of zero-crossing net heat flux respectively.

each profiles except for the last profile of float 24c in the deep and surface layer (Fig. 34b, yellow squares and triangles). In new mixing layers, both Chla and b_{bp} increase as a response to phytoplankton growth. The accumulation rate of Chla (0.15 d^{-1} and 0.26 d^{-1}) is higher than the accumulation rate of b_{bp} (0.04 d^{-1} and 0.08 d^{-1}) for float 22b and 24c respectively. In remnant layers, both Chla and b_{bp} decrease probably as a response to heterotrophic activity. Like surface layers, loss rate of Chla (0.1 d^{-1} and 0.08 d^{-1}) is higher than loss rate of b_{bp} (0.03 d^{-1} and 0 d^{-1}) for float 22b and 24c respectively. In deep layers, Chla and b_{bp} are stable with values nearly null for Chla and values higher than 1.10^{-4} m^{-1} for b_{bp}. This deep b_{bp} signal is a constant background value.
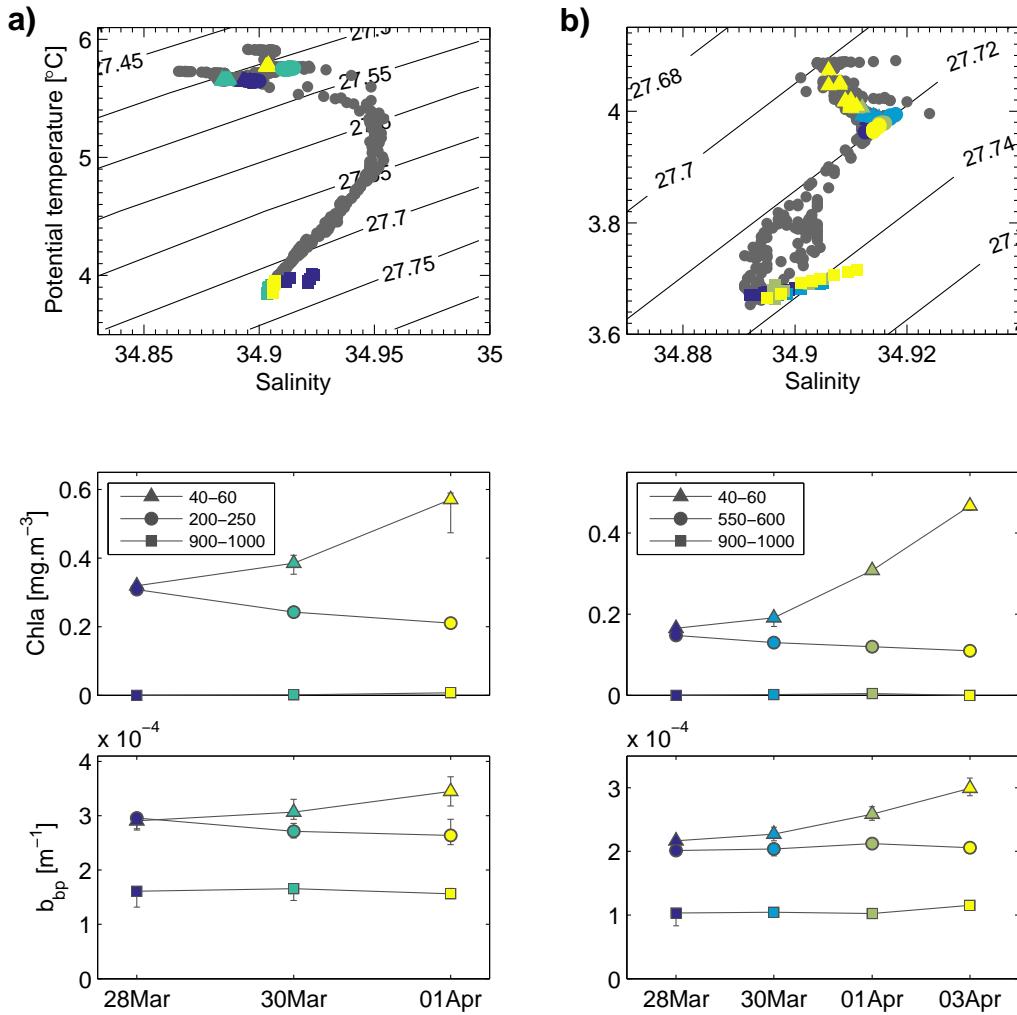
Figure. 34. BGC-Argo float profiles along 2 sections of float trajectories 22b (a) and 24c (b) acquired in 2014 (see location in Fig. 30). Top panels show potential temperature and salinity diagram for each profiles of the 2 sections. Bottom panels show time evolution of mean Chla and b_{bp} from each profile over 3 different layers : surface (triangle), remnant (filled circle) and deep layer (square). Vertical error bars indicate the range of data points within each layers. Color of the symbols differentiates each profiles.

As soon as the remnant layer forms and sequesters particles at depth, the Chla to b_{bp} ratio in this layer starts to decrease (Fig. 35). Thus, Chla to b_{bp} ratio in the remnant layer can be considered as a proxy for the freshness of the exported material. Interestingly, the attenuation rate of the Chla to b_{bp} ratio in the remnant layer is similar for both floats located in different region of the subpolar gyre. Time series of Chla to b_{bp} ratio at each depth along the float trajectories 22b (February to July 2014) shows that the ML pump export fresh material to depth up to 400 m during the whole winter-spring transition period (Fig. 36). Hence, the intermittent behavior of the ML pump in the winter-spring transition generates pulses of fresh organic material into the mesopelagic zone. During the spring bloom in June, such fresh material remains restricted to the first hundred meters.
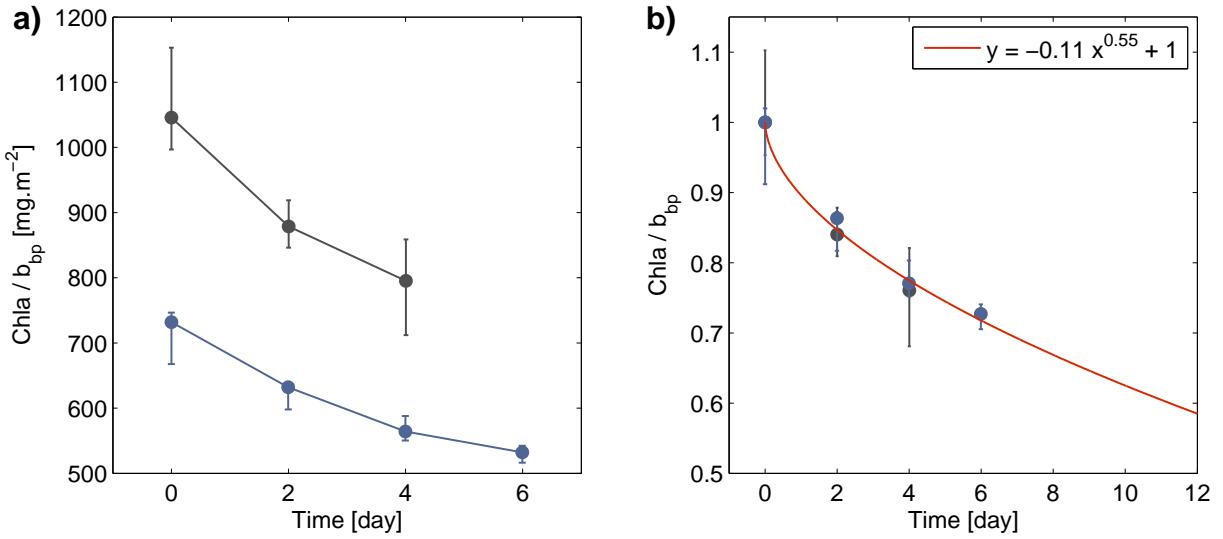
Figure. 35. a) Chla to b_{bp} ratio in the remnant layer as a function of time for sections of float trajectories 22b (black line) and 24c (blue line) shown in Fig. 30 and 34. b) Same curve as in a) but data normalized by their maximum value. The red line represents the best-fit power law function for both float sections. The vertical error bars indicate the range of data points within the remnant layer.
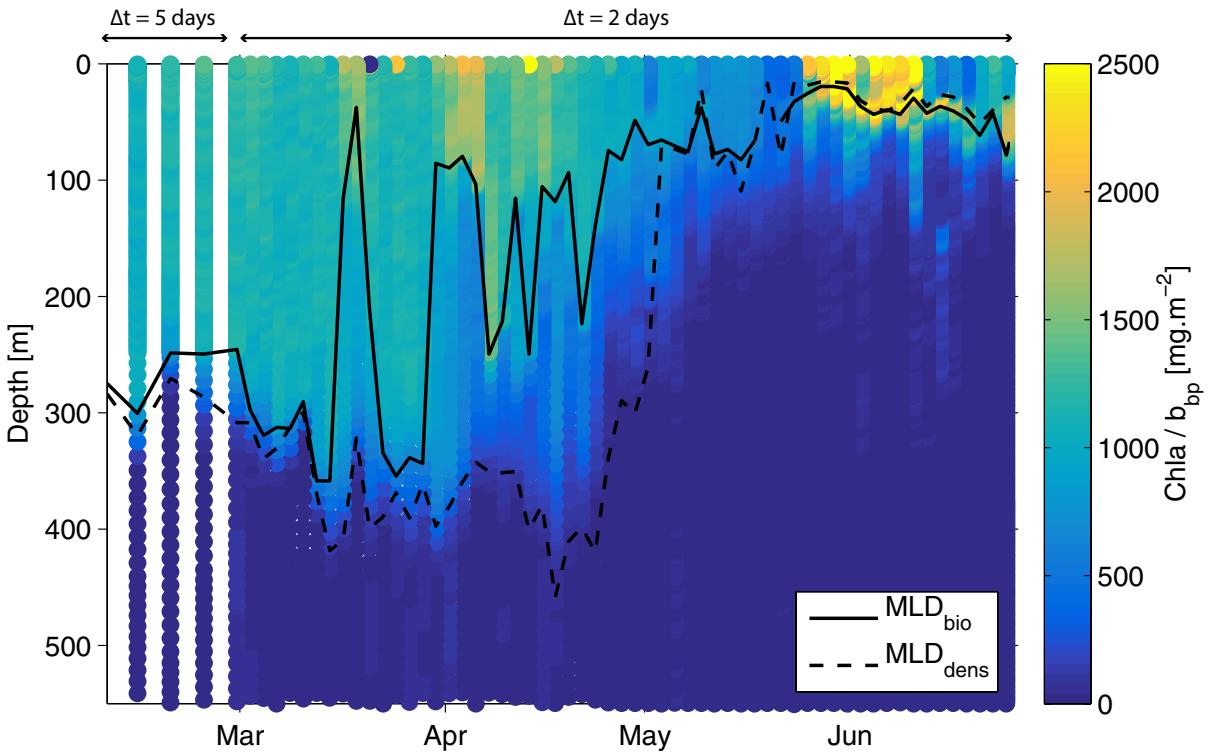

Figure. 36. Time series of Chla to b_{bp} ratio at each depth along the float trajectories 22b (February-July 2014). Solid black line and dashed black line represent MLD_{bio} and MLD_{dens} respectively.

Spatiotemporal variability of ML pump events

Using the signature of ML pump export (i.e. POC stock in the remnant layer), the spatiotemporal variability of this mechanism can be investigated in the whole subpolar gyre. However, submesoscale subduction, which involves 3D processes, may also produce similar signatures (Fig. 37). Before in-

vestigating spatiotemporal variability of the ML pump, this mechanism has to be discriminated from submesoscale subduction. RSD_{spice} was calculated for all the profiles with a ML pump signature to detect submesoscale subduction events (see an example in Fig. 37b). Submesoscale subduction is driven by instabilities growing from horizontal density gradients. This subduction index clearly exhibits high values in the strong density gradient areas (Fig. 37c), thus validating its pertinence. Profiles with RSD_{spice} higher than 5% were removed from the analysis in order to focus exclusively on ML pump mechanism.
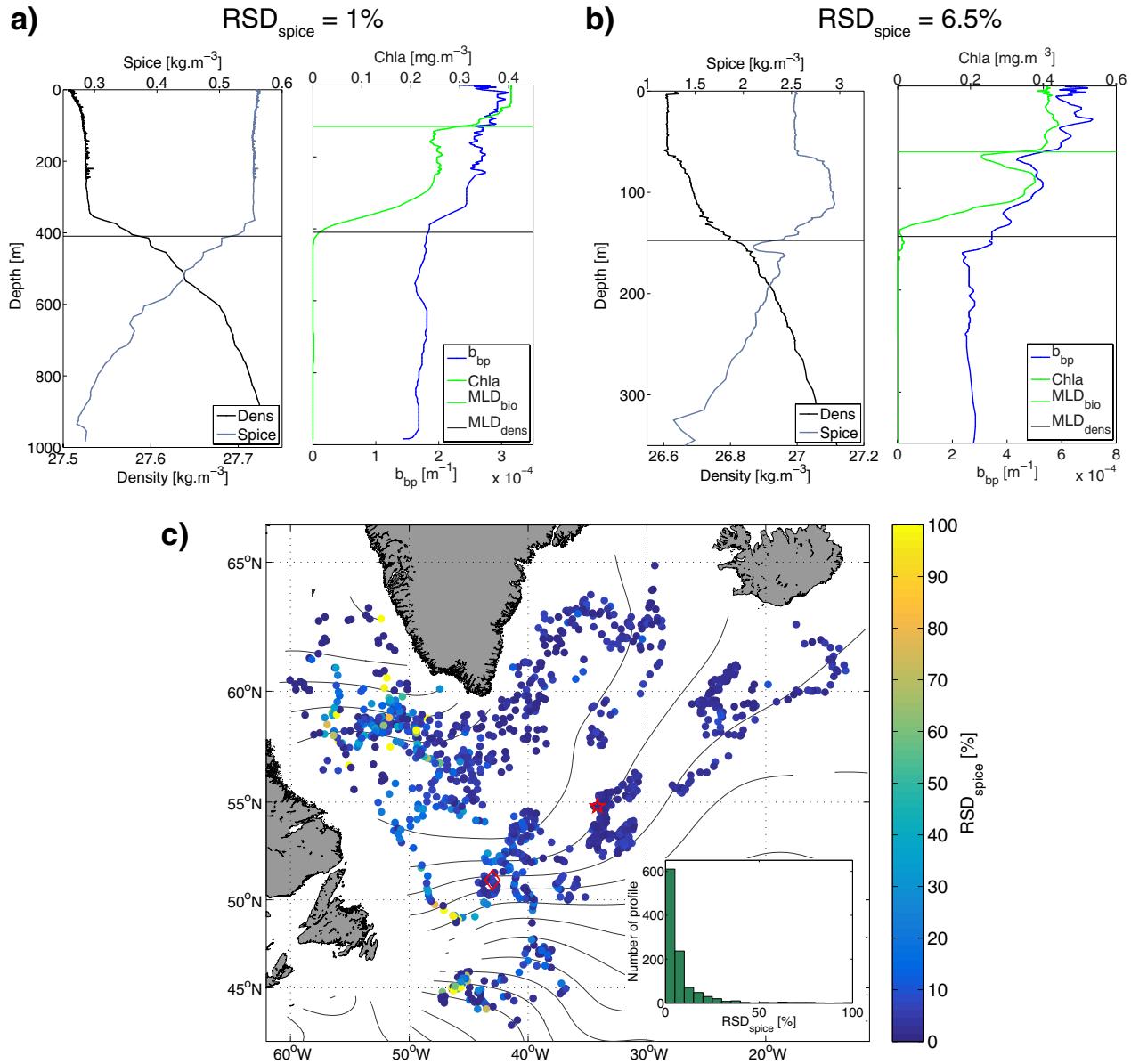

Figure. 37. Mixed layer pump versus subduction in the North Atlantic subpolar gyre. RSD_{spice} is the relative standard deviation (standard deviation / mean) of spice from surface to MLD_{dens}. a) Example of Spice, Density, Chla and b_{bp} profile after an export event by ML pump. b) Same as a) but for an export event by subduction. High RSD_{spice} indicates lateral intrusions of water. Horizontal black and green lines mark the depth of MLD_{dens} and MLD_{bio} respectively. c) Spatial distribution of BGC-Argo float profiles with an export signature color-coded by RSD_{spice}. Red star and diamond mark the location of profile in a) and b) respectively. At lower left, a histogram of the RSD_{spice} associated to each float profiles.

Each profile, from each float trajectory, with a ML pump signature is shown on Figure 38. Maximum POC stocks exported by the ML pump are centered on the day where the sign of the smoothed heat flux changes from negative to positive (Fig. 38a). The frequency of ML pump events is high (~40%) during all the winter and early spring period (120 days). Furthermore, the ML pump events appear to be widespread over the whole subpolar gyre (Fig. 38b). This mechanism connects the upper to the deep ocean and supplies food to mesopelagic ecosystems during the winter and early spring period.

Discussion

The ML pump signature

Dall'Olmo et Mork (2014) estimated the seasonal carbon flux mediated by the ML pump using rate of change of POC stock below the mixed layer, along the float trajectory ($E = \triangle POC / \triangle t$ where $\triangle t$ is the integration time), assuming a spatial homogeneity. $\triangle t$ was chosen as the time between seasonal minimum and maximum of POC stock (few months). Furthermore, they estimated the MLD with a density difference criteria of 0.1 kg.m^{-3} which matches the seasonal pycnocline (MLD$_{dens}$, see Fig. 33b). Therefore, the intra-seasonal dynamics of the mixing layer was not taken into account and the episodic nature of carbon export was not considered. The innovative approach, here, is to use a single profile to retrace the water mass history of mixing and thus relax the assumption of spatial homogeneity. Using MLD$_{bio}$ as the depth limit of a recent mixing and MLD$_{dens}$ as the depth limit of a past mixing, the presence of a remnant layer can be identified and used as a signature of the ML pump. Although the typical timescale of MLD$_{bio}$ is known (~1-2 days), the timescale of MLD$_{dens}$ is more difficult to assess. Figure 31b shows that MLD$_{dens}$ is still deep after 4 days after convection stopped and figure 33b reveals a 10 days delay between the permanent "shoaling" of MLD$_{bio}$ around 100 m and the "shoaling" of MLD$_{dens}$. It is thus assumed that MLD$_{dens}$ roughly corresponds to a mixed layer on a 10-day timescale. Thereby, the signature of ML pump likely reveals recent export of organic matter thus allowing the assessment of the episodic nature of this mechanism.

The strongest signatures of the ML pump are recorded when the net heat flux switches from negative to positive values in early spring. Interestingly, the switch from positive to negative values in fall does not affect MLD$_{bio}$ which remains closely related to MLD$_{dens}$ (Fig. 33). This dissymmetry is likely due to the mechanical effect of wind, that mixes the upper layer even if the heat flux is positive (Woods, 1980). The wind-driven mixing may be sufficiently strong to redistribute phytoplankton cells within MLD$_{dens}$ (< 100 m) at this time of the year. Although strong ML pump signatures are not detected during fall, the deepening of the mixing layer should contribute, in a more continuous way, to the export of organic material produced during summer or fall blooms.

Warming of the upper layer is not the only source of stratification. In addition to freshwater flux (i.e. rain or evaporation), 3D processes involving lateral advection are known to quickly restratify deep mixed layers (Brainerd et Gregg, 1993; Hosegood *et al.*, 2006, 2008; Johnson *et al.*, 2016). Submesoscale eddies or Ekman buoyancy flux can slump horizontal density gradient to create vertical stratification (Thomas et Lee, 2005; Boccaletti *et al.*, 2007). These processes, which generate a
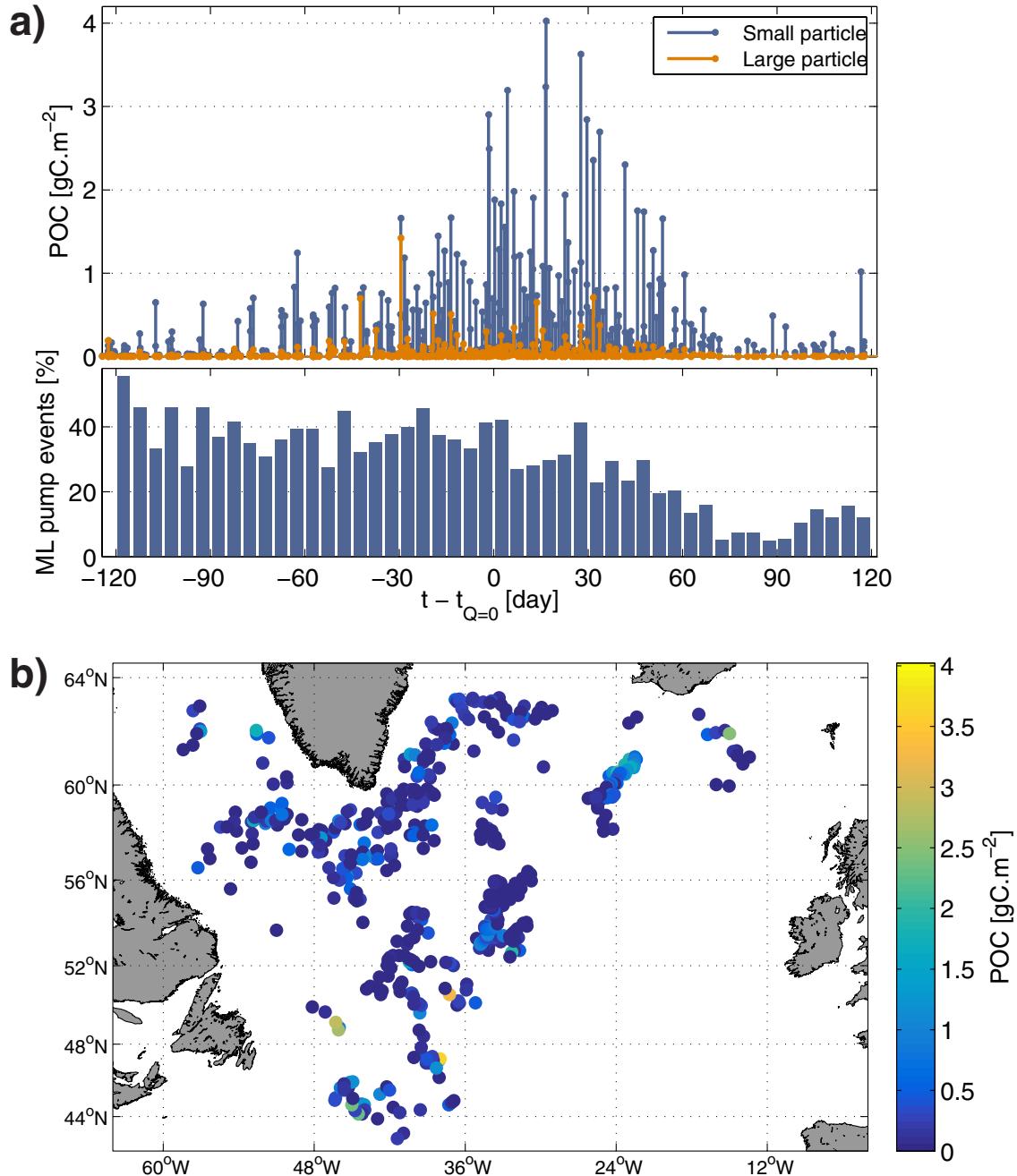
Figure. 38. a) POC stock transferred to the mesopelagic by mixed layer pump events measured by floats over the whole subpolar gyre (top). The frequency of the ML pump events calculated as the number of profiles with ML pump signature divided by the total number of profiles within each time interval (5 days) (bottom). The time axis refers to the day of observation relative to the day where the sign of heat flux changes from negative to positive (see Fig. 33c). b) Location of the mixed layer pump events. Color denotes the amount of small particles transferred to the mesopelagic.

signature similar to the ML pump, are often associated with submesoscale subduction (Omand *et al.*, 2015). Based on a RSD$_{spice}$ threshold of 5%, it can be estimated that almost 40% of the profiles displaying a ML pump signature were concerned by lateral water intrusion. As mentioned by Ho et Marra (1994), quantifying ML pump export is difficult since local and advective effects have to be distinguished. Here, a RSD$_{spice}$ threshold of 5% appeared to be enough to remove profiles affected

by advective effects. However, it is worth noting that lateral restratifications could contribute to the export due to the ML pump. Indeed, lateral restratification could stimulate phytoplankton production (Mahadevan *et al.*, 2012), even during winter (Lacour et al., submitted), and the resulting biomass could be exported later, following a deep mixing event. Although this study focuses on 1D processes, lateral restratification may also stimulate the ML pump export, especially in winter when positive heat fluxes are scarcer.

Fate of Chla and b_{bp} signal in the remnant layer

Quasi-lagrangian sections of float trajectories allowed us to investigate the fate of Chla and b_{bp} signal in the surface and in remnant layers after a stratification event (Fig. 34). Chla signal increased faster in the surface layer and decreased faster in the remnant layer than the b_{bp} signal. The reason for this discrepancy between the two proxies of phytoplankton biomass is probably different between the surface and the remnant layers. In the surface layer, taxonomical changes in the phytoplankton community could explain the faster increase in the Chla signal. The local restratification could enhance the light environment and stimulate large phytoplankton such as diatoms with higher Chla to b_{bp} ratio (Cetinić *et al.*, 2015, Lacour et al., submitted). In the remnant layer, the reasons could be twofold. First, changes in the autotroph to heterotroph ratio have to be considered. The consumption of phytoplankton cells, which leads to a decrease in the Chla signal, could enhance the growth of heterotroph organisms such as bacteria or protists which could contribute to the b_{bp} signal. Second, assuming that heterotrophs affect the Chla and b_{bp} signal in a similar fashion, additional decrease in Chla could be attributed to physiological adaptations to darkness which involve a reduced fluorescence per unit of Chla (Murphy et Cowles, 1997).

Despite different loss rates of Chla and b_{bp} between two different regions within the subpolar gyre, the attenuation rate of Chla to b_{bp} ratio remains similar. These observations give support to the second hypothesis. Such physiological adaptation to darkness could be ubiquitous in subpolar phytoplancton species. The relation obtained when fitting a power law function to both attenuation curves (Fig. 35b) could be used to estimate the time spent since particles left the mixing layer and thus estimate the rate of POC export due to the ML pump. However, initial value of Chla to b_{bp} ratio in the mixing layer must be known to use this relation. Unfortunately, the use of individual float profiles in "eulerian mode" does not allow to provide an estimate of export rate.

Role of the ML pump in sustaining mesopelagic ecosystems

The occurence of widespread and recurrent ML pump events during a relatively large time period (> 120 days) implies that this mechanism may be of great significance in supplying the energy required by the mesopelagic heterotrophic community. The particles mixed downward through the ML pump are rich in fresh phytoplankton and detritus, so potentially of high nutritional content for grazers and bacteria located below the mixing layer. Export of both small and large particles to the mesopelagic region suggest that this mechanism could sustain different zooplankton population with different feeding preferences. Furthermore, the ML pump should also export DOC and sustain bac-

terial activity. Thereby, ML pump could supply a major source of energy to the whole mesopelagic ecosystem during the winter and early spring period. On the contrary, the biological pump mainly depends on the spring bloom and the associated inputs of fresh organic substrate are restricted to the upper mesopelagic layer.

Many studies reported that the bulk of zooplankton populations occurs just below the turbulent mixing layer (Mackas *et al.*, 1993; Lagadeuc *et al.*, 1997; Incze *et al.*, 2001). The turbulence-avoidance behavior of grazers has been invoked to explain their vertical distribution in the water column (Franks, 2001). However, the reason of this behavior is not clear. Turbulence is known to influence encounter and ingestion rate of zooplankton and larger predators, but both positive and negative effect have been reported (MacKenzie, 2000). In winter and early spring, the vertical distribution of grazers could be a direct consequence of the ML pump. These organisms could stay at depth, in the low-turbulence remnant layer, waiting for pulses of fresh food induced by the ML pump. A similar strategy has been reported during the spring bloom where zooplankton act as gatekeepers at the base of the particle maximum layer, feeding on sinking aggregates (Jackson, 1993; Lampitt *et al.*, 1993; Jackson et Checkley, 2011). This feeding strategy would be energy efficient as vertical migrations would not be necessary.

Finally, the ML pump during the winter-spring transition could trigger the seasonal development of overwintering organisms such as copepods so that their reproduction would coincide with the forthcoming spring bloom. We can thus speculate that the frequency of episodic ML pump export events during the pre-bloom period may modulate the timing of the maturation phase of copepods and indirectly impact the magnitude of the spring bloom.

Conclusion

The density of the BGC-Argo float network enabled to capture and quantify the frequency and intensity of episodic export events on a basin scale, for the first time. ML pump export events are widespread over the North Atlantic Subpolar Gyre, and span a large temporal window preceding the spring bloom. To date, the high-frequency bio-physical mechanism had clearly been overlooked due to the lack of well suited observational tools. Yet, the ML pump may contribute significantly to the export of carbon during the winter and early spring periods. This mechanism may sustain the development of overwintering organisms such as copepods with potential impact on the characteristics of the subsequent spring bloom through predator-prey interactions. Further investigations of episodic events will provide new insights on life strategies and food web interactions, provide information for developing stochastic models, and potentially address the fundamental limitations of assuming steady-state conditions.

4.4 Conclusion

Cette étude a mis en évidence le caractère épisodique de l'export de carbone induit par la dynamique de la couche turbulente. Les événements d'export sont répartis sur l'ensemble du gyre subpolaire de l'Atlantique Nord et sont particulièrement fréquents et intenses pendant la transition hiver-printemps. Ils pourraient être d'une importance cruciale pour alimenter l'écosystème mésopélagique pendant une période où les flux par sédimentation sont a priori limités. De plus amples investigations sont nécessaires pour comprendre comment les organismes hétérotrophes exploitent ces sources épisodiques d'énergie dans la zone mésopélagique. La considération des événements épisodiques devrait ouvrir de nouvelles perspectives sur les stratégies d'alimentation des organismes hétérotrophes, ainsi que sur les interactions trophiques qui s'opèrent dans la zone mésopélagique.

Cette étude s'est focalisée sur le contrôle de la dynamique de la couche turbulente par des processus 1D tels que les flux de chaleur. Il faut cependant noter que des processus 3D tels que les tourbillons de méso- et sous-mésoéchelle sont aussi susceptibles de restratifier les couches de mélanges profondes, notamment pendant la période hivernale. Ces processus pourraient ainsi participer à la dynamique de la couche turbulente et à l'export de carbone associé. De plus, les structures de sous-mésoéchelle sont directement impliquées dans la subduction de masses d'eau potentiellement riches en matière organique. Ces deux pompes bio-physiques sont donc intimement liées et ont en commun le caractère épisodique de l'export de carbone.

CHAPITRE 5

Conclusion générale et perspectives

Les processus bio-physiques qui contrôlent la dynamique de la biomasse phytoplanctonique et l'export de carbone sont complexes et interviennent sur des échelles spatio-temporelles très diverses. Les nombreuses études réalisées dans ce domaine se sont focalisées seulement sur certaines d'entre elles, de par la limitation des outils d'observation. L'expérience NAB08 qui s'est déroulée dans le bassin d'Islande fut l'une des premières à montrer le formidable potentiel d'une utilisation synergique des différents outils d'observation disponibles. Malheureusement, ce genre d'approche est limité à une période donnée, généralement pendant le bloom printanier. Les résultats de cette thèse, que nous allons brièvement résumer dans les trois prochains paragraphes, soutiennent l'idée qu'il est essentiel de considérer l'ensemble du cycle annuel de biomasse phytoplanctonique pour comprendre la dynamique des blooms aux hautes latitudes.

Nous avons commencé par poser un cadre climatologique aux cycles annuels de biomasse phytoplanctonique. La couverture, à grande échelle, des observations satellites a permis d'apprécier la variabilité spatiale des cycles de biomasse et de discerner des biorégions océaniques au sein du gyre subpolaire de l'Atlantique Nord. Les conditions hydrologiques ont pu être évaluées au sein de chaque biorégion grâce aux données de flotteurs Argo. Nous avons accordé une attention particulière à la mer du Labrador qui est divisée en deux biorégions aux cycles annuels de biomasse très contrastés et a priori paradoxaux. Les conditions particulières de mélange hivernal dans la région au nord de la mer du Labrador sont responsables d'un environnement lumineux plus favorable à la croissance du phytoplancton. Il en résulte un bloom printanier plus précoce, court et intense que celui de la région au sud. La formation récurrente de tourbillons sur la côte ouest du Groenland pourrait être à l'origine des faibles couches de mélange observées dans le nord de la mer du Labrador qui influencent les caractéristiques du bloom printanier à l'échelle climatologique.

La nouvelle génération de flotteurs BGC-Argo a permis d'explorer pour la première fois la dynamique de la biomasse phytoplanctonique dans le gyre subpolaire durant la période hivernale. Des restratifications intermittentes de la couche de mélange, liées à un transport horizontal de masse d'eau, probablement induit par des structures de sous-mésoéchelle, initient des blooms phytoplanctoniques transitoires. Ces restratifications, ici encore, modifient l'environnement lumineux du phytoplancton, ce qui influence non seulement la production mais aussi la structure de la communauté en favorisant

la croissance des diatomées. Ces blooms transitoires pourraient ainsi maintenir une population active de diatomées pendant l'hiver et influencer les caractéristiques du bloom printanier. En effet, des simulations numériques simples ont montré que l'augmentation de la fréquence de ces événements épisodiques avance la date d'initiation et augmente l'intensité du bloom printanier. Ces résultats rappellent le rôle potentiel des tourbillons de mésoéchelle sur le cycle annuel de biomasse à l'échelle climatologique dans le nord de la mer du Labrador. Le pré-conditionnement biologique pendant la période hivernale pourrait participer à l'initiation précoce du bloom dans cette région. La confirmation d'un tel mécanisme requiert cependant un jeu de données beaucoup plus conséquent, notamment sur la composition des communautés phytoplanctoniques. Le lien entre les blooms transitoires hivernaux et le bloom printanier ne pourra être confirmé que si les espèces phytoplanctoniques impliquées sont les mêmes. Des capteurs d'imagerie tels que le "FlowCytobot" pourraient apporter des éléments de réponse mais leur utilisation implique une intervention par bateau qui peut s'avérer délicate dans les conditions de mer difficiles rencontrées en hiver dans le gyre subpolaire.

L'intermittence du mélange hivernal à l'origine des blooms transitoires stimule également l'exportation épisodique de matière organique en profondeur. La densité du réseau BGC-Argo dans le gyre subpolaire de l'Atlantique Nord permet d'apprécier la variabilité spatio-temporelle de ces événements. Il faut cependant pouvoir les identifier sur un profil unique. Si un bloom de phytoplancton est facilement reconnaissable à partir de l'analyse d'un profil de Chla, l'identification d'un événement d'export de carbone n'est pas triviale. L'utilisation de différents critères a permis de distinguer la profondeur d'une couche de mélange récente de celle d'une couche de mélange passée. Ces deux profondeurs délimitent une couche de mélange dite fossile qui contient la matière organique récemment exportée par le mélange. Cette signature permet d'identifier et de quantifier l'export de carbone (POC, dérivé du b_{bp}) généré par la dynamique haute fréquence de la couche de mélange. Ces événements d'export sont particulièrement fréquents et intenses pendant la période de transition hiver-printemps. Ils sont donc susceptibles d'alimenter l'écosystème mésopélagique avant le développement du bloom printanier et le flux de sédimentation qui en résulte. Les organismes hétérotrophes en dormance en profondeur tels que les copépodes pourraient bénéficier de cet apport épisodique de matière organique fraîche pour initier leur phase de maturation. La fréquence de ces événements pourrait notamment moduler le temps de maturation du zooplancton et ainsi influencer les interactions prédateur-proie pendant le bloom printanier (notion de "match-mismatch"). Connaissant le rôle majeur de ces organismes sur le contrôle de la durée et de l'intensité du bloom, cette hypothèse mériterait d'être confirmée par de plus amples investigations.

Ainsi, bien que le cycle annuel de biomasse, tel que perçu par satellite, soit dominé par le bloom printanier, il semble important de considérer également les événements épisodiques précédant le bloom. En effet, celui-ci n'est pas un événement indépendant mais découle en partie du pré-conditionnement physique et biologique pendant la période hivernale. L'intermittence du mélange hivernal pourrait ainsi favoriser à la fois la production phytoplanctonique en surface et le développement des organismes hétérotrophes en profondeur influençant dans les deux cas les caractéristiques du bloom printanier à venir.

Une approche climatologique, telle que menée en première partie de cette thèse, ne permet pas de résoudre la variabilité haute fréquence de la couche de mélange liée aux structures de méso- ou sous-mésoéchelle. Les événements épisodiques tels que les blooms transitoires, lissés par un effet de moyennage, ont-ils tout de même une influence sur le cycle annuel de biomasse à grande échelle ? La modélisation a apporté des éléments de réponse à cette question. Plusieurs études ont effectivement montré que l'augmentation de la résolution spatiale d'un modèle, afin de résoudre les structures de sous-mésoéchelle, affecte significativement l'estimation des flux biogéochimiques à grande échelle spatiale et temporelle (Lévy *et al.*, 2001, 2012). La sous-mésoéchelle notamment contribuerait à la variabilité inter-annuelle du bloom phytoplanctonique à l'échelle d'un bassin océanique (Lévy et Jahn, 2014). Cependant, ces modèles sont extrêmement idéalisés et ne reflètent que très partiellement la réalité. Par exemple, l'impact local des structures de méso- et sous-mésoéchelle sur la composition des communautés phytoplanctoniques n'est pas considéré mais pourrait pourtant modifier les cycles biogéochimiques à l'échelle régionale (Sinha *et al.*, 2010; Clayton *et al.*, 2016). Une approche similaire a été utilisée par Mahadevan *et al.* (2012) et Omand *et al.* (2015) en utilisant à la fois des données *in situ* et un modèle numérique. Mahadevan *et al.* (2012) ont d'abord identifié à l'aide de données *in situ* des structures de sous-mésoéchelle qui permettent de restratifier localement la couche de mélange. Ils ont ensuite paramétrisé ce processus pour l'intégrer dans un modèle, et ainsi étudier son rôle à l'échelle d'un bassin océanique (sans augmenter la résolution spatiale du modèle). Ils ont ainsi montré que ces processus de sous-mésoéchelle permettent d'initier le bloom printanier avant la restratification printanière. De même, Omand *et al.* (2015) ont identifié, sur des profils de planeurs sous-marins, la signature d'un export de carbone par subduction à sous-mésoéchelle. La paramétrisation de ce processus a permis d'évaluer son impact à l'échelle globale avec un modèle simple.

La première perspective de cette thèse serait de montrer, sur la base de données *in situ*, comment les événements épisodiques aux petites échelles spatio-temporelles peuvent influencer les cycles biogéochimiques à l'échelle d'un bassin ou d'une région océanique. Typiquement, est-ce que des blooms épisodiques pendant la période hivernale influencent le cycle annuel de biomasse phytoplanctonique d'une biorégion océanique (comme identifié dans la première partie de cette thèse) ? Est ce que les structures de méso- et sous-mésoéchelle sont responsables du bruit observé autour du cycle annuel moyen ou peuvent-elles également influencer un cycle climatologique ? La stratégie serait d'utiliser la densité du réseau de flotteurs BGC-Argo pour réaliser un transfert d'échelle, de la méso- ou sous-mésoéchelle à l'échelle régionale. En identifiant la signature d'un événement épisodique tel qu'un bloom transitoire, on pourrait quantifier la fréquence et l'intensité de ces événements au sein d'une biorégion et évaluer leur impact régional, en particulier sur les caractéristiques du bloom printanier. Avec l'augmentation attendue du nombre de profils, on pourra, par une approche statistique, évaluer ce qui peut différencier les biorégions lors de la période de pré-conditionnement hivernal.

Les premières observations satellites aux hautes et moyennes latitudes de la biomasse phytoplanctonique ont naturellement guidé la grande majorité des études vers le bloom printanier, la biomasse hivernale de surface étant très faible et la biomasse de subsurface potentiellement présente en été n'étant pas directement visible. Puis l'utilisation complémentaire de différents outils d'observation a

permis de révéler des stocks non négligeables de biomasse phytoplanctonique en dehors de la période du bloom printanier. Finalement, de nombreux processus bio-physiques ont été mis en évidence pour expliquer la dynamique annuelle de la biomasse phytoplanctonique (Lindemann et St. John, 2014; Chiswell *et al.*, 2015). Les travaux de cette thèse ont également contribué à montrer l'importance de la dynamique de la biomasse sur un cycle annuel complet. Etonnamment, les études sur l'export de carbone organique n'ont pas suivi la même évolution et sont restées principalement focalisées sur l'export lié au bloom printanier. Des études menées pendant le bloom printanier ont montré que le flux de carbone par sédimentation des particules et agrégats n'est pas suffisant pour soutenir la demande métabolique des organismes hétérotrophes dans la zone mésopélagique. Il semble alors peu probable que le flux de particules pendant le bloom printanier soit la seule source d'énergie exploitable au cours d'un cycle annuel. Bien qu'il existe une source alternative d'énergie liée à la chimiosynthèse, d'autres processus d'export devraient intervenir sur différentes fenêtres temporelles afin de soutenir durablement l'écosystème mésopélagique.

La deuxième perspective de cette thèse serait donc d'étudier l'export de carbone comme un processus multifactoriel qui se manifeste tout au long d'un cycle annuel. Dans cette optique, la région inter-gyre (40-50°N) de l'Atlantique Nord semble particulièrement intéressante de par la dynamique annuelle de la biomasse phytoplanctonique. La matière organique, produite pendant la période hivernale dans les couches de mélange profondes ou lors des restratifications intermittentes, peut être exportée par la dynamique de la couche de mélange ou par la subduction à sous-mésoéchelle et/ou à grande échelle. Le bloom de surface intense pendant la période printanière alimente la pompe biologique et se poursuit en profondeur (DBM, "Deep Biomass Maximum") pendant la période estivale lorsque les nutriments deviennent limitants en surface et que la lumière pénètre plus profondément. Ces DBM pourraient apporter une source significative d'énergie à l'écosystème mésopélagique. Pendant cette période, les structures de sous-mésoéchelle peuvent aussi favoriser une remontée de nutriments à l'origine de blooms localisés en surface qui participeront à l'export épisodique de matière organique. Enfin, l'approfondissement de la couche de mélange en automne ré-injecte des éléments nutritifs en surface et initie le bloom automnal également susceptible d'exporter de la matière organique par sédimentation. La poursuite du mélange entraine en profondeur les produits issus des blooms estivaux et automnaux (POC et DOC) pour clore le cycle annuel d'export. Une région aussi dynamique que la zone inter-gyre de l'Atlantique Nord a un potentiel d'export de carbone qui ne se limite clairement pas à la seule pompe biologique pendant le bloom printanier.

Les deux perspectives de recherche évoquées précédemment sont délicates à entreprendre du fait de la diversité des échelles spatio-temporelles à résoudre. La mise en place d'un système d'observation intégré, associant campagnes en mer, plateformes autonomes et télédétection spatiale, complété par des études de modélisation, semble indispensable à la bonne réussite d'une telle entreprise. Les flotteurs Argo et BGC-Argo ainsi que les observations satellites pourraient apporter une vision complète du cycle annuel, que ce soit pour la production ou l'export de matière organique. Des campagnes, dédiées à des périodes clés (idéalement une par saison), pourraient résoudre des processus aux échelles plus fines, typiquement la formation d'un tourbillon de sous-mésoéchelle, à l'aide de flotteurs

lagrangiens et d'un réseau de planeurs sous-marins. Enfin, la modélisation apparaît comme un outil adapté pour réaliser un transfert d'échelle afin d'étendre les observations *in situ* sur un domaine plus vaste.

Bibliographie

Alldredge A.L., Passow U. et Logan B.E. (1993). The abundance and significance of a class of large, transparent organic particles in the ocean. *Deep Sea Research Part I : Oceanographic Research Papers*, 40 (6), 1131–1140, ISSN 09670637, doi :10.1016/0967-0637(93)90129-Q.

Álvarez M., Ríos A.F., Pérez F.F., Bryden H.L. et Rosón G. (2003). Transports and budgets of total inorganic carbon in the subpolar and temperate North Atlantic. *Global Biogeochemical Cycles*, 17 (1), 2–1–2–21, ISSN 08866236, doi :10.1029/2002GB001881.

Arrigo K.R. (2007). Carbon cycle : Marine manipulations. *Nature*, 450 (7169), 491–492, ISSN 0028-0836, doi :10.1038/450491a.

Backhaus J.O., Hegseth E.N., Wehde H., Irigoien X., Hatten K. et Logemann K. (2003). Convecion and primary production in winter. *Mar. Ecol. Progr. Ser.*, 251 (1953), 1–14.

Banse K. (1994). Grazing and Zooplankton Production as Key Controls of Phytoplankton Production in the Open Ocean. *Oceanography*, 7 (l), 13–20, ISSN 10428275, doi :10.5670/oceanog.1994.10.

Barth J.A., Cowles T.J., Kosro P.M., Shearman R.K., Huyer A. et Smith R.L. (2002). Injection of carbon from the shelf to offshore beneath the euphotic zone in the California Current. *Journal of Geophysical Research*, 107 (C6), 3057, ISSN 0148-0227, doi :10.1029/2001JC000956.

Barton A.D., Lozier M.S. et Williams R.G. (2014). Physical controls of variability in North Atlantic phytoplankton communities. *Limnology and Oceanography*, 60 (1), 181–197, ISSN 00243590, doi :10.1002/lno.10011.

Behrenfeld M.J. (2010). Abandoning Sverdrup's Critical Depth Hypothesis on phytoplankton blooms. *Ecology*, 91 (4), pp. 977–989, ISSN 00129658.

Behrenfeld M.J. et Boss E.S. (2014). Resurrecting the ecological underpinnings of ocean plankton blooms. *Annual review of marine science*, 6 (September 2013), 167–194, ISSN 1941-1405, doi :10.1146/annurev-marine-052913-021325.

Behrenfeld M.J., Doney S.C., Lima I., Boss E.S. et Siegel D.A. (2013). Annual cycles of ecological disturbance and recovery underlying the subarctic Atlantic spring plankton bloom. *Global Biogeochemical Cycles*, 27 (2), 526–540, ISSN 1944-9224, doi :10.1002/gbc.20050.

Behrenfeld M.J., O'Malley R.T., Boss E.S., Westberry T.K., Graff J.R., Halsey K.H., Milligan A.J., Siegel D.a. et Brown M.B. (2015). Revaluating ocean warming impacts on global phytoplankton. *Nature Climate Change*, 6 (3), 323–330, ISSN 1758-678X.

Behrenfeld M.J., O'Malley R.T., Siegel D.a., McClain C.R., Sarmiento J.L., Feldman G.C., Milligan A.J., Falkowski P.G., Letelier R.M. et Boss E.S. (2006). Climate-driven trends in contemporary ocean productivity. *Nature*, 444 (7120), 752–755, ISSN 1476-4687, doi :10.1038/nature05317.

Bishop J., Conte M., Wiebe P., Roman M. et Langdon C. (1986). Particulate matter production and consumption in deep mixed layers : observations in a warm-core ring. *Deep Sea Research Part A. Oceanographic Research*

Papers, 33 (11-12), 1813–1841, ISSN 01980149, doi :10.1016/0198-0149(86)90081-6.

Blain S., Renaut S., Xing X., Claustre H. et Guinet C. (2013). Instrumented elephant seals reveal the seasonality in chlorophyll and light-mixing regime in the iron-fertilized Southern Ocean. *Geophysical Research Letters*, 40 (24), 6368–6372, ISSN 00948276, doi :10.1002/2013GL058065.

Boccaletti G., Ferrari R. et Fox-Kemper B. (2007). Mixed Layer Instabilities and Restratification. *Journal of Physical Oceanography*, 37 (9), 2228–2250, ISSN 0022-3670, doi :10.1175/JPO3101.1.

Boss E. et Behrenfeld M. (2010). In situ evaluation of the initiation of the North Atlantic phytoplankton bloom. *Geophysical Research Letters*, 37 (18), ISSN 00948276, doi :10.1029/2010GL044174.

Boss E., Stramski D., Bergmann T., Pegau S. et Lewis M. (2004). Why Should We Measure the Optical Backscattering Coefficient ? *Oceanography*, 17 (2), 44–49, ISSN 10428275, doi :10.5670/oceanog.2004.46.

Brainerd K.E. et Gregg M.C. (1993). Diurnal restratification and turbulence in the oceanic surface mixed layer : 1. Observations. *Journal of Geophysical Research*, 98 (C12), 22645, ISSN 0148-0227, doi : 10.1029/93JC02297.

Brainerd K.E., Gregg M.C. et Sciences F. (1995). Surface mixed and mixing layer depths. *Deep Sea Research Part I : Oceanographic Research Papers*, 42 (9), 1521–1543, ISSN 09670637, doi :10.1016/0967-0637(95) 00068-H.

Briggs N., Perry M.J., Cetinić I., Lee C., D'Asaro E., Gray A.M. et Rehm E. (2011). High-resolution observations of aggregate flux during a sub-polar North Atlantic spring bloom. *Deep Sea Research Part I : Oceanographic Research Papers*, 58 (10), 1031–1039, ISSN 09670637, doi :10.1016/j.dsr.2011.07.007.

Brody S.R. et Lozier M.S. (2014). Changes in dominant mixing length scales as a driver of subpolar phytoplankton bloom initiation in the North Atlantic. *Geophysical Research Letters*, p. n/a–n/a, ISSN 00948276, doi :10.1002/2014GL059707.

Brody S.R. et Lozier M.S. (2015). Characterizing upper-ocean mixing and its effect on the spring phytoplankton bloom with in situ data. *ICES Journal of Marine Science : Journal du Conseil*, 72 (6), 1961–1970, ISSN 1054-3139, doi :10.1093/icesjms/fsv006.

Buesseler K.O. et Boyd P.W. (2009). Shedding light on processes that control particle export and flux attenuation in the twilight zone of the open ocean. *Limnology and Oceanography*, 54 (4), 1210–1232, ISSN 00243590, doi :10.4319/lo.2009.54.4.1210.

Burd A.B., Anderson T.R., Arístegui J., Baltar F., Beaupré S.R., Buesseler K.O., DeHairs F., Jackson G.A., Kadko D.C., Koppelmann R., Lampitt R.S., Nagata T., Reinthaler T., Robinson C., Robison B.H., Tamburini C. et Tanaka T. (2010). Assessing the apparent imbalance between geochemical and biochemical indicators of meso- and bathypelagic biological activity : What the ! ! ! ! is wrong with present calculations of carbon budgets ? *Deep Sea Research Part II : Topical Studies in Oceanography*, 57 (16), 1557–1571, ISSN 09670645, doi :10.1016/j.dsr2.2010.02.022.

Calinski T. et Harabasz J. (1974). A Dendrite Method for Cluster Analysis, doi :10.1080/03610917408548446.

Callies J., Ferrari R., Klymak J.M. et Gula J. (2015). Seasonality in submesoscale turbulence. *Nature communications*, 6, 6862, ISSN 2041-1723, doi :10.1038/ncomms7862.

Caniaux G., Prieur L., Giordani H., Hernandez F. et Eymard L. (2001). Observation of the Circulation in the Newfoundland Basin in Winter 1997. *Journal of Physical Oceanography*, 31 (3), 689–710, ISSN 0022-3670, doi :10.1175/1520-0485(2001)031<0689:OOTCIT>2.0.CO;2.

Carlson C.A., Ducklow H.W. et Michaels A.F. (1994). Annual flux of dissolved organic carbon from the

euphotic zone in the northwestern Sargasso Sea. *Nature*, 371 (6496), 405–408, ISSN 0028-0836, doi : 10.1038/371405a0.

Caron D.A. (2016). Mixotrophy stirs up our understanding of marine food webs. *Proceedings of the National Academy of Sciences of the United States of America*, 113 (11), 2806–2808, ISSN 1091-6490, doi :10.1073/pnas.1600718113.

Cetinić I., Perry M.J., Briggs N.T., Kallin E., D'Asaro E.a. et Lee C.M. (2012). Particulate organic carbon and inherent optical properties during 2008 North Atlantic Bloom Experiment. *Journal of Geophysical Research*, 117 (C6), C06028, ISSN 0148-0227, doi :10.1029/2011JC007771.

Cetinić I., Perry M.J., D'Asaro E., Briggs N., Poulton N., Sieracki M.E. et Lee C.M. (2015). A simple optical index shows spatial and temporal heterogeneity in phytoplankton community composition during the 2008 North Atlantic Bloom Experiment. *Biogeosciences*, 12 (7), 2179–2194, ISSN 1726-4189, doi : 10.5194/bg-12-2179-2015.

Chanut J., Barnier B., Large W., Debreu L., Penduff T., Molines J.M. et Mathiot P. (2008). Mesoscale Eddies in the Labrador Sea and Their Contribution to Convection and Restratification. *J. Phys. Oceanogr.*, 38 (8), 1617–1643, ISSN 0022-3670.

Chiswell S. (2011). Annual cycles and spring blooms in phytoplankton : don't abandon Sverdrup completely. *Marine Ecology Progress Series*, 443, 39–50, ISSN 0171-8630, doi :10.3354/meps09453.

Chiswell S.M., Calil P.H.R. et Boyd P.W. (2015). Spring blooms and annual cycles of phytoplankton : a unified perspective. *Journal of Plankton Research*, p. fbv021–, ISSN 0142-7873, doi :10.1093/plankt/fbv021.

Claustre H., Antoine D., Boehme L., Boss E., D'Ortenzio F., Fanton D'Andon O., Guinet C., Gruber N., Handegard N.O., Hood M., Johnson K., Kortzinger A., Lampitt R., LeTraon P.Y., Le Quere C., Lewis M., Perry M.J., Platt T., Roemmich D., Sathyendranath S., Send U., Testor P. et Yoder J. (2010). Guidelines towards an integrated ocean observation system for ecosystems and biogeochemical cycles. *Proceedings of Ocean-Obs'09 : Sustained Ocean Observations and Information for Society*, 1 (1), 21–25, ISSN 0379-6566, doi : 10.5270/OceanObs09.pp.14.

Clayton S., Dutkiewicz S., Jahn O., Hill C., Heimbach P. et Follows M.J. (2016). Biogeochemical versus ecological consequences of modeled ocean physics. *Biogeosciences Discussions*, 0, 1–20, ISSN 1810-6285, doi :10.5194/bg-2016-337.

Cullen J.J. et Lewis M.R. (1995). Biological processes and optical measurements near the sea surface : Some issues relevant to remote sensing. *Journal of Geophysical Research*, 100 (C7), 13255, ISSN 0148-0227, doi :10.1029/95JC00454.

Cushing D.H. (1959). The seasonal variation in oceanic production as a problem in population dynamics. *J. Cons. int. Explor. Mer*, 24 (3), 455–464, ISSN 1054-3139, doi :doi:10.1093/icesjms/24.3.455.

Dale T., Rey F. et Heimdal B.R. (1999). Seasonal development of phytoplankton at a high latitude oceanic site. (Stn M), 419–435.

Dall'Olmo G., Dingle J., Polimene L., Brewin R.J.W. et Claustre H. (2016). Substantial energy input to the mesopelagic ecosystem from the seasonal mixed-layer pump. *Nature Geoscience*, ISSN 1752-0894, doi : 10.1038/ngeo2818.

Dall'Olmo G. et Mork K.A. (2014). Carbon export by small particles in the Norwegian Sea. *Geophysical Research Letters*, 41 (8), 2921–2927, ISSN 00948276, doi :10.1002/2014GL059244.

D'Asaro E. (2008). Convection and the seeding of the North Atlantic bloom. *Journal of Marine Systems*, 69 (3-

4), 233–237, ISSN 09247963, doi :10.1016/j.jmarsys.2005.08.005.

de Boyer Montégut C., Madec G., Fischer A.S., Lazar A. et Iudicone D. (2004). Mixed layer depth over the global ocean : An examination of profile data and a profile-based climatology. *Journal of Geophysical Research C : Oceans*, 109 (12), 1–20, ISSN 01480227, doi :10.1029/2004JC002378.

de Jong M.F., Bower A.S., Furey H.H., de Jong M.F., Bower A.S. et Furey H.H. (2014). Two Years of Observations of Warm-Core Anticyclones in the Labrador Sea and Their Seasonal Cycle in Heat and Salt Stratification. *Journal of Physical Oceanography*, 44 (2), 427–444, ISSN 0022-3670, doi :10.1175/JPO-D-13-070.1.

DeTracey B. et Tang C.L. (1997). Monthly climatological atlas of surface atmospheric conditions of the northwest Atlantic. *Canadian data report of hydrography and ocean science*.

Devred E., Sathyendranath S. et Platt T. (2007). Delineation of ecological provinces using ocean colour radiometry. *Marine Ecology Progress Series*, 346, 1–13, ISSN 0171-8630, doi :10.3354/meps07149.

Dickey T.D. (2003). Emerging ocean observations for interdisciplinary data assimilation systems. *Journal of Marine Systems*, 40 à 41 (0), 5–48, ISSN 0924-7963, doi :10.1016/S0924-7963(03)00011-3.

D'Ortenzio F. et Ribera d'Alcalà M. (2009). On the trophic regimes of the Mediterranean Sea : a satellite analysis. *Biogeosciences*, 6 (2), 139–148, doi :10.5194/bg-6-139-2009.

Ducklow H., Steinberg D. et Buesseler K. (2001). Upper Ocean Carbon Export and the Biological Pump. *Oceanography*, 14 (4), 50–58, ISSN 10428275, doi :10.5670/oceanog.2001.06.

Durbin E.E.G., Campbell R.G.R., Casas M.C.M., Ohman M.M.D., Niehoff B., Runge J. et Wagner M. (2003). Interannual variation in phytoplankton blooms and zooplankton productivity and abundance in the Gulf of Maine during winter. *Marine Ecology Progress Series*, 254 (Sverdrup 1953), 81–100, ISSN 0171-8630, doi :10.3354/meps254081.

Ebert U., Arrayás M., Temme N., Sommeijer B. et Huisman J. (2001). Critical conditions for phytoplankton blooms. *Bulletin of mathematical biology*, 63 (6), 1095–1124, ISSN 0092-8240, doi :10.1006/bulm.2001.0261.

Edwards M. et Richardson A.J. (2004). Impact of climate change on marine pelagic phenology and trophic mismatch. *Nature*, 430 (7002), 881–4, ISSN 1476-4687, doi :10.1038/nature02808.

Emery W. (2001). Water types and water masses.

Eppley R.W., Renger E.H., Venrick E.L., Mullin M.M. et Jul N. (1973). A Study of Plankton Dynamics and Nutrient Cycling in the Central Gyre of the North Pacific Ocean. *Limnology and Oceanography*, 18 (4), 534–551, ISSN 00243590, doi :10.4319/lo.1973.18.4.0534.

Eymard L., Caniaux G., Dupuis H., Prieur L., Giordani H., Troadec R., Bessemoulin P., Lachaud G., Bouhours G., Bourras D., Guérin C., Le Borgne P., Brisson A. et Marsouin A. (1999). Surface fluxes in the North Atlantic current during CATCH/FASTEX. *Quarterly Journal of the Royal Meteorological Society*, 125 (561), 3563–3599, ISSN 00359009, doi :10.1002/qj.49712556121.

Falkowski P., Kiefer D.A., Division O.S. et Angeles L. (1985). Chlorophyll a fluorescence in phytoplankton : relationship to photosynthesis and biomass. 7 (5), 715–731.

Ferrari R., Merrifield S.T. et Taylor J.R. (2014). Shutdown of convection triggers increase of surface chlorophyll. *Journal of Marine Systems*, ISSN 09247963, doi :10.1016/j.jmarsys.2014.02.009.

Field C.B. (1998). Primary Production of the Biosphere : Integrating Terrestrial and Oceanic Components. *Science*, 281 (5374), 237–240, doi :10.1126/science.281.5374.237.

Fischer A., Moberg E., Alexander H., Brownlee E., Hunter-Cevera K., Pitz K., Rosengard S. et Sosik H. (2014).

Sixty Years of Sverdrup : A Retrospective of Progress in the Study of Phytoplankton Blooms. *Oceanography*, 27 (1), 222–235, ISSN 10428275, doi :10.5670/oceanog.2014.26.

Flament P. (2002). A state variable for characterizing water masses and their diffusive stability : spiciness. *Progress in Oceanography*, 54 (1), 493–501, ISSN 00796611, doi :10.1016/S0079-6611(02)00065-4.

Follows M.J., Williams R.G. et Marshall J.C. (1996). The solubility pump of carbon in the subtropical gyre of the North Atlantic. *Journal of Marine Research*, 54 (4), 605–630, ISSN 00222402, doi : 10.1357/0022240963213682.

Fontela M., García-Ibáñez M.I., Hansell D.A., Mercier H. et Pérez F.F. (2016). Dissolved Organic Carbon in the North Atlantic Meridional Overturning Circulation. *Scientific Reports*, 6 (May), 26931, ISSN 2045-2322, doi :10.1038/srep26931.

Fox-Kemper B. et Ferrari R. (2008). Parameterization of Mixed Layer Eddies. Part II : Prognosis and Impact. *Journal of Physical Oceanography*, 38 (6), 1166–1179, ISSN 0022-3670, doi :10.1175/2007JPO3788.1.

Fox-Kemper B., Ferrari R. et Hallberg R. (2008). Parameterization of Mixed Layer Eddies. Part I : Theory and Diagnosis. *Journal of Physical Oceanography*, 38 (6), 1145–1165, ISSN 0022-3670, doi :10.1175/ 2007JPO3792.1.

Frajka-Williams E. et Rhines P.B. (2010). Physical controls and interannual variability of the Labrador Sea spring phytoplankton bloom in distinct regions. *Deep Sea Research Part I : Oceanographic Research Papers*, 57 (4), 541–552, ISSN 0967-0637, doi :10.1016/j.dsr.2010.01.003.

Franks P.J.S. (2001). Phytoplankton blooms in a fluctuating environment : the roles of plankton response time scales and grazing. *Journal of Plankton Research*, 23 (12), 1433–1441, ISSN 14643774, doi :10.1093/plankt/ 23.12.1433.

Franks P.J.S. (2014). Has Sverdrup's critical depth hypothesis been tested ? Mixed layers vs. turbulent layers. *ICES Journal of Marine Science*, p. fsu175–, ISSN 1054-3139, doi :10.1093/icesjms/fsu175.

Frost B.W. (1991). The role of grazing in nutrient-rich areas of the open sea. *Limnology and Oceanography*, 36 (8), 1616–1630, ISSN 00243590, doi :10.4319/lo.1991.36.8.1616.

Gardner W.D., Chung S.P., Richardson M.J. et Walsh I.D. (1995). The oceanic mixed-layer pump. *Deep Sea Research Part II : Topical Studies in Oceanography*, 42 (2-3), 757–775, ISSN 09670645, doi :10.1016/ 0967-0645(95)00037-Q.

Garside C. et Garside J.C. (1993). The "f-ratio" on 20°W during the North Atlantic Bloom Experiment. *Deep-Sea Research Part II*, 40 (1-2), 75–90, ISSN 09670645, doi :10.1016/0967-0645(93)90007-A.

Geider R.J. (1987). Light and Temperature Dependence of the Carbon to Chlorophyll a Ratio in Microalgae and Cyanobacteria : Implications for Physiology and Growth of Phytoplankton. *New Phytologist*, 106 (1), 1–34, ISSN 0028-646X, doi :10.1111/j.1469-8137.1987.tb04788.x.

Geider R.J., Osbonie B.A. et Raven J.A. (1986). Growth, Photosynthesis and Maintenance Metabolic Cost in the Diatom Phaeodactylum Tricornutum At Very Low Light Levels. *Journal of Phycology*, 22 (1), 39–48, ISSN 15298817, doi :10.1111/j.1529-8817.1986.tb02513.x.

Giering S.L.C., Sanders R., Lampitt R.S., Anderson T.R., Tamburini C., Boutrif M., Zubkov M.V., Marsay C.M., Henson S.A., Saw K., Cook K. et Mayor D.J. (2014). Reconciliation of the carbon budget in the ocean's twilight zone. *Nature*, 507 (7493), 480–483, ISSN 0028-0836, doi :10.1038/nature13123.

Giering S.L.C., Sanders R., Martin A.P., Lindemann C., Möller K.O., Daniels C.J., Mayor D.J. et St. John M.A. (2016). High export via small particles before the onset of the North Atlantic spring bloom. *Journal of*

Geophysical Research : Oceans, p. n/a–n/a, ISSN 2169-9291, doi :10.1002/2016JC012048.

Goldman J.C., McCarthy J.J. et Peavey D.G. (1979). Growth rate influence on the chemical composition of phytoplankton in oceanic waters. *Nature*, 279 (5710), 210–215, ISSN 0028-0836, doi :10.1038/279210a0.

Gordon H.R. et Morel A. (1983). Remote assessment of ocean color for interpretation of satellite visible imagery : A review. *Lecture Notes on Coastal and Estaurine Study*, 4, 1–114, ISSN 0025-3154, doi : 10.1029/LN004.

Gran H.H. et Braarud T. (1935). A Quantitative Study of the Phytoplankton in the Bay of Fundy and the Gulf of Maine (including Observations on Hydrography, Chemistry and Turbidity). *Journal of the Biological Board of Canada*, 1 (5), 279–467, ISSN 0368-1424, doi :10.1139/f35-012.

Granskog M.A., Pavlov A.K., Sagan S., Kowalczuk P., Raczkowska A. et Stedmon C.A. (2015). Effect of sea-ice melt on inherent optical properties and vertical distribution of solar radiant heating in Arctic surface waters. *Journal of Geophysical Research : Oceans*, 120 (10), 7028–7039, ISSN 21699291.

Große F., Lindemann C., Pätsch J. et Backhaus J.O. (2015). The influence of winter convection on primary production : A parameterisation using a hydrostatic three-dimensional biogeochemical model. *Journal of Marine Systems*, 147, 138–152, ISSN 09247963, doi :10.1016/j.jmarsys.2014.07.002.

Guidi L., Legendre L., Reygondeau G., Uitz J., Stemmann L. et Henson S.A. (2015). A new look at ocean carbon remineralization for estimating deepwater sequestration. *Global Biogeochemical Cycles*, 29 (7), 1044–1059, ISSN 08866236, doi :10.1002/2014GB005063.

Guidi L., Stemmann L., Jackson G.A., Ibanez F., Claustre H., Legendre L., Picheral M. et Gorsky G. (2009). Effects of phytoplankton community on production, size, and export of large aggregates : A world-ocean analysis. *Limnology and Oceanography*, 54 (6), 1951–1963, ISSN 00243590, doi :10.4319/lo.2009.54.6. 1951.

Hanna E., Huybrechts P., Steffen K., Cappelen J., Huff R., Shuman C., Irvine-Fynn T., Wise S. et Griffiths M. (2008). Increased Runoff from Melt from the Greenland Ice Sheet : A Response to Global Warming. *J. Climate*, 21 (2), 331–341, ISSN 0894-8755.

Hansell D., Carlson C., Repeta D. et Schlitzer R. (2009). Dissolved organic matter in the ocean : A controversy stimulates new insights.

Hartigan J.A. et Wong M.A. (1979). Algorithm AS 136 : A K-Means Clustering Algorithm. *Journal of the Royal Statistical Society. Series C (Applied Statistics)*, 28 (1), 100–108, ISSN 00359254.

Hatun, Eriksen C.C. et Rhines P.B. (2007). Buoyant Eddies Entering the Labrador Sea Observed with Gliders and Altimetry. *J. Phys. Oceanogr.*, 37 (12), 2838–2854, ISSN 0022-3670.

Head E.J.H., Harris L.R. et Campbell R.W. (2000). Investigations on the ecology of Calanus spp. in the Labrador Sea. I. Relationship between the phytoplankton bloom and reproduction and development of Calanus finmarchicus in spring. *Mar Ecol Prog Ser*, 193, 53–73.

Henson S.A., Dunne J.P. et Sarmiento J.L. (2009). Decadal variability in North Atlantic phytoplankton blooms. *Journal of Geophysical Research : Oceans*, 114 (C4), ISSN 2156-2202, doi :10.1029/2008JC005139.

Henson S.A., Robinson I., Allen J.T. et Waniek J.J. (2006). Effect of meteorological conditions on interannual variability in timing and magnitude of the spring bloom in the Irminger Basin, North Atlantic. *Deep-Sea Research Part I : Oceanographic Research Papers*, 53 (10), 1601–1615, ISSN 09670637, doi :10.1016/j.dsr. 2006.07.009.

Ho C. et Marra J. (1994). Early-spring export of phytoplankton production in the northeast Atlantic Ocean.

Marine Ecology Progress Series, 114 (1), 197–202, ISSN 0171-8630, doi :10.3354/meps114197.

Holte J. et Talley L. (2009). A New Algorithm for Finding Mixed Layer Depths with Applications to Argo Data and Subantarctic Mode Water Formation. *J. Atmos. Oceanic Technol.*, 26 (9), 1920–1939, ISSN 0739-0572.

Hosegood P., Gregg M.C. et Alford M.H. (2006). Sub-mesoscale lateral density structure in the oceanic surface mixed layer. *Geophysical Research Letters*, 33 (22), L22604, ISSN 0094-8276, doi :10.1029/2006GL026797.

Hosegood P.J., Gregg M.C. et Alford M.H. (2008). Restratification of the Surface Mixed Layer with Submesoscale Lateral Density Gradients : Diagnosing the Importance of the Horizontal Dimension. *Journal of Physical Oceanography*, 38 (11), 2438–2460, ISSN 0022-3670, doi :10.1175/2008JPO3843.1.

Huisman J., Arrayás M., Ebert U. et Sommeijer B. (2002). How do sinking phytoplankton species manage to persist ? *The American naturalist*, 159 (3), 245–254, ISSN 0003-0147, doi :10.1086/338511.

Huisman J., van Oostveen P. et Weissing F.J. (1999). Critical Depth and Critical Turbulence : Two Different Mechanisms for the Development of Phytoplankton Blooms. *Limnology and Oceanography*, 44 (7), 1781–1787, ISSN 00243590.

Incze L., Hebert D., Wolff N., Oakey N. et Dye D. (2001). Changes in copepod distributions associated with increased turbulence from wind stress. *Marine Ecology Progress Series*, 213, 229–240, ISSN 0171-8630, doi :10.3354/meps213229.

IOC, SCOR et IAPSO (2010). The International thermodynamic equation of seawater–2010 : Calculation and use of thermodynamic properties. *Intergovernmental Oceanographic Comission, UNESCO*, 56, 196.

Jackson G.A. (1993). Flux feeding as a mechanism for zooplankton grazing and its implications for vertical particulate flux 1. *Limnology and Oceanography*, 38 (6), 1328–1331, ISSN 00243590, doi :10.4319/lo.1993.38.6.1328.

Jackson G.A. et Checkley D.M. (2011). Particle size distributions in the upper 100m water column and their implications for animal feeding in the plankton. *Deep Sea Research Part I : Oceanographic Research Papers*, 58 (3), 283–297, ISSN 09670637, doi :10.1016/j.dsr.2010.12.008.

Ji R., Edwards M., Mackas D.L., Runge J.a. et Thomas A.C. (2010). Marine plankton phenology and life history in a changing climate : current research and future directions. *Journal of plankton research*, 32 (10), 1355–1368, ISSN 0142-7873, doi :10.1093/plankt/fbq062.

Johnson G.C., Schmidtko S. et Lyman J.M. (2012). Relative contributions of temperature and salinity to seasonal mixed layer density changes and horizontal density gradients. *Journal of Geophysical Research : Oceans*, 117 (4), ISSN 21699291.

Johnson L., Lee C.M. et D'Asaro E.A. (2016). Global Estimates of Lateral Springtime Restratification. *Journal of Physical Oceanography*, 46 (5), 1555–1573, ISSN 0022-3670, doi :10.1175/JPO-D-15-0163.1.

Jónasdóttir S.H., Visser A.W., Richardson K. et Heath M.R. (2015). Seasonal copepod lipid pump promotes carbon sequestration in the deep North Atlantic. *Proceedings of the National Academy of Sciences of the United States of America*, 112 (39), 12122–6, ISSN 1091-6490, doi :10.1073/pnas.1512110112.

Karleskind P., Lévy M. et Memery L. (2011). Subduction of carbon, nitrogen, and oxygen in the northeast Atlantic. *Journal of Geophysical Research*, 116 (C2), 1–17, ISSN 0148-0227, doi :10.1029/2010JC006446.

Katsman C.A., Spall M.A., Pickart R.S. et Hole W. (2004). Boundary Current Eddies and Their Role in the Restratification of the Labrador Sea *. *Journal of Physical Oceanography*, 34, 1967–1983, ISSN 0022-3670, doi :10.1175/1520-0485(2004)034<1967:BCEATR>2.0.CO;2.

Keeling R.F. et Peng T.h. (1995). Transport of heat, CO2 and O2 by the Atlantic's thermohaline circulation, doi :10.1098/rstb.1995.0055.

KIRK J.T.O. (1984). Dependence of relationship between inherent and apparent optical properties of water on solar altitude. *Limnology and Oceanography*, 29 (2), 350–356, ISSN 00243590, doi :10.4319/lo.1984.29.2.0350.

Klein P. et Lapeyre G. (2009). The Oceanic Vertical Pump Induced by Mesoscale and Submesoscale Turbulence. *Annual Review of Marine Science*, 1 (1), 351–375, doi :10.1146/annurev.marine.010908.163704.

Koeve W. et Pollehne F. (2002). Storm-induced convective export of organic matter during spring in the northeast Atlantic Ocean. *Deep Sea Research Part I : . . . .*

Körtzinger A., Send U., Lampitt R.S., Hartman S., Wallace D.W.R., Karstensen J., Villagarcia M.G., Llinás O. et DeGrandpre M.D. (2008). The seasonal p CO 2 cycle at 49°N/16.5°W in the northeastern Atlantic Ocean and what it tells us about biological productivity. *Journal of Geophysical Research*, 113 (C4), C04020, ISSN 0148-0227, doi :10.1029/2007JC004347.

Lacour L., Claustre H., Prieur L. et Ortenzio F.D. (2015). Phytoplankton biomass cycles in the North Atlantic subpolar gyre : A similar mechanism for two different blooms in the Labrador Sea. *Geophysical Research Letters*, p. 1–8, doi :10.1002/2015GL064540.Received.

Lagadeuc Y., Boulé M. et Dodson J.J. (1997). Effect of vertical mixing on the vertical distribution of copepods in coastal waters. *Journal of plankton research*, 19 (9), 1183–1204, ISSN 01427873 (ISSN), doi :10.1093/plankt/19.9.1183.

Lampitt R.S., Salter I., de Cuevas B.A., Hartman S., Larkin K.E. et Pebody C.A. (2010). Long-term variability of downward particle flux in the deep northeast Atlantic : Causes and trends. *Deep-Sea Research Part II : Topical Studies in Oceanography*, 57 (15), 1346–1361, ISSN 09670645, doi :10.1016/j.dsr2.2010.01.011.

Lampitt R.S., Wishner K.F., Turley C.M. et Angel M.V. (1993). Marine snow studies in the Northeast Atlantic Ocean : distribution, composition and role as a food source for migrating plankton. *Marine Biology*, 116 (4), 689–702, ISSN 0025-3162, doi :10.1007/BF00355486.

Lavigne H., D'Ortenzio F., Migon C., Claustre H., Testor P., D'Alcalà M.R., Lavezza R., Houpert L. et Prieur L. (2013). Enhancing the comprehension of mixed layer depth control on the Mediterranean phytoplankton phenology. *Journal of Geophysical Research : Oceans*, 118 (7), 3416–3430, ISSN 21699275, doi :10.1002/jgrc.20251.

Lehahn Y., Koren I., Schatz D., Frada M., Sheyn U., Boss E., Efrati S., Rudich Y., Trainic M., Sharoni S., Laber C., DiTullio G., Coolen M., Martins A., Van Mooy B., Bidle K. et Vardi A. (2014). Decoupling Physical from Biological Processes to Assess the Impact of Viruses on a Mesoscale Algal Bloom. *Current Biology*, ISSN 09609822, doi :10.1016/j.cub.2014.07.046.

Lévy M. (2008). The modulation of biological production by oceanic mesoscale turbulence, Lect. Notes Phys., dans J.B. Weiss et A. Provenzale, rédacteurs, *Transport in Geophysical flow : Ten years after*, 744, p. 219–261, Springler, doi :10.1007/978-3-540-75215-8-9.

Lévy M., Iovino D., Resplandy L., Klein P., Madec G., a. M. Tréguier, Masson S. et Takahashi K. (2012). Large-scale impacts of submesoscale dynamics on phytoplankton : Local and remote effects. *Ocean Modelling*, 43-44, 77–93, ISSN 14635003, doi :10.1016/j.ocemod.2011.12.003.

Lévy M. et Jahn O. (2014). Phytoplankton diversity and community structure affected by oceanic dispersal and mesoscale turbulence. . . . *Fluids and Environments*.

Lévy M., Klein P. et Treguier A.M. (2001). Impact of sub-mesoscale physics on production and subduction of phytoplankton in an oligotrophic regime. *Journal of Marine Research*, 59 (4), 535–565, ISSN 00222402, doi :10.1357/002224001762842181.

Levy M. et Martin A.P. (2013). The influence of mesoscale and submesoscale heterogeneity on ocean biogeochemical reactions. *Global Biogeochemical Cycles*, ISSN 1944-9224, doi :10.1002/2012GB004518.

Lindemann C., Backhaus J.O. et St John M.A. (2015). Physiological constrains on Sverdrup's Critical-Depth-Hypothesis : the influences of dark respiration and sinking. *ICES Journal of Marine Science : Journal du Conseil*, 72 (6), 1942–1951, ISSN 1054-3139, doi :10.1093/icesjms/fsv046.

Lindemann C. et St. John M.A. (2014). A seasonal diary of phytoplankton in the North Atlantic. *Frontiers in Marine Science*, 1, 37, ISSN 2296-7745, doi :10.3389/fmars.2014.00037.

Litchman E. (2000). Growth rates of phytoplankton under fluctuating light. *Freshwater Biology*, 44 (2), 223–235, ISSN 0046-5070, doi :10.1046/j.1365-2427.2000.00559.x.

Longhurst A., Sathyendranath S., Platt T. et Caverhill C. (1995). An estimate of global primary production in the ocean from satellite radiometer data. *Journal of Plankton Research*, 17, 1245–1271, ISSN 0142-7873, doi :10.1093/plankt/17.6.1245.

Longhurst A.R. (2007). Chapter 9 - The Atlantic Ocean, dans A.R. Longhurst, rédacteur, *Ecological Geography of the Sea (Second Edition)*, p. 131–273, Academic Press, Burlington, second edi édition, ISBN 978-0-12-455521-1, doi :http://dx.doi.org/10.1016/B978-012455521-1/50010-3.

Mackas D.L., Sefton H., Miller C.B. et Raich A. (1993). Vertical habitat partitioning by large calanoid copepods in the oceanic subarctic Pacific during Spring. *Progress in Oceanography*, 32 (1), 259–294, ISSN 00796611, doi :10.1016/0079-6611(93)90017-8.

MacKenzie B.R. (2000). Turbulence, larval fish ecology and fisheries recruitment : a review of field studies. *Oceanologica Acta*, 23 (4), 357–375, ISSN 03991784, doi :10.1016/S0399-1784(00)00142-0.

Mahadevan A. (2016). The Impact of Submesoscale Physics on Primary Productivity of Plankton. *Annual review of marine science*, 8, 161–84, ISSN 1941-0611, doi :10.1146/annurev-marine-010814-015912.

Mahadevan A., Lee C., Perry M.J. et D'Asaro E. (2012). RESEARCH ARTICLES Eddy-Driven Stratification Initiates North Atlantic Spring Phytoplankton Blooms. *Science*, 337 (6090), 54–58, doi :10.1126/science.1218740.

Mahadevan A. et Tandon A. (2006). An analysis of mechanisms for submesoscale vertical motion at ocean fronts. *Ocean Modelling*, 14 (3), 241–256, ISSN 14635003, doi :10.1016/j.ocemod.2006.05.006.

Mahadevan A., Tandon A. et Ferrari R. (2010). Rapid changes in mixed layer stratification driven by submesoscale instabilities and winds. *Journal of Geophysical Research*, 115 (C3), C03017, ISSN 0148-0227, doi :10.1029/2008JC005203.

Marra J. (2004). The compensation irradiance for phytoplankton in nature. *Geophysical Research Letters*, 31 (6), L06305, ISSN 0094-8276, doi :10.1029/2003GL018881.

Marra J. et Barber R.T. (2005). Primary productivity in the Arabian Sea : A synthesis of JGOFS data. *Progress in Oceanography*, 65 (2-4), 159–175, ISSN 00796611, doi :10.1016/j.pocean.2005.03.004.

Martin P., Lampitt R.S., Jane Perry M., Sanders R., Lee C. et D'Asaro E. (2011). Export and mesopelagic particle flux during a North Atlantic spring diatom bloom. *Deep Sea Research Part I : Oceanographic Research Papers*, 58 (4), 338–349, ISSN 09670637, doi :10.1016/j.dsr.2011.01.006.

Martinez E., Antoine D., D'Ortenzio F. et Gentili B. (2009). Climate-driven basin-scale decadal oscillations

of oceanic phytoplankton. *Science (New York, N.Y.)*, 326 (5957), 1253–6, ISSN 1095-9203, doi :10.1126/science.1177012.

Martinez E., Raitsos D.E. et Antoine D. (2016). Warmer, deeper, and greener mixed layers in the North Atlantic subpolar gyre over the last 50 years. *Global Change Biology*, 22 (2), 604–612, ISSN 13652486, doi :10.1111/gcb.13100.

Martinez-Vicente V., Dall'Olmo G., Tarran G., Boss E. et Sathyendranath S. (2013). Optical backscattering is correlated with phytoplankton carbon across the Atlantic Ocean. *Geophysical Research Letters*, p. n/a–n/a, ISSN 1944-8007, doi :10.1002/grl.50252.

Martinez-Vicente V., Tilstone G., Sathyendranath S., Miller P. et Groom S. (2012). Contributions of phytoplankton and bacteria to the optical backscattering coefficient over the Mid-Atlantic Ridge. *Marine Ecology Progress Series*, 445, 37–51, ISSN 0171-8630, doi :10.3354/meps09388.

Matsuoka A., Babin M., Doxaran D., Hooker S.B., Mitchell B.G., Bélanger S. et Bricaud A. (2014). A synthesis of light absorption properties of the Arctic Ocean : application to semianalytical estimates of dissolved organic carbon concentrations from space. *Biogeosciences*, 11 (12), 3131–3147, ISSN 1726-4189, doi : 10.5194/bg-11-3131-2014.

McGillicuddy D.J. (2015). Mechanisms of Physical-Biological-Biogeochemical Interaction at the Oceanic Mesoscale. *Annual review of marine science*, ISSN 1941-0611, doi :10.1146/annurev-marine-010814-015606.

McGillicuddy D.J., Anderson L.A., Doney S.C. et Maltrud M.E. (2003). Eddy-driven sources and sinks of nutrients in the upper ocean : Results from a 0.1 resolution model of the North Atlantic. *Global Biogeochemical Cycles*, 17 (2), ISSN 08866236, doi :10.1029/2002GB001987.

McQuoid M.R. et Hobson L.A. (1996). Diatom resting stages. *Journal of Phycology*, 32, 889–902.

Mignot A., Claustre H., Uitz J., Poteau A., D'Ortenzio F. et Xing X. (2014). Understanding the seasonal dynamics of phytoplankton biomass and the deep chlorophyll maximum in oligotrophic environments : A Bio-Argo float investigation. *Global Biogeochemical Cycles*, 28 (8), 856–876, ISSN 19449224, doi : 10.1002/2013GB004781.

Milligan G. et Cooper M. (1985). An examination of procedures for determining the number of clusters in a data set. *Psychometrika*, 50 (2), 159–179, ISSN 0033-3123, doi :10.1007/BF02294245.

Morel A. (1991). Light and marine photosynthesis : a spectral model with geochemical and climatological implications. *Progress in Oceanography*, 26 (3), 263–306, ISSN 00796611, doi :10.1016/0079-6611(91)90004-6.

Morel A., Claustre H. et Gentili B. (2010). The most oligotrophic subtropical zones of the global ocean : Similarities and differences in terms of chlorophyll and yellow substance. *Biogeosciences*, 7 (10), 3139–3151, ISSN 17264170, doi :10.5194/bg-7-3139-2010.

Murphy A.M. et Cowles T.J. (1997). Effects of darkness on multi-excitation in vivo fluorescence and survival in a marine diatom. *Limnology and Oceanography*, 42 (6), 1444–1453, ISSN 00243590, doi :10.4319/lo.1997.42.6.1444.

Omand M.M., D'Asaro E.A., Lee C.M., Perry M.J., Briggs N., Cetinić I. et Mahadevan A. (2015). Eddy-driven subduction exports particulate organic carbon from the spring bloom. *Science*, 348 (6231), 222–225, ISSN 1095-9203, doi :10.1126/science.1260062.

Organelli E., Claustre H., Bricaud A., Schmechtig C., Poteau A., Xing X., Prieur L., D'Ortenzio F., Dall'Olmo G. et Vellucci V. (2016). A novel near real-time quality-control procedure for radiometric profiles measu-

red by Bio-Argo floats : protocols and performances. *Journal of Atmospheric and Oceanic Technology*, p. 160303130530002, ISSN 0739-0572, doi :10.1175/JTECH-D-15-0193.1.

Passow U. (2002). Transparent exopolymer particles (TEP) in aquatic environments. *Progress in Oceanography*, 55 (3), 287–333, ISSN 00796611, doi :10.1016/S0079-6611(02)00138-6.

Paulsen M., Riisgaard K., Thingstad T., St John M. et Nielsen T. (2015). Winter-spring transition in the subarctic Atlantic : microbial response to deep mixing and pre-bloom production. *Aquatic Microbial Ecology*, 76 (1), 49–69, ISSN 0948-3055, doi :10.3354/ame01767.

Pérez F.F., Mercier H., Vázquez-Rodríguez M., Lherminier P., Velo A., Pardo P.C., Rosón G. et Ríos A.F. (2013). Atlantic Ocean CO2 uptake reduced by weakening of the meridional overturning circulation. *Nature Geoscience*, 6 (2), 146–152, ISSN 1752-0894, doi :10.1038/ngeo1680.

Platt T., Bird D.F. et Sathyendranath S. (1991). Critical Depth and Marine Primary Production. *Proceedings of the Royal Society B : Biological Sciences*, 246 (1317), 205–217, ISSN 0962-8452, doi :10.1098/rspb.1991.0146.

Poulton A.J., Holligan P.M., Hickman A., Kim Y.N., Adey T.R., Stinchcombe M.C., Holeton C., Root S. et Woodward E.M.S. (2006). Phytoplankton carbon fixation, chlorophyll-biomass and diagnostic pigments in the Atlantic Ocean. *Deep Sea Research Part II : Topical Studies in Oceanography*, 53 (14-16), 1593–1610, ISSN 09670645, doi :10.1016/j.dsr2.2006.05.007.

Price J., Weller R. et Pinkel R. (1986). Diurnal cycling : Observations and models of the upper ocean response to diurnal heating, cooling, and wind mixing. . . . *Geophysical Research : Oceans* . . . .

Price J.F. (1979). Observations of a Rain-Formed Mixed Layer. *Journal of Physical Oceanography*, 9 (3), 643–649, ISSN 0022-3670, doi :10.1175/1520-0485(1979)009<0643:OOARFM>2.0.CO;2.

Prieur L. et Legendre L. (1988). Oceanographic criteria for new phytoplankton production. *Toward a Theory on Biological-Physical Interactions in the World Ocean*, 239, pp 71–112.

Provenzale A. (1999). Transport by coherent barotropic vortices. *Annual Review of Fluid Mechanics*, 31, 55–93, doi :10.1146/annurev.fluid.31.1.55.

Racault M.F., Le Quéré C., Buitenhuis E., Sathyendranath S. et Platt T. (2012). Phytoplankton phenology in the global ocean. *Ecological Indicators*, 14 (1), 152–163, ISSN 1470160X, doi :10.1016/j.ecolind.2011.07.010.

Reverdin G., Niiler P.P. et Valdimarsson H. (2003). North Atlantic Ocean surface currents. *Journal of Geophysical Research : Oceans*, 108 (C1), 2–21, ISSN 2156-2202, doi :10.1029/2001JC001020.

Reygondeau G., Longhurst A., Martinez E., Beaugrand G., Antoine D. et Maury O. (2013). Dynamic biogeochemical provinces in the global ocean. *Global Biogeochemical Cycles*, 27 (4), 1046–1058, ISSN 08866236, doi :10.1002/gbc.20089.

Riley G.A. (1942). The relationship of vertical turbulence and spring diatom flowerings. *Journal of Marine Research*, V, 67–87.

Riley G.a. (1957). Phytoplankton of the North Central Sargasso Sea. *Limnology and Oceanography*, 2 (3), 252–270, ISSN 1939-5590, doi :10.1002/lno.1957.2.3.0252.

Riley G.A. et Bumpus D.F. (1946). *Phytoplankton-zooplankton Relationships on Georges Bank*.

Sabine C.L., Feely R.A., Gruber N., Key R.M., Lee K., Bullister J.L., Wanninkhof R., Wong C.S., Wallace D.W.R., Tilbrook B., Millero F.J., Peng T.H., Kozyr A., Ono T. et Rios A.F. (2004). The oceanic sink for anthropogenic CO2. *Science (New York, N.Y.)*, 305 (5682), 367–71, ISSN 1095-9203, doi :10.1126/science.1097403.

Sackmann B.S., Perry M.J. et Eriksen C.C. (2008). Seaglider observations of variability in daytime fluorescence quenching of chlorophyll-*a* in Northeastern Pacific coastal waters. *Biogeosciences Discussions*, 5 (4), 2839–2865, ISSN 1810-6285, doi :10.5194/bgd-5-2839-2008.

Sallee J.B., Matear R.J., Rintoul S.R. et Lenton A. (2012). Localized subduction of anthropogenic carbon dioxide in the Southern Hemisphere oceans. *Nature Geoscience*, 5 (8), 579–584, ISSN 1752-0894, doi : 10.1038/ngeo1523.

Sanders R., Henson S.A., Koski M., De La Rocha C.L., Painter S.C., Poulton A.J., Riley J., Salihoglu B., Visser A., Yool A., Bellerby R. et Martin A.P. (2014). The Biological Carbon Pump in the North Atlantic. *Progress in Oceanography*, 129 (PB), 200–218, ISSN 00796611, doi :10.1016/j.pocean.2014.05.005.

Schmechtig C., Claustre H., Poteau A. et D'Ortenzio F. (2014). Bio-Argo quality control manual for the Chlorophyll-A concentration. *Ifremer*, p. 13, doi :http://dx.doi.org/10.13155/35385Bio-Argo.

Schmidt S. et Send U. (2007). Origin and Composition of Seasonal Labrador Sea Freshwater. *Journal of Physical Oceanography*, 37 (6), 1445–1454, ISSN 0022-3670, doi :10.1175/JPO3065.1.

Schulze L.M., Pickart R.S. et Moore G. (2016). Atmospheric forcing during active convection in the Labrador Sea and its impact on mixed-layer depth. *Journal of Geophysical Research : Oceans*, ISSN 21699275, doi : 10.1002/2015JC011607.

Siegel D.A., Buesseler K.O., Behrenfeld M.J., Benitez-Nelson C.R., Boss E., Brzezinski M.A., Burd A., Carlson C.A., D'Asaro E.A., Doney S.C., Perry M.J., Stanley R.H.R. et Steinberg D.K. (2016). Prediction of the Export and Fate of Global Ocean Net Primary Production : The EXPORTS Science Plan. *Frontiers in Marine Science*, 3, 22, ISSN 2296-7745, doi :10.3389/fmars.2016.00022.

Siegel D.A., Doney S.C. et Yoder J.A. (2002). The North Atlantic Spring Phytoplankton Bloom and Sverdrup's Critical Depth Hypothesis. *Science*, 296 (5568), 730–733, doi :10.1126/science.1069174.

Sinha B., Buitenhuis E.T., Quéré C.L. et Anderson T.R. (2010). Comparison of the emergent behavior of a complex ecosystem model in two ocean general circulation models. *Progress in Oceanography*, 84 (3), 204–224, ISSN 00796611, doi :10.1016/j.pocean.2009.10.003.

Smayda T.J. (1970). The suspension and sinking of phytoplankton in the sea. *Oceanogr. Mar. Biol. Ann. Rev.*, 8, 353–414.

Smayda T.J. et Mitchell-Innes B. (1974). Dark survival of autotrophic, planktonic marine diatoms. *Marine Biology*, 25 (3), 195–202, ISSN 00253162, doi :10.1007/BF00394965.

Smetacek V. (1999). Diatoms and the ocean carbon cycle. *Protist News*, 150 (1), 25–32, ISSN 1434-4610, doi :10.1016/S1434-4610(99)70006-4.

Smetacek V. et Passow U. (1990). Spring bloom initiation and Sverdrup's critical-depth model. *Limnology and Oceanography*, 35 (1), 228–234, ISSN 00243590, doi :10.4319/lo.1990.35.1.0228.

Smetacek V.S. (1985). Role of sinking in diatom life-history cycles : ecological, evolutionary and geological significance. *Marine Biology*, 84 (3), 239–251, ISSN 0025-3162, doi :10.1007/BF00392493.

Steinberg D.K., Carlson C.A., Bates N.R., Goldthwait S.A., Madin L.P. et Michaels A.F. (2000). Zooplankton vertical migration and the active transport of dissolved organic and inorganic carbon in the Sargasso Sea. *Deep Sea Research Part I : Oceanographic Research Papers*, 47 (1), 137–158, ISSN 09670637, doi :10.1016/S0967-0637(99)00052-7.

Steinberg D.K., Van Mooy B.A.S., Buesseler K.O., Boyd P.W., Kobari T. et Karl D.M. (2008). Bacterial vs. zooplankton control of sinking particle flux in the ocean's twilight zone. *Limnology and Oceanography*,

53 (4), 1327–1338, ISSN 00243590, doi :10.4319/lo.2008.53.4.1327.

Stramska M. et Dickey T.D. (1994). Modeling phytoplankton dynamics in the northeast Atlantic during the initiation of the spring bloom. *Journal of Geophysical Research*, 99 (C5), 10241, ISSN 0148-0227, doi : 10.1029/93JC03378.

Sverdrup H.U. (1953). On conditions for the vernal blooming of phytoplankton. *Journal du conseil international pour l'exploitation de la mer*, 18, 287–295.

Takahashi T., Sutherland S.C., Wanninkhof R., Sweeney C., Feely R.A., Chipman D.W., Hales B., Friederich G., Chavez F., Sabine C., Watson A., Bakker D.C.E., Schuster U., Metzl N., Yoshikawa-Inoue H., Ishii M., Midorikawa T., Nojiri Y., Kortzinger A., Steinhoff T., Hoppema M., Olafsson J., Arnarson T.S., Tilbrook B., Johannessen T., Olsen A., Bellerby R., Wong C.S., Delille B., Bates N.R. et de Baar H.J.W. (2009). Climatological mean and decadal change in surface ocean pCO2, and net sea-air {CO2} flux over the global oceans. *Deep Sea Research Part II : Topical Studies in Oceanography*, 56, 554–577, ISSN 0967-0645, doi : 10.1016/j.dsr2.2008.12.009.

Taylor J.R. et Ferrari R. (2011a). Ocean fronts trigger high latitude phytoplankton blooms. *Geophysical Research Letters*, 38 (23), n/a–n/a, ISSN 00948276, doi :10.1029/2011GL049312.

Taylor J.R. et Ferrari R. (2011b). Shutdown of turbulent convection as a new criterion for the onset of spring phytoplankton blooms. *Limnol. Oceanogr.*, 56(6), 2293–2307.

Thomas L.N. et Lee C.M. (2005). Intensification of ocean fronts. *Bulletin of the American Meteorological Society*, 86 (6), 783, ISSN 00030007, doi :10.1175/JPO2737.1.

Tian R.C., Deibel D., Rivkin R.B. et Vézina A.F. (2004). Biogenic carbon and nitrogen export in a deep-convection region : simulations in the Labrador Sea. *Deep Sea Research Part I : Oceanographic Research Papers*, 51 (3), 413–437, ISSN 09670637, doi :10.1016/j.dsr.2003.10.015.

Townsend D.W., Keller M.D., Sieracki M.E. et Ackleson S.G. (1992). Spring phytoplankton blooms in the absence of vertical water column stratification. *Nature*, 360 (6399), 59–62.

Turner J. (2002). Zooplankton fecal pellets, marine snow and sinking phytoplankton blooms. *Aquatic Microbial Ecology*, 27 (1), 57–102, ISSN 0948-3055, doi :10.3354/ame027057.

Turner J.T. (2015). Zooplankton fecal pellets, marine snow, phytodetritus and the ocean's biological pump. *Progress in Oceanography*, 130, 205–248, ISSN 00796611, doi :10.1016/j.pocean.2014.08.005.

Vardi A., Haramaty L., Van Mooy B.A.S., Fredricks H.F., Kimmance S.A., Larsen A. et Bidle K.D. (2012). Host-virus dynamics and subcellular controls of cell fate in a natural coccolithophore population. *Proceedings of the National Academy of Sciences of the United States of America*, 109 (47), 19327–32, ISSN 1091-6490, doi :10.1073/pnas.1208895109.

Vichi M., Allen J.I., Masina S. et Hardman-Mountford N.J. (2011). The emergence of ocean biogeochemical provinces : A quantitative assessment and a diagnostic for model evaluation. *Global Biogeochemical Cycles*, 25 (2), n/a–n/a, ISSN 08866236, doi :10.1029/2010GB003867.

Vidussi F., Claustre H., Manca B.B., Luchetta A. et Marty J.C. (2001). Phytoplankton pigment distribution in relation to upper thermocline circulation in the eastern Mediterranean Sea during winter. *Journal of Geophysical Research*, 106 (C9), 19939, ISSN 0148-0227, doi :10.1029/1999JC000308.

Villa-Alfageme M., de Soto F.C., Ceballos-Romero E., Giering S., Le Moigne F.A.C., Henson S. et Sanders R.J. (2016). Geographical, seasonal and depth variation in sinking particle speeds in the North Atlantic. *Manuscript submitted for publication*, ISSN 00948276, doi :10.1002/2016GL069233.

Walter B., Peters J., van Beusekom J.E.E. et St. John M.A. (2015). Interactive effects of temperature and light during deep convection : a case study on growth and condition of the diatom Thalassiosira weissflogii. *ICES Journal of Marine Science : Journal du Conseil*, 72 (6), 2061–2071, doi :10.1093/icesjms/fsu218.

Wong A., Keeley R., Carval T. et Argo Data Management Team (2015). Argo Quality Control Manual For CTD and Trajectory Data. (December), 1–56.

Woods J. et Onken R. (1982). Diurnal variation and primary production in the ocean preliminary results of a Lagrangian ensemble model. *Journal of Plankton Research*, 4 (3), 735–756, ISSN 0142-7873, doi :10.1093/plankt/4.3.735.

Woods J.D. (1980). Diurnal and seasonal variation of convection in the wind-mixed layer of the ocean. *Quarterly Journal of the Royal Meteorological Society*, 106 (449), 379–394, ISSN 00359009, doi :10.1002/qj.49710644902.

Wu Y., Platt T., Tang C.C.L. et Sathyendranath S. (2008). Regional differences in the timing of the spring bloom in the Labrador Sea. *Mar Ecol Prog Ser*, 355, 9–20.

Xing X., Claustre H., Blain S., D'Ortenzio F., Antoine D., Ras J. et Guinet C. (2012). Quenching correction for in vivo chlorophyll fluorescence acquired by autonomous platforms : A case study with instrumented elephant seals in the Kerguelen region (Southern Ocean). *Limnology and Oceanography : Methods*, 10 (7), 483–495, ISSN 1541-5856, doi :10.4319/lom.2012.10.483.

Xing X., Morel A., Claustre H., Antoine D., D'Ortenzio F., Poteau A. et Mignot A. (2011). Combined processing and mutual interpretation of radiometry and fluorimetry from autonomous profiling Bio-Argo floats : Chlorophyll a retrieval. *Journal of Geophysical Research*, 116 (C6), C06020, ISSN 0148-0227, doi : 10.1029/2010JC006899.

Zawada D.G., Zaneveld J.R.V., Boss E., Gardner W.D., Richardson M.J. et Mishonov A.V. (2005). A comparison of hydrographically and optically derived mixed layer depths. *Journal of Geophysical Research*, 110 (C11), C11001, ISSN 0148-0227, doi :10.1029/2004JC002417.

ANNEXE A

Supporting information for : *Phytoplankton biomasse cyles in the North Atlantic subpolar gyre : a similar mechanism for two different blooms in the Labrador Sea*

AGU PUBLICATIONS

Geophysical Research Letter

Supporting Information for

Phytoplankton biomass cycles in the North Atlantic sub-polar gyre: a similar mechanism for two different blooms in the Labrador Sea

Léo Lacour[1,2], Hervé Claustre[1,2], Louis Prieur[1,2], Fabrizio D'Ortenzio[1,2]

[1]Sorbonne Universités, UPMC Univ Paris 06, UMR 7093, LOV, Observatoire océanologique, F-06230, Villefranche/mer, France

[2]CNRS, UMR 7093, LOV, Observatoire océanologique, F-06230, Villefranche/mer, France

Contents of this file

Introduction

This supporting information provides explanations on the calculation of Eddy Kinetic Energy (EKE) map in the background of Figure 1 (Text S1), gives details on the test for choosing the appropriate number of cluster (Text S2 and Figure S1) and bring more precisions on criteria used by *Holte and Talley* [2009] algorithm to estimate the MLD (Text S2). Figure S2 shows the bioregionalization of the Labrador Sea. Figure S3 shows a monthly climatology of sea ice concentration in the Labrador Sea, Figure S4 shows the location of float data used in this study, Figure S5 is the density time series of both bioregions of the Labrador Sea and Figure S6 shows nutrient availability in the Labrador Sea.

Text S1.

ANDRO database [*Ollitrault and Rannou*, 2012] is an Argo-based deep displacement atlas. Each float cycle (deep displacement between 2 profiles) gives an estimation of the zonal and meridional current velocities at their drifting depth (mostly around 1000 m). During 1998-2010, around 5800 cycles were available in the LS. These velocities were binned into 1° by 1° box and then averaged in space and time. Only the box containing more than 5 data were kept. Standard deviation of the zonal (u') and meridional (v') velocity components in each box were used to calculate the mean deep eddy kinetic energy (EKE) as follows : EKE=1/2 (u'2 + v'2) where the overbar denotes the time average over the whole period (1998-2010). EKE was

then interpolated on a finer grid by a Gaussian correlation function, weighted by the local number of data, with a decorrelation radius of 100 km.

Text S2.

The optimal number of cluster to bioregionalize the North Atlantic is estimated using the Calinski and Harabazs index (Figure S1). This index measures the ratio between the dispersion of the Chla data within a cluster and the dispersion between the clusters. The optimal number of clusters is obtained when the index remains unaltered for the increasing number of cluster (from 2 to 10, [*Calinski and Harabasz*, 1974; *Milligan and Cooper*, 1985; *D'Ortenzio and Ribera d'Alcalà*, 2009]). Here, from 5 clusters, the index does not decrease significantly. A final visual check allowed us to choose 6 clusters. To test the relevance and the stability of the regionalization with 6 clusters, two statistical tests were performed. The original data set was modified with two resampling methods, the subsetting method which randomly samples half of the original dataset and the noise method which randomly replaces 5% of the original data set with noise data [*Hennig*, 2007]. The clusterization was applied to both modified data set and the results were compared to the clusters obtained from the original data set. The comparison was performed with the Jaccard coefficient, which is a similarity measure between various sets. A Jaccard coefficient greater than 0.75 indicates that the cluster is relevant and stable [*Hennig*, 2007]. The results of both tests, summarized in Table S1 show that the 6 clusters chosen are relevant and stables.

Text S3.

In this study, the density algorithm from *Holte and Talley* [2009] is used for estimating the mixed layer depth (MLD). A suite of possible MLD is calculated based on different criteria. Some physical features of the temperature and density profile are used to help choosing the final MLD value. The different criteria and physical features used are the density threshold (0.03 kg.m-3), the density gradient (0.0005 kg.m-3.dbar-1), the intersection of the density mixed layer and thermocline fits, the temperature threshold (0.2 °C), the collocated temperature and temperature gradient maxima, the temperature maximum and the final MLDs from the temperature and salinity algorithm (see Figure 3, 8 and 9 in Holte and Talley [2009]). The range of possible mixed layer depth according to the different criteria used in the method does not exceed a mean value of 52 m in the North LS and 187 m in the South LS over the year. The weak MLD range in the North LS demonstrates that the choice of the criteria does not impact significantly the results of the light-mixing model. The results in the South LS could be more influenced by the choice of the criteria.
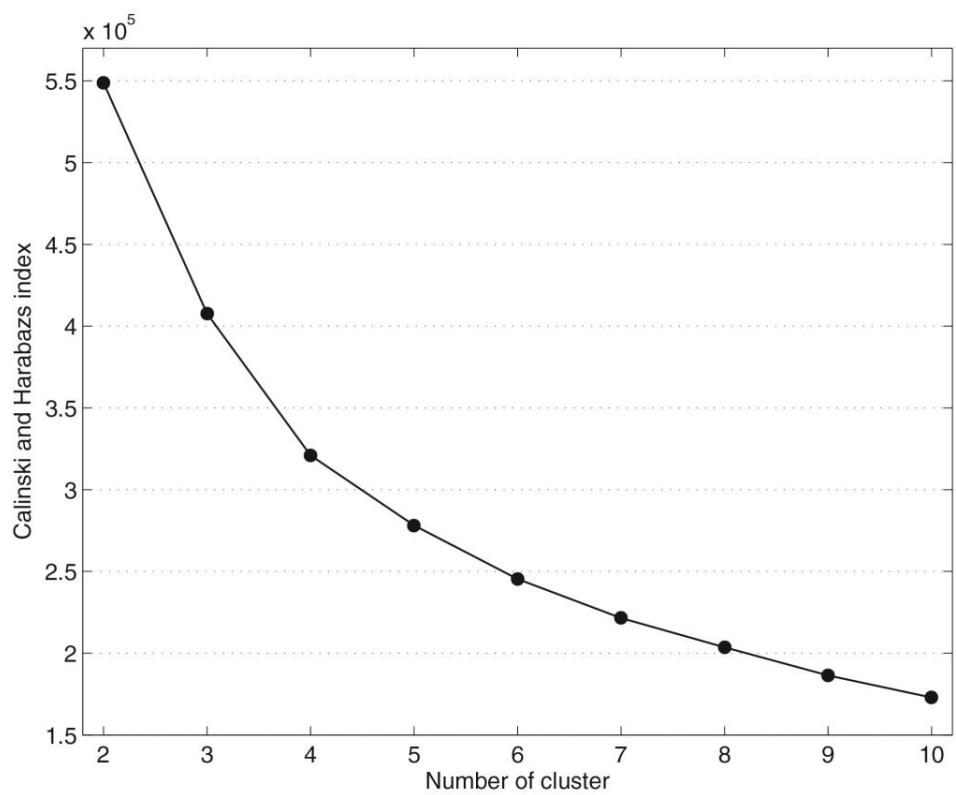
Figure S1. Calinski and Harabazs index to estimate the optimal number of cluster to use for the bioregionalization of the North Atlantic.
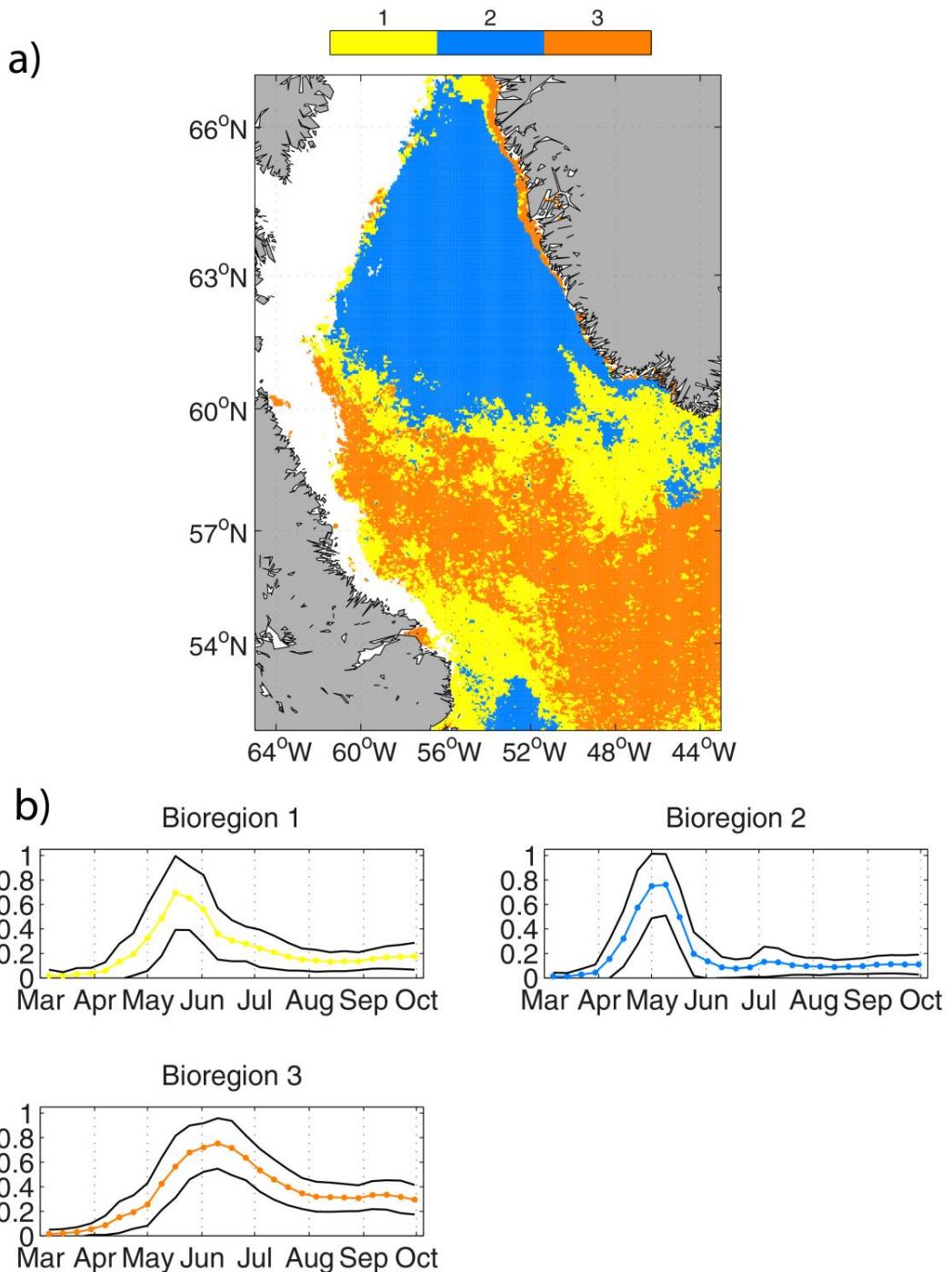
Figure S2. Spatial distribution of the clusters obtained from the K-means analysis (a) and mean normalized Chla annual cycles in each cluster +/- one standard deviation. Each cluster is considered as a bioregion with a spatiotemporal coherence with respect to phytoplankton biomass cycles. Bioregion 2 and 3 are the so called North LS and South LS region respectively. Bioregion 3 is a transitional region between bioregion 2 and 3. The use of 3 clusters allows defining more precisely the North LS and South LS regions.
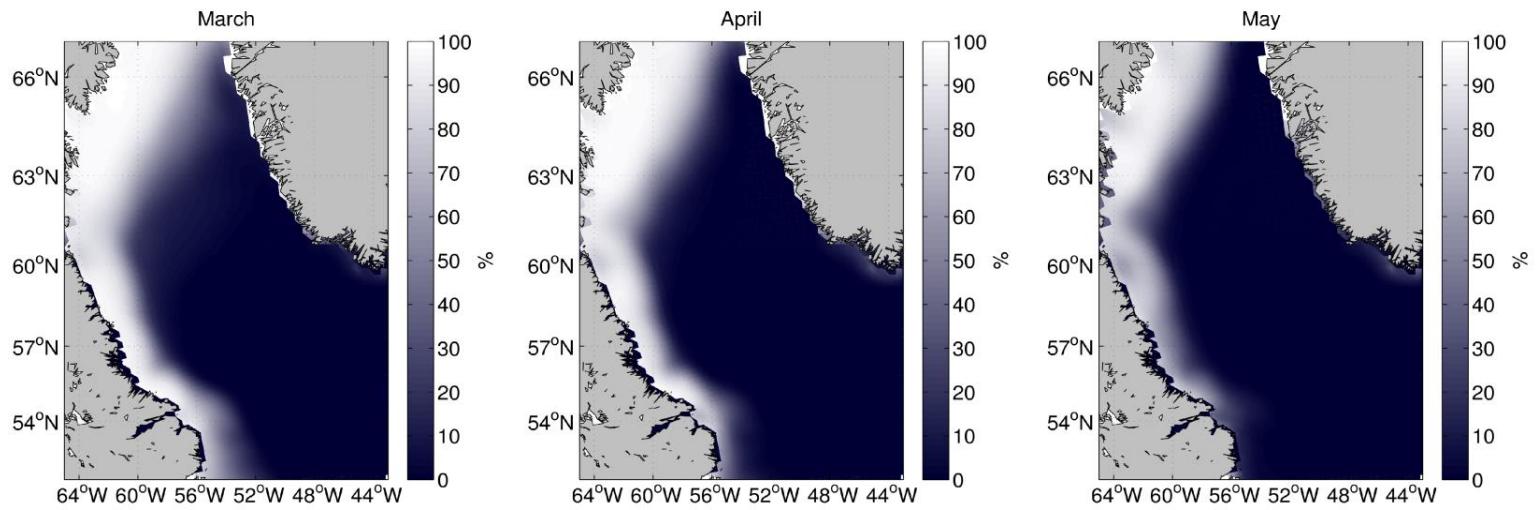
Figure S3. Monthly climatology of the fraction of ocean area covered by sea ice (%) from passive microwave data (NOAA/NSIDC) at a spatial resolution of 25 km (http://nsidc.org/data/G02202)
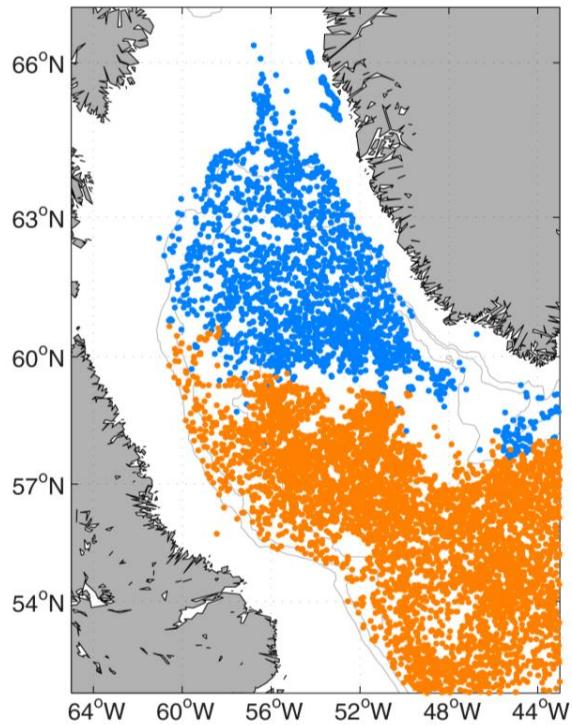
Figure S4. Data location of Argo float profiles used for calculation of area-averaged time series of temperature and salinity in bioregions North LS (blue) and South LS (orange).
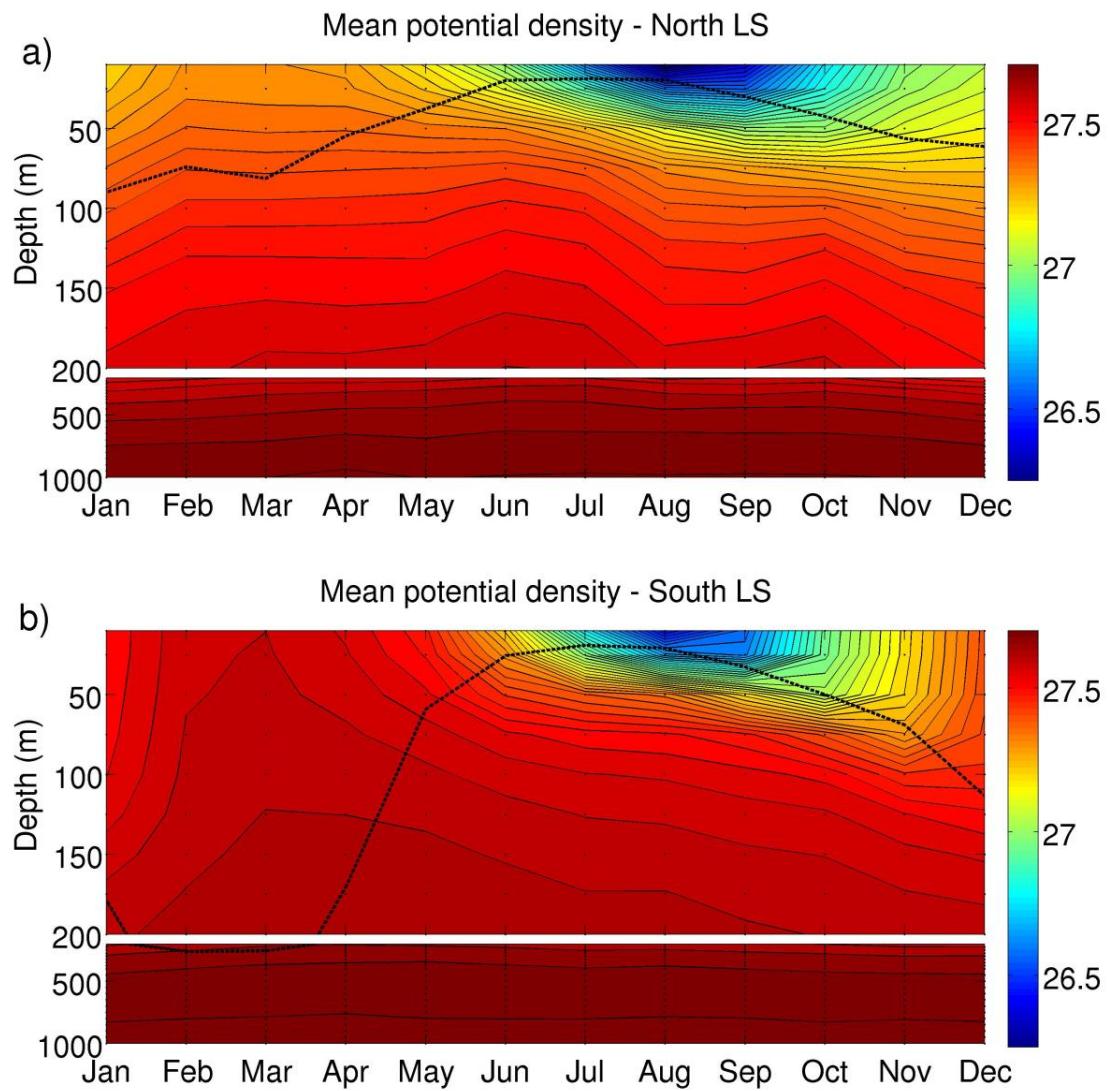
Figure S5. Climatological area-averaged time series of potential density in the North LS (a) and in the South LS (b) over the 1998-2014 period. Dashed lines denote the climatological MLD. The data (black points) were interpolated using the matlab function "contour". Thin black lines represent contours, with a resolution of 0.03 kg.m⁻³.
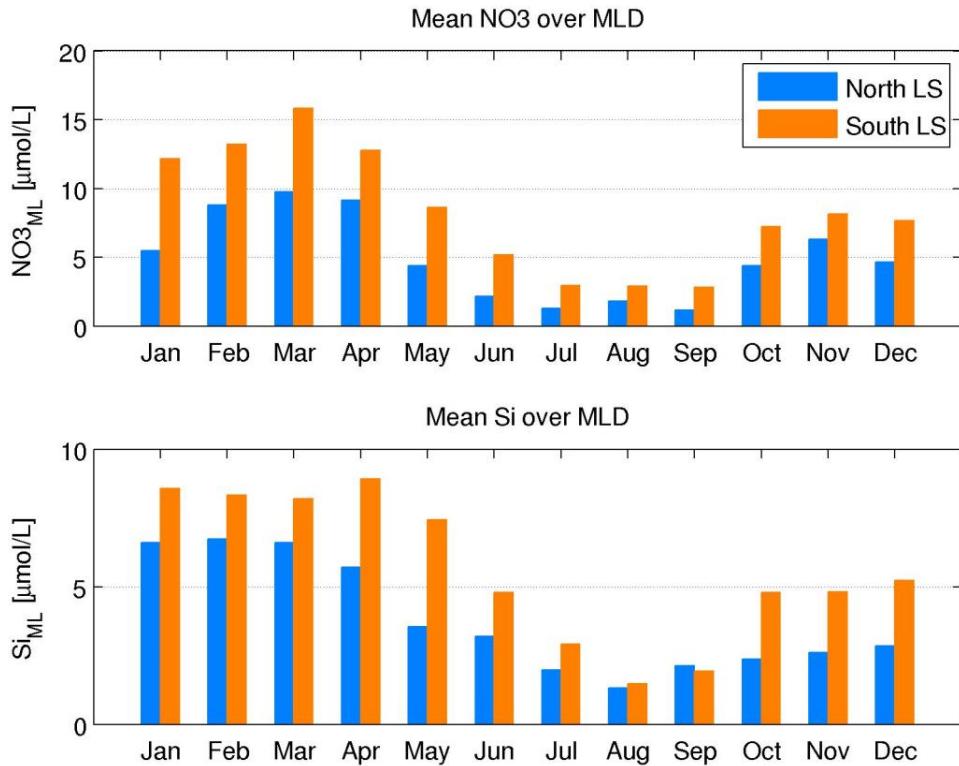
Figure S6. Monthly climatological nitrate (NO₃) (a) and silicate (Si) concentration (b) averaged over the MLD, and area-averaged in both bioregions of the Labrador Sea.

Table S1. Jaccard coefficient of the six clusters used to bioregionalize the North Atlantic for subsetting and noise method.

	Cluster 1	Cluster 2	Cluster 3	Cluster 4	Cluster 5	Cluster 6
Subsetting	0.997	0.991	0.995	0.991	0.992	0.995
Noise	0.90	0.93	0.95	0.85	0.94	0.97

References

Calinski, T., and J. Harabasz (1974), A Dendrite Method for Cluster Analysis, *Commun. Stat. - Simul. Comput.*, *3*, 1–27, doi:10.1080/03610917408548446.

D'Ortenzio, F., and M. Ribera d'Alcalà (2009), On the trophic regimes of the Mediterranean Sea: a satellite analysis, *Biogeosciences*, *6*(2), 139–148, doi:10.5194/bg-6-139-2009.

Hennig, C. (2007), Cluster-wise assessment of cluster stability, *Comput. Stat. Data Anal.*, *52*(1), 258–271, doi:10.1016/j.csda.2006.11.025.

Holte, J., and L. Talley (2009), A New Algorithm for Finding Mixed Layer Depths with Applications to Argo Data and Subantarctic Mode Water Formation, *J. Atmos. Ocean. Technol.*, *26*(9), 1920–1939.

Milligan, G., and M. Cooper (1985), An examination of procedures for determining the number of clusters in a data set, *Psychometrika*, *50*(2), 159–179.

Ollitrault, M., and J.-P. Rannou (2012), ANDRO: An Argo-Based Deep Displacement Dataset, *J. Atmos. Ocean. Technol.*, *30*(4), 759–788.

Supporting information for : *Unexpected winter phytoplankton blooms in the North Atlantic subpolar gyre*

Supplementary Materials for

Unexpected Winter Phytoplankton Blooms in the North Atlantic Subpolar Gyre

L. Lacour[1]*, M. Ardyna[1], K. F. Stec[2], H. Claustre[1], L. Prieur[1], M. Ribera D'Alcala[2], D. Iudicone[2]

correspondence to: leo.lacour@obs-vlfr.fr.

This file includes:

1. Materiel and Methods

1.1. BGC-Argo float data

PROVOR CTS-4 profiling floats used in this study are equipped with: a SBE 41 CTD; an ECO3 (Combined Three Channel Sensors) composed of a chlorophyll *a* (chla) fluorometer, a Colored Dissolved Organic Matter (CDOM) fluorometer, and an optical backscattering sensor at 700 nm and angle of 124° (b_{bp}); an OCR-504 radiometer measuring Photosynthetically Available Radiation integrated over 400-700 nm (PAR). Measurements were collected during upward profiles every 5 or 10 days, from the parking depth at 1000 m to the surface. Vertical resolution of acquisition was 10 m between 1000 m and 250 m, 1 m between 250 m and 10 m, and 0.2 m between 10 m and the surface. Radiometric measurements were acquired only in the upper 250 m. Data were transmitted via Iridium communication each time the floats surface, usually around local noon. A "real time" quality control procedure was performed on CTD data [1], chla [2] and PAR measurements [3] after the factory calibration was applied . The instrumental dark signal was removed from the chla profile and the non-photochemical quenching was corrected following the method in [4]. Spikes were removed from chla and b_{bp} profiles using a 5-point running median filter and a 7-point running mean filter [5].

1.2. Atmospheric data and Sea ice fraction

Net heat flux and wind data were extracted from the ECMWF ERA Interim dataset (reanalysis) freely available at http://apps.ecmwf.int/datasets/data/interim-full-daily/levtype=sfc. Atmospheric data, with spatial resolution of 0.25°, were averaged over 12 hours periods. Daily mean sea ice product with spatial resolution of 0.05° was provided by the OSTIA global foundation (http://marine.copernicus.eu). Pixels with sea ice fraction > 50% are plotted in Fig. 1D.

1.3. Stratification and Turner angle analysis

More than 2000 Argo float temperature and salinity profiles were acquired during January-March 2014 and 2015 in the North Atlantic Subpolar Gyre. Derived density profiles were used to estimate the depth of the mixed layer (see section 1.4). Buoyancy frequency $N^2 = -(g / \rho_0) \partial \rho / \partial z$ (where g is the acceleration due to gravity, ρ is the potential density and ρ_0 is a reference density) averaged over 5-100 m depth was calculated to provide a quantitative measure of stratification. Surface temperature, salinity and density data (averaged over 5-15 m depth) from Argo float were interpolated on a regular grid by a Gaussian correlation function, weighted by the local number of data, with a decorrelation radius of 200 km. Both vertical Argo profiles and surface horizontal map of temperature and salinity were used to calculate Turner angle (Matlab function gsw_Turner_Rsubrho from Gibbs Sea Water toolbox) as follow [6,7]:

$$Tu_v = tan^{-1}(\alpha \frac{\partial \theta}{\partial z} - \beta \frac{\partial S_A}{\partial z}, \alpha \frac{\partial \theta}{\partial z} + \beta \frac{\partial S_A}{\partial z})$$

$$Tu_H = tan^{-1}(\alpha \partial \theta - \beta \partial S_A, \alpha \partial \theta + \beta \partial S_A)$$

where ∂ is the difference between data points calculated across isopycnals, α and β are the thermal expansion and saline contraction coefficients, respectively, θ is the conservative temperature and S_A is the absolute salinity (TEOS-10, [8]). Vertical Turner angle Tu_v was determined for each Argo profile using data points of θ and S_A at 5 m and the depth of the mixed layer (Fig. S1). Horizontal Turner angle Tu_H was calculated for each 0.25° grid points of the surface map using θ and S_A at the maximum and minimum density points in a 3x3 square centered around the grid point. Thus, the difference between data points is calculated across gradients. A turner angle provides a metric to quantify the relative contribution of temperature and salinity to density gradients. The slumping of horizontal density gradient induced by mixed layer eddies (MLEs) produces vertical density gradient with a similar Turner angle ($Tu_H = Tu_v$) [7]. Frequency distribution of Tu_v (from all Argo profiles) and Tu_H (from all grid points), each normalized by the maximum frequency of the distribution, allow to compare temperature and salinity structure of horizontal and vertical gradients in the whole subpolar gyre in the winters 2014 and 2015. Similar distribution of horizontal and vertical Turner angle indicate that horizontal density gradients slump to produce vertical stratification. It is important to note that although MLEs seems to be a leading-order mechanism that slump horizontal density gradient, other lateral processes such as mesoscale dynamics or wind through Ekman buoyancy fluxes also modify upper-ocean stratification [7].
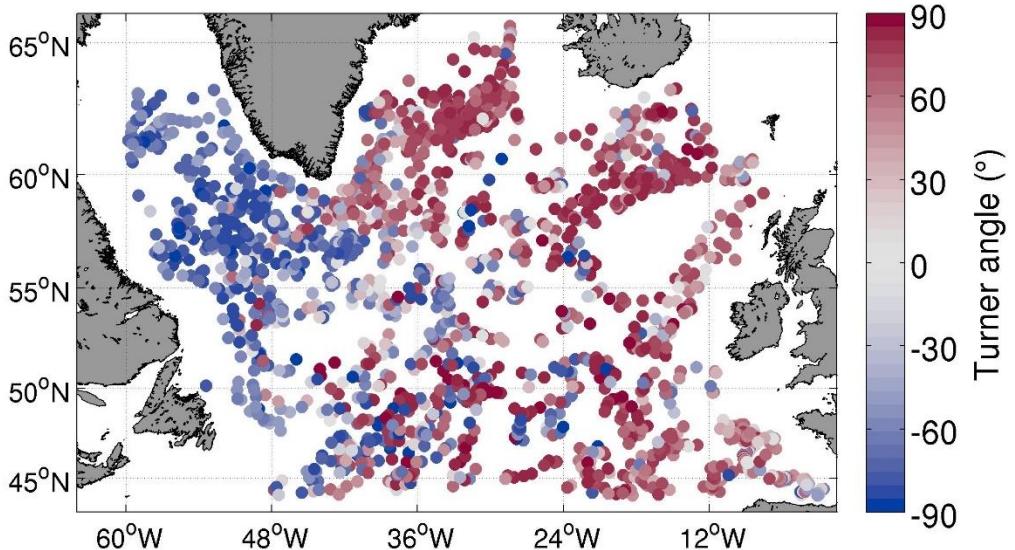
Fig. S1. Vertical Turner angle Tu_v for more than 2000 Argo float profiles in the North Atlantic Subpolar Gyre in the winters 2014 and 2015. Turner angles $> 0°$ indicate that temperature is the main contributor to the density gradient whereas angles $< 0°$ indicate that salinity is the main contributor. Around $0°$, both temperature and salinity contribute equally to the density gradient. Angles $> 45°$ or $< -45°$ indicate that salinity is working against temperature and vice versa.

1.4. MLD estimation

The mixed layer depth (MLD) was estimated using a density difference of 0.01 kg m^{-3} from a reference value at 5 m depth. MLD was used to distinguish deep mixed conditions (MLD > 100 m) from stratified conditions, in the sense of shallow mixed layer (MLD < 100 m). The threshold of 100 m corresponds approximately to the deeper limit of the euphotic zone. Although we don't have any information about mixing intensity, we assumed that the mixed layer depth estimation, using a criteria of 0.01 kg m^{-3}, matches well the active mixing layer depth in winter [9]. As a quality control of the mixed layer depth estimation, we checked the shape of the chla profiles in the MLD. If the MLD is actively mixed, the chla is expected to be homogeneous in this layer. The relative standard deviation (RSD = standard deviation / mean) was calculated to quantify the homogeneity of the chla profile in the MLD (Fig. S2). This quality control was done before the quenching correction given that this correction needs an accurate estimation of the MLD. Therefore, in order to avoid the bias by quenching at the surface, the RSD was calculated between the isolume 20 µmol photons m^{-2} s^{-1}, which marks the beginning of the quenching effect (dashed grey line), and the MLD (dashed black line, Fig. S2). All the winter profiles with RSD > 20% (57 profiles) were removed from the present analysis.
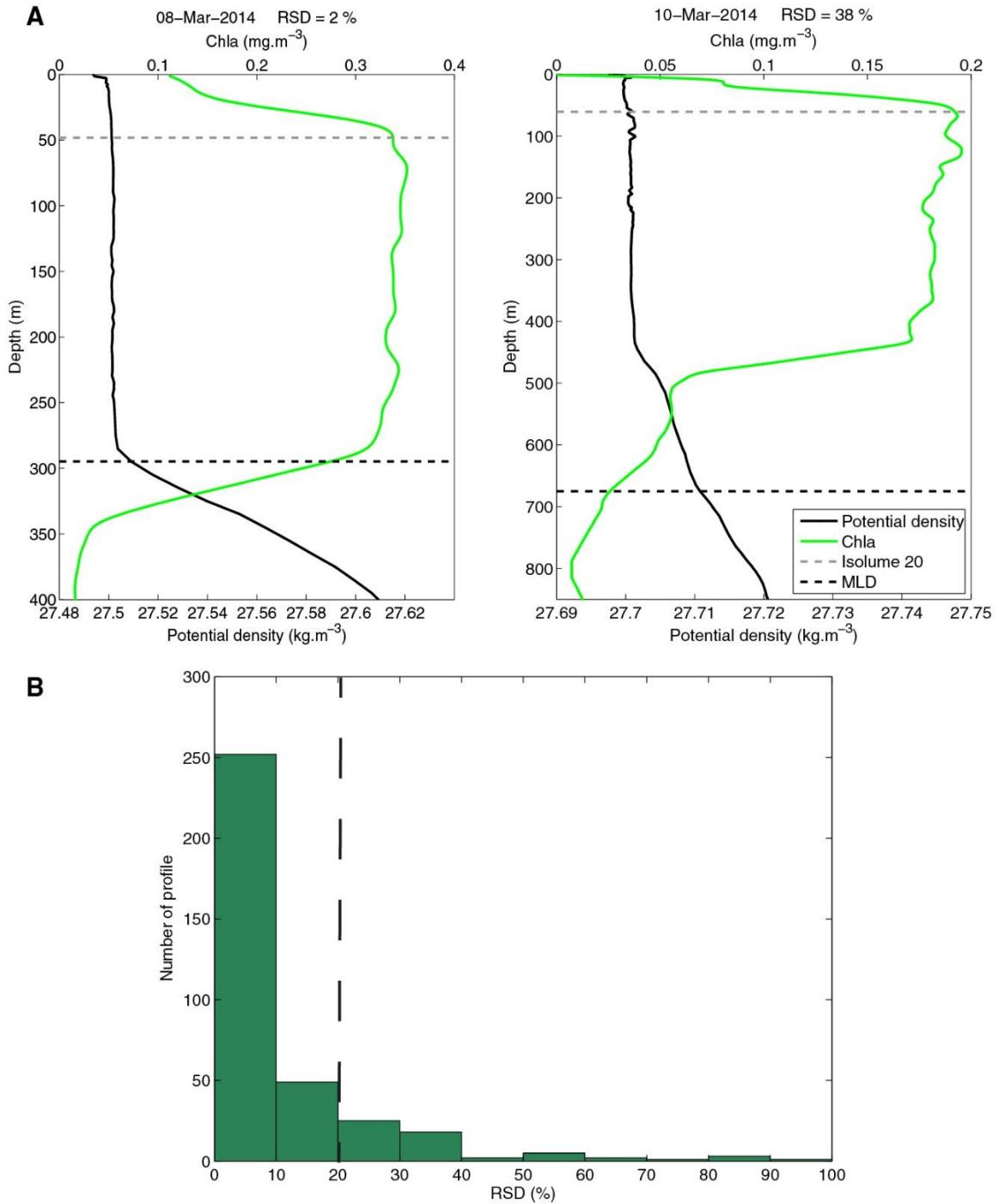
Fig. S2. Quality control of the mixed layer depth (MLD) estimation using chla profiles. (**A**) Examples of a good MLD estimation (RSD = 2%, left panel) and a bad MLD estimation (RSD = 38%, right panel). Dashed grey line marks the isolume 20 μmol photons m^{-2} s^{-1} and black dashed line marks the MLD. (**B**) All winter profiles with RSD > 20% (57 profiles) were removed from the analysis.

1.5. Historical Argo analysis

Historical MLD estimation (criteria 0.01 kg.m^{-3}) was obtained from the Argo database for a period 1995-2010 [10]. Within pixels of 9x6 degrees, we calculated for each year and each month the probability that MLD was lower than 100 m. Figure S3 shows the median probability (period 1995-2010) for January, February and March. This figure gives an historical context to

demonstrate that observations made in winters 2014 and 2015 by Argo and BGC-Argo floats (Fig. 1A and 2A) are not peculiarities of these specific years.
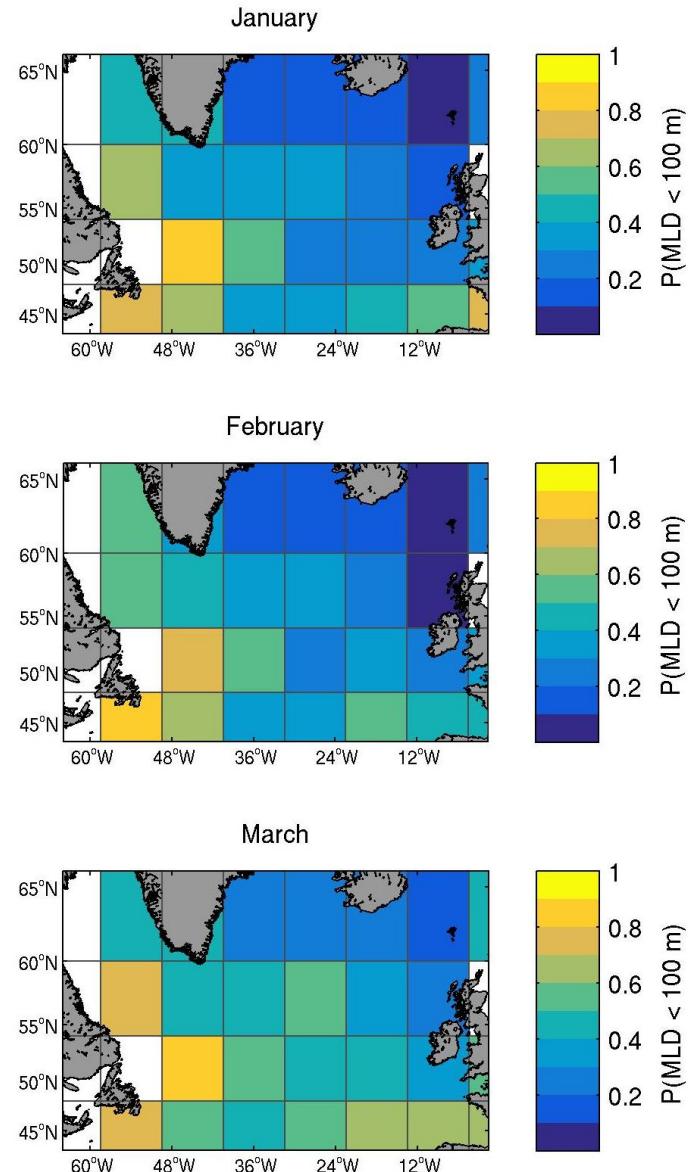
Fig. S3. Median probability that MLD was lower than 100 m for January, February and March in the North Atlantic Subpolar Gyre.

1.6. Calm periods

Calm periods were defined as a decrease of wind lower than 10 m s^{-1} and net heat flux higher than -100 W m^{-2} (i.e. positive or weakly negative) during at least 24 hours, the time scales needed to develop stratifying buoyancy flux from MLEs [11]. The stratifying buoyancy flux, which competes with surface cooling and winds, is proportional to $(b_y H)^2/f$ where b_y is the horizontal buoyancy gradient, H is the mixed layer depth and f is the Coriolis frequency. The wind and heat flux threshold used in this study are typical values allowing restratification by lateral buoyancy flux in the Iceland basin ($H = 300$ m, $b_y = -0.3$ x 10^{-7} s^{-2} and $f = 1.28$ x 10^{-4} s^{-}

[1]). However, similar conditions were observed across most of the subpolar gyre, with the westward shallowing of the mixed layer depth compensated by increasing horizontal gradients [12]. Therefore, we used the same thresholds across the whole subpolar gyre to define calm periods. Figure S4 shows an example of the wind and heat flux intermittency at a given location (55°N -40°W). Numerous data points fall below the atmospheric thresholds defined above (orange dots) during both winters 2014 and 2015. This example shows that calm periods (at least two consecutive data points) are frequent and intermittent in winter in the subpolar gyre. The probability to have calm periods during both winters 2014 and 2015 is the total duration of calm periods divided by total duration of the period of observation (180 days).
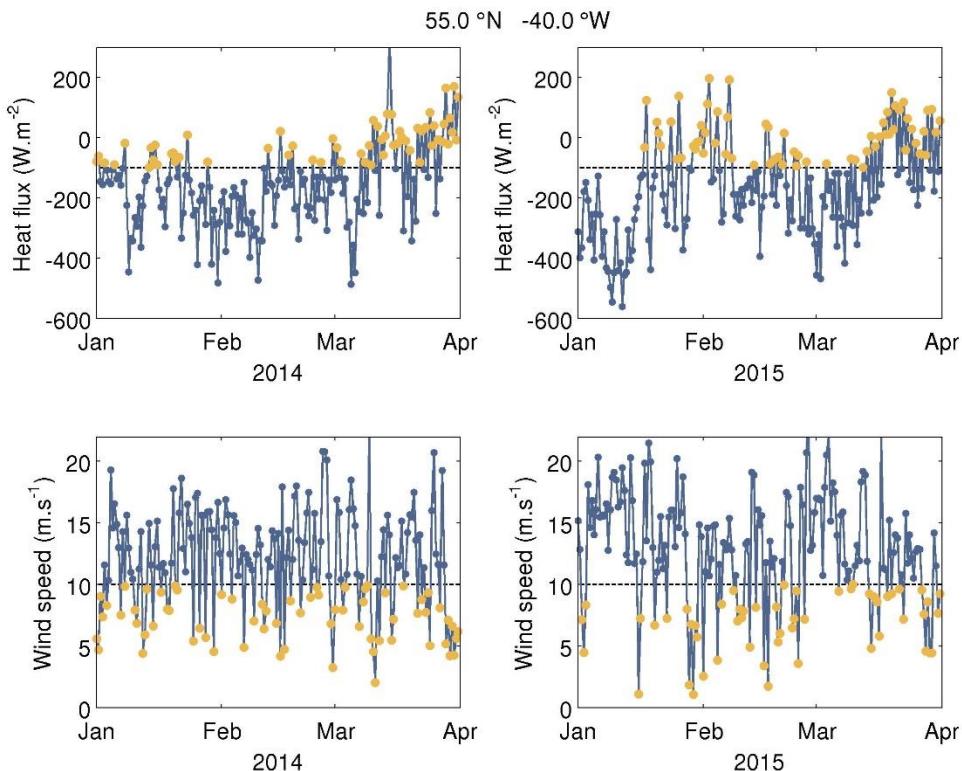
Fig. S4. Wind and heat flux intermittency at 55°N -40°W during the winters 2014 and 2015. 12h-averaged wind speed and heat flux < 10 m s^{-1} and > -100 W m^{-2} respectively are marked in orange.

1.7. Sea state derived from BGC-Argo floats

A profiling float uses a pump to regulate his buoyancy so that it controls its ascent to the surface. From 10 m depth to the surface, the pump is off and the float is supposed to reach the surface under its own momentum. After 600 seconds, if the float does not reach the surface, the pump is reactivated. The time spend during the ascent, between 10 m and the surface, where the pump is off, is well correlated with maximum wave height (Fig. S5). This proxy of the sea state is used in the North Atlantic Subpolar Gyre as an independent estimation of the frequency of calm periods with a flat sea (ascent time < 100 s) (method developed by Antoine Poteau). Note that this calm period estimation is only based on sea state and is not related to the restratification mechanism as above.
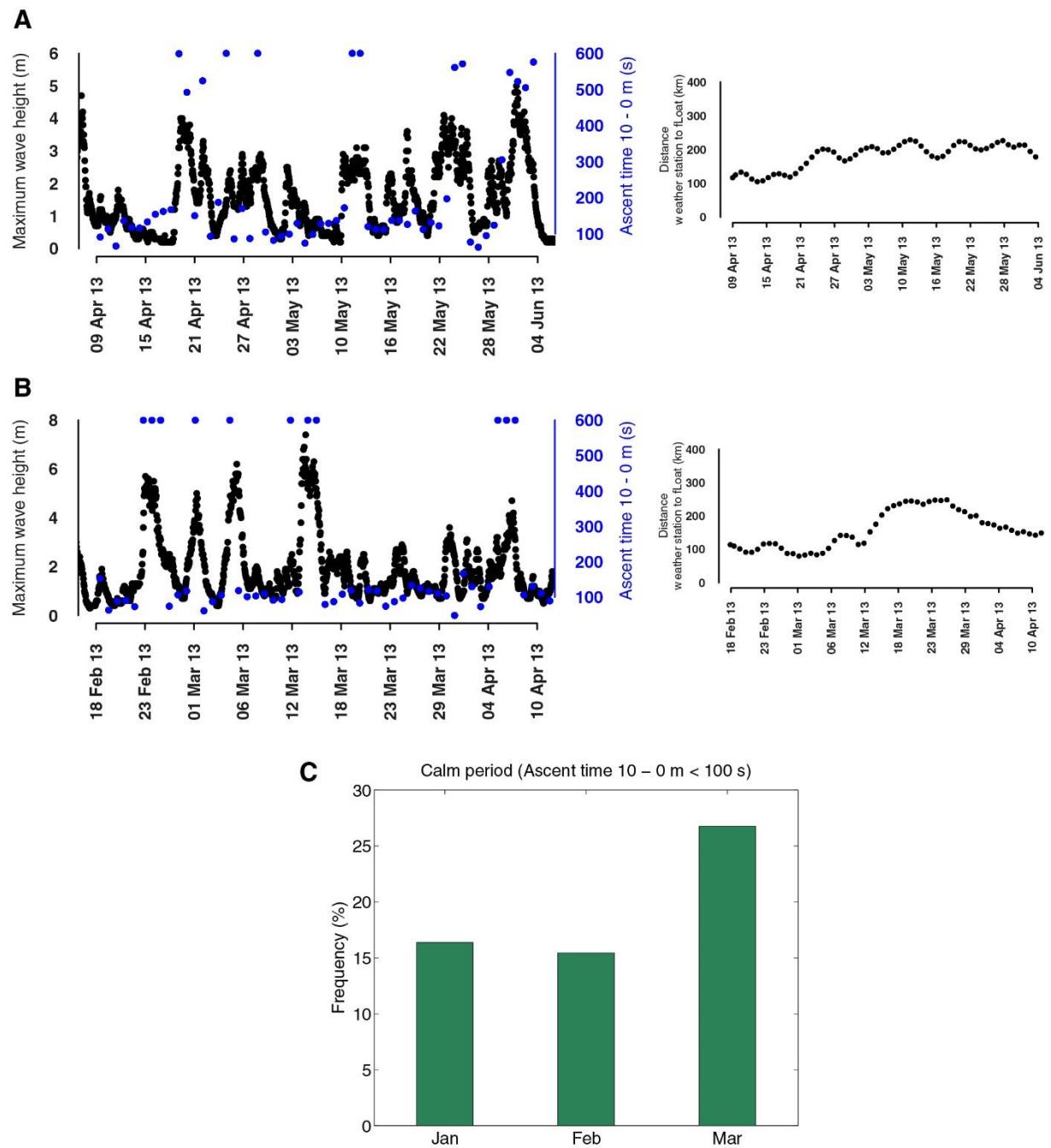
Fig. S5. Sea state estimation from BGC-Argo float profiles. Comparison of ascent time and maximum wave height for 2 BGC-Argo floats near weather station LION (**A**) and weather station COTE d'AZUR (**B**) in the North-western Mediterranean Sea. Distances between weather stations and floats are shown on the right. (**C**) Frequency of calm periods (ascent time $10 - 0$ m < 100 s) for the 301 BGC-Argo float profiles in the subpolar gyre.

1.8. Light model

A radiative transfer model [13], was used to assess daily-integrated PAR along the float trajectory. This model takes into account the water vapor content (which can reduces PAR up to 0.7% when the sun is at zenith), the total ozone content (up to 1%) and the tropospheric aerosol load (up to 6%). However, the more crucial effect of the cloud cover is not taken into account in this so-called "clear sky" model. The transmission across the air-water interface is separately computed for the diffuse light component using a constant reflectance (6.6%) and for the direct component using a sun-altitude dependent reflectance. The modeled instantaneous PAR (iPAR) just below the surface is propagated through the water column using a diffuse attenuation coefficient derived from the chla profile measured by the float [14,15]. By comparing the clear sky iPAR profile with the float iPAR profile, the light attenuation due to the cloud cover can be estimated (Fig. S6). The median, over the vertical profile, of the ratio of float iPAR to clear sky iPAR gives a correction factor which quantifies the average light attenuation due to cloud cover during the float ascent (cloud cover is not necessarily stable, see Fig. S6). To avoid any potential bias due to dark signal at depth, the median is computed only in the upper layer where iPAR > 5 µmol photons m^{-2} s^{-1}. Assuming that the average cloud cover estimated during float ascent is representative of the entire day, this correction factor is subsequently applied to all the modeled profiles of the day (time increment $1/60^{th}$ of the day length). The integration of all these cloud-corrected modeled iPAR profiles over the day length gives an estimate of daily-integrated PAR (in mol photons m^{-2}). The surface daily-integrated PAR used in this study is the first value recorded below the sea surface. In the main text, the term cloudiness refers to the correction factor (i.e. the attenuation of light). The modeled daily-integrated PAR profile is used to estimate Ze, the depth to which the euphotic zone extends. Ze is here defined as the depth of the 0.1 mol photons m^{-2} isolume, a light threshold adapted to subarctic species [16,17]. The modeled daily-integrated PAR profile is also used to calculate the average PAR in the mixed layer (PAR_{ML}).
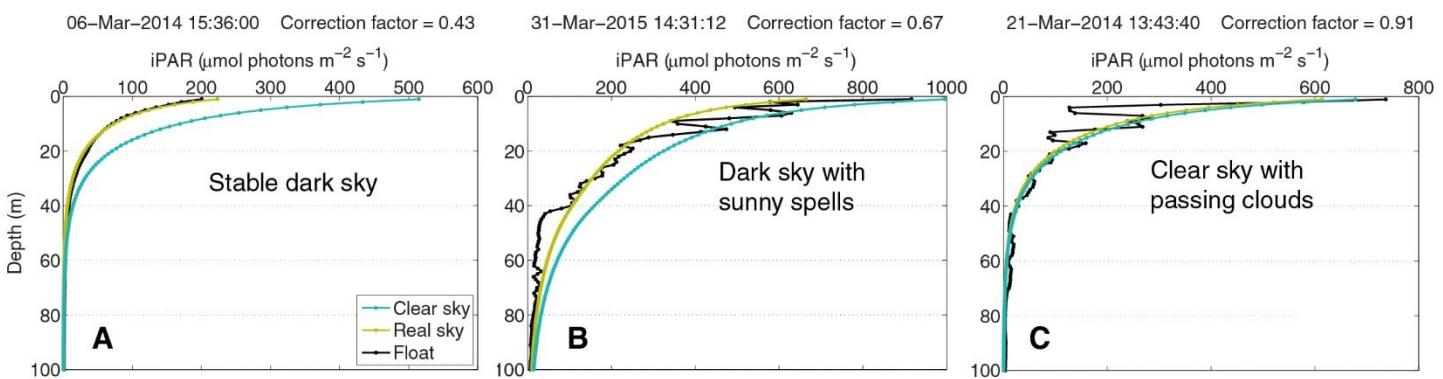

Fig. S6. Three examples of the impact of the cloud cover on the instantaneous photosynthetically available radiation (iPAR). Blue line is the modeled clear sky iPAR profile. Black line is the iPAR profile measured by BGC-Argo floats. Yellow line is the corrected modeled iPAR profile. The correction factor (see in tittle) describes the average light attenuation due to the cloud cover during the float ascent. A stable dark sky reduces the light level by 67% (**A**). A partly cloudy sky with sunny spells reduces by 33% on average (**B**). A clear sky with few passing clouds reduces by only 9% on average (**C**).

1.9. Optical community index

A simple optical community index (CI) was used to assess changes in phytoplankton community composition (see also section 2.1 and 2.2). Cetinić et al. 2015 [18] have shown that high and low chla fluorescence to b_{bp} ratio was correlated with diatom- and pico-nanophytoplankton-dominated communities, respectively. They chose to use chla fluorescence (volt) and not calibrated chla (mg m^{-3}) to homogenize their dataset which came from different platforms (with different sensors). In the present study, the optical community index was calculated with chla and b_{bp} calibrated in the same way for all the BGC-Argo fleet used (Fig. S7). Thus, the use of chla instead of chla fluorescence does not affect the interpretation of the optical index. CI was calculated as the ratio of MLD integrated values. It ranged from 50 to 1600 mg m^{-2}. For clarity, the ratio has been normalized by the minimum and the maximum value of the dataset so that the optical community index ranges from 0 to 1. The maximum of the ratio reached 60% of the average value, recorded by floats in different location of the subpolar gyre, at the peak of the spring bloom when diatoms are dominant. However, at the peak of the spring bloom, the chla to b_{bp} ratio is boosted due to physiological adaptation to silicate limitation, as shown by Cetinić et al. 2015 (*18, their figure 6*). In their study, 60% of the value of chla fluorescence to b_{bp} ratio at the peak of the spring bloom (~150 V m) gives a ratio of ~90 V m which corresponds to a fraction of diatom cell carbon to total autotrophic cell carbon of 40-60%. We conclude that a community index close to 1 indicates a large contribution of diatoms to the community whereas index close to 0 indicates a dominance of the pico- and nanophytoplankton.
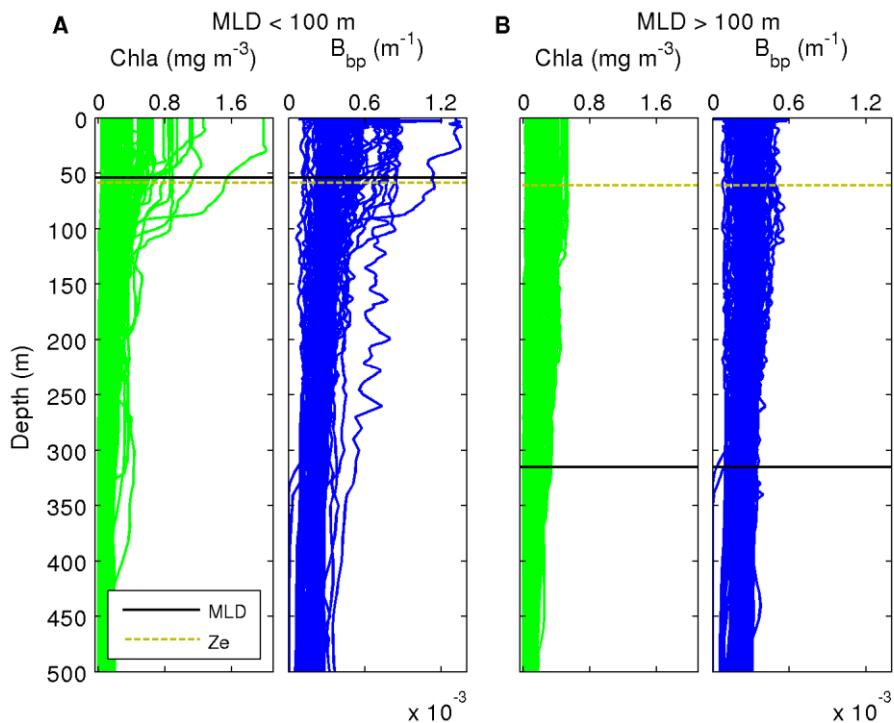

Fig. S7. Chla and bbp profile from BGC-Argo float in the North Atlantic Subpolar Gyre in 2014 and 2015 winters. (**A**) Stratified profiles (MLD < 100 m, n = 86). (**B**) Deeply mixed profiles (MLD > 100 m, n = 215). Horizontal black and yellow lines indicate the median MLD and euphotic depth (Ze) respectively.

1.10. Pigment analysis

High Performance Liquid Chromatography (HPLC) pigment data were acquired during the CATCH (Couplage avec l'Atmosphère en Conditions Hivernales) experiment [19] which took place in the Newfoundland Basin in January-February 1997 (37 stations coupled with CTD measurements). Diagnostic pigment (DP) analysis was used to explore patterns of dominance among phytoplankton assemblages [20]. DP is the sum of seven depth-integrated pigments (Table S1):

$$DP = Zea + Tchl\ b + Allo + 19'HF + 19'BF + Fuco + Peri$$

The biomass proportion (BP) associated with each size class is defined as:

$$BP_{pico} = \frac{Zea + Tchl\ b}{DP}$$

$$BP_{nano} = \frac{Allo + 19'HF + 19'BF}{DP}$$

$$BP_{micro} = \frac{Fuco + Peri}{DP}$$

Where the subscripts pico, nano and micro refer to picophytoplankton (<2 μm), nanophytoplankton (2-20 μm) and microphytoplankton (20-200 μm). The use of this method allowed us to investigate the role of mixing intermittency on the community structure as a whole and not only on diatoms abundance (see section 2.4).

Table S1. Taxonomic pigments (modified from Vidussi et al. [20])

Pigments	Abbreviations	Taxonomic significance	Size (μm)
Zeaxanthin	Zea	Cyanobacteria and prochlorophytes	< 2
Chlorophyll b+Divinylchlorophyll b	Tchl b	Green flagellates and prochlorophytes	< 2
Hexanoyloxyfucoxanthin	19'HF	Chromophytes nanoflagellates	2-20
Butanoyloxyfucoxanthin	19'BF	Chromophytes nanoflagellates	2-20
Alloxanthin	Allo	Cryptophytes	2-20
Fucoxanthin	Fuco	Diatoms	>20
Peridinin	Peri	Dinoflagellates	>20

2. Supplementary text
2.1. Main drivers of optical community index variability

For assessing potential sources of variability in the community index, a Principal Component Analysis (PCA) was performed on 344 BGC-Argo float profiles (Fig. S8A). Input parameters were daily-integrated surface PAR (PAR), mixed layer depth (MLD), mean surface

0 – 20 m salinity (SAL), mean surface colored dissolved organic matter (CDOM) and optical community index (CI). Prior to analysis, these parameters were standardized by subtracting the mean and dividing by the standard deviation. Together, principal component 1 and 2 explain 73% of the variance. CI is well positively correlated with surface PAR and in a lesser extent negatively correlated with MLD. Stations with high CI show high loading on PAR and stations with low CI show high loading on MLD and SAL/CDOM (negatively correlated). A hierarchical clustering analysis allowed us to define 3 main groups (Fig. S8B and C). Cluster 3 is characterized by high surface PAR and shallow MLD, cluster 2 by deep MLD and low surface PAR and cluster 1 by low salinity and high CDOM. These last two variables allowed us to identify stations influenced by terrigeneous inputs from the Arctic, as already shown in previous studies [21,22]. Terrigeneous matter strongly increased the b_{bp} signal thus decreasing the CI (<200 mg m^{-2}). This variability being not linked to changes in community composition, stations from this cluster 1 (shown in Fig. S8D) were removed from the analysis (43 stations).
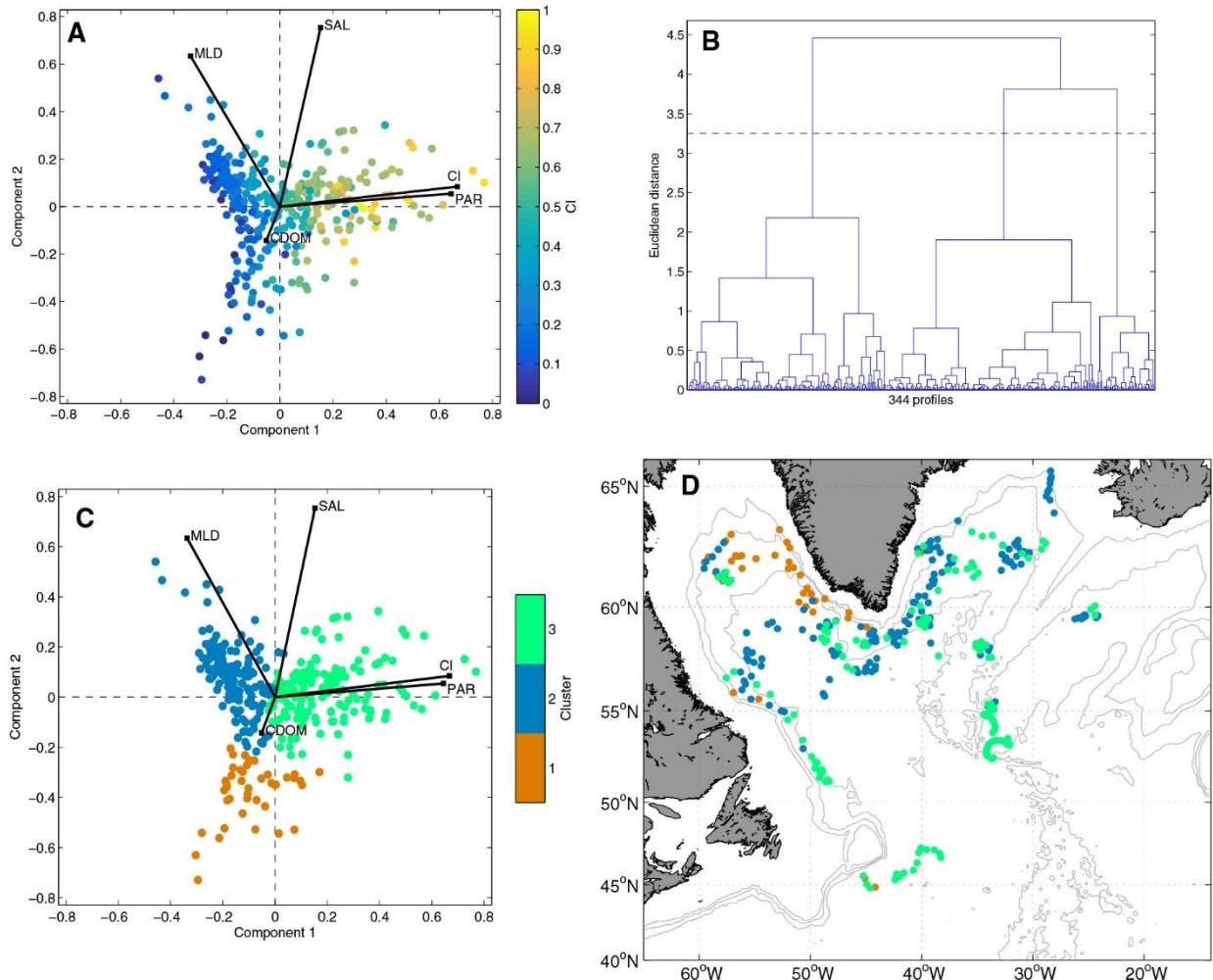
Fig. S8. Principal component analysis (PCA) applied on BGC-Argo float data (n=344). Input parameters are daily-integrated surface PAR (PAR), mixed layer depth (MLD), surface 0 - 20 m salinity (SAL), surface colored dissolved organic matter (CDOM) and optical community index (CI). Together, component 1 and 2 explain 73% of the variance. (**A**) Dots are color-coded by the community index. (**B**) A hierarchical cluster tree allows defining 3 clusters of stations.

(**C**) Same as (A) but color-coded by the 3 clusters. (**D**) Location of the stations belonging to each cluster.

2.2. Photoacclimation

Chla is not simply a measure of phytoplankton biomass, but varies as a response of physiological adaptation to changing light (i.e. photoacclimation) [23]. Indeed, at global scale, the seasonal variability of chla to b_{bp} ratio seems to be mainly driven by photoacclimation [24]. However, at local scale, over a limited temporal window (3 months), our results show that photoacclimation is not a dominant factor. Chla to b_{bp} ratio increases when light level increases which is opposite to a photoacclimation effect (Fig. S8A and S10A-B).

2.3. Light level / Light regime

The light level experienced by phytoplankton cells within an active mixed layer is not obvious to quantify. The average light in the MLD, used to estimate the light level, has clearly an influence on phytoplankton growth in such a way that it is frequently used to explain the bloom onset [25–27]. However, this descriptor shows only a weak correlation with the optical community index (Fig. S9), suggesting that average light in the MLD is not sufficient to characterize the light environment. The light regime (light/dark period), mainly controlled by the depth of the mixed layer relative to the depth of the euphotic zone (Ze), could also play a crucial role on the community composition (Fig. S10). Diatom growth is enhanced when cells are mixed in the euphotic layer (i.e. longer light period) as also evidenced by laboratory experiment [28].
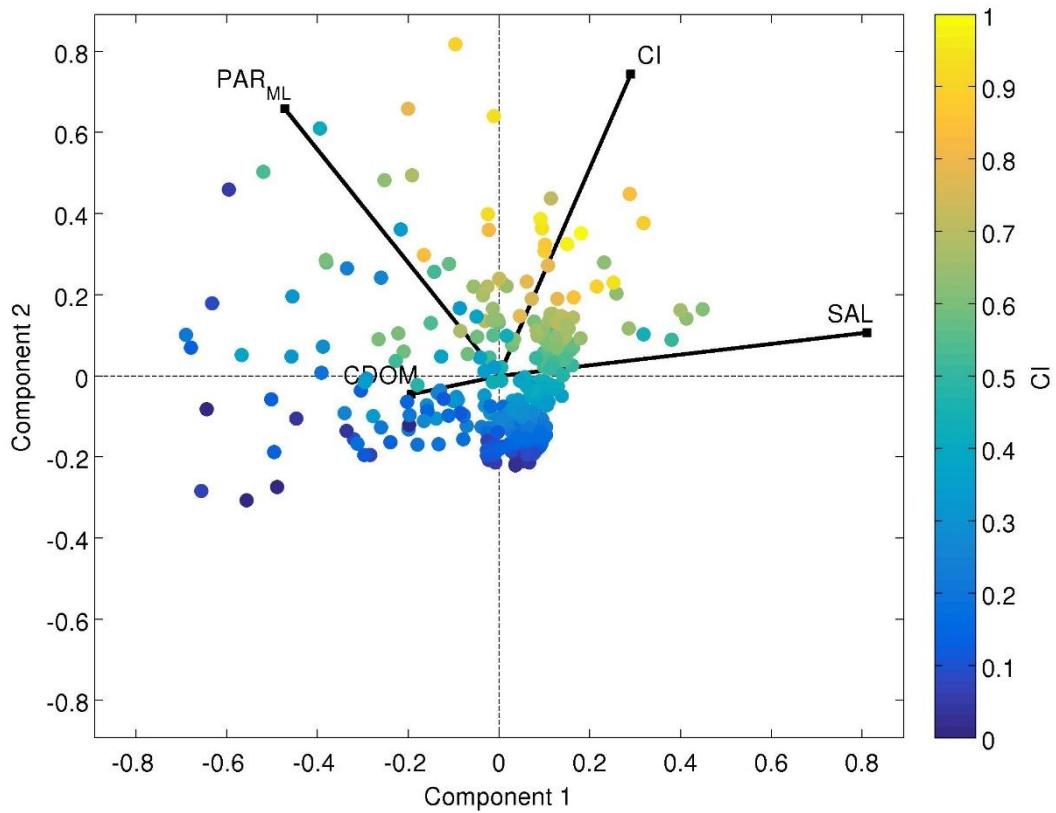
Fig. S9. Same as Fig. S8 with PAR_{ML} instead of MLD and PAR. Together, component 1 and 2 explain 77% of the variance.
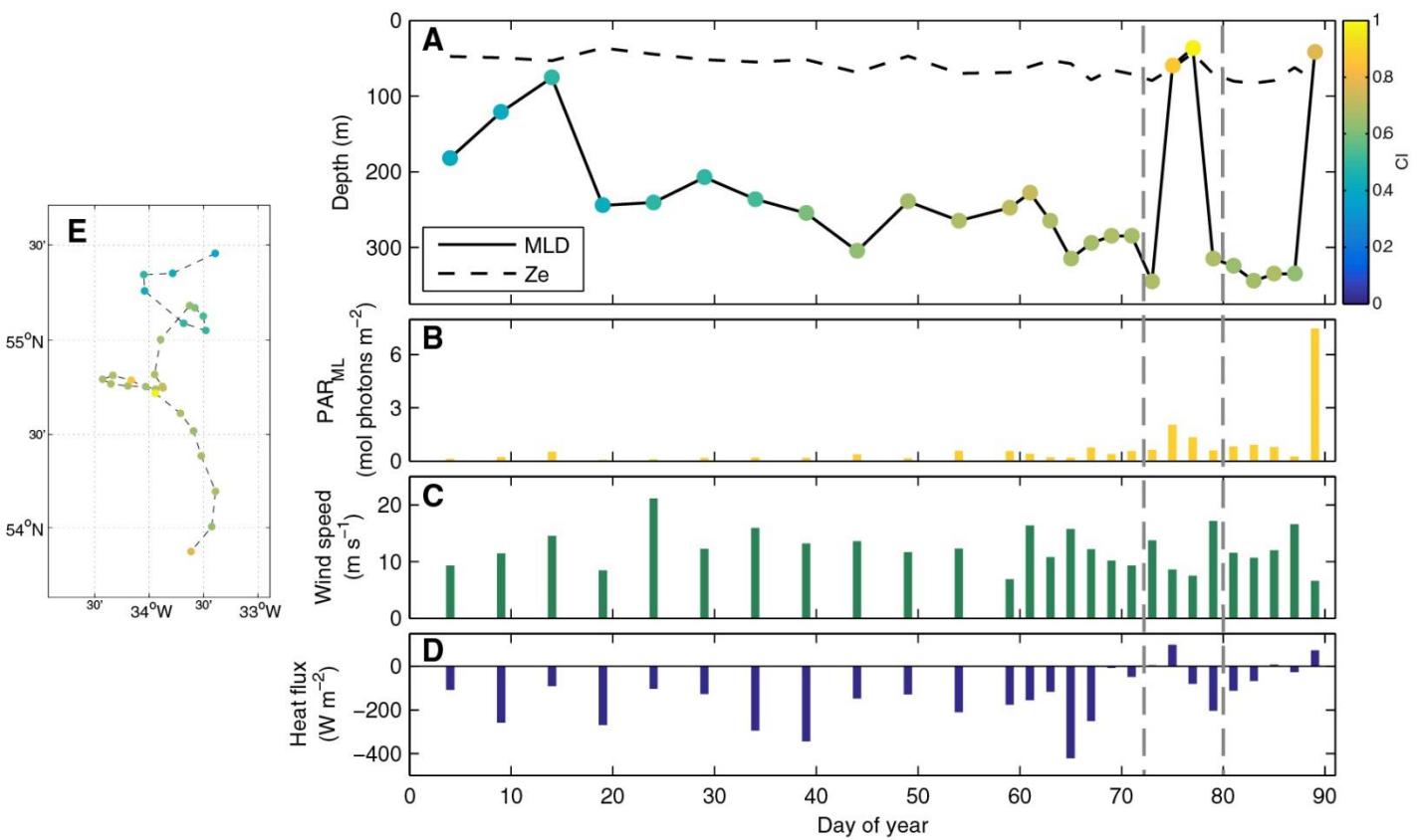
Fig. S10. A restratification event supported by a relaxation of the wind and heat flux in mid-March (~day 75) induces a transient diatom bloom as evidenced by high community index (CI). (**A**) MLD and Ze along a Bio-Argo float trajectory, color-coded by CI. Match up of PAR_{ML} (**B**), wind speed (**C**) and heat flux (**D**) at each surfacing of the float. (**E**) Trajectory of the float color-coded by CI.

2.4. CATCH expedition: HPLC validation

The CATCH expedition is one of the few midwinter survey carried out in the subpolar gyre with HPLC data available. The reason for the poor winter sampling in this region is evidenced by rough weather conditions suffered during the CATCH experiment. Strong storms with winds as high as 20 m s^{-1} were frequently recorded along the ship track. Even so, 25% of the wind measurements were lower than 10 m s^{-1} [19], which highlights the intermittency of the atmospheric forcing. The study area was characterised by strong horizontal density gradients due to the convergence of two contrasting waters, cold and fresh Labrador Sea water and warm and saline subtropical water. Numerous fronts and eddies were observed in this highly energetic region [29]. As a consequence, mixing length scale was highly intermittent and patchy with MLDs ranging from 20 to 800 m depth. Figure S11A shows two examples of all diagnostic pigment concentration profiles acquired within two-day intervals, one in stratified conditions (MLD = 60 m) and one in deeply mixed conditions (MLD = 460 m). The concentration of diatoms (Fuco) clearly increases in the stratified case. However, in both cases, nanoflagellates (HF) concentration remains the highest. The depth of the mixed layer clearly impacts the biomass proportion of the nano- and microphytoplankton (Fig. S11B). The microphytoplankton abundance increases with MLD shallowing and reaches almost 40% of the community when MLD shoals above 100 m. The nanophytoplankton, identified as nanoflagellates, remain

dominant in early winter whatever the depth of the mixed layer (50-70%). The picophytoplankton abundance (~20%, not shown) is almost unaffected by mixing, as also noted in the Iceland Basin [30]. Interestingly, before January 15th, the community structure appears to be not influenced by the MLD shallowing (grey dots in Fig. S11B). Especially, a critical light threshold could limit the diatom growth, even in shallow MLD. Based on this chemotaxonomic analysis, we confirm that short-term restratification of the water column affects not only the phytoplankton production but also the community structure, initiating transient diatom blooms, provided that daily-integrated surface PAR reaches a critical threshold.
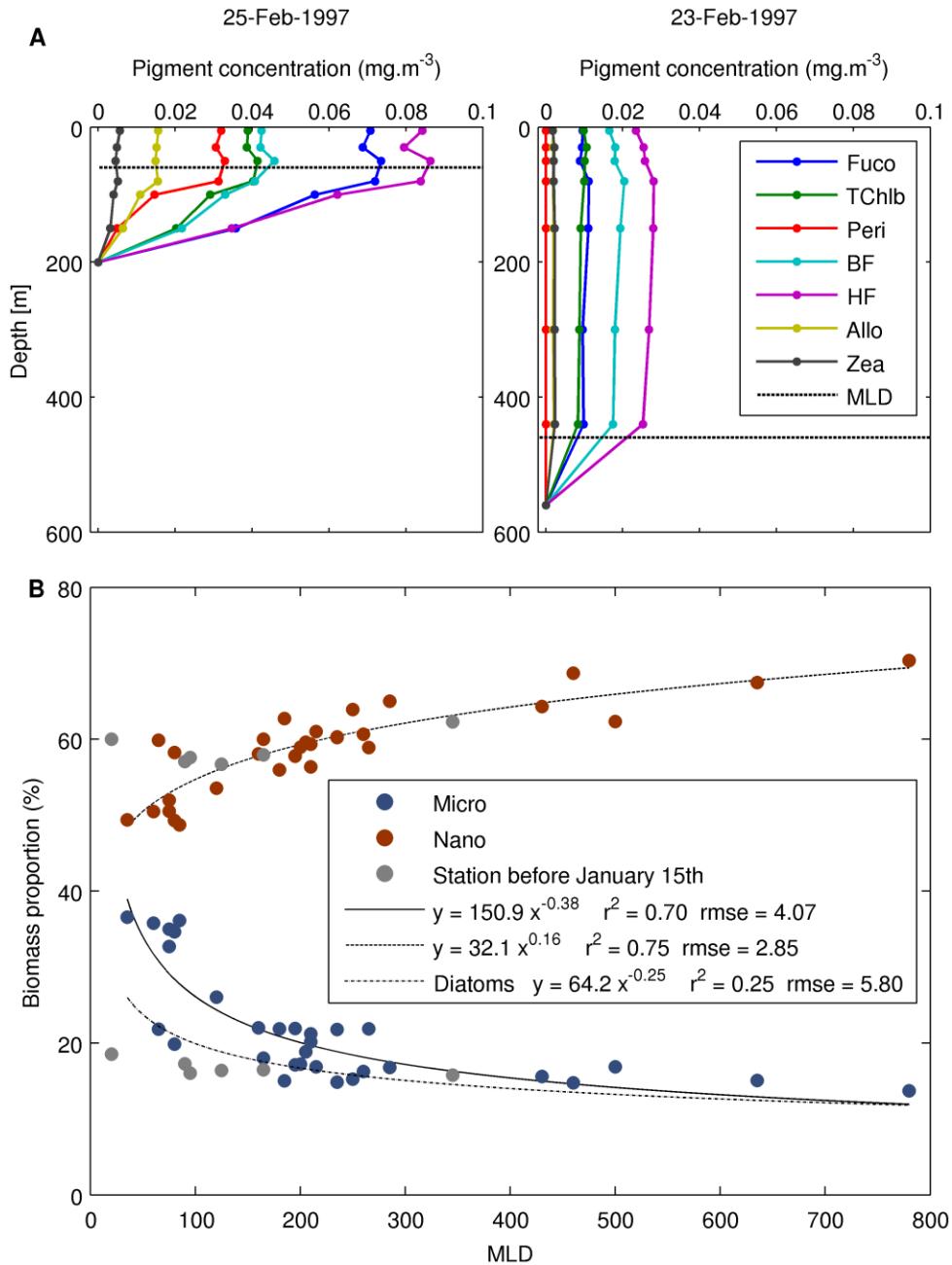
Fig. S11. Chemotaxonomic analysis from the CATCH expedition (January-February 1997), see location of the stations on Fig. 2A. (**A**) Examples of one stratified profile (left) and one deeply mixed profile (right) of pigment concentrations. The horizontal dashed black line marks the MLD. (**B**) Biomass proportion of nano- and microphytoplankton as function of MLD. Solid and dashed lines represent the best-fit power law function of the data excluding grey dots, which correspond to stations before January 15th (assumed to be extremely light limited). Dash-dot line represent the best-fit power law function of the proportion of diatoms (Fuco / DP).

2.5. Physiological adaptation to darkness

Restratification events are intermittent, interspersed with long and deep mixing events. Therefore, strategies to manage periods of darkness are needed at short time scale (hours) [31]. Both reduction of metabolic rates [32,33] and use of energy storage products (e.g. lipids, carbohydrates, etc.) have been pointed out as physiological adaptation to darkness, especially for diatoms [28]. Intermittent restratification events may allow phytoplankton species to restore their intracellular energy storage products.

2.6. Ecosystem model description

Conceptually, this 0-D ecosystem model consists of a set of coupled differential equations (Eqs. 1-6) respectively resolving the concentration of nutrients: Nitrate (N) and Silicate (Si), phytoplankton (P), zooplankton (Z) and dead organic matter: detrital nitrogen (D_N) and silicate (D_{Si}), within an idealized formulation of seasonally changing environmental forcing. Specifically, the model equations are:

$$\frac{dN}{dt} = \frac{-q_N + w_{mix}(N_0 - N)}{H} - \sum_{i=1}^{m} \mu_i(N, Si, I)P_i + \sum_{k=1}^{n} \varepsilon(1-e)\left(G_{P_{ik}} + G_{D_k}\right) + \beta D_N \qquad (1)$$

$$\frac{dSi}{dt} = \frac{-q_{Si} + w_{mix}(Si_0 - Si)}{H} - \sum_{i=1}^{m} \mu_i(N, Si, I)P_i R_i + \beta D_{Si} \qquad (2)$$

$$\frac{dP_i}{dt} = \frac{-q_{P_i}}{H} + \mu_i(N, Si, I)P_i + -m_{P_i}P_i - \sum_{k=1}^{n} G_{P_{ik}} \qquad (3)$$

$$\frac{dZ_k}{dt} = \frac{-q_{Z_k}}{H} + \omega\left(\varepsilon e\left(\sum_{i=1}^{m} G_{P_{ik}} + G_{D_k}\right) - m_{Z_k}Z_k - m_{Z2_k}Z_k^2\right) \qquad (4)$$

$$\frac{dD_N}{dt} = \frac{-q_{D_N}}{H} + \sum_{k=1}^{n} m_{Z_k}Z_k + \sum_{i=1}^{m} m_{P_i}P_i - \beta D_N - w_g\frac{D_N}{H} + \sum_{k=1}^{n}(1-\varepsilon)\left(\sum_{i=1}^{m} G_{P_{ik}} + G_{D_k}\right) - \sum_{k=1}^{n} G_{D_k} \quad (5)$$

$$\frac{dD_{Si}}{dt} = \frac{-q_{D_{Si}}}{H} + \sum_{i=1}^{m} m_{P_i} P_i R_i - \beta D_{Si} - w_g \frac{D_{Si}}{H} + \sum_{k=1}^{n} \sum_{i=1}^{m} R_i G_{P_{ik}} \qquad (6)$$

Species' growth rate formulation

Phytoplankton growth, $\mu(N, Si, I)$, was determined as a product of a species specific sensitivity to essential nutrients and photosynthetic activity:

$$\mu_i(N, Si, I) = min\left\{\frac{N}{N + H_{Ni}}, \frac{Si}{Si + H_{Sii}}\right\} \frac{1}{24H} \int_0^{24} \int_0^{H} \frac{r_i \alpha I(t, z)}{\sqrt{r_i^2 + (\alpha_i I(t, z))^2}} dz dt \qquad (7)$$

The effect on growth rate of nutrients availability was represented by a Michaelis-Menten function and the resources limitation of growth was determined by the most limiting one, where: H_{Ni} - nitrate half-saturation of species i, H_{Sii} - silicate half-saturation of species i, N, Si - nitrate and silicate concentration respectively.

Photosynthesis was calculated using a Smith P-I curve [34], where: I(t,z) is the local light level at time t at depth z, r is the growth rate of species i, and α is the initial slope of the P-I curve.

Zooplankton grazing

Zooplankton was assumed to graze on both phytoplankton and detritus [35]. The zooplankton growth rate was described with a basic multi-species Holling Type III functional response with a half-saturation coefficient (H_k for zooplankton species k) regulating grazing efficiency at high prey concentrations (Eq. 4) grazing rate (g_k selectivity coefficient of zooplankton species k for phytoplankton species i (S_{ik}), and a relative preference for detritus and phytoplankton (Φ_D and Φ_P respectively) (Table S3). Therefore the specific grazing rate of a zooplankton species k on phytoplankton species i ($i=1...k$) was expressed by the term:

$$G_{Pik} = \frac{g_k(\Phi_P S_{ik} P_i) P_i}{H_k^2 + \sum_{i=1}^{m}(\Phi_P S_{ik} P_i) P_i + (\Phi_D D) D} Z \qquad (8)$$

In an analogous manner the specific grazing rate of a zooplankton species k on detritus was expressed by:

$$GD_k = \frac{g_k(\Phi_D D) D}{H_k^2 + \sum_{i=1}^{m}(\Phi_P S_{ik} P_i) P_i + (\Phi_D D) D} Z \qquad (9)$$

Description of physical forcing

The model requires that the forcing functions in form of the annual cycle of solar radiation I(z,t), nutrient concentrations in the seasonal nutricline and annual cycle of the mixed

layer depth (MLD) be specified. Nutrient (NO_3, SiO_2) concentration data were extracted from World Ocean Atlas 2013 and linearly interpolated with depth. Surface irradiance was computed as in Evans et al. [36]. The parametrization of the MLD (Eq. 10) captures the main features of its behavior observed in most regions of the world ocean: fast deepening during the late autumn and winter, abrupt shoaling in the spring, prolonged stratification in the summer, and relatively slow shallowing during the end of the summer and beginning of autumn. The annual cycle of MLD was considered in an idealized form described with an analytical function:

$$h(t) = \begin{cases} if\ \varDelta_T + T_0 \leq t < S_L + \varDelta_T + T_1 : H_{min} \\ \\ if\ S_L + \varDelta_T + T_1 \leq t < T + T_1 : -0.5(H_{max} - H_{min})\left(\sin\left(\varPi\dfrac{t - S_L}{T - \varDelta_T - S_L} + \varPi/2\right) - 1\right) + H_{min} \\ \\ if\ T_1 \leq t < \varDelta_T + T_1 : -0.5(H_{max} - H_{min})\left(\sin\left(\varPi\dfrac{t - T - \varDelta_T}{-\varDelta_T} + 3\varPi/2\right) - 1\right) + H_{min} \end{cases} \quad (10)$$

where $T=365$, $Hmin/Hmax$ - minimum/maximum MLD thickness during the year, $T1$ - time point indicating end of deep winter mixing period and beginning of spring restratification, $\varDelta T$ - duration of spring restratification, S_L - length of summer stratified period.

Winter intermittency

The formation of the temporal water column restratification was represented by a product of a scaling factor $f(t, \tau_1, \tau_2)$ reproducing the calm period, and the function $h(t)$ describing seasonal form of the MLD. The scaling factor $f(t, \tau_1, \tau_2)$ was given by:

$$f(t, \tau_1, \tau_2) = \frac{1}{1 + e^{-\xi(t - \tau_1 - \tau_2)}}\left(1 - \frac{1}{1 + e^{-\xi(t - \tau_1)}}\right) \quad (11)$$

where: $\xi = 10$ - rate of water column shoaling and deepening during the calm period, τ_1 - initiation of the calm period, τ_2 - duration of the calm period, t - time. The values of τ_1 and τ_2 were assigned according to the considered scenarios (see paragraph: Simulation setup).

Processes related to MLD change

With increasing mixed layer depth h, nutrients are entrained from the underlying layer into the water column, increasing their concentration. Phytoplankton and zooplankton concentrations become diluted as the mixed layer deepens (case (a)). Shoaling of the MLD causes loss (detrainment) of the non-motile compartments of biomass (phytoplankton and small zooplankton) (case (b)) and concentrates motile compartments (copepods) (case (c)). The turbulent fluxes at the lower boundary of the MLD are parameterized in terms of an entrainment velocity ($w_e = \dfrac{dH}{dt}$) in the ordinary way:

$$q_i = \begin{cases} (X_i - X_{pi})\dfrac{w_e}{h} & if\ w_e \geq 0\ ; \text{case (a)} \\[2mm] 0\ if\ w_e < 0\ \text{and nonmotile organisms; case (b)} \\[2mm] X_i\dfrac{w_e}{h}\ if\ w_e < 0\ \text{and motile organisms; case (c)} \end{cases} \tag{12}$$

where: h - depth of the MLD, $X_i = \{N,\ Si,\ P,\ Z,\ D_N,\ D_{Si}\}$, and $X_{pi} = \{N_p,\ Si_p,\ P_p,\ Z_p,\ D_{Np},\ D_{Sip}\}$ are the concentrations of the components below the seasonal nutricline which are assumed to be equal to zero for all components except for nutrients.

Nutrients and detritus

      At the end of summer, as physical mixing increases, the mixed layer penetrates the deep layers, thereby providing a source of nutrients to the upper water column layers; nutrients become elevated throughout the upper water column and homogeneously distributed in the water column mixed layer. Conversely, the increase in thermal stratification deprives the upper water column of nutrients supply. The phytoplankton present in the water column consume the available resources leading to a progressive deepening of the nutricline that consequently closely parallels the depth of the photic zone.

      To capture the nutrient depletion in the photic zone during summer and to emphasizes the role of the nutrient entrainment related to rapid deepening of the MLD in autumn, N_0 and Si_0 concentration data from World Ocean Atlas 2013 (profiles from September for 47°N 20°W - NABE area) were linearly interpolated and used as model forcing.

      Dissolved nitrogen is regenerated in the system as a result of remineralisation of detritus ($\beta D_N; \beta = 0.05[d^{-1}]$) and zooplankton excretion ($\epsilon(1-e)(G_{P_{ik}} + G_{D_k})$). The surface nutrient concentration is also influenced by net transport due to mixing, thus associated with entrainment of water from deep layers ($\frac{-q_N}{H}$) and diffusion ($\frac{w_{min}(N_0 - N)}{H}; w_{mix} = 0.1[d^{-1}]$). Dissolved silicate is regenerated in a similar manner but excluding zooplankton excretion. Because of this assumption all the silicon processed by grazers goes into detritus.

      Nitrogen and silicate detritus (Eq. 5 and 6) are produced by natural mortality of phytoplankton and zooplankton (linear term), and as zooplankton egestion (faecal pellet production). Additionally, in case of nitrogen detritus, zooplankton egestion contributes to detritus pool. The loss of detritus is attributed to remineralisation (with a constant rate β) and to gravitational sinking (with a constant sinking rate $w_g = 5\ [m\ d^{-1}]$). Loss of detritus is also due to changes in the MLD (the terms $\frac{-q_{D_N}}{H}$ and $\frac{-q_{D_{Si}}}{H}$). Furthermore, zooplankton is capable of grazing on nitrogen detritus, as represented by the term $-\sum_{k=1}^{n} G_{D_k}$ in equation 5.

Phytoplankton community description

      The phytoplankton community was based on the explicit representation of four functional groups of phytoplankton: diatoms, coccolitophores, dinoflagellates and small flagellates. Each phytoplankton group was distinguished by its physiological properties (i.e., traits describing growth rate and resources requirements (Table S2) in broad ranges. In the case of light-dependent growth parameters, the values were chosen to represent general ranking of the modeled taxonomic groups: small flagellates and diatoms have the lowest light requirements, followed by dinoflagellates and coccolithophores [37–39].

Ecological trade-offs were imposed through highly simplified allometric constraints [40,41] bounding the phytoplankton physiological properties and size: large phytoplankton species were distinguished by higher intrinsic maximum growth rates, higher nutrient half-saturations and were assumed to be high-light adapted due to packaging effects [42,43].

The marine ecosystem model represents a broad spectrum of phytoplankton species representing each phytoplankton functional group. In order to overcome some difficulties attributed to limited knowledge of physiological properties of the species in each functional group, a stochastic approach was applied. More specifically, each phytoplankton functional group was distinguished by the range of the parameters ruling their physiologies. The specific values of coefficients describing each species in the community were provided by random drawing from these broad ranges (Table S2). The community assemblage was formed by 40 generated species (10 in each functional group).

Nonetheless, 40 species do not reflect the astonishing phytoplankton diversity observed in marine ecosystems. Thus, to correctly consider the limitations given by the finite selection of the species, an ensemble approach [44] was employed. Namely, 30 phytoplankton communities were generated and treated as an ensemble set.

The phytoplankton community was initially saturated with species, though the interactions of model species with the seasonally fluctuating environment, competition with other phytoplankton, and grazing determine the composition of the phytoplankton community in a sustainable ecosystem. Because of this initial species saturation, neither community structure nor diversity were imposed, but were an emergent properties [45,46].

Table S2: Phytoplankton parameters.

Parameter	Units	Meaning	Diatoms	Dinoflagellates	Coccolitophores	Small flagellates
r	d^{-1}	maximum growth rate	0.76 - 1.94	0.47 - 0.77	0.91 - 1.2	1.27 - 1.59
H_N	$mmol\ m^{-3}$	half-saturation for N uptake	0.93 - 1.58	2.5 - 6.3	0.15 - 0.21	1.94 - 4.88
H_{Si}	$mmol\ m^{-3}$	half-saturation for Si uptake	1	0	0	0
α	$d^{-1}\ (Wm^{-2})^{-1}$	initial slope of P-I curve	0.019 - 0.1271	0.085 - 0.115	0.028-0.038	0.019 -0.127
$R_{N:Si}$	-	elemental ratios	1	0	0	0
m_P	d^{-1}	mortality rate	0.05	0.025	0.06	0.05

Zooplankton community description

The model zooplankton community includes two generalist grazers distinguished by the size. Large zooplankton (copepods) preferentially graze on large phytoplankton (in here diatoms and dinoflagellates), but can graze on small phytoplankton (in here coccolitophores and small flagellates) and vice versa for small zooplankton (microzooplankton) (Table S3).

The description of the large zooplankton species representing copepods was augmented with a winter dormancy strategy tightly connected with environmental cues, triggered by the deepening of MLD, and is meant to reflect their life cycles. A dormancy function was described by an equation:

$$\omega(t) = \frac{1}{1+e^{-s(t-t_1)}} \left(1 - \frac{1}{1+e^{-s(t-t_2)}} \right)$$ (13)

where t is time in days, s is an arbitrary shape parameter, t_1 and t_2 are the days indicating end and beginning of dormancy period. The values of $\omega(t)$ ranged from 0 to 1 and were used as a scaling factor for copepods grazing and mortality rates. Therefore for copepods, $g_k = \omega \hat{g}_k$, $m_{Zk} = \omega \hat{m}_{Zk}$, $m_{Z2k} = \omega \hat{m}_{Z2k}$. Since the life cycles were not considered for microzooplankton the parameters were as follows: $g_k = \hat{g}_k$, $m_{Zk} = \hat{m}_{Zk}$, $m_{Z2k} = \hat{m}_{Z2k}$.

Table S3: Zooplankton specific parameter

Parameter	Meaning	Units	Mesozooplankton	Microzooplankton
H_k	half-saturation for intake	$mmolN\ m^{-3}$	0.5	0.5
e	net production efficiency	-	0.75	0.75
ε	absorption efficiency	-	0.69	0.69
Φ_P	grazing preference for P	-	0.67	0.67
Φ_D	grazing preference for D	-	0.33	0.33
$\hat{g}$	max ingestion rate for large P	d^{-1}	1	0.17
	max ingestion rate for small P		0.17	1
$\hat{m}_Z$	linear mortality rate	d^{-1}	0.02	0.02
$\hat{m}_{Z2}$	quadratic mortality rate	$(mmol\ m^{-3})^{-1}\ d^{-1}$	0.1	0.1

Simulations setup

A phytoplankton community was initialized with an identical, very low concentration (10^{-6} mmol C m^{-3}) in every simulated environment and the model was integrated for 100 years, over which time a repeating annual cycle in ecosystem structure emerged. The integration was repeated 30 times, each time with a different random selection of 40 phytoplankton species. As a result an ensemble of 30 communities was created, and analysed statistically with focus on some relevant ecological metrics.

The model equations were solved in Matlab (MATLAB R2012a, The MathWorks Inc., Natick, MA, 2000) with an implicit ode15s scheme that guarantees high order of accuracy. The source code and the scripts used for data analyses are freely available from the authors.

Modeling scenarios

The modeling scenarios explored in this study considered winter intermittency in form

of calm periods accounting for 30, 20, 10 and 0% of the winter period which were referred to as 30%, 20%, 10% and reference case. All calm periods were considered to last for 3 days and were uniformly distributed during the winter months, hence 3, 2, 1 and 0 calm period per month were resolved in the scenarios 30%, 20%, 10% and reference case respectively.

The shoaling of the water column during each calm period reached the euphotic zone. The phytoplankton trapped below the euphotic zone during the calm period was subjected to the natural mortality and grazing resolved in the model. These two populations, from the photic zone and from below it, were mixed together during water column deepening at the end of calm period.

An identical set of phytoplankton communities was simulated in all the above scenarios, thus allowing for the analysis of how winter intermittency affected each community dynamics with respect to its composition.

Further details about the model can be found in Stec 2015 [47], freely available on Open University and EThOS webpage.

Model predictive skill assessment

The model predictive skill was assessed by comparison of model results and *in situ* observations obtained during the North Atlantic Bloom Experiment in 1989 at 47N 20W. This shows how well the model is able to reproduce the short term, high frequency variability of the system, i.e. the phenology of the phytoplankton blooms.

The model forced by MLD adapted to the conditions observed during NABE was able to reproduce the typical mid-latitude seasonal succession pattern consisting low phytoplankton abundance in winter, a spring bloom of diatoms with a subsequent bloom of non-diatom phytoplankton, often other flagellates, followed by coccolithophorids observed during stratified conditions.

The seasonal patterns of phytoplankton abundance were consistent across all the tested communities and, despite considerable spread of correlation values, indicate that the timing and the magnitude of the bloom was in an agreement with the NABE data (Fig. S12). The North Atlantic Bloom Experiment was designed to capture the spring bloom dynamics, hence the model validation against NABE data has a strong bias towards the spring bloom period and the spread of indicators' values used for model skill assessment (correlation R, normalised standard deviation $\sigma^\star$, and root-mean-square-distance RMSD) was mainly related to spring bloom phenology, i.e. its initiation, termination and intensity. Overall, the model chlorophyll versus reference data correlation ranged from 0.3 to 0.8, normalised standard deviation was close to 1 for the great majority of the ensemble members, and median RMSD was lower than 0.35 for all the communities.

Despite having significant correlation values (R>0.8) and rather low RMSD values (<0.5), the model nitrate has considerably lower normalised standard deviation with respect to the reference data (Fig. S12). The model reproduces well the winter nutrient concentrations, yet it underestimates nitrate drawdown during the spring bloom. The NO_3 model concentration observed shortly after spring bloom was higher with respect to observations and consequently their standard deviation was lower. The model silicate concentration was in a good agreement with NABE measurements with R>0.7, $\sigma^\star$ close to 1 and RMSD <0.4 for the vast majority of the explored communities (Fig. S12)
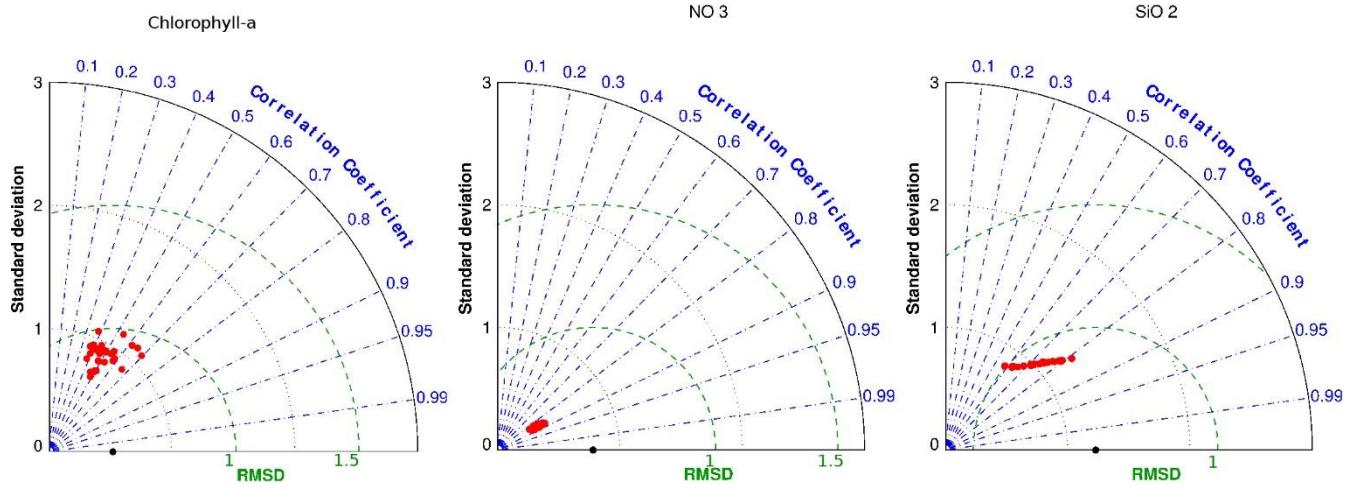
Fig. S12. A quantitative approach based on assessment indices and skill scores was provided to evaluate model performance, where each simulation result was validated against the available in situ observations of a) chlorophyll-a b) nitrate and c) silicate obtained during the NABE. Normalized standard deviation, correlation coefficient and root-mean-square difference of appropriate model variables and field observations was computed for each of the explored 30 communities and displayed with a Taylor diagram. Black dots on x-axis depict the origin of the RMSD plane.

2.7. Modelling results

The growth rates of all species were comparable at the beginning of the winter (Fig. S13). Because of the increasing solar irradiance towards the end of winter and the physiological discrepancies amongst the phytoplankton functional groups, the gap between the species' net growth rates increases both during the deep mixing and, above all, the calm periods when the diatom growth rate may exceed that of small flagellates by two-fold (Fig. S13).
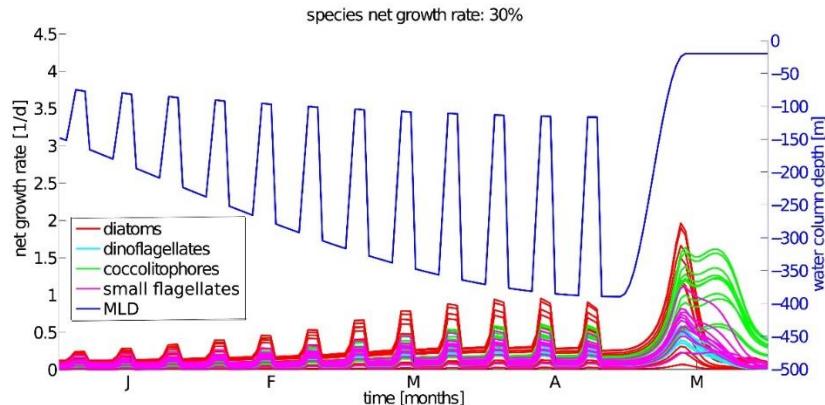
Fig. S13. Net growth rates of all the species in the intermittency scenario 30%. Each line depicts a single species. The blue line depicts the depth of the MLD which represent the water column depth considered in the model (OD model).

Because of their physiological characteristics diatoms clearly benefit from a temporal change in the light environment, i.e. a series of a growth rate boosts observed during consecutive calm periods resulting in small but recurrent diatoms blooms (Fig. S14). These

small blooms modulated the accumulation rate of diatoms, restructuring the community at the functional group level (Fig. S15), i.e. increasing the biomass of diatoms relative to small flagellates by factors of 1.17, 1.8 and 3.2 in the 10, 20 and 30% scenarios, or advancing time point when diatom biomass exceeded that of small flagellates by 6, 11 and 17 days respectively (Table S4).
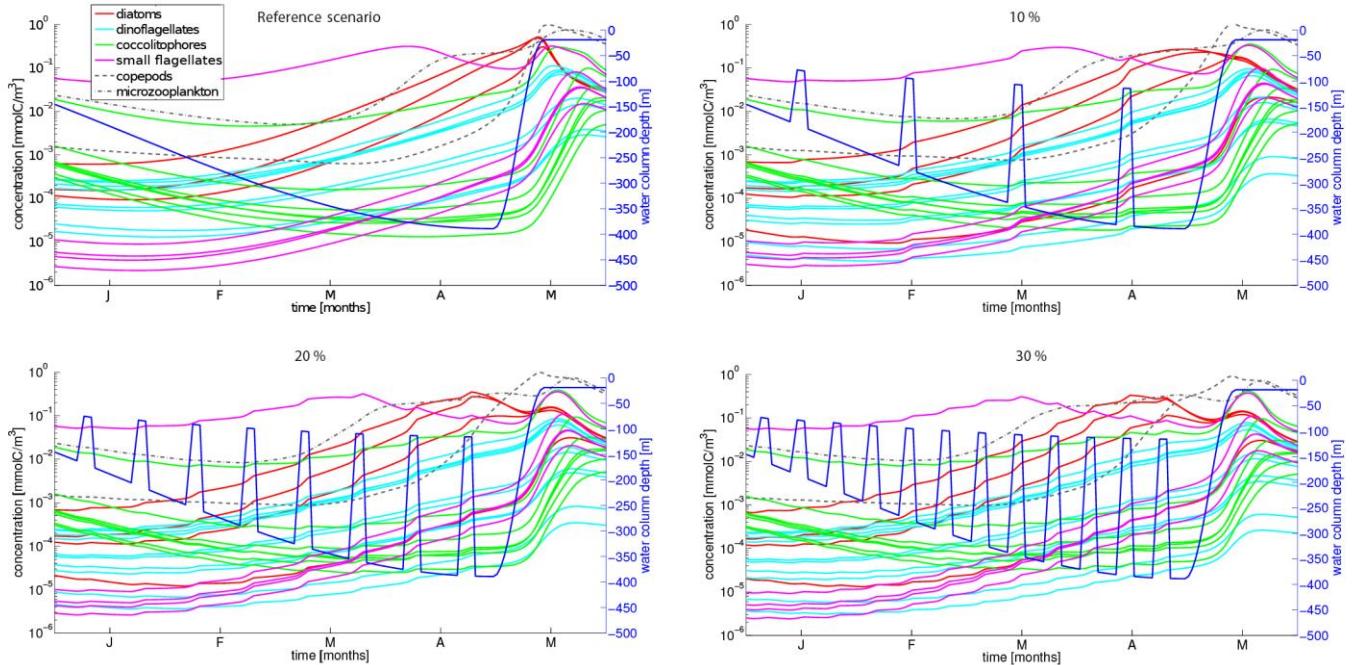
Fig. S14. Species concentration in the intermittency scenarios: reference, 10%, 20% and 30%. Each line depicts a single species. The blue line depicts the depth of the MLD which represent the water column depth considered in the model (0D model).

Small flagellates, diatoms, and dinoflagellates started accumulating in mid-winter while the seasonal mixed layer was deepening (Fig. S15), consistent with the "Disturbance-Recovery hypothesis" [48]. However, transient restratification of the mixed layer generating Sverdrup-like blooms also allowed additional accumulation of diatoms throughout winter (Fig. S14 and Fig. 3B in the main text). The diatom concentration at the end of winter increased by 2.3, 5.9 and 10.6 folds (Table S4) impacting both spring bloom magnitude and timing. Indeed the bloom advanced in time by 6, 20 and 28 days in terms of the concentration and by 4, 10 and 19 in terms of depth-integrated biomass peak in the scenarios 10, 20 and 30% respectively (Table S4). While the maximal volumetric concentration decreased (0.45, 0.43 and 0.41 relative to the reference scenario) the maximal depth-integrated biomass increased by factors of 1.5, 2.13 and 2.05 in the scenarios 10, 20 and 30% respectively (Table S4). This ambiguity was related to the depth of the water column during the maximal concentration, i.e. even though the peak concentration decreased it was observed in a higher volume, thus the accumulated biomass was greater. The mismatch between diatoms and copepods due to an early bloom could explain the impact on the bloom magnitude observed in the simulations [49].
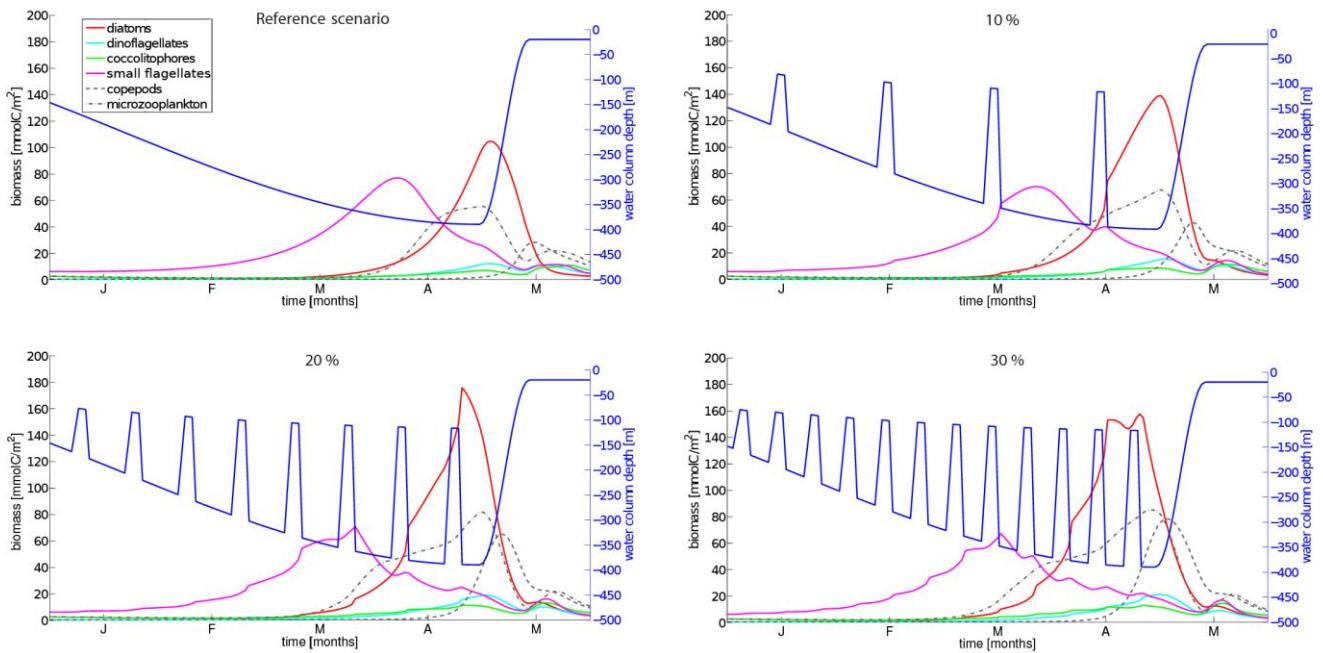
Fig. S15. Depth-integrated biomass of phytoplankton functional groups and zooplankton in the intermittency scenarios reference, 10%, 20% and 30%. Each line depicts the depth-integrated biomass of all the species within the functional group in a single, randomly selected community across all the considered scenarios. The blue line depicts the depth of the MLD which represent the water column depth considered in the model (OD model).

These results not only corroborate BGC-Argo and CATCH observations, but also reinforce the predicted causative link between the frequency of restratification events and the observed interannual variability of spring bloom phenology.

In addition, winter mixing intermittency seems to impact species diversity. The volumetric concentration-based diversity was elevated by 29, 39 and 43%, and the integrated biomass-based diversity by 35, 53 and 41% in the 10, 20 and 30% scenarios with respect to the reference case (Table S5). The most pronounced diversity increase was found in the case of small flagellates and dinoflagellates, though a considerable increase in diversity was observed in all PFTs.

Table S4. Model results. The values presented here indicate the median ± median absolute deviation value computed for all 30 communities explored in the four intermittency scenarios. In this table, biomass refers to depth-integrated biomass.

Parameter	*reference*	*10%*	*20%*	*30%*
diatoms:small flagellates end of winter ratio	0.35 ± 0.19	0.41 ± 0.31	0.64 ± 0.77	1.13 ± 2.25
cumulative diatoms winter biomass ($[mmolC\ m^{-2}]$)	85.78 ± 25.04	167.04 ± 89.05	298.02 ± 134.71	483.95 ± 281.08
cumulative small flagellates winter	589.59 ±	885.22 ±	1255.47 ±	1666.10 ±

biomass ([$mmolC\ m^{-2}$])	427.49	675.67	887.12	983.19
diatoms dominance over small flagellates ([yd])	108.50 ± 14.00	102.50 ± 10.00	97.50 ± 8.50	91.00 ± 5.50
diatoms concentration at the end of winter ([$mmolC\ m^{-3}$])	5.64 ± 2.79	13.07 ± 7.78	33.03 ± 15.27	60.18 ± 37.71
diatoms bloom peak (biomass) ([$mmolC\ m^{-2}$])	129.15 ± 34.13	194.10 ± 69.83	275.35 ± 38.28	265.02 ± 33.49
diatoms bloom peak (concentration) ([$mmolC\ m^{-3}$])	1.89 ± 0.85	0.85 ± 0.26	0.82 ± 0.08	0.77 ± 0.07
diatoms bloom peak time (biomass) ([yd])	127.00 ± 9.50	123.00 ± 2.00	117.00 ± 1.00	108.00 ± 9.00
diatoms bloom peak time (concentration) ([yd])	136.00 ± 1.00	130.00 ± 9.00	116.00 ± 3.50	108.00 ± 9.00

Table S5. Species diversity. The values presented here indicate the median ± median absolute deviation computed for all 30 communities explored in the four intermittency scenarios. The species diversity was measured as a total number of species whose median biomass over the seasonal cycle exceeded 0.004 [$mmol\ C\ m^{-2}$] (top value in each cell) or maximal concentration throughout the whole year exceeded 0.05 [$mmol\ C\ m^{-3}$] (bottom value in each cell).

Diversity	*reference*	*10%*	*20%*	*30%*
All PFTs	14.5±2.5	18.5±3.5	20±3	20.5±2.5
	8.5±2.5	11.5±2.5	13±2	12±3
Diatoms	3±1	4±1	4±1	4±1
	3±1	3±1	3±1	3±1
Small flagellates	6±2	8±1	8±1	8±1
	2±1	4±1	4±1.5	4±1.5
Dinoflagellates	4±1.5	4.5±1.5	5±1	5±1
	1.5±0.5	2±1	2±1	2±1

References

1. Wong, A., Keeley, R., Carval, T. & Argo Data Management Team. Argo Quality Control Manual For CTD and Trajectory Data. 1–56 (2015).

2. Schmechtig, C., Claustre, H., Poteau, A. & D'Ortenzio, F. Bio-Argo quality control manual for the Chlorophyll-A concentration. *Ifremer* 13 (2014). doi:http://dx.doi.org/10.13155/35385 Bio-Argo

3. Organelli, E. *et al.* A novel near real-time quality-control procedure for radiometric profiles measured by Bio-Argo floats: protocols and performances. *J. Atmos. Ocean. Technol.* 160303130530002 (2016). doi:10.1175/JTECH-D-15-0193.1

4. Xing, X. *et al.* Quenching correction for in vivo chlorophyll fluorescence acquired by autonomous platforms: A case study with instrumented elephant seals in the Kerguelen region (Southern Ocean). *Limnol. Oceanogr. Methods* **10,** 483–495 (2012).

5. Briggs, N. *et al.* High-resolution observations of aggregate flux during a sub-polar North Atlantic spring bloom. *Deep Sea Res. Part I Oceanogr. Res. Pap.* **58,** 1031–1039 (2011).

6. Johnson, G. C., Schmidtko, S. & Lyman, J. M. Relative contributions of temperature and salinity to seasonal mixed layer density changes and horizontal density gradients. *J. Geophys. Res. Ocean.* **117,** (2012).

7. Johnson, L., Lee, C. M. & D'Asaro, E. A. Global Estimates of Lateral Springtime Restratification. *J. Phys. Oceanogr.* **46,** 1555–1573 (2016).

8. IOC, SCOR & IAPSO. The International thermodynamic equation of seawater–2010: Calculation and use of thermodynamic properties. *Intergov. Oceanogr. Com. UNESCO* **56,** 196 (2010).

9. Brainerd, K. E., Gregg, M. C. & Sciences, F. Surface mixed and mixing layer depths. *Deep Sea Res. Part I Oceanogr. Res. Pap.* **42,** 1521–1543 (1995).

10. de Boyer Montégut, C., Madec, G., Fischer, A. S., Lazar, A. & Iudicone, D. Mixed layer depth over the global ocean: An examination of profile data and a profile-based climatology. *J. Geophys. Res. C Ocean.* **109,** 1–20 (2004).

11. Boccaletti, G., Ferrari, R. & Fox-Kemper, B. Mixed Layer Instabilities and Restratification. *J. Phys. Oceanogr.* **37,** 2228–2250 (2007).

12. Mahadevan, A., Lee, C., Perry, M. J. & D'Asaro, E. RESEARCH ARTICLES Eddy-Driven Stratification Initiates North Atlantic Spring Phytoplankton Blooms. *Science* **337,** 54–58 (2012).

13. Morel, A. Light and marine photosynthesis: a spectral model with geochemical and climatological implications. *Prog. Oceanogr.* **26,** 263–306 (1991).

14. KIRK, J. T. O. Dependence of relationship between inherent and apparent optical properties of water on solar altitude. *Limnol. Oceanogr.* **29,** 350–356 (1984).

15. Gordon, H. R. & Morel, A. Remote assessment of ocean color for interpretation of satellite visible imagery: A review. *Lect. Notes Coast. Estaurine Study* **4,** 1–114 (1983).

16. Smetacek, V. & Passow, U. Spring bloom initiation and Sverdrup's critical-depth model. *Limnol. Oceanogr.* **35,** 228–234 (1990).

17.   Geider, R. J., Osbonie, B. A. & Raven, J. A. Growth, Photosynthesis and Maintenance Metabolic Cost in the Diatom Phaeodactylum Tricornutum At Very Low Light Levels. *J. Phycol.* **22,** 39–48 (1986).

18.   Cetinić, I. *et al.* A simple optical index shows spatial and temporal heterogeneity in phytoplankton community composition during the 2008 North Atlantic Bloom Experiment. *Biogeosciences* **12,** 2179–2194 (2015).

19.   Eymard, L. *et al.* Surface fluxes in the North Atlantic current during CATCH/FASTEX. *Q. J. R. Meteorol. Soc.* **125,** 3563–3599 (1999).

20.   Vidussi, F., Claustre, H., Manca, B. B., Luchetta, A. & Marty, J.-C. Phytoplankton pigment distribution in relation to upper thermocline circulation in the eastern Mediterranean Sea during winter. *J. Geophys. Res.* **106,** 19939 (2001).

21.   Matsuoka, A. *et al.* A synthesis of light absorption properties of the Arctic Ocean: application to semianalytical estimates of dissolved organic carbon concentrations from space. *Biogeosciences* **11,** 3131–3147 (2014).

22.   Granskog, M. A. *et al.* Effect of sea-ice melt on inherent optical properties and vertical distribution of solar radiant heating in Arctic surface waters. *J. Geophys. Res. Ocean.* **120,** 7028–7039 (2015).

23.   Geider, R. J. Light and Temperature Dependence of the Carbon to Chlorophyll a Ratio in Microalgae and Cyanobacteria: Implications for Physiology and Growth of Phytoplankton. *New Phytol.* **106,** 1–34 (1987).

24.   Behrenfeld, M. J. *et al.* Revaluating ocean warming impacts on global phytoplankton. *Nat. Clim. Chang.* **6,** 323–330 (2015).

25.   Sverdrup, H. U. On conditions for the vernal blooming of phytoplankton. *J. Cons. Int. Expl. Mer* **18,** 287–295 (1953).

26.   Siegel, D. A., Doney, S. C. & Yoder, J. A. The North Atlantic Spring Phytoplankton Bloom and Sverdrup's Critical Depth Hypothesis. *Science* **296,** 730–733 (2002).

27.   Lacour, L., Claustre, H., Prieur, L. & Ortenzio, F. D. Phytoplankton biomass cycles in the North Atlantic subpolar gyre: A similar mechanism for two different blooms in the Labrador Sea. *Geophys. Res. Lett.* 1–8 (2015). doi:10.1002/2015GL064540.Received

28.   Walter, B., Peters, J., van Beusekom, J. E. E. & St. John, M. A. Interactive effects of temperature and light during deep convection: a case study on growth and condition of the diatom Thalassiosira weissflogii. *ICES J. Mar. Sci. J. du Cons.* **72,** 2061–2071 (2015).

29.   Caniaux, G., Prieur, L., Giordani, H., Hernandez, F. & Eymard, L. Observation of the Circulation in the Newfoundland Basin in Winter 1997. *J. Phys. Oceanogr.* **31,** 689–710 (2001).

30.   Paulsen, M., Riisgaard, K., Thingstad, T., St John, M. & Nielsen, T. Winter-spring transition in the subarctic Atlantic: microbial response to deep mixing and pre-bloom production. *Aquat. Microb. Ecol.* **76,** 49–69 (2015).

31.   McMinn, A. & Martin, A. Dark survival in a warming world. *Proc. Biol. Sci.* **280,** 20122909 (2013).

32.   Jochem, F. J. Dark survival strategies in marine phytoplankton assessed by cytometric

measurement of metabolic activity with fluorescein diacetate. *Mar. Biol.* **135,** 721–728 (1999).

33. Lindemann, C., Backhaus, J. O. & St John, M. A. Physiological constrains on Sverdrup's Critical-Depth-Hypothesis: the influences of dark respiration and sinking. *ICES J. Mar. Sci.* fsv046- (2015). doi:10.1093/icesjms/fsv046

34. Smith, E. L. Photosynthesis in Relation to Light and Carbon Dioxide. *Proc. Natl. Acad. Sci. U. S. A.* **22,** 504–11 (1936).

35. Fasham, M. J. R., Ducklow, H. W. & McKelvie, S. M. A nitrogen-based model of plankton dynamics in the oceanic mixed layer. *J. Mar. Res.* **48,** 591–639 (1990).

36. Evans, G. T. & Parslow, J. S. A Model of Annual Plankton Cycles. *Biol. Oceanogr.* **3,** 327–347 (1985).

37. Brand, L. E. & Guillard, R. R. L. The effects of continuous light and light intensity on the reproduction rates of twenty-two species of marine phytoplankton. *J. Exp. Mar. Bio. Ecol.* **50,** 119–132 (1981).

38. Richardson, K., Beardall, J. & Raven, J. a. Adaption of unicellular algae to irradiance: an analysis of strategies. *New Phytol.* **93,** 157–191 (1983).

39. Langdon, C. On the Causes of Interspecific Differences in the Growth Irradiance Relationship for Phytoplankton .2. a General-Review. *J. Plankton Res.* **10,** 1291–1312 (1988).

40. Sarthou, G., Timmermans, K. R., Blain, S. & Tréguer, P. Growth physiology and fate of diatoms in the ocean: A review. *J. Sea Res.* **53,** 25–42 (2005).

41. Follows, J. Modeling and prediction of marine microbial populations in the genomic era. *Oceanography* **20,** 155 (2007).

42. Kirk, J. T. O. *Light and photosynthesis in aquatic ecosystems*. (Cambridge university press, 1994).

43. Finkel, Z. V & Rwin, A. N. J. I. Modeling Size-dependent Photosynthesis : Light Absorption and the Allometric Rule. *J. Theor. Biol.* 361–369 (2000). doi:10.1006/jtbi.2000.2020

44. Murphy, J. M. *et al.* Quantification of modelling uncertainties in a large ensemble of climate change simulations. *Nature* **430,** 768–772 (2004).

45. Follows, M. J., Dutkiewicz, S., Grant, S. & Chisholm, S. W. Emergent biogeography of microbial communities in a model ocean. *Science* **315,** 1843–1846 (2007).

46. Dutkiewicz, S., Follows, M. J. & Bragg, J. G. Modeling the coupling of ocean ecology and biogeochemistry. *Global Biogeochem. Cycles* **23,** (2009).

47. Stec, K. F. Role of life strategies in diatom biodiversity: a modelling approach. (Open University, 2015).

48. Behrenfeld, M. J. Abandoning Sverdrup's Critical Depth Hypothesis on phytoplankton blooms. *Ecology* **91,** 977–989 (2010).

49. Edwards, M. & Richardson, A. J. Impact of climate change on marine pelagic phenology and trophic mismatch. *Nature* **430,** 881–4 (2004).

Liste des figures

Remerciements

Je souhaite adresser de chaleureux remerciements à :

Hervé, pour m'avoir fait partager sa vision de l'exploration en océanographie

Fabrizio, notre indispensable chef d'équipe

Daniele et Gilles, toujours très sympathiques et enthousiastes

Mes anciens colocs et collègues Nico, Fabio, Simon, David (Jack, Bobby, Billy) et Laurent

Mes voisins de mezzanine, Raph, Marie, Orens, Christophe et de nouveau Nico

Nos chères gestionnaires, Linda et Corinne

Et enfin, l'ensemble des occupants de la Corderie Ouest